Proteomic insights into the modulation of foetal neurogenesis by the anti-retroviral efavirenz

CLAUDIA ALBELDAS

(ALBCLA003)

SUBMITTED TO THE UNIVERSITY OF CAPE TOWN in fulfilment of the requirements of the degree MSc (Med) in Chemical Biology

Faculty of Health Sciences

UNIVERSITY OF CAPE TOWN

July 2019

Supervisor: Professor Jonathan Blackburn

Integrative Biomedical Sciences, University of Cape Town

Declaration

I, *Claudia Albeldas,* hereby declare that the work on which this dissertation/thesis is based is my original work (except where acknowledgements indicate otherwise) and that neither the whole work nor any part of it has been, is being, or is to be submitted for another degree in this or any other university.

I empower the university to reproduce for the purpose of research either the whole or any portion of the contents in any manner whatsoever.

Signed: Signed by candidate Date: 04.21.2019

בס"ד

Acknowledgments

Firstly, thank you to my supervisor, Professor Jonathan Blackburn, for giving me the opportunity to work in your laboratory and for your support and encouragement throughout this process.

To Brandon Murugan, you were not only a friend to me but a mentor and a teacher. Thank you for teaching me the skills I needed for this work, for having unlimited patience with me, for always looking out for me, and for believing in me even when I did not believe in myself. As I have said before, without you, I would not have made it to this point.

Thank you to Brandon, Shaun, Tariq, and Bridget for assisting me with lab work, data analysis, proof reading, and mass spectrometry related queries. You all played invaluable roles and I am truly grateful for your help. To the rest of the Blackburn Laboratory members, thank you for always pitching in to help when needed and for the words of encouragement that were always necessary.

Thank you to the NRF, Jonathan Blackburn, the Ernst and Ethel fund, and my parents for financial support throughout this degree.

Thank you to my parents and my sister for always believing in me and supporting me. I could not have done this without the three of you as my rock. To my granny, Felicia, for being my biggest fan and cheerleader, this is for you.

Abstract

Background: South African guidelines recommend that HIV-positive pregnant women immediately initiate antiretroviral therapy (efavirenz, emtricitabine, and tenofovir), regardless of trimester. Efavirenz causes central nervous system neuropathy and has been linked to birth defects such as encephalocoele. Cohort studies of HIV-uninfected children exposed to antiretroviral treatment *in utero* report minor learning delays but are inconclusive.

Non-transformed human derived neuroepithelial stem (NES) represent a unique pre-clinical model in which to investigate the effects of efavirenz on the developing neural system. Efavirenz-induced global cellular molecular changes may be characterised using mass spectrometry (MS).

Aims: To optimise an MS-based efavirenz extraction and detection assay, and to investigate efavirenz-induced NES proteomic responses.

Methods: A TSQ Vantage triple quadrupole mass spectrometer was employed to optimise targeted detection of efavirenz extracted from cultured cells and supernatant. Cells were cultured for 72 hours, incorporating a 24-hourly efavirenz treatment. Efavirenz concentration dynamics were assessed over this period, and cells were harvested every 24 hours for discovery proteomic analysis using a Q-Exactive quadrupole-Orbitrap mass spectrometer.

Results: Drug extraction with acetonitrile was selected as the optimal extraction and detection technique. In cell culture, efavirenz concentration increased after 24 hours and decreased after 48 hours. A total of 1663 protein groups were identified, with 26, 39, and 80 protein groups differentially expressed 24, 48, and 72 hours respectively post EFV treatment. The most significantly enriched deregulated pathways included cholesterol biosynthesis, mRNA splicing, and JAK/STAT and Wnt signalling.

Conclusions: Efavirenz-altered protein expression reflects functional pathway perturbations, which may contribute to clinically-observed neurological effects. Orthoganal and *in vivo* confirmation is required.

List of abbreviations

3TC	Lamivudine
ACAT	acetyl-CoA acetyltransferase
ACLY	ATP citrate lyase
ACN	Acetonitrile
ALS	amyotrophic lateral sclerosis
ANI	asymptomatic neurocognitive impairment
ANOVA	analysis of variance
ANXA2	annexin 2
AUC	area under the curve
BBB	blood brain barrier
CE	collision energy
CID	collision induced dissociation
CLIP2	cytoplasmic linker gene
CM	chloroform-methanol
CMV	Cytomegalovirus
CNS	central nervous system
CO2	carbon dioxide
CPSF1	cleavage and polyadenylation specificity factor subunit 1
CSF	cerebrospinal fluid
CTNNB1	ß-catenin
CV	coefficient of variation
DMSO	dimethyl sulphoxide
DTI	diffusion tensor imaging
EGF	epidermal growth factor
EMT	epithelial to mesenchymal transition
ESI	electrospray ionisation
FA	formic acid
FADS2	fatty acid desaturase
FASN	fatty acid synthase
FASP	filter aided sample preparation
FDA	Food and Drug Administration
FDC	fixed dose combination
FDFT1	squalene synthase
FDR	false discovery rate
FGF2	fibroblast growth factor 2
FT-ICR	Fourier transform ion cyclotron resonance analysers
GSK3B	glycogen synthase kinase 3β
GuHCl	guanidinium hydrochloride
HAD	HIV associated dementia
HAND	HIV associated neurocognitive disorder
HCD	higher energy collisional dissociation

HESI	heated electrospray ionisation
HEU	HIV exposed uninfected
HGMCS1	hydroxymethylglutaryl-CoA synthase
HMDB	human metabolome data base
HPLC	high performance liquid chromatography
IAA	Iodoacetamide
IFN	Interferon
IL-6	interleukin 6
iTRAQ	isobaric tags for absolute and relative quantification
JAK	Janus kinase
KSHV	Kaposi's sarcoma-associated herpesvirus
LC	liquid chromatography
LC-MS/MS	tandem mass spectrometry
LFQ	label free quantitation
LSM4	U6 snRNA-associated protein
LTNP	long-term nonprogressor
m/z	mass to charge ratio
MALDI	matrix assisted laser desorption/ionisation
miRNA	micro RNAs
MND	mild neurocognitive disorder
mRNA	messenger RNA
MS	mass spectrometry
MS1	precursor ion spectra
MS2	product ion spectra
MTC	multiple testing correction
MTCT	mother to child transmission
mtDNA	mitochondrial DNA
MTT	3-(4, 5-dimethylthiazolyl-2)-2, 5-diphenyltetrazolium bromide
NES	neuroepithelial stem
PAK2	p21 activated kinase 2
PBS	phosphate buffered saline
PEG	polyethylene glycol
PEP	posterior error probability
PPIE	peptidyl prolyl isomerase E
ppm	parts per million
PSM	peptide-spectrum match
RAC1	ras related GTPase binding protein
ROS	reactive oxygen species
SF	splicing factor
SHR	steroid hormone receptors
SHSY-5Y	Neuroblastoma
SILAC	stable isotope labelling by amino acids in cell culture

snRNA	small nuclear RNA
snRNPs	small nuclear ribonucleoproteins
SQLE	squalene epoxidase
SRM	selected reaction monitoring
STAT3	signal transducer and activator of transcription 3
SVZ	the sub-ventricular zone
TCEP	tris(2-carboxyethyl)phosphine
TGF-ß	transforming growth factor ß
TIC	total ion chromatogram
TNF-α	tumour necrosis factor α
TOF	time of flight
TSQ	triple stage quadrupole
UBXN7	UBX domain protein
V	Volts
WHO	World Health Organisation
XICs	extracted ion chromatograms

Table of contents

Contents

List of figures

List of tables

Chapter 1: Literature review

1.1 Introduction

The human immunodeficiency virus (HIV) epidemic in South Africa is the largest worldwide, with an estimated 13% of the population infected in 2018.[1] HIV is classified as a lentivirus, a subset of retroviruses consisting of RNA instead of DNA, which infect humans and animals and cause a slow progressing chronic disorder.[2] HIV differs from animal lentiviruses as it causes major immunodeficiency, whereas animal lentiviruses cause slightly impaired immune responses.[2]

Once HIV enters the host, it targets and depletes host CD4+ T-cells via apoptosis and pyroptosis.[3] This causes a major inflammatory response, which attracts and activates more T-cells, ultimately resulting in a cycle of inflammation and immune cell destruction.[4] A CD4+ cell count below 200 cells/mm^3 and a high viral load is indicative of immunodeficiency that results in vulnerability to secondary infections.[5] Most commonly, tuberculosis (TB) and the development of certain types of cancer are seen in patients that progress to acquired immunodeficiency syndrome (AIDS). Left untreated, HIV infection will usually result in progression to AIDS, and subsequently, death within 11 years.[6] AIDS can be a debilitating disease, causing major financial strain and emotional trauma within families. With the introduction of anti-retroviral (ARV) drugs, the implementation of various sustainable intervention strategies within affected communities, and general education, there has been a steady decline in HIV infection rates, as well as morbidity and mortality rates.[7,8]

As a result of ARV medication, HIV has become a chronic disease, necessitating life-long treatment that allows those infected to live longer and healthier lives. Another major success of ARV treatment has resulted in HIV-infected women being able to give birth to uninfected children. The benefit of ARV treatment in protecting the foetus from HIV is undeniable, although concerns have been raised about the side effects of certain ARV drugs that the foetus may experience during development, both pre- and post-natally. In adults, the side effects of ARV treatment are well documented, while a limited amount of information on the effects of ARV exposure *in utero* exists. Thus as the use of ARVs become more wide-spread, it is pertinent to obtain a deeper understanding of the effects of ARV usage during pregnancy.

1.2 Aetiology and pathogenesis of HIV

Since the identification of HIV 1981, many studies have been conducted to better understand the origin, transmission, and pathogenicity of the virus.[9] ARV drugs need to target processes that are vital to viral replication, while causing minimal side effects to the host. Therefore, in order to develop effective ARV treatment, an understanding of the viral life cycle and mechanisms essential for infection is needed.

Transmission of HIV can occur via bodily fluids such as blood, semen, or breast milk, among others. Most commonly, HIV is transmitted through unprotected sexual intercourse with an infected person. Once the virus enters the blood stream of an uninfected person, usually via a mucous membrane in the genital tract, it attacks the host immune cells. HIV is an enveloped virus and therefore needs to fuse with the host cell membrane in order to insert the viral core particles into the host cells. The viral envelope protein gp120 targets the host cell CD4+ receptor and a co-receptor (either CCR5 or CXCR4) in order to successfully bind to the cell.[10] Gp41 of the viral envelope protein then initiates fusion between the host and viral membranes and the viral core particle enters the host cell where viral RNA is transcribed to double stranded viral DNA by reverse transcriptase.[11–13] The viral DNA enters the host cell nucleus where integrase removes the 3' ends from the viral DNA and, via transesterification, joins it to the 5' end of the host DNA.[14,15] Protease enzymes then cleave polyprotein precursors for gag and gag-pol, both of which are essential for maturation and infectivity of the virus.[16–18] The newly transcribed viral proteins and viral RNA assemble at the surface of the host cell and bud from the cell as a mature virus. HIV hijacks many host cell proteins, but reverse transcriptase, integrase, and protease are all exclusively virally transcribed, making them extremely attractive as targets for ARV treatment of HIV infection.[10,14,18]

1.3 Classes of ARV treatments and their mechanisms

There are several classes of ARVs, each targeting a different vital part of the viral life cycle, including cell recognition and entry, DNA transcription, DNA integration, and cleavage of essential viral proteins (Figure 1.1).

Entry/fusion inhibitors prevent the virus from fusing with the host cell membrane, either acting as a CCR5 antagonist, or by targeting CXCR4 co-receptors.[10] For example, maraviroc is a CCR5 antagonist that blocks gp120 from associating with the receptor.[19] Enfuvirtide is a synthetic peptide that mimics part of the viral membrane protein gp41 and inhibits fusion with the host cell membrane.[10,20]

Nucleoside/nucleotide reverse transcriptase inhibitors (NRTI/NtRTI respectively) were the first class of ARV drugs to be developed. NRTIs are phosphorylated intracellularly, and are incorporated into the lengthening viral DNA strand. The NRTI either lacks a 3'-OH group or contains a modified group that prevents subsequent addition of nucleotides to the strand, thus preventing all downstream viral action.[13] NRTIs are widely used in treatment cocktails, as they are effective and generally well tolerated.[20] Some of the more common NRTIs used regularly to treat of HIV infection are tenofovir (TFV), emtricitabine (FTC), zidovudine (ZDV) and abacavir (ABC).

Non-nucleoside reverse transcriptase inhibitors (NNRTI), the third class of ARV drugs produced, inhibit viral reverse transcriptase by specific binding to a non-substrate binding site of the enzyme, allosterically inhibiting DNA polymerisation by changing the conformation of the enzyme at its active site.[13,20,21] Efavirenz (EFV) and neviraprine (NVP) are two commonly used NNRTIs.

Integrase inhibitors, such as raltegravir and dolutagravir, are the most recent class of ARVs to be developed.[19] These drugs bind to the enzyme and mimic the DNA substrate/integrase interaction.[14]

Integrase inhibitors are attractive as an ARV treatment as there are no equivalent enzymes found in the host cell, limiting possible side effects.[14]

Protease inhibitors block the viral enzyme by acting as competitive peptidomic inhibitors, mimicking the transition state of the protease catalysis and blocking the binding of viral proteins.[16,18] This class consists of drugs including saquinavir, ritonavir, and lopinavir.

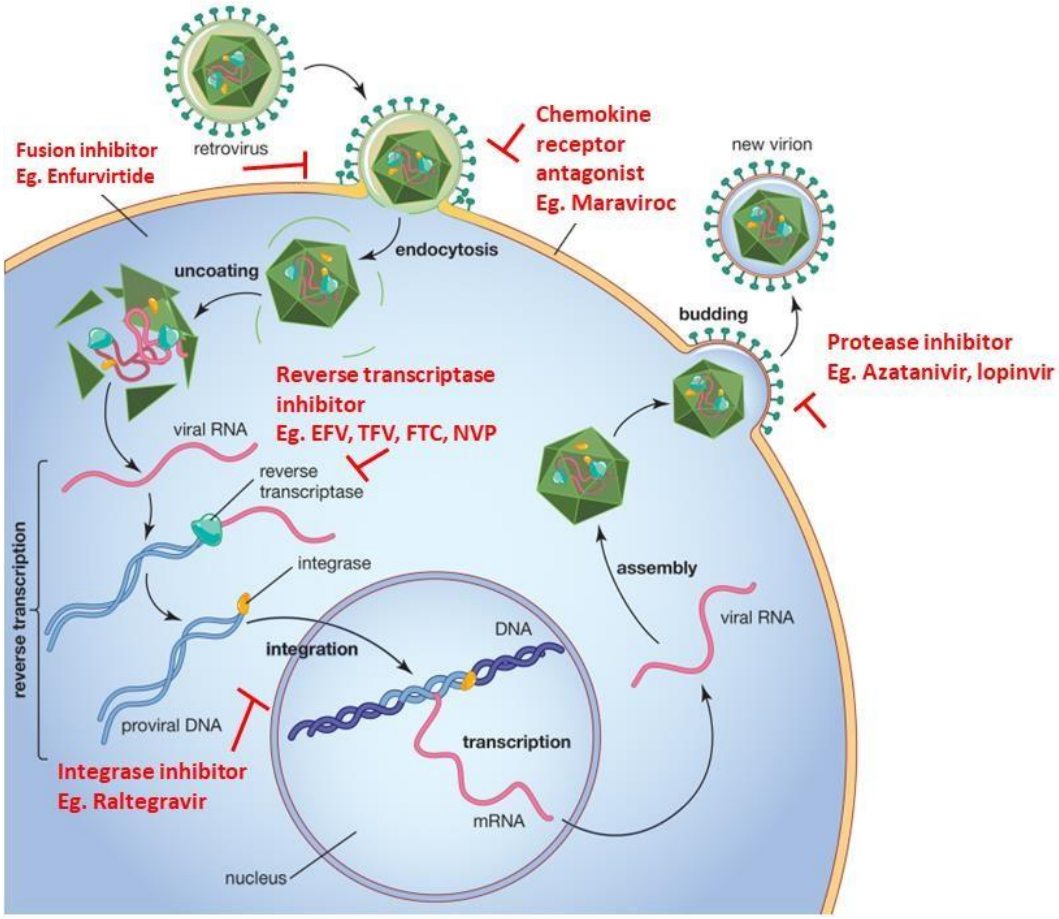

Figure 1.1: Schematic representation of the key points in the life cycle of HIV and the main drug classes that interfere with viral infection and replication. The class of drug as well as specific examples are in red text. The point of disruption is indicated by a red line. Schematic adapted from Encyclopaedia Britannica.[22]

1.3.1 Current ARV treatment recommendations

In 1987 the first NRTI drug, ZDV, was used in monotherapy with great and rapid benefit to patients. It soon became apparent that the virus was developing resistance to the drug, causing virologic failure.[23]

Subsequently, other drugs, such as didanosine and zalcitabine, were used as sequential monotherapies, and eventually as dual NRTI therapies.[19] Although dual therapy was a vast improvement on monotherapy, the timeframe for success was limited. Almost 20 years after the introduction of ARV monotherapy, triple drug therapy regimens were developed, known as highly active anti-retroviral therapy (HAART) or combination therapy.[19] HAART treatment usually consists of one NNRTI and two NRTIs, and is more effective than mono or dual therapy as it targets multiple points of the viral life cycle. HAART decreased the viral load significantly, leading to stalled development of resistance, as well as a drastic increase in survival expectation across all ages.[24–27]

1.3.1.1 Treatment regimen development for low income settings

With strict adherence to a HAART regimen, the viral load can remain undetectable, known as virologic control. An adherence level below 80% leads to virologic failure in up to 87% of patients, and is a major factor contributing to the development of ARV resistant strains of HIV.[28] Combination therapy such as HAART has an increased risk of non-adherence, which is associated with the increased dose frequency and pill count.[29] The risk of non-adherence is also compounded by limited accessibility to health care facilities and resources in low-income settings.[29,30]

In order to minimize side effects and maximize adherence and viral suppression, a fixed dose combination (FDC) pill has been prescribed as a first line treatment in South Africa. This is a single tablet taken once a day, as opposed to multiple tablets taken multiple times in the day. The drugs used in any fixed dose pill have to be carefully selected so as to provide the highest potency and the lowest side effect profile possible. The components of the FDC must be carefully selected as ARV drugs interact not only with other ARVs, but also with anti-tubercular drugs.[31,32] This is particularly pertinent in the South African context as it is estimated that over 60% of HIV infected patients are co-infected with TB, which is the primary cause of death in those with HIV.[33]

1.3.1.2 The constituents of the current first line FDC treatment in South Africa

The South African Department of Health implemented roll-out of an FDC consisting of EFV (600mg), FTC (200 mg), and tenofovir disoproxil fumarate ([TDF] 300 mg), the latter metabolised in the gut into its active form, TFV.[34–36] The combination of these three drugs is the preferred first line treatment currently in use in South Africa.[37]

EFV is a NNRTI that inhibits HIV replication by binding specifically to a non-substrate binding site of the HIV reverse transcriptase.[21,38] EFV has a plasma half-life of roughly 46 hours, and reaches steady state within ten days.[39] In adults, EFV has most commonly been associated with central nervous system (CNS) neuropathy including dizziness, headaches, confusion, stupor, impaired concentration, agitation, amnesia, depersonalization, hallucinations, insomnia, and abnormal or vivid dreams, all of which are generally resolved within a month after treatment commencement.[39–42] Gastrointestinal effects such as nausea, diarrhoea, and vomiting have also been reported.[39] Clinical manifestations of EFV toxicity have been well documented in adults in relatively short term studies, and in recent years there has been more focus on the cellular and molecular effects of EFV.

FTC is an NRTI analogue of the nucleoside cytidine. When the analogue enters the nucleus, it is phosphorylated and incorporated by the viral reverse transcriptase. Once incorporated, elongation is prohibited as the analogues lack a 3'-OH group and/or contain a modified sugar moiety, both of which block the addition of another nucleotide.[13,43] FTC has a serum half-life of roughly ten hours, although its intracellular half-life can be as long as 39 hours.[42] Toxicity from FTC is uncommon and it is generally well tolerated. Side effects include hyperpigmentation, headaches, rash, and gastrointestinal upset.[42]

TFV is an acyclic nucleotide diester analogue of deoxyadenosine 5'-monophosphate, lacking the 3'-OH group, preventing phosphodiester linkage that is essential for DNA chain elongation.[13,42] TFV has a serum half-life of roughly 15 hours and a low toxicity profile, with side effects such as gastrointestinal upset, nausea, abdominal pain, and dizziness.[42] TFV is recommended as treatment for patients who are co-infected with hepatitis B virus and HIV, and the combination of FTC and TFV is recommended as a preventative prophylaxis treatment for HIV.[38,44]

1.3.1.3 ARV drug interactions

When drugs are used in combination, there are three potential interaction effects. The non-interaction of drugs (as described by the Bliss independence model[45]) is known as an additive effect, whereby each drug achieves the individual pharmacological effect, without influencing the other. Non-interaction can be likened to the null hypothesis or the baseline of the drugs interaction. A deviation from the baseline, where the combined effect of two drugs results in a reduced response than that of each drug individually, is known as an antagonistic effect.[45] This can either be in terms of the desired response, such as pathogen death, or an undesired response such as a negative side effect for the patient. Antagonistic drugs can be useful to minimise negative side effects, as long as other drugs are used to maintain the desired responses such as pathogen death. When two drugs result in a greater response than that of each individual drug, it is known as a synergistic effect. This is highly desirable in many drug treatments as it allows for a lower dosage of drugs to be administered while still achieving high efficacy. At the same time, lower doses of drugs may result in fewer adverse side effects. Drug interactions influence the selection of the constituents of ARV FDC regimens.

NRTIs, such as ZDV or FTC, are transported across the host cell membrane and phosphorylated to become metabolically active nucleotides lacking a 3'-OH group, thus causing termination of elongation by the viral reverse transcriptase. Viral resistance to NRTIs occurs when the reverse transcriptase catalyses ATP to act as a nucleophile that is able to remove chain terminating analogues, thus allowing transcription to continue.[46] NNRTIs such as EFV, which bind allosterically to reverse transcriptase, are able to inhibit ATP catalysis of nucleotide analogue removal, thus decreasing the rate of acquiring resistance.[46] Based on this synergistic action, NRTIs and NNRTIs are recommended to be used in combination. The first line FDC regimen in South Africa contains one NNRTI (EFV), one NRTI (FTC), and one NtRTI (TFV). In combination, both FTC and TFV increase in intracellular concentration. This may be as a result of a decrease in the efflux of the drugs via the ABCC transporters, as ABC transporter functionality decreases in the presence of all three drugs.[47] EFV concentration is not affected by the combined administration, possibly due to the ability of EFV to induce its own metabolism, minimising the effect of the ABCC decrease in functionality.[47,48] According to most opinions, the FDC regimen is safe for use by HIV infected adults. The side effects caused by FTC and TFV are minimal, although there have been reports of up to 50% of patients on EFV containing regimens developing CNS-related side effects.[49–51]

1.4 ARVs and the CNS

During HIV infection the CNS, specifically the brain, is the second most frequently infected organ following the lungs, and is thought to be a primary infection site of the HI-virus.[52,53] The virus infects microglia and astrocytes and can remain within these cells in a latent state, acting as a reservoir of infection, unaffected by many current ARVs in use. [53–56] Infection of the CNS can result in a range of neurological complications classified as HIV associated neurocognitive disorder (HAND) that includes asymptomatic neurocognitive impairment (ANI), mild neurocognitive disorder (MND), and HIV associated dementia (HAD).[57]

While the introduction of ARVs has resulted in a 40-50% decline in the incidence of severe HAD cases, there has been little to no improvement in the reported incidence of milder forms of HAND, indicating that new patients are still presenting with HIV related CNS disease, even with treatment and virologic control.[57,58] Low level viral replication in the CNS or immune activation triggered by HIV infection may be responsible for continual HAND emergence, necessitating ARVs with a higher CNS penetrance.[59] ARVs themselves may contribute to the mild forms of HAND, as the nature of HAND has somewhat changed in the ARV era. For example, although HAD is much less frequently diagnosed, it is now observed in patients with less severe immunosuppression than previously seen, as well as in patients with lower viral loads.[60] Before the ARV treatment era, HAND affected mostly motor skills, cognitive speed, and verbal fluency. Post ARV era, memory, learning skills, and executive function are the most noticeably impaired neurocognitive areas.[61] The subtle change in the nature of HAND and the change in relevant biomarkers for HAND has brought the safety profiles of certain ARV drugs into question.[61] ARV treatment greatly decreases the risk of HAD, but it is important to investigate the long-term side effects of the drugs as the lifespan of those living with HIV, and thus lifetime usage of the drugs, increases.

The three constituents of the FDC (EFV, FTC, and TFV) are able to cross into the CNS to some extent.[34,62,63] EFV is strongly recommended for use in first-line treatment by the World Health Organisation (WHO) due to its high potency and ability to cross the blood brain barrier (BBB).[64] Reaching approximately 1% of the plasma concentration in the cerebrospinal fluid (CSF), it is still well above the 50% inhibitory concentration of EFV on the wild type virus.[62,65] EFV is therefore a useful agent in reducing the viral load in the CNS in order to prevent the development of HAD, as well as reducing the risk of a latent reservoir of HIV forming in the CNS. Aside from the necessary benefits of EFV with regards to systemic viral suppression and CNS viral suppression, EFV is notorious for having strong CNS-related side effects. Despite neurocognitive side effects presenting in up to 50% of those administered

EFV as a constituent of HAART,[51] the FDC containing EFV is still recommended as a first line treatment for all patients, including pregnant women. In order to minimise the risk of mother to child transmission (MTCT) of HIV, pregnant, HIV-positive women receive priority treatment regardless of their CD4+ cell count and stage of pregnancy. The treatment with this often toxic drug during critical stages of foetal development necessitates investigation into the effects of EFV during pregnancy, and specifically during foetal neurogenesis.

1.5 ARV treatment in vulnerable populations: pregnant mothers and foetuses

The chance of MTCT of HIV is between 25-35%, which can be lowered to approximately 2% with ARV treatment.[66] With an estimated 30% of women of child-bearing age infected with HIV in South Africa, pregnant women infected with HIV are considered priority patients in the roll out of the FDC, regardless of their CD4+ cell count, clinical staging, or the gestational age of pregnancy.[1,67,68] Children who contract HIV through vertical transmission, either during pregnancy, childbirth, or breastfeeding, have a very low survival rate, with close to 50% mortality in the first two years of life.[69] It is therefore imperative to minimise vertical transmission with ARV treatment.

Due to pregnant women and children generally being excluded from drug trials, animal models were used to create an initial preclinical safety profile for treatment with ARV drugs. The generalizability of these models to human populations is questionable,[70] and thus there is still a need for deeper insights into the effects of the FDC drugs on during the development and neurogenesis of foetuses.

1.5.1 The safety profile of the FDC during pregnancy

The three constituents of the FDC are able to cross the placenta, which has the desirable effect of reducing viral load in the mother and the foetus, allowing the infant to be born HIV-negative.[35,71–74] Literature regarding the effects of these drugs on infants exposed *in utero* is limited, but in recent years there have been increasing numbers of retrospective and prospective studies investigating the effects of *in utero* exposure to ARVs, and whether exposure increases the risk of birth defects. Findings are mixed and generally not definitive regarding the safety of the drugs during pregnancy and each study highlights the need for larger cohorts, longer follow up periods, and standardized testing. In infant populations exposed *in utero*, the FDC consisting of TFV, FTC, and EFV has the lowest risk for birth defects when compared to other drug combinations,[75] although the risk of pre-term birth and stillbirth is significantly higher in infants exposed to the FDC compared to unexposed infants.[76]

1.5.2 The safety profile of EFV during pregnancy

Of the three FDC drugs, EFV has the most thoroughly documented and severe side effects in adults. EFV is classified as a category D drug for use in pregnancy, which indicates positive evidence of risk to the foetus.[77] Case studies have reported increased risks of myelomeningocele and encephalocoele after EFV exposure in the first trimester,[78–81] but the benefit of the drug outweighs the potential risk, and for this reason, EFV was initially recommended for pregnant women only after the first trimester as a foetus is most vulnerable to teratogens during organogenesis at this time. NVP was initially used as the first trimester NNRTI instead of EFV, but it was found that women on NVP had consistently higher viral loads and that NVP interacts with rifampicin, a first line treatment for TB.[82] Women treated with EFV and unaware of the pregnancy for the first six weeks did not have a significantly increased risk of birth defects, and as a result, in 2012 pregnant women in lower income countries such as South Africa were recommended to take EFV as a first line treatment, regardless of the stage of pregnancy.[64,82] Subsequently, there were multiple reports of first trimester exposure to EFV causing an increase in negative pregnancy outcomes, including neurological defects.[81,83,84] The risk was further elevated when including elective termination of pregnancy due to observed neurological defects.[85] Foetuses exposed to EFV were also found to have elevated lactate levels, indicating mitochondrial dysfunction, which has been linked to neuropathy.[58,86–89]

The use of EFV during pregnancy remains controversial, as the increased risk is often small, and there are too few cohort studies of adequate size to draw any concrete conclusions. Neurological defects in the general population are rare, and therefore larger sample sizes are needed to detect increased risk in EFV exposed populations. For this reason, a small increase in observed neurological defects in EFV-exposed populations, even if insignificant, is still noteworthy. The safety of EFV during pregnancy and the neurological risk it poses can therefore neither be confirmed nor refuted currently.[90–92]

1.5.3 The conflicting evidence regarding long term effects of *in utero EFV* exposure

The great success of the WHO in decreasing MTCT has been invaluable to the millions of children born to HIV-positive mothers.[66] As a result, there are many children who have been exposed to both the HI-virus and ARV drugs *in utero,* as well as HIV prophylaxis treatment post-partum. This increasing population therefore needs to be better understood as they face many challenges, such as living with HIV positive caregivers, increased risk of illness, and potential risk of exposure to both the virus and the drugs during foetal and postnatal development.[93] The first 1000 days of neural development, from conception to approximately two years old, are vital. Exposure to toxic stress can affect different areas of the brain, depending on which point during development the exposure occurred.[94] During the critical periods of development, damage in a particular area may be irreversible, while exposure during the sensitive period may not be deterministic.[94] The impact of toxic drugs might only manifest later in life, when the exposed children begin to participate in more complex tasks relating to cognitive function such as reading, concept learning, critical thinking, and problem solving.[95,96]

With the increasing population of HIV exposed, uninfected (HEU) children there is a need to gain a deeper understanding of the long term effects of *in utero* exposure to both the virus and the ARV drugs. The majority of the literature focusses on congenital abnormalities, with some emphasis on neurological defects. When investigating the long term effects of exposure, there are conflicting results, with some studies indicating no increased risk of any long term neurological deficit, while others show an increased risk. Due to the recent introduction of the FDC as a first line treatment for treating HIV in pregnant women, the majority of long-term studies include drugs such as ZDV, lamivudine (3TC), and NVP, with few studies including EFV.

1.5.3.1 The HEU child

Upon investigation of the long-term effects of ARV exposure *in utero*, multiple studies found that children exposed to ARV drugs *in utero* experienced neurological deficits when compared to peers that were not exposed. Although these deficits were correlated to ARV exposure after sensitivity analysis, there was generally no link to any specific drug.[97–99] HEU children had deficits in language-related tasks such as delayed language emergence or lower scores in reading skills. [86,96,99–102] HEU children also had motor developmental delays[95,103] as well as scores in cognitive ability,[98,104] executive function levels,[105]

and mathematical ability[106] slightly below those of their unexposed peers. Elevated lactate levels, indicative of mitochondrial dysfunction and linked to *in utero* ARV exposure,[97,103,107] have been associated with neurological dysfunctions including behavioural problems.[97,107] The deficits in neurocognitive function caused by mitochondrial dysfunction can be supported by findings in a primate model, which found that primates exposed to an NRTI regimen *in utero* and for an additional six weeks postnatally had accumulative mitochondrial damage in the brain cortex when assessed at one year after birth.[10] In contrast to the aforementioned findings, there are reports that claim that there is no correlation between *in utero* ARV exposure and long term neurodevelopmental risks. The biochemical profile and gross structure of the brains of HEU children and their non-exposed peers were the same between the ages of five and ten years old, indicating that HEU children have typical brain development.[109] This study only included HEU children who had no CNS-related disorders or dysmorphic syndromes, excluding the population of HEU children suffering from CNS disorders potentially caused by ARV exposure. In America, the majority of drug regimens in longitudinal studies contained ZDV or 3TC, and there was no statistically significant difference between HEU and their unexposed peers in neurological development.[98,110] These studies were all performed in high income countries and lacked appropriate control groups. Often the HEU group was from lower income communities and thus lower cognitive scores or mental health problems were attributed to socioeconomic background and caregiver health.[111]

When compared to similar studies performed in Africa, it was found that the HEU children had poorer outcomes than those predicted for HEU children in high income settings.[95] The distinction in long term exposure effects between high and low income settings highlights the need for early intervention to mitigate potential negative effects of *in utero* ARV exposure, as early intervention has been shown to improve cognitive functioning of affected children.[112]

Although there has been an increase in interest in HEU children specifically in Africa, there are many contradictory findings and methodological shortcomings. A study performed in Zambia reported no difference in language and cognitive development in HEU and unexposed children.[113] In this study, children up to two years of age were assessed, excluding detection of developmental deficits that would only become apparent at a later age when performing more complex tasks. The standardized Capute Scales Clinical Adaptive Test/Clinical Linguistic and Auditory Milestone Scale testing that was used in this study is unable to detect specific cognitive or language delays in children and as a result the study was unable to rule out the possibility of cognitive or language delays in HEU children.[113] In South Africa similar results indicated that HEU children had no cognitive developmental deficits when compared to

their unexposed peers. This study had major confounding factors, whereby the control group was mostly comprised of children from Afrikaans population groups, while the HEU group was mostly Xhosa.[114] The control group surprisingly had a higher rate of maternal substance abuse, and subsequently, a higher rate of growth stunting, which has been shown to delay neurodevelopment.[115] It is possible that the control group was not representative of a population mean, confounding the results. In contrast to these findings, in the Democratic Republic of Congo, HEU children were found to have lower cognitive scores than the control group, although this was attributed to HIV-positive status of the caregivers as well as poor living conditions.[116]

Most longitudinal studies are unable to either confirm or deny the safety of ARV usage in pregnancy due to confounding factors. Even more concerning is the lack of data regarding the use of EFV in pregnancy, as it is a first line treatment in South Africa. The question remains whether the potential increased risk of aberrant neurodevelopment in HEU children is as a result of exposure to ARVs *in utero,* and specifically EFV, which is known to cause seizures, aggressive behaviour, ataxia, tremors, and cerebellar dysfunction in children,[117,118] and other CNS symptoms in adults. In order to create early interventions for the growing population of HEU children, a deeper understanding of the mechanisms by which EFV can affect the developing neural system needs to be attained. Seemingly minor alterations in the neurocognitive functions on an individual level can have a large impact on public health, indicating a need to address the potential long term side effects of *in utero* EFV exposure. The present study aims to investigate the biochemical effects of EFV at a cellular level, using human derived foetal neuroepithelial stem (NES) cells as a model for EFV exposure during early development. Understanding the effects of EFV at the molecular level may provide compelling pre-clinical evidence to emphasize the importance of further research in order to provide optimal protection for both the mother and the foetus from HIV, as well as for the long-term health and development of the neural system.

1.6 Cell culture as a means to investigate molecular effects of EFV on developing neurons

Several studies attempting to elucidate the effects of ARVs on the CNS have used methodologies including cohort studies, animal models, and cell culture models. In most cases, cohort studies contain many confounding factors which limit the ability to draw conclusions. Animal models allow for more controlled studies, although their applicability to human settings has been questioned as there are reports of only 2-3% of animal teratogens having the same effect in humans.[70,119] Cell culture models are the easiest to control and offer insights into the molecular mechanisms of ARVs and their side effects. By building a solid foundation of understanding at the cellular level, further studies can be more targeted and precise. Previous cell culture models attempting to elucidate the effects of ARVs on the neural system have used either animal neural cells, or human non-neural cell lines.[120–122] Transformed human neural cell lines such as neuroblastoma (SHSY-5Y) have been used, but are also not necessarily representative of the functioning of primary neuronal tissue.

Non-transformed, human-derived NES cells have been isolated from the hind brain of a five week old foetus and successfully passaged up to 100 times while maintaining genetic stability.[123] These proliferating neuroepithelial cells spontaneously form rosettes that are responsive to patterning signals and are the sole cell type found in developing neural tubes.[124] Upon removal of various growth factors such as EGF and FGF, the NES cells are able to spontaneously differentiate into an almost pure population of synaptically active neurons *in vitro,* forming elaborate neural networks within four weeks from growth factor removal.[123,125] The NES cell line can act as a model that represents early neural tube development, the neurogenesis process, and a pure population of neurons *in vitro*.[123,124] The NES cells thus provide a model that allows for a deeper insight into the molecular effects of EFV on the developing neural system. This model can be used to assess global cellular molecular changes during early neural development, as well as in mature neuronal populations. The effects of EFV at the molecular level can be used in conjunction with cohort and animal studies to further the understanding of the effects of EFV on the developing neural system in this growing population of infants exposed to ARVs *in utero*.

1.6.1 Using proteomics to investigate global cellular changes

Traditionally, biological research followed a reductionist approach, where one component of a system was examined and its function described. This approach lacks the ability to describe the complex pluralistic nature of cause and effect in a biological system. Systems biology offers a more holistic approach, by observing the system and its interactions as a whole. The term "omics" is often used to describe the network under observation. Genomics, the most well-known approach to systems biology, is considered to be the blueprint of an organism and offers many insights to the makeup of different organisms. Proteins can be likened to the building blocks or the functional aspect of the genome. Genes are translated into proteins which can then be modified to suit the immediate needs of the organism or cell, thus the snapshot in time provided by observing cell wide protein changes, known as the proteome, gives a clearer indication of the cellular response to the environment.

1.7 Mass spectrometry for proteome analysis

Mass spectrometry (MS) has been a cornerstone in the advancement of proteomics, allowing thousands of proteins to be identified in a single experiment. Experiments can be approached in a top-down or bottom-up workflow, which involves the analysis of whole, intact proteins, or digested peptides, respectively. Smaller peptides are preferred for MS analysis over whole proteins, as peptides have a higher ionisation and fragmentation efficiency than the larger proteins.[126,127] In order to prepare peptide samples for MS analysis, proteins from cell lysate or tissues are precipitated and digested, and the peptides are suspended in an organic solvent such as an acetonitrile (ACN)/water mixture. The acquisition of MS data from the peptide mixture can then be performed in discovery or targeted mode. Discovery, or shotgun, proteomics is a hypothesis generating investigation which identifies and quantifies several thousand proteins from a complex mixture of proteins. Targeted experiments can be used to validate hypotheses generated from discovery data or to search for a predetermined list of proteins by setting the MS experiment to detect peptides of specified retention times or masses. MS experiments can be performed on various instruments, each with advantages and disadvantages, and commonly used instruments or techniques will be discussed in more detail. A typical MS workflow for cell culture shotgun proteomics is illustrated below (Figure 1.2).

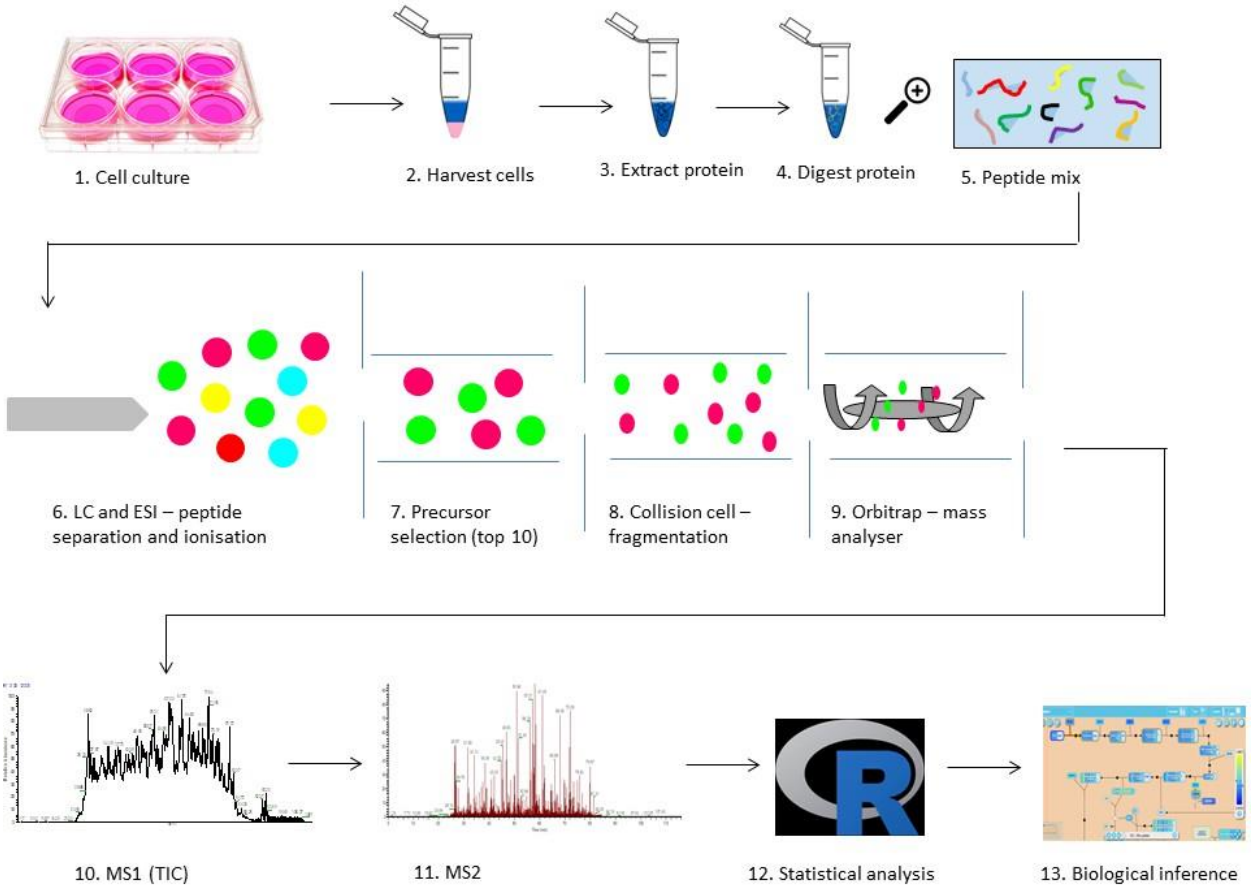

Figure 1.2: Schematic representation of a typical MS workflow. **1)** A treatment and control condition are prepared. **2)** Cells are harvested, frozen with liquid nitrogen, and stored until needed for further processing. **3)** Cell pellets are lysed, and proteins are extracted via protein precipitation methods. **4)** Proteins are digested over night with trypsin. **5)** The peptides are desalted and suspended in 2% ACN. **6)** The peptide mixture is separated by liquid chromatography (LC) based on hydrophobicity. As the peptides reach the charged emitter tip they are ionised by electrospray ionisation (ESI). **7)** Ionised peptides flow through the MS into the first quadrupole where the precursor ions are selected, generally by data dependent "top 10" precursor selection. **8)** In a precursor scan (MS1), precursor ions are transferred to the C-trap, and then analysed on the Orbitrap. In a product ion scan (MS2), selected precursor ions travel via the C-trap into a collision cell where fragmentation of the ions occurs. **9)** The Orbitrap mass analyser uses an electrostatic field and the frequency of the ion oscillation to determine the mass to charge ratio. **10)** An MS1 chromatogram is generated by the detection of precursor ions. **11)** An MS2 chromatogram is generated by the detection of fragmented product ions. **12)** Statistical analysis is performed with software such as R, Perseus, and Excel to determine significance of differences observed in the data. **13)** Enrichment and pathway analysis is performed in order to assess the relevance of the observed proteome differences.

1.7.1 Liquid chromatography

Prior to analysis by MS, the complexity of the peptide mixture is reduced to ensure the detection of the majority of the peptides. The pre-fractionation of peptide samples results in fewer peptides reaching the ion source of the MS at any given time. This prevents competition for charge that results in the lower abundance peptides being masked by the highly abundant peptides. MS instruments have limited dynamic range, and thus by decreasing sample complexity with liquid chromatography (LC), the sensitivity of the experiment is increased and very low abundance peptides are more likely to be detected.

High performance LC (HPLC) is commonly used in proteomics and offers higher resolution than regular LC. A hydrophobic stationary phase (reverse phase) consisting of c18 silica beads is packed into a column, and a mobile phase containing water, an ion pairing agent (usually formic acid [FA]), and organic solvent is able to flow through the column. Strongly hydrophobic peptides adsorb to the stationary phase, while less hydrophobic peptides are eluted. An increasing gradient of non-polar solvent, generally ACN or methanol, causes increasingly hydrophobic peptides to elute into the ion source.[126,128]

1.7.2 Ion Sources

Typically, an MS instrument consists of an ion source, a mass analyser, and a detector. To be detected by the mass analyser, analytes are first ionised by the ion source. The development of soft ionisation techniques enabled the ionisation of non-volatile and thermolabile compounds, such as peptides (or biological macromolecules), with minimal fragmentation. Matrix assisted laser desorption/ionisation (MALDI) and electrospray ionisation (ESI) are most commonly used as ionisation techniques for MS and can both be coupled to LC systems.

1.7.2.1 MALDI

Samples are co-crystallised in a matrix made up of small organic molecules, which serve to absorb energy from a laser pulse, as well as ionise the analyte in question. MALDI is especially useful for simple samples, mass fingerprinting, and analysis of proteins *in situ*, as whole tissue sections can be coated with matrix, which allows for spatial distribution within a sample to be maintained.[129,130] MALDI generally produces singly charged peptides, which results in fewer fragmented ions than ESI.[126]

1.7.2.2 ESI

Peptides in solution are passed through a charged metal capillary tip, where positive and negative charges are separated, forming a charged Taylor cone which extends into a liquid filament. The filament is unstable and breaks off into charged droplets - the charge depending on the ionisation mode of the capillary. A neutral gas, such as nitrogen, can be continually pumped around the capillary, causing solvent evaporation. As the solvent evaporates, the surface area of the droplet shrinks, and the Columbic repulsion between charges eventually overcomes the surface tension cohesive force (the Rayleigh limit), causing Columbic fission and the formation of smaller droplets.[131,132] This process repeats until a single gas phase ion is produced. The exact mechanism by which this happens is unknown, although three models have been proposed.[133] The ion evaporation model suggests that the decreasing size of the droplet and the increasing field strength causes the charged ion to be ejected into the gas phase. The charge residue model suggests that eventually, each droplet contains a single charged ion, and once the solvent completely evaporates, the charged ion remains in the gas phase.[131,134] The chain ejection model suggests that in solution, polymer chains may become disordered, with more hydrophobic sections becoming exposed to the solvent. This in turn causes ejection from the solvent droplet, as the interior of the droplet is unfavourable for hydrophobic polypeptide chains.[133] Once the ion is in the gas phase, it is detected by the mass analyser.

1.7.3 Mass analysers

There are four mass analysers currently used in proteomics. Time of flight (TOF) analysers simply record the amount of time taken for the analyte to travel across the flight tube. An analyte with a larger mass to charge ratio (m/z) will take longer to traverse the flight tube. TOF instruments are often coupled to a MALDI ion source, and can be placed in tandem with a collision cell between them.[135,136] Fourier transform ion cyclotron resonance (FT-ICR) analysers trap ions with magnetic fields and use cyclotron resonance to detect the ions.[135] Quadrupole mass analysers consist of four metal rods which create an electric field by means of radio frequency and direct current which alters the flight of the ions through the quadrupole. Quadrupoles can be placed in tandem, with the first acting as a mass filter, the second acting as a collision cell, and the third acting as another mass filter.[137] An ion trap, such as the Orbitrap, uses static electrostatic fields to trap ions. The ions oscillate around the central electrode of the Orbitrap at a frequency related to the m/z value of each ion. A Fourier transform algorithm is used to accurately convert the time/domain signal into the m/z value.[138,139] The Orbitrap comes with a large trapping volume, high mass accuracy, a large dynamic range, and a high m/z range. The Orbitrap is both a mass analyser and a detector, while other mass analysers will be coupled to detectors such as electron multipliers to increase the signal detected.

1.7.3.1 Tandem MS

As the peptide mixture elutes and flows through the MS, charged ions (subsequently referred to as precursor ions) are detected by the mass analyser. The m/z values of each precursor ion are plotted on a chromatogram (MS1). The intensity value on the y-axis represents the relative quantity of the peptide eluting at a specific retention time. All plotted MS1 scans make up a total ion chromatogram (TIC). The Q-Exactive instrument contains a C-trap in which precursor ions are stored and subsequently transferred and analysed in the Orbitrap, creating the MS1 chromatogram. In discovery MS, ten or 20 of the precursor ions with the highest intensity are transferred via the C-trap and enter a collision chamber where they interact with a gas, often nitrogen, which causes collision induced dissociation (CID). The resultant ions are referred to as product ions, which are then transferred back into the C-trap, followed by analysis in the Orbitrap.[140,141] Higher energy collisional dissociation (HCD) is common in Obritrap instruments, and results in a wide range of fragmentation patterns and high quality product ion spectra (MS2).[138,142] In order to prevent the same highly abundant precursor ions from being fragmented constantly, dynamic exclusion essentially ignores already seen parent ions for a small window in time. Fragmentation along the peptide backbone occurs and the dissociated product ions are detected by the

mass analyser, creating the MS2 spectra.[143] When fragmented, the charge either remains on the N-terminus (b-ion) or on the C-terminus (y-ion). Adjacent fragments differ by the mass of an amino acid and can thus be used to identify the peptide sequence.[135,143]

1.7.4 Protein quantitation with MS analysis

In addition to protein identification, MS is an indispensable tool for protein quantitation. Relative or absolute quantitation can be assessed depending on the experimental design and sample preparation.

1.7.4.1 Isotope labelling

Stable isotope labelling is considered the gold standard for protein quantitation, with many different types of labels, each with their own advantages and disadvantages.[144,145] There are two broad categories for isotope labelling, namely, pre- and post-harvest.

Pre-harvest labelling occurs when metabolically active cells incorporate isotopic labels during protein synthesis. This allows the samples to be mixed together once they have been harvested, eliminating much of the variation due to sample processing. Stable isotope labelling by amino acids in cell culture (SILAC) uses media containing either heavy or light amino acids that become incorporated into each new synthesised protein. The heavy amino acids cause a mass shift, allowing for relative quantitation of the two conditions.[145,146] Major drawbacks of SILAC are that it cannot be used to label primary tissues and few conditions can be studied at one time. Post-harvest tagging, such as isobaric tagging, overcomes these issues and can be used to tag tissue samples, as well as multiplexing the number of samples analysed. Isobaric tags for absolute and relative quantification (iTRAQ) react with peptides via a peptide reactive group.[147] The tag consists of a reporter and a balancer group, which ensures that the relative mass increase for each peptide is equivalent, and thus differentially tagged peptides appear initially as a single peak, reducing complexity. In MS2, the relative abundance of the reporter ion is proportional to the relative abundance of the peptide in each sample, allowing for relative quantitation between samples. iTRAQ is a reliable method for relative protein quantitation, although it is limited to only eight different tags.[145]

1.7.4.2 Label free quantitation

With recent advances in MS and LC performance, such as nano-electrospray, label free quantitation (LFQ) has become an increasingly popular method of quantitation.[148,149] Higher mass resolution and peptide identification rates increase the number of data points available for pairing corresponding peptides across samples, improving the quality of LFQ.[150] By using LFQ, it is possible to obtain an unlimited number of "snapshots" of the proteome, making LFQ attractive for time course analyses or characterisation of an entire proteome, as the number of samples is not limited to the number of tags.[151] LFQ is the most economical and simple method used for MS analysis and is able to achieve quantitation equivalent to SILAC labelling.[150] LQF uses either spectral counting or peak intensity to quantify peptides. If a peptide is more abundant, there will be more MS2 spectra detected, which allows for simultaneous protein identification and quantitation by MS2 data collection. The more highly abundant peptides in a sample are thus favoured in spectral counting. Another drawback of spectral counting is that poor quality data can lead to inaccurate protein identification and thus inaccurate quantitation.[151]

Extracted ion chromatograms (XICs) are another means of performing LFQ, and use the area under the curve (AUC) of the peak corresponding to the peptide as a surrogate for peptide quantity, as peak intensity increases linearly with peptide abundance.[152] Intensity measurements can distinguish between peptides with a similar mass but a different amino acid sequence, which minimises false positive identification, thus improving accurate protein quantitation.[151] Quantitation by XICs has also shown superior performance to spectral counting, especially in the case of low abundance peptides.[150]

1.8 Data analysis

1.8.1 MaxQuant

A shotgun MS experiment typically generates large amounts of raw data, presenting a challenge for data analysis. Software packages such as MaxQuant have been specifically developed for high accuracy quantitation and identification of shotgun MS data.[153,154] MS1 spectra consist of information regarding the peptide mass and the intensity, while the MS2 spectra are used to identify the peptide by matching the fragment spectrum against a database. Andromeda, the search engine integrated into the MaxQuant workflow, scores peptide-spectrum matches (PSM) based on probability calculations.[155] Each PSM is tested against a decoy database and assigned with a posterior error probability (PEP) score that represents the probability of error for that particular PSM. The false discovery rate (FDR) determines the error rate associated with the collection of all PSMs. The PEP and FDR scores ensure that false positive PSMs are minimised.[156] The MaxQuant workflow was originally designed for analysis of SILAC raw data,[153] but with the recent increase in the number of LFQ experiments, a MaxQuantLFQ algorithm specifically designed to handle LFQ data has been integrated into the workflow and is recommended for use in comparative shotgun proteomics.[150,157]

1.8.2 Skyline

Skyline is software that can be used to develop and analyse targeted MS experiments.[158,159] During method development, peptides belonging to proteins of interest can be empirically detected via a shotgun experiment, or can be created *in silico* by Skyline. Collision energy (CE) ramping is integrated into the Skyline method development pipeline to ensure target peptides with the highest intensity are detected.[158] Raw data are imported back into Skyline for processing, whereby each product ion is grouped with the precursor ion and stored graphically.[159] The best peak for each peptide will be picked by Skyline based on various parameters, such as log intensity, identified count, library intensity score, co-elution count, shape score, and weighted co-elution.[158] Quantitation is assessed by the AUC for each product ion, and the total area is related to the precursor ion. The intensity and the interference for each product ion can be individually inspected in Skyline.[158–160]

1.8.3 Statistical analysis and biological inference

Outputs from MaxQuant and Skyline can be easily exported to R, Perseus, or Microsoft Excel software for further statistical analysis. The intensity values are used as a proxy for the relative abundance of each peptide and statistical testing can then be performed to evaluate the relative protein expression between samples.[152] In differential proteomics, a Student's t-test is considered the best test for significance when there are three or more replicates per group.[150,161]

Peptides are assigned to protein groups rather than individual proteins, as this takes protein isoforms as well as peptide redundancy in certain proteins into account. Thus further analysis is based on protein groups that are identified by a set or subset of peptides as opposed to specific individual proteins. A list of statistically significant differentially expressed protein groups can then be interrogated further using various bioinformatics workflows available. Data bases such as Panther, StringDB, Reactome, and GSEA are curated protein function databases that can be used to infer interactions between differentially expressed protein groups, which can result in a deeper understanding of the biological significance of the condition tested.

1.9 Aims and objectives

Due to the severity of the HIV epidemic, the approval of ARV drugs was initially accelerated, without full knowledge of the long term side effects.[162,163] CNS side effects caused by EFV in adults are well documented but due to pregnant women and children generally being excluded from clinical trials, there remains a gap in the knowledge of how EFV exposure affects the developing neural system of children exposed *in utero*. This study aims to characterise the proteomic cell wide changes caused by EFV in proliferating NES cells at biologically relevant concentrations. Based on the literature reviewed, it seems reasonable to hypothesise that EFV may cause perturbations in the proteome of neural stem cells in vitro, ultimately affecting neural differentiation and development in vivo.

Aim 1: Understand the movement and degradation of EFV in cell culture using small molecule targeted MS.

Objectives 1:

a) Optimise the detection of EFV on the Vantage Triple-Stage quadrupole (TSQ) with different solvents such as ACN, methanol and dimethyl sulphoxide (DMSO).

b) Develop a targeted MS experiment to detect EFV, optimising gradient elution, CE, and ensuring reproducible results.

c) Optimise the extraction of EFV from cell suspension and supernatant using protein precipitation.

d) Assess whether EFV is able to enter NES cells at detectable levels.

e) Assess the degradation of EFV in NES cell culture.

Aim 2: Characterise the global cellular changes in NES cells caused by EFV treatment

Objectives 2:

a) Design a treatment schedule over 72 hours for NES cells based on EFV concentrations over 72 hours as elucidated in aim 1.

b) Investigate cytotoxic effect of EFV in cells using cell counting and cell viability assays.

c) Create a time-course proteomic profile over 72 hours for NES cells treated with EFV using a discovery MS workflow with LFQ on the Q-Exactive.

Chapter 2: Optimisation of the detection of EFV using targeted MS.

2.1 Introduction

Small molecules have a wide range of functions, serving as pharmaceutical drugs, secondary metabolites, pesticides, and signalling molecules. Assays are needed to determine the amount of the small molecule present in a system, their activity, and their cellular location. Most biochemical assays used to detect or quantify small molecules are unable to directly measure the molecule, instead measuring either enzymes or proteins which interact with the molecules, such as immunological or colorimetric assays.[164–166] The small molecule in question may bind to an antibody, an aptamer, or may act in a biochemical reaction, all of which result in a measurable signal that acts as a proxy for the presence and quantity of the small molecule. Immunological and colorimetric assays are generally simple and fast, and minimal training is required. There is no need for specialised, expensive equipment or training to perform these assays, although in some cases, antibodies may be costly for a single experiment.[167] Immunological assays are useful for studies in which the outcome is predicted, but are blind to unexpected biological events.[144]

MS is another way to detect and quantify small molecules by measuring the m/z of the ionized molecule. It is generally accepted that MS has lower limits of detection than immunological assays, and lends itself to high throughput experiments.[168] Another appealing aspect of using MS is that the molecule is being directly measured, as opposed to quantification occurring via a proxy. MS experiments also allows for performance of multiplexed experiments, whereby multiple small molecules can be detected in one experiment at no extra cost, as opposed to needing multiple antibodies and multiple tests.[167] LC coupled to MS separates complex mixtures and allows for higher sensitivity by minimizing interference, which is particularly important in biological samples. Initial method development for drug detection assays can be lengthy and costly, but ultimately allow for automated, high throughput experiments.

Selected reaction monitoring (SRM) is a targeted MS method that is often used in drug detection assays. A triple quadrupole instrument is considered the gold standard for SRM quantitative analysis as it maintains high selectivity in complex samples. The first quadrupole acts as a mass filter, selecting analytes of a specific m/z value from a target list. The second quadrupole acts as a collision cell, fragmenting the selected analytes. The third quadrupole acts as the second mass filter, once again

selecting ions of a pre-specified m/z value.[137] By having two levels of mass filtering within a narrow mass window, high selectivity is achieved as co-eluting ions are effectively filtered out.[137,169]

This chapter describes various optimisation steps taken to confidently identify EFV by SRM analysis. Factors such as drying and reconstitution of EFV, as well as multiple instrument parameters were optimized to ensure high quality data.

2.2 Materials and methods

2.2.1 Optimisation of instrument parameters and detection of EFV by direct infusion.

EFV (99.4% purity) was obtained through the NIH AIDS Reagent Program, Division of AIDS, NIAID, NIH. EFV powder (10 µg) was reconstituted in 50% DMSO (Sigma Aldrich) and diluted by a factor of 100 and 1000 in 2% ACN (HPLC grade, Sigma Aldrich), 0.1% formic acid (FA, Sigma Aldrich). At low concentrations DMSO has been found to improve ionization, specifically for hydrophobic compunds[170,171] such as EFV.[13,172] EFV powder was also reconstituted in 100% ACN, 100% methanol, 50% ACN, and 50% methanol. Each sample was infused directly into the TSQ Vantage Triple-Stage quadrupole (Thermo Scientific) at 2 µl/min with a Hamilton syringe. Source parameters were optimized according to the heated electrospray ionization (HESI) probe manual.[173] The capillary and vaporizer temperatures were set to 360^{o}C and 350^{o}C, respectively. The sheath gas and auxiliary gas were set to 40 and 15, respectively. The spray voltage was set to 3000 V.

2.2.2 Optimisation of EFV ionisation and detection

Sample was loaded onto a 10 cm reverse phase monolithic column (C18 silica-based, pore size 130 Å, Phenomenex) using the Accela 600 auto sampler (Thermo Scientific). The sample was separated over 20 minutes using a standard gradient optimised for separation of peptides in complex mixtures. The mobile phase consisted of solvent A (0.1% FA in HPLC grade water, Sigma Aldrich) and solvent B (0.1% FA in ACN). Solvent B was increased from 2% to 60% over nine minutes, increased to 80% in one minute, followed by a hold at 80% for six minutes. Solvent B was then decreased to 2% in one minute, and held for four minutes to equilibrate the column before the next sample. Ionisation occurred via a heated electrospray ionisation (HESI) probe (HESI-II, Thermo Scientific).

To optimize detection in complex mixtures, a full scan, or parent ion scan, was performed in positive and negative ionization mode.[174–176] Different ionisation modes cause the fragmentation pattern of the molecule to differ, resulting in different product ions, which can improve the sensitivity when identifying the molecule in complex mixture.[177] Changing the ionisation mode could also decrease interference by co-eluting molecules that ionise in one mode only. The TSQ was operated in full scan mode across a scan

range of 10-1500 m/z over 1.5 seconds. EFV in 100% ACN or methanol and in 50% ACN or methanol was injected and analysed with a full scan in both positive and negative mode.

2.2.3 Developing a reliable drug detection assay using SRM

Subsequent to detection of EFV in MS1, as well as the selection of solvent and gradient optimisation, a more selective and sensitive method was created using SRM to improve detection of EFV in complex samples. A product ion scan was performed and the resultant product ions were then verified using known and predicted tandem mass spectrometry (LC-MS/MS) EFV spectra from the human metabolome data base (HMDB).[178] Subsequently, the raw files were imported into Skyline[159] to obtain a product ion target list, which was achieved by selecting the highest ranking ions. Transitions are evaluated by Skyline according to signal intensity and interference.[160] High ranking transitions have high signal intensity and low interference values. Transitions that were ranked poorly or had less than 1 Da mass difference to previously selected transitions were discarded. Once this list was completed, it was exported to the Xcalibur software (Thermo Scientific v2.2) and an SRM method was created to target the selected product ions. In order to increase overall peak area and sensitivity of detection, CE was optimised for each product ion by performing a manual ramping of CE ranging from 10 to 40 volts (V) in increments of 10 V.[179,180] Once the CE for each transition was optimized, a final transition list was generated for future detection assays.

2.2.4 Standard curve of EFV in ACN

Increasing concentrations of EFV from 3.9 ng to 2000 ng was reconstituted in 100% ACN in triplicate. Samples were analysed on the TSQ vantage using the optimised SRM assay in order to assess if the intensity of EFV increased linearly with the concentration. Raw data was imported into Skyline, and total peak area values were exported into GraphPad Prism (v7 for Windows) for statistical analysis and visualisation. Intensity values and concentration values were $\log_2$ transformed for ease of visualisation and a linear regression line was fitted to the graph.

2.3 Results

2.3.1 Optimisation of instrument parameters and detection of EFV by direct infusion.

EFV powder (99.4% purity) was reconstituted in 50% DMSO 10 µg/µl. Stocks were stored at -20^{o}C until needed. When infused onto the TSQ, a 1:100 dilution of 1 µg EFV stock (10 µg/µl) in 2% ACN, 0.1% FA was not detected in positive or negative mode. Polyethylene glycol (PEG), characterised by 44 m/z repeating peaks, was detected in diluted DMSO samples. EFV was detected by infusion when reconstituted in 50% and 100% methanol or ACN. Detection optimisation was subsequently performed using 50% and 100% methanol or ACN (Figure 2.1).

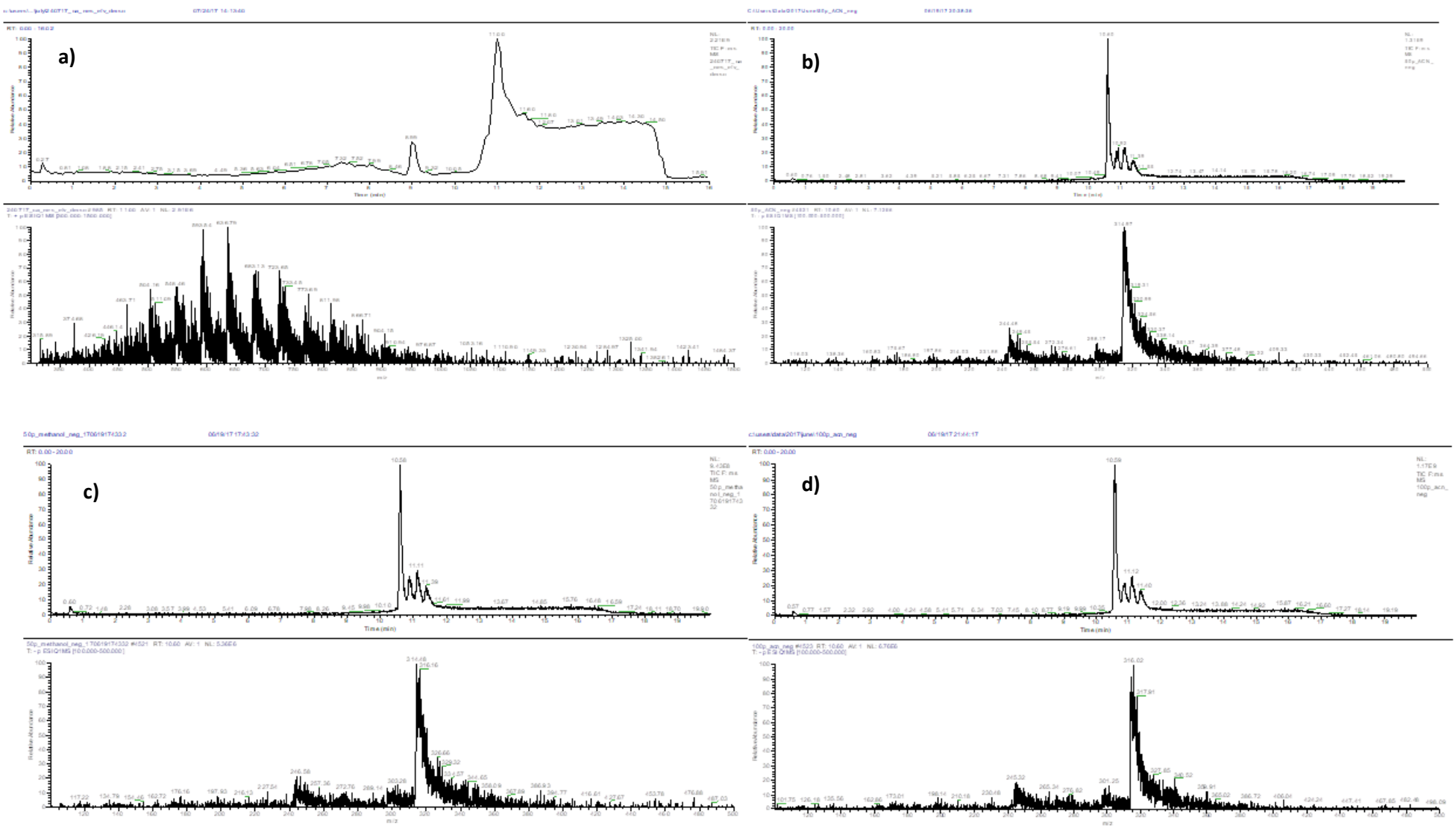

***Figure 2.1: Optimisation of EFV detection in organic solvents*.** Neat EFV was solubilised in **a)** DMSO (50%), diluted in 2% ACN, and 0.1% FA. **b)** Methanol (50%), **c)** ACN (50%), and **d)** ACN (100%). The upper panel represents the total ion count from the infusion. The lower panel represents the mass spectrum, indicating the m/z value of the peaks in the total ion count. The repetitive peaks in a) are Polyethylene glycol (PEG) peaks. EFV was detected in 50% methanol, 100% methanol (not shown), 50% ACN, and 100% ACN.

2.3.2 Optimisation of EFV ionisation and detection

When ionised, a molecule is either protonated (positive mode) or deprotonated (negative mode). The difference in charge results in a mass difference of 2 Da. Neutral EFV has a molecular mass of 315 g/mol, and was detected in negative mode with a m/z value of 314, as expected, as it becomes deprotonated. No EFV peak of 316 m/z was detected in positive mode when solubilised in either concentration of methanol or ACN (Figure 2.2). In negative mode, the intensity of the EFV peak did not differ significantly when reconstituted in 100% or 50% methanol or ACN. The average intensity value of the EFV peak in 50% methanol was 8.19 $x10^8$ and 1.24 $x10^9$ in 50% ACN, although the ACN samples had a slightly higher average intensity the difference was not statistically significant ($p = 0.061$) (Figure 2.3).

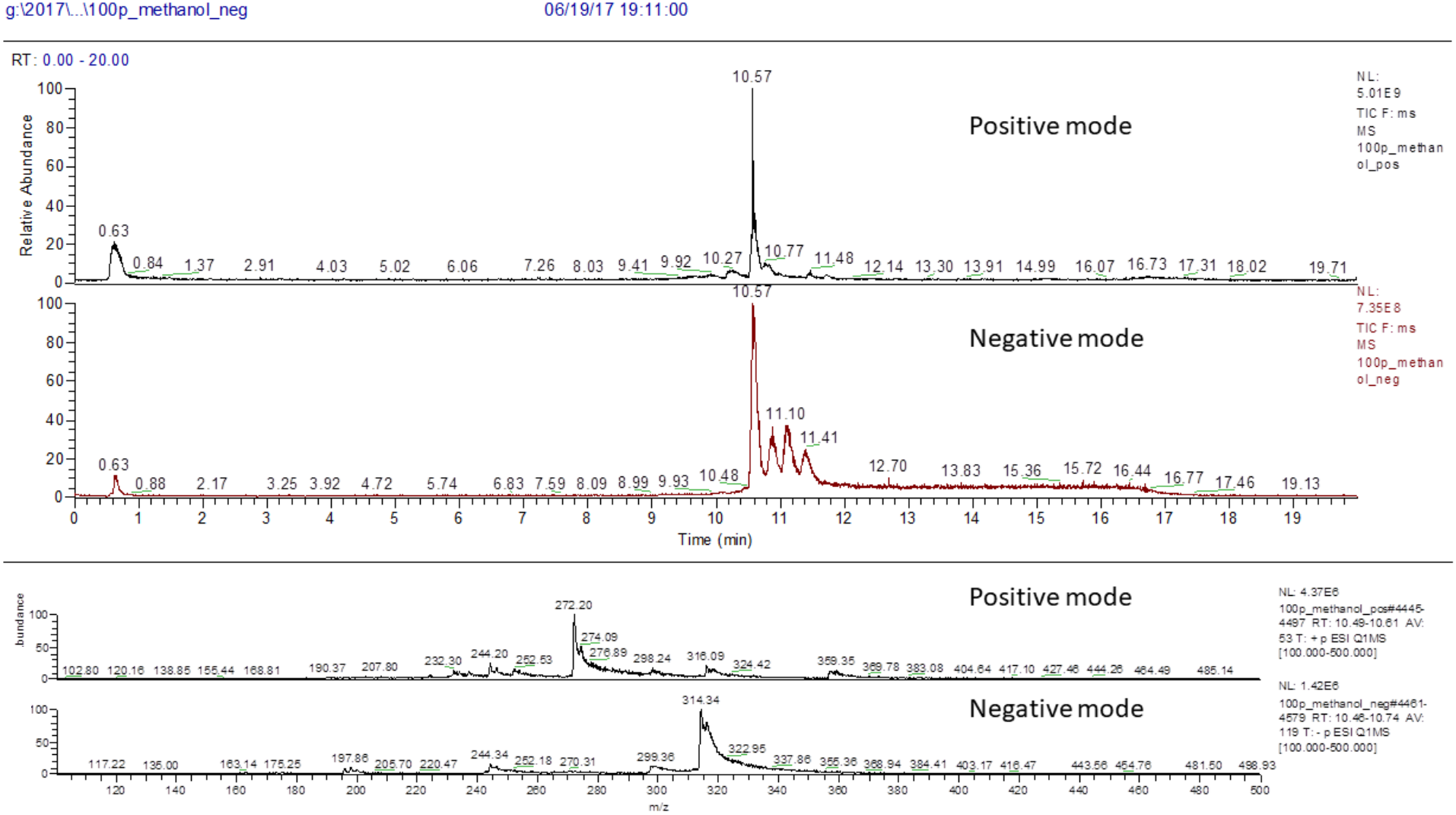

Figure 2.2: Optimisation of EFV detection in positive and negative ionisation mode. The upper panels **(a)** represent the TIC, and the lower panels **(b)** represent the respective extracted chromatogram (XIC). The XIC corresponding to the positive mode TIC shows a molecule with an m/z value of 272. The XIC corresponding to the negative mode TIC shows a molecule with an m/z value of 314. EFV is expected to have an m/z value of 316 in positive mode and 314 in negative mode. The three smaller peaks in negative mode represent the isotopes of EFV.

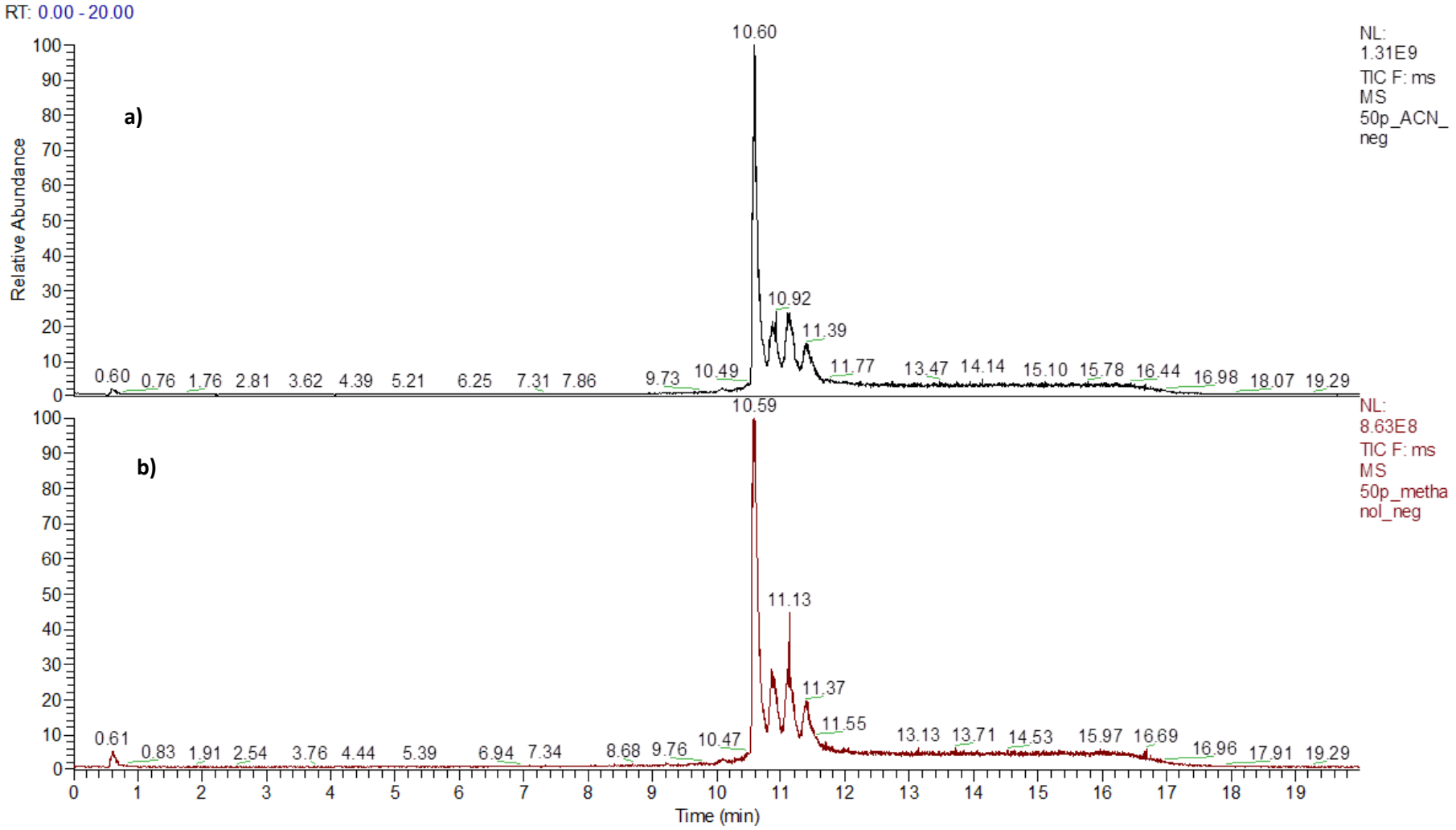

Figure 2.3: EFV detection in full scan mode when solubilised in 50% ACN and 50% methanol. EFV was detected when solubilised in ACN and in methanol (100% and 50%). ACN (upper panel, a) signal of1.31 x10^9 was slightly higher than the signal of 8.63 x10^8 in methanol (lower panel, b) although this was not significantly different (p = 0.061).

2.3.3 Developing a reliable drug detection assay using SRM

CE ramping was performed to optimise the fragmentation of each transition. All of the product ions fragmented optimally at 20 V apart from the 69.01 ion that had the highest ranking at 30 V (Figure 2.4). Table 2.1 shows the final list as imported into Xcalibur. The completed transition list consisted of five distinct and high ranking product ions for the parent molecule of EFV. The parent ion of EFV was 314 m/z, and the product ions were 69.01; 215.67; 242.13; 243.88 and 249.83 m/z.

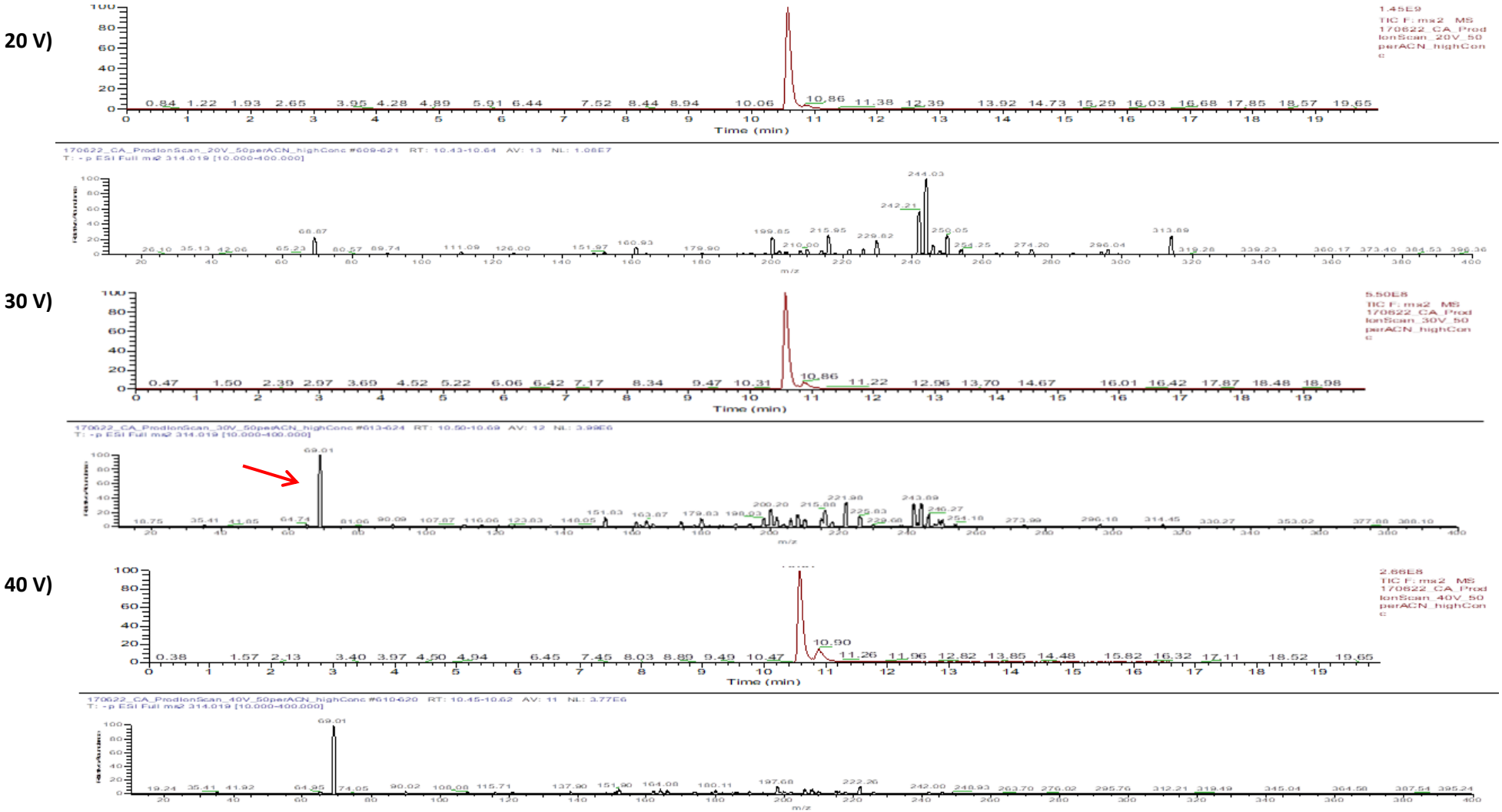

Figure 2.4: CE optimisation for the EFV SRM assay. The collision energy (CE) for the five top ranking product ions was optimised with manual CE ramping. Each red peak in the upper panels represents the parent ion detection. The black peaks in the panels directly below represent the product ions. The collision energy measured in volts (V) causes different fragmentation of the product ions. The collision energy with the highest intensity product ions was selected for the final SRM list. In this figure, the product ion 69.01 was optimally detected at 30V, indicated by a red arrow.

Table 2.1: SRM transition list for EFV detection

	Parent	Product	SRM Collision Energy	Start Time	Stop Time	Polarity	Trigger	Reference	Name
1	314.019	69.014	30	0.00	30.00	-	0	No	Efavirenz
2	314.019	215.675	20	0.00	30.00	-	0	No	Efavirenz
3	314.019	242.137	20	0.00	30.00	-	0	No	Efavirenz
4	314.019	243.887	20	0.00	30.00	-	0	No	Efavirenz
5	314.019	249.837	20	0.00	30.00	-	0	No	Efavirenz

2.3.4 Standard curve of EFV in ACN

The $\log_2$ transformed intensities of EFV peaks were found to increase linearly with increasing EFV concentration. The coefficient of determination (R^2 value) was 0.9915.

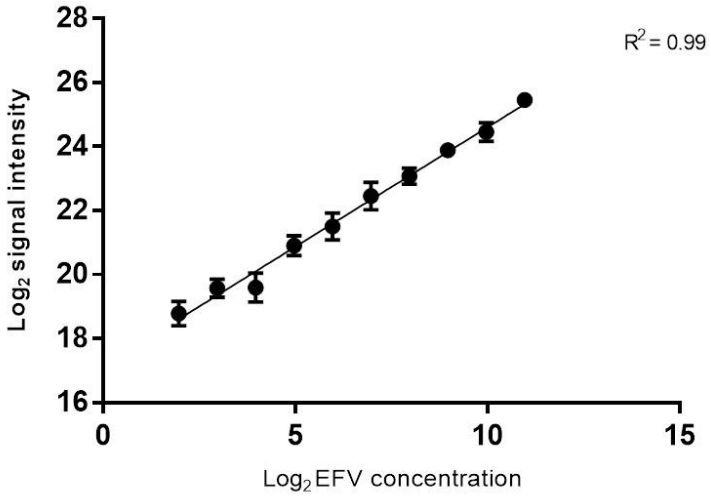

Figure 2.5: Standard curve for EFV. Neat EFV was solubilised in 100% ACN. The relationship between EFV concentration and intensity was linear between 3.9 ng and 2000 ng.

2.4 Discussion

To detect EFV in complex samples, a method was created using an EFV standard (99.4% purity). The reconstitution solvent, gradient, and SRM method were optimised to ensure sensitive and reliable detection of EFV.

2.4.1 Optimisation of instrument parameters and detection of EFV by direct infusion.

In this work, the vehicle used for EFV was DMSO. DMSO has been suggested to improve ionization, especially in hydrophobic compounds, such as EFV,[13,170–172] which was considered as an advantage for EFV detection. EFV solubilised in DMSO and diluted 1:100 in ACN and FA resulted in large PEG contamination peaks (Figure 2.1). This may have been due to the DMSO washing off contaminants stuck to the column , but considering the high concentration of EFV initially used(10 µg), it is possible that the contaminants were causing ionisation suppression of EFV, thus making EFV undetectable. DMSO is also known to leach plastic, and may have stripped the plastic lines, causing PEG contamination.[181,182]

2.4.2 Optimisation of ionisation of EFV

For further analysis, 50% ACN was used to reconstitute EFV, as the solvent is already used within the MS system, and ACN peak intensities were 10-fold higher than methanol (Figure 2.3). There were insignificant differences found between 100% and 50% ACN reconstitution, although 50% reconstitution resulted in slightly higher peak intensities. The EFV peak of 314 m/z was not detected in positive mode when reconstituted with either ACN or methanol, indicating that EFV was unable to ionise in these conditions (Figure 2.2). All subsequent runs were performed in negative mode.

2.4.3 Developing a reliable drug detection assay using SRM

A total of five transitions were selected for the identification of EFV. For accurate detection of the molecule in question, it is recommended that there be no less than 12 data points acquired over the elution time of the molecule.[169] EFV was found to elute over 25 seconds at 80% ACN. The cycle time was set to one second, resulting in a scan time for each transition of 0.2 seconds. This resulted in a total of 25 data points for each transition over the elution of EFV, which is well above the minimum recommendation of 12 data points.

2.4.4 Standard curve of EFV in ACN

The standard curve for EFV in ACN indicated that the concentration and intensity values increased linearly. The R^2 value of 0.9915 indicated that the linear regression was an accurate fit to the data (Figure 2.5). This confirmed that intensity could be used as a proxy for the relative concentration of EFV in further experiments.

2.5 Conclusion

Targeted MS using SRM can be used for drug detection assays. Optimisation for the detection of the analyte EFV was performed and ACN was selected as the solvent for reconstitution of EFV as it resulted in higher intensity values when compared to DMSO and methanol. EFV was detected in negative ionisation mode but not in positive ionisation mode. An SRM assay was created, resulting in five high quality transitions with optimised CE values for further analysis. Using the SRM assay, a standard curve for EFV in ACN was analysed, and indicated that signal intensity and EFV concentration increased linearly. This allowed for further experiments to be performed using signal intensity as a proxy for concentration. All further work was performed using the optimised parameters specified in this chapter.

Chapter 3: Optimisation of EFV extraction from cell culture media and cell suspension

3.1 Introduction

Pharmacokinetics is an investigation into the fate of a drug once administered, leading to information pertaining to its degradation or metabolism. The efficient extraction of a drug from a biological system is an integral part of a study aiming to describe the relationship between the two components. A biological system in this respect ranges from cell culture to human tissue. There are various extraction procedures such as solid-phase extraction, whereby sample is loaded onto a cartridge of silca beads and eluted with organic solvent .[174,183] Liquid-liquid extraction partitions solutes based on their relative solubility in two immiscible liquids.[175,184] Protein precipitation is performed with miscible organics solvents, which cause proteins to aggregate, leaving small molecules in the solvent.[185–187] Proteins can also be depleted from the sample by use of proteinase K.[185,188]

When using MS for drug detection, complex samples such as cell supernatant or cell lysates compete with the analyte for charge, resulting in ion suppression and reducing the sensitivity of detection. Simplifying the sample also improves the sensitivity and specificity of the experiment as an MS instrument has a limited dynamic range. By reducing sample complexity, accurate detection of a low abundance target is more likely. Ostensibly, protein precipitation is the fastest and most cost-effective method of small molecule extraction, and requires very little method development,[185,189] and as such, it was the starting point for drug extraction optimization. Organic solvents such as ACN, methanol, and chloroform among others can be used to extract small molecules such as EFV by precipitating the protein and retaining the supernatant.[185,190,191] Although all methods lead to the majority of proteins being precipitated, the detection of the small molecule by MS is dependent on the solvent used for extraction as well as the properties of the small molecule.[185]

EFV is soluble in ACN, methanol, and chloroform, all of which have been routinely used for protein precipitation in various drug extraction techniques with plasma samples.[184,185,187,188,191–193] ACN and chloroform-methanol (CM) were used as the solvents for drug extraction optimisation.

3.2 Materials and methods

3.2.1 Drug extraction optimisation using protein precipitation methods

Fresh DMEM: Hams F12 media (Invitrogen, Gibco) was spiked with 1 µg of EFV per 1 ml of media. Untreated cells were pelleted and resuspended in 1 ml fresh media, as the phenol red component of the media was needed for subsequent steps during method development. The cell suspension was then spiked with 1 µg of EFV. All protein precipitation was performed in 400 µl flat bottomed glass vials (Separations) so as to avoid leaching of plastic by the organic solvents. The optimisation was performed with three experimental replicates for each extraction method applied to both the cell suspension and supernatant. The organic solvents had a dual purpose of lysing the cells and precipitating the proteins.

3.2.1.1 CM protein precipitation

A CM (both HPLC grade, Sigma Aldrich) solution (2:1) was added to 100 µl of the supernatant or cell suspension fractions (4:1). The samples were shaken on vortex for 20 seconds, incubated at room temperature for 40 minutes, then transferred to 1.5 ml polypropylene high-quality reaction tubes (Eppendorf), and centrifuged at 15 000 g for five minutes at 23°C (LabNet Z233MK2 Microcentrifuge). EFV is a polar molecule and was therefore retained in the methanol-water phase (upper phase) which was isolated for further processing.[194] The middle and lower phases contained chloroform and non-polar molecules and were discarded.

3.2.1.2 Acetonitrile precipitation

ACN (100%, HPLC grade, Sigma Aldrich) was added to spiked media and cell suspension fractions in a 3:1 ratio. Samples were vortexed for 20 seconds, incubated at room temperature for 40 minutes, transferred to high quality reaction tubes, and centrifuged at 15 000 g for five minutes at 23°C. The supernatant was retained and the pellet containing the protein was discarded. Retained supernatants from both precipitation methods were then transferred into 400 µl flat bottom glass inserts and dried at 30^{o}C in an SPD SpeedVac (ThermoSavant) for approximately one hour. Dried samples were then resuspended in 50 µl 50% ACN, transferred into auto sampler vials with 100 µl tapered glass inserts (Separations) and analysed on the TSQ Vantage in full scan and SRM mode (section 2.3.3).

3.2.2 Assessment of inter- and intra- daily sample variation

The relative drug concentration in cell culture was to be measured over the course of 72 hours, which required supernatant and cell suspension samples to be harvested on three subsequent days. It was therefore necessary to ensure the accuracy of the standard curve to predict concentrations, as well as the consistency over time of the chromatogram intensity as a predictor of drug concentration. The volume of sample for extraction as well as the effect of sample processing on different days was assessed. On three consecutive days EFV extraction was performed on three replicates, each containing 1 ml of media spiked with 1 µg of EFV. The drug was extracted from 100 µl of each replicate using the ACN method (section 3.2.1.2). A further three 100 µl extractions were performed from one replicate, to assess whether the 100 µl volume was sufficient for reproducibility (triplicate extraction). This resulted in three experimental replicates and a subset of three technical replicates for each day. In order to assess whether day to day variability was caused by processing on different days, 100 µl from each replicate was stored in glass auto sampler vials (Separations) at -20°C in 75% ACN. Once three samples were collected from three consecutive days and stored at -20°C for at least 24 hours, samples were processed according to the ACN method (section 3.2.1.2). The workflow is represented in figure 3.1. The batch-to-batch variability was quantified by calculating the percentage coefficient of variation (CV), with a lower value indicating higher precision. A value of <20% was considered to be an acceptable level of precision as indicated by the Food and Drug Administration (FDA) guidelines for method validation.[195]

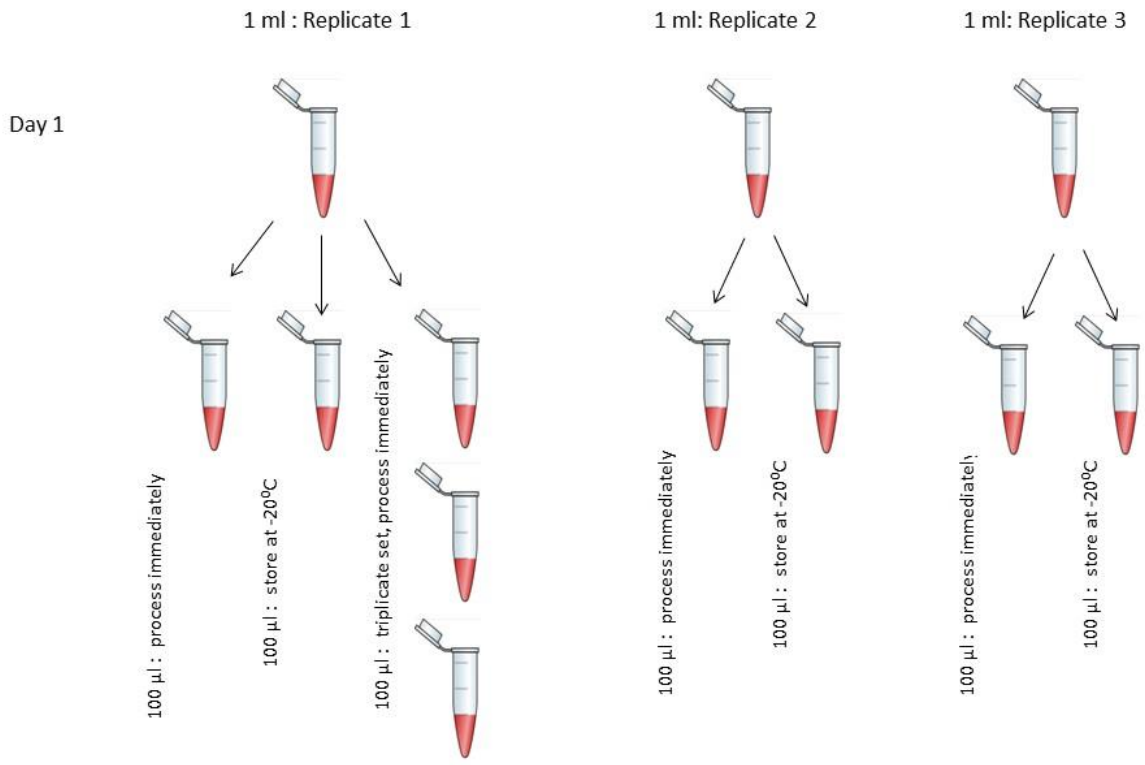

Figure 3.1: Workflow to assess daily variability of sample processing. Representation of day 1 of EFV extraction with ACN protein precipitation. Fresh media was spiked with 1 µg of EFV per 1 ml of media. Samples were either processed immediately on sequential days or stored at -20°C for at least 24 hours, until all samples were collected over three days. A set of triplicates was processed from one of the replicates and processed immediately on sequential days. This work flow was followed over three sequential days.

3.2.3 Decreasing inter- and intra- daily sample variation

3.2.3.1 Assessment of plastic leaching with ACN in high quality reaction tubes during protein precipitation.

High quality reaction tubes were needed for protein precipitation in order to obtain a protein pellet via centrifugation. PEG is a common contaminant in MS which causes ion suppression, specifically in ESI-MS, and a resulting decrease in resolution and sensitivity.[132,196] The binding of PEG to the column also limits peptides binding to the column,[197] causing poor chromatography of the peptide mixture. Polypropylene tubes (Eppendorf) have been specifically enhanced to resist damage by various chemicals, and are resistant to ACN for up to 24 hours.[198] In order to ensure that plastic leaching did not occur in MS detectable amounts, protein precipitation was performed for 20, 40, and 60 minutes. Full scans were performed in positive and negative mode. Equivalent glass and plastic EFV extractions were compared on the TSQ in full scan and SRM mode (section 2.3.3) to observe any effect on the detection caused by method of extraction. After pelleting the protein, the supernatant was transferred to a glass tube and dried down. Due to the higher extraction volume, a larger pellet remained and resolubilisation with 50% ACN was increased from 50 to 200 µl.

3.2.3.2 Increasing the number of replicates and the starting volume of extraction

To mitigate the high degree of observed variability the number of experimental replicates was increased to four, as variation decreased when a higher number of replicates were processed (data not shown). Extractions were performed with the whole 1ml of media spiked with 1 µg EFV over three days, as opposed to 100 µl from 1 ml (section 3.2.2). As the volume for extraction was increased, larger reaction tubes were needed for the protein precipitation step. High quality reaction tubes were used as an alternative to glass tubes as the latter required a specialised centrifuge to obtain high enough speeds to pellet the proteins. Plastic leaching tests indicated that protein precipitation could be performed for up to 60 minutes with no PEG contamination.

3.2.3.3 Extraction of EFV from the organic phase

A phase separation was observed when the volume of 50% ACN for pellet solubilisation was increased to 200 µl, which consisted of water and ACN fractions. The separation was highlighted by the presence of phenol red in the water fraction. The resolubilised EFV/phenol red solution (200 µl) was transferred into a 400 µl glass auto sampler insert (Separations) and centrifuged at 2000 g for one minute in a reaction tube to maximise the phase separation. The upper ACN layer was carefully removed using a micropoint 200 µl gel loading pipette tip (Corning), ensuring that the entire fraction was removed. Any contamination by the aqueous fraction quickly migrated to the bottom of the glass insert and was carefully removed with the micropoint tip. Both the aqueous and organic fractions were analysed on the TSQ Vantage in positive, negative, full scan, and SRM mode (methods described in chapter 2). The needle height from the bottom of the vial was also increased to 3 mm, and the syringe speed was decreased to 0.8 µl/second in order to prevent contamination by any residual phenol red left at the bottom of the vial.

3.2.4 Comparing gradient elution and isocratic elution for detection optimisation

To minimize analysis time, an isocratic elution that held at 75% solvent B for four minutes was assessed. The sensitivity of the isocratic elution was compared to the 20-minute gradient elution using the optimised SRM method (section 2.3.3). The equilibration time at the end of the gradient was subsequently extended to 15 minutes.

3.2.5 Data analysis for SRM in Skyline

Raw SRM data was imported into Skyline which contained the transition list from the optimization steps as described in section 2.2.3. In Skyline, the raw data was processed and generated an output file. The area under the curve for each transition or product ion was summed to obtain the total intensity of EFV in each sample. Each product ion was measured 25 times during the elution of the molecule over 25 seconds. The total area values were exported to GraphPad Prism for statistical analysis and graphical representation. Daily variability was assessed with CV values and a one-way analysis of variance (ANOVA) test.

3.3 Results

3.3.1 Drug extraction optimisation using protein precipitation methods

Samples from ACN and CM drug extraction methods were analysed on the TSQ in both full scan and SRM mode. Full scan analysis showed the EFV peak (m/z = 314) was detected with the ACN extraction but not with the CM extraction (Figure 3.2, upper panels). Using the SRM method, EFV was detected in both conditions (Figure 3.2, lower panels). The CM method resulted in less smooth peaks with lower intensity and higher background noise than the ACN method (Figure 3.3). The average intensity for the CM method was $1.17x10^5$ and the average intensity for the ACN method was $1.57x10^7$, two orders of magnitude higher than that of the CM method (CV = 9.6% and 4%, respectively).

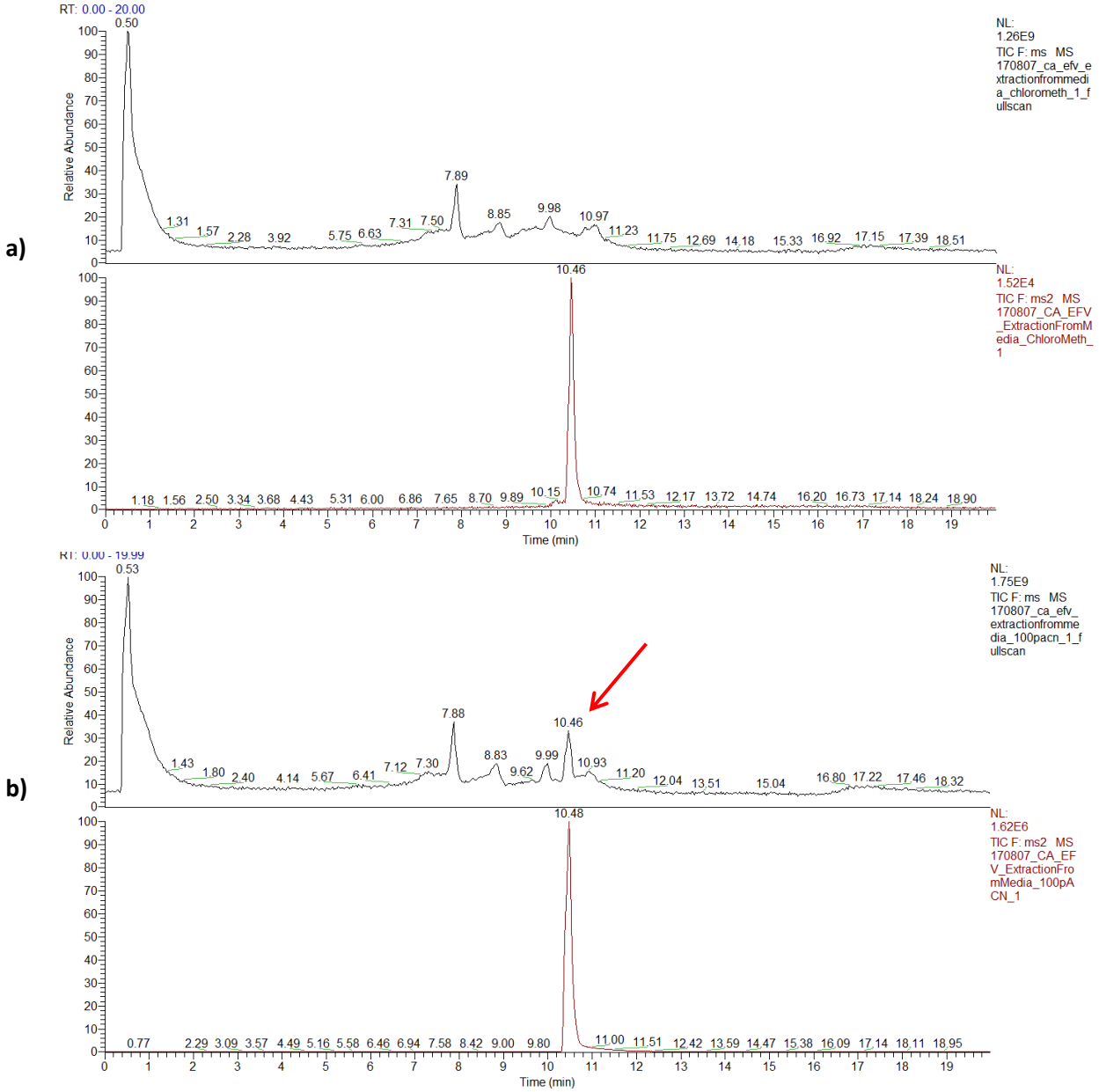

Figure 3.2: Detection of EFV after protein precipitation extraction. EFV was extracted by a) chloroform- methanol (CM) or b) ACN protein precipitation. The upper panels (black peaks) represent the full scan (MS1). The lower panel (red peaks) shows the detection of EFV by SRM (MS2). EFV is not detected in the CM precipitation full scan, but is detected in the SRM. EFV is detected in both the full scan and SRM mode with ACN protein precipitation. EFV in the ACN extraction full scan is indicated by a red arrow. This peak was not present in the CM extraction full scan

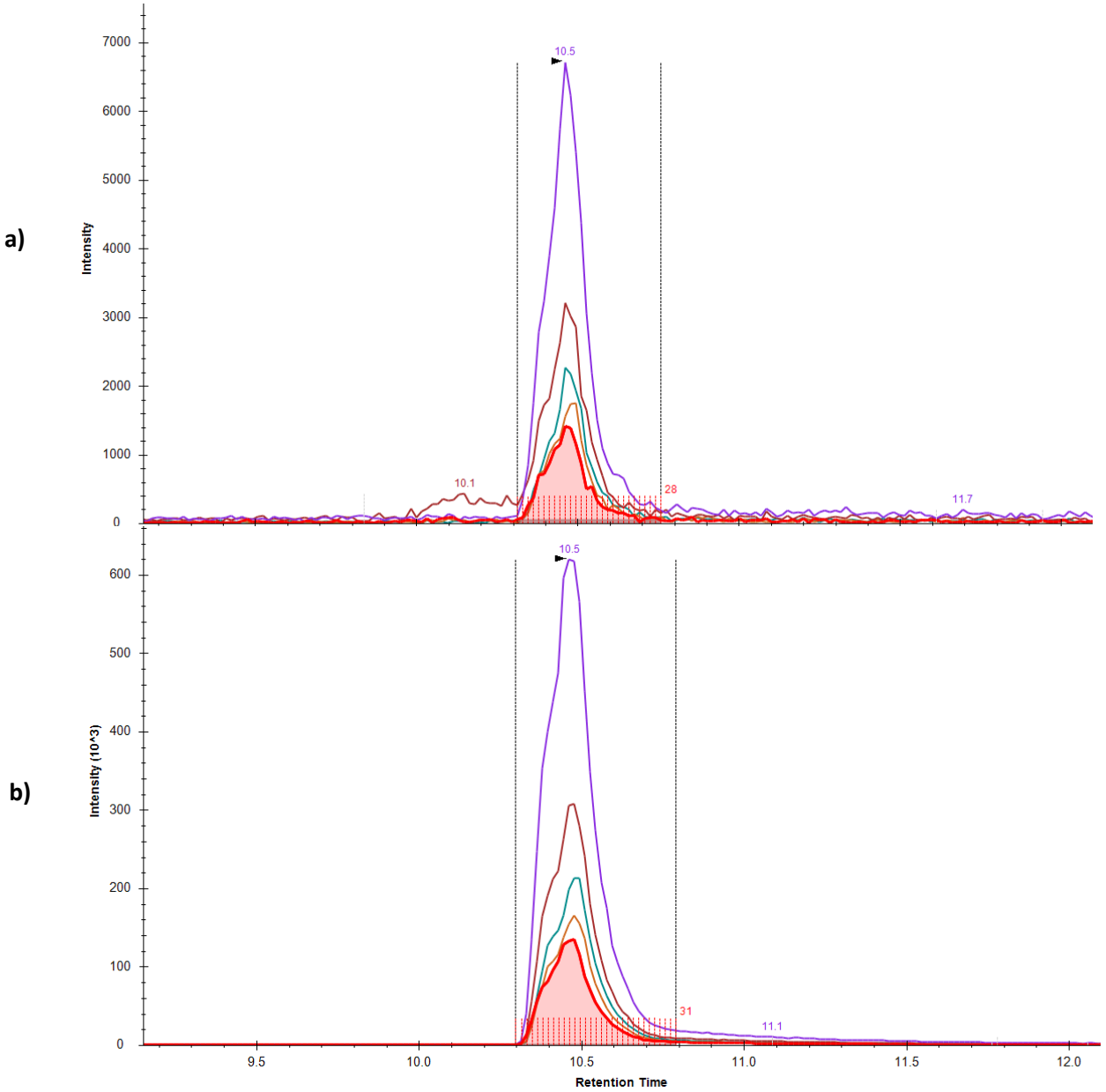

Figure 3.3: Transition peaks of EFV after protein precipitation extraction. The average peak intensity was two orders of magnitude lower with **a)** chloroform-methanol (CM) extraction compared to **b)** ACN extraction. The smooth peaks in the ACN extraction are due to higher signal intensity and less background noise, indicating a more efficient extraction. The intensity of the SRM peak was 1.17×10^5 for the CM method, and 1.57×10^7 for the ACN method.

3.3.2 Assessment of inter- and intra- daily sample variation

The CV of each set of replicates in both conditions over three days was assessed. When samples containing 1 μg/ml of EFV were processed on sequential days, none of the three sets had acceptable CV values (CV > 20%). Samples processed on the same day after storage at -20^{o}C only had one of three sets with acceptable CV values. The triplicate extraction to assess whether the volume of extraction was sufficient for reproducibility had two of three sets with acceptable CV values (Table 3.1). A one-way ANOVA test performed on replicates processed on sequential days indicated that the intensities of EFV measured on each day were significantly different ($p < 0.005$) from each other. Samples stored at -20^{o}C and processed on the same day were also found to be significantly different from each other ($p < 0.005$).

Table 3.1: CV values for EFV extraction to assess inter- and intra-daily variation

	Processed on sequential days	Processed on same day (freezer)	Processed on same day (triplicate)	Four replicates, 1 ml starting volume
Day 1	0.479	0.230	0.315	0.174
Day 2	0.253	0.173	0.147	0.372
Day 3	0.485	0.515	0.163	0.254

3.3.3 Decreasing inter- and intra- daily sample variation

3.3.3.1 Assessment of plastic leaching with ACN in high quality reaction tubes during protein precipitation

High quality reaction tubes with 75% ACN were used to assess plastic leaching. No PEG was detected in any samples when incubated at room temperature for up to 60 minutes in positive or negative mode full scans (data not shown). Drug extraction in glass vials or plastic reaction tubes did not differ significantly based on EFV intensity values (data not shown)

3.3.3.2 Increasing the number of replicates and the starting volume of extraction

Processing the whole 1 ml of four replicates on sequential days resulted in a decrease in CV values when compared to processing 100 µl from three replicates on sequential days, but not when compared to stored samples processed on the same day (Table 3.1). A one-way ANOVA showed that there was no significant difference between EFV intensities detected on different days when four samples were processed with a 1 ml starting volume ($p > 0.05$).

3.3.3.3 Extraction of EFV from the organic phase

Performing the extraction on the full 1 ml resulted in organic and aqueous phases containing EFV and phenol red respectively. EFV was not detected by the full scan in the aqueous fraction, but was detected by a full scan in the organic fraction (Figure 3.4 a and 3.5 a). EFV was detected by SRM with intensity 6.46 $x10^3$ and 3.39 $x10^5$ in the aqueous and organic fractions respectively (Figure 3.4 and 3.5). The blank sample after the water fraction showed a large phenolic acid contaminant peak that was not present after the ACN fraction (Figure 3.6).

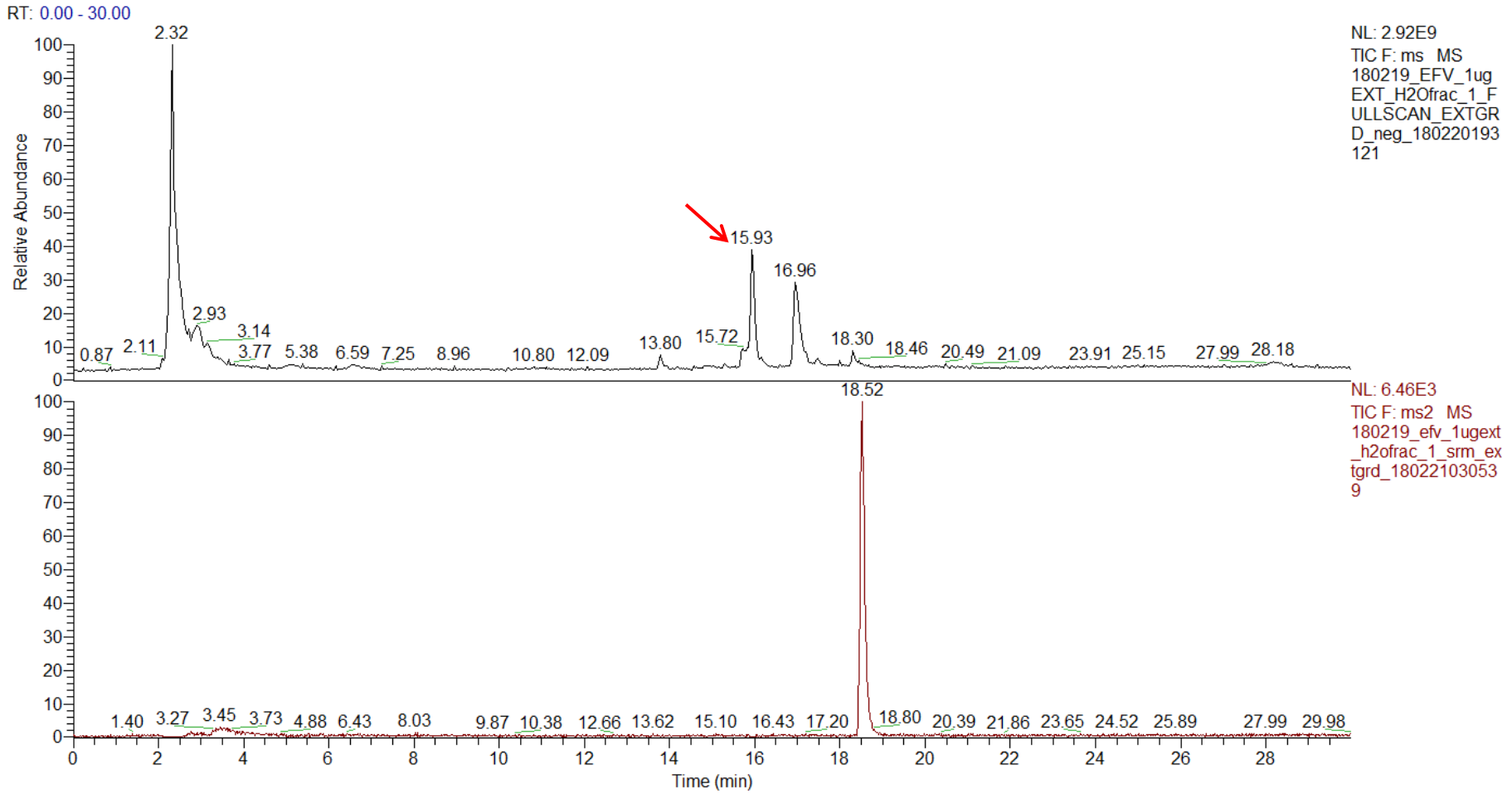

Figure 3.4: EFV extraction from the aqueous phase. A phase separation resulted in an organic and aqueous phase. The upper panel **(a)** represents the TIC from the aqueous fraction. The peak at 15.96 represents a molecule of 354 m/z, the mass of phenol red, indicated by a red arrow. The lower panel **(b),** shows the SRM chromatogram, whereby EFV was detected. The lack of smooth lines indicates low intensity of the detected analyte.

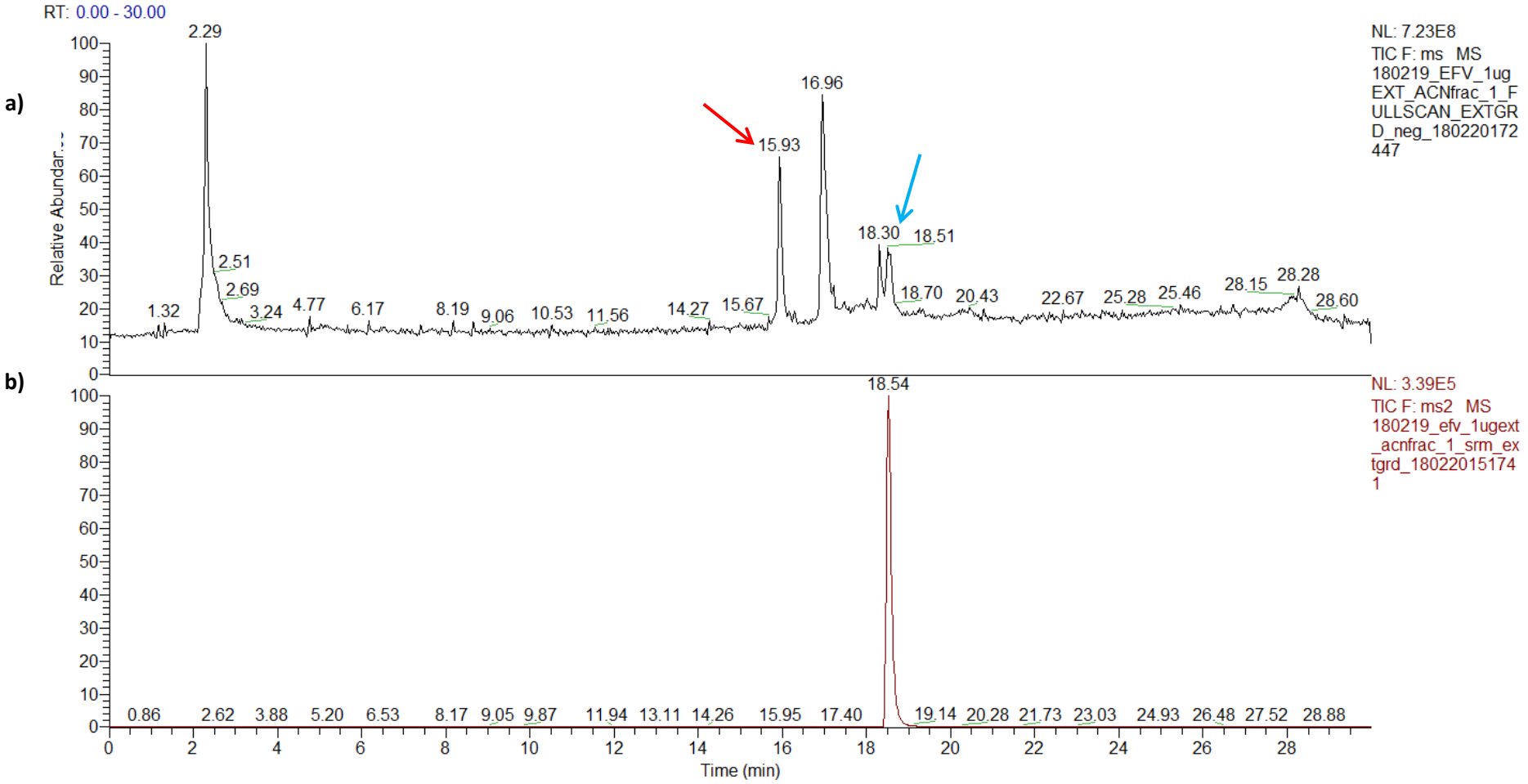

Figure 3.5: EFV extraction from the organic phase. The upper panel **(a)** represents the TIC from the organic phase. EFV was detected at 18.51 in the full scan (indicated by a blue arrow), as well as phenol red at 15.93 (indicated by a red arrow). The lower panel **(b)** shows the SRM chromatogram, the smooth lines indicate high signal intensity and low background noise

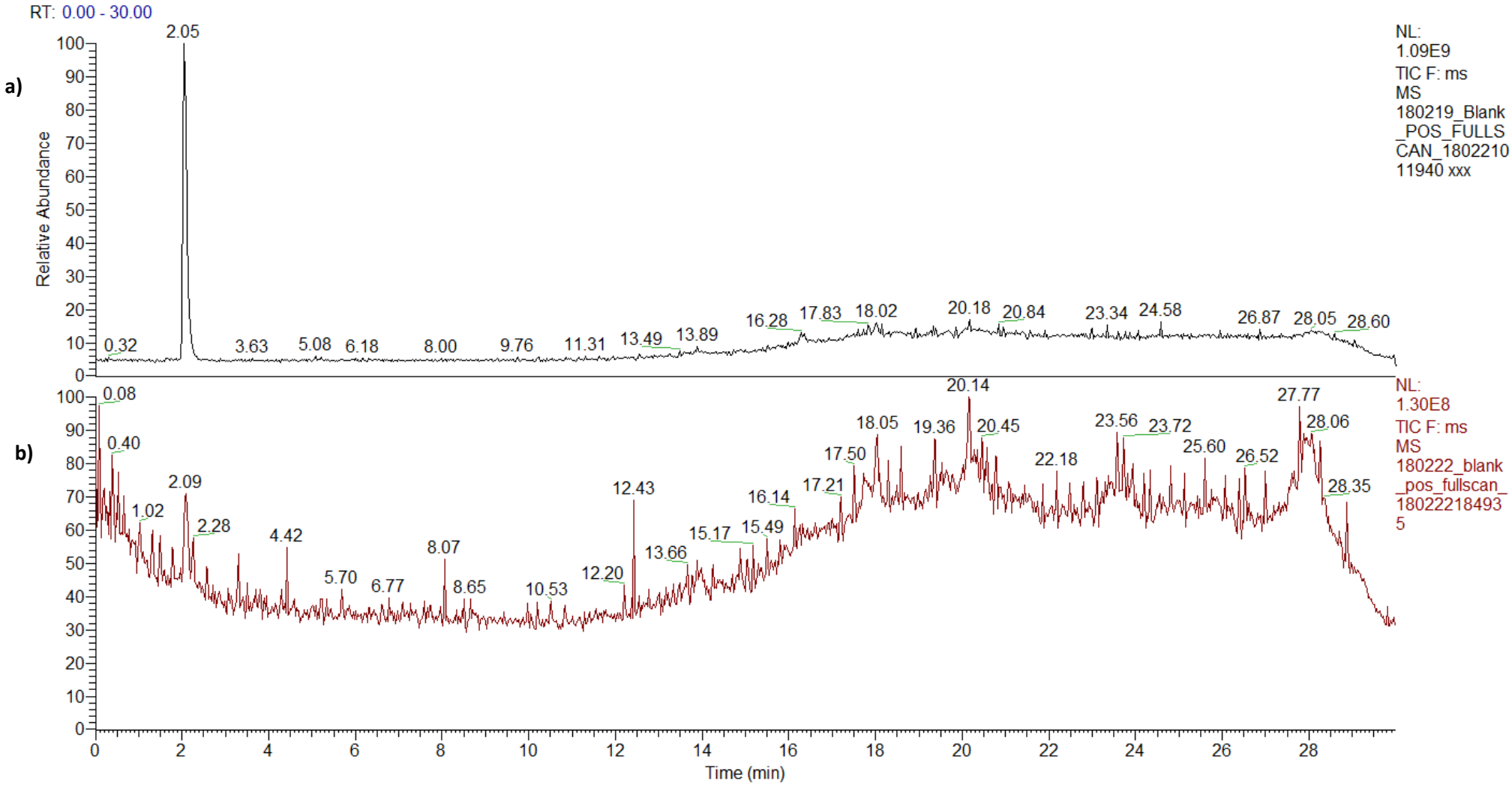

Figure 3.6: Blank runs after aqueous and organic phase EFV extraction. The upper panel **(a)** shows the blank run directly after an aqueous phase EFV sample. The large contamination peak was identified as phenolic acid. The lower panel **(b)** shows a blank sample run directly after an organic phase EFV sample. The TIC shows the gradient and is typical of a blank sample with no contamination..

3.3.4 Comparing gradient elution and isocratic elution for detection optimisation

The gradient elution resulted in much narrower peak widths as well as higher intensity values when compared to the isocratic gradient. The average intensity value for isocratic elution was $1.36x10^4$, which was 24-fold lower than the gradient elution with an average intensity of $3.24x10^5$ (Figure 3.7). There was a shift in retention time of EFV over multiple sample analyses (Figure 3.8). The extension of post-gradient equilibration time resulted in a reproducible elution of the analyte over multiple consecutive analyses (data not shown).

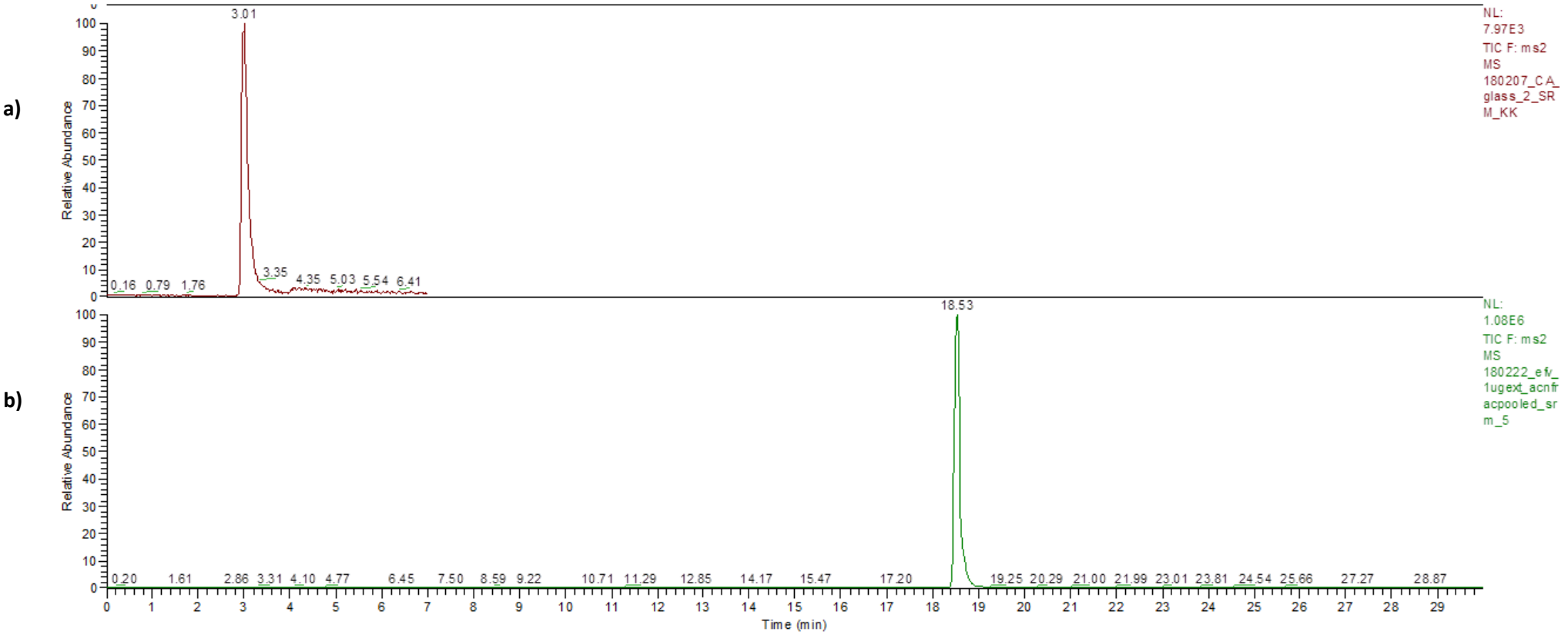

Figure 3.7: Comparison of isocratic and gradient methods. The upper panel **(a)** shows the isocratic elution of EFV. The analyte elutes at 3.01 on a 7 minute run with an intensity of 7.97 x10^3. The lower panel **(b)** shows the gradient method, with the analyte eluting at 18.53 on a 30 minute run with the intensity of 1.08 x10^6.

3.4 Discussion

Protein precipitation was performed with organic solvents ACN and CM to optimise extraction of EFV from media and the cell lysate. Optimisation steps were performed to improve reproducibility between days, as well as the chromatographic gradient.

3.4.1 Drug extraction optimisation using protein precipitation methods

The signal intensity of EFV in ACN was shown to increase linearly with increasing concentration, indicating that intensity could be used as a proxy for analyte amount (Chapter 2, section 2.3.4). For assessment of extraction efficiency, higher signal intensity indicates a higher relative abundance, and thus a more efficient extraction method. EFV intensity was $1.57x10^7$ and $1.17x10^5$ for ACN and CM extraction respectively, indicating that ACN was ~100 times more efficient at extracting EFV from spiked media and lysate than the CM method (Figure 3.2 and 3.3). It is interesting to note the inefficiency of CM extraction as EFV is soluble in and was detected in methanol (Chapter 2, section 2.3.1). Methanol is often a preferred solvent for drug extraction, although its efficiency depends on the properties of the small molecule being extracted.[185] Photolysis of EFV (the decomposition or separation of the molecule by the action of light) is affected by the solvent in which it was reconstituted in.[199] A bathochromic shift indicates a change in the absorption of light by the molecule, caused by photolysis. EFV solubilised in chloroform showed a larger bathochromic shift than methanol, and the smallest effect was that of ACN.[199] This may be caused by stabilization of the polarized imidic acid phototautomer of EFV, which occurred with chloroform and methanol, as they both have strong hydrogen bond donor ability, as opposed to ACN which has no hydrogen bonding ability.[199] It is possible that the lower efficiency of the CM method to extract EFV was due to the solvents enabling photolysis during the sample preparation.

Another explanation for the lower efficiency of the CM extraction method could be that the EFV fraction was contaminated by proteins and lipids, caused by the inability to discern the phase separation, which may have resulted in ion suppression and thus lower detection efficiency. It is also plausible that the CM method, often selected for top-down proteomics as it does not fully denature proteins during the precipitation process, resulted in EFV remaining bound to non-denatured precipitated proteins.[200]

3.4.2 Assessment of inter- and intra- daily sample variation

Inter- and intra- daily variation between samples was assessed in three ways. Samples processed on sequential days were all significantly different from each other and had high CV values. Samples processed on the same day after storage were also significantly different from each other and had high CV values. The triplicate extractions from a single replicate had two CV values < 20% and one triplicate with CV > 20%. The outlier triplicate set from the first day of processing had significantly lower intensities than the two following days. This trend was also observed in the first day replicates of samples processed on sequential days, as well as those stored at -20^{o}C and processed on the same day, which suggests that the low intensity was due to an error either in the initial spiking of EFV into the media, or due to pipetting error during the 100 µl extraction for processing and/or storage steps (Table 3.1). These results indicated that the inter- and intra- daily variation was too high to use this assay as a semi-quantitative method for detection of EFV within cell culture. It was hypothesised that higher starting amounts for processing and thus a higher final concentration of EFV would ensure that the lower limit of EFV detection was not reached, as well as preventing pipetting error when removing a small volume for processing.

3.4.3 Decreasing inter- and intra- daily sample variation

3.4.3.1 Assessment of plastic leaching with ACN in high quality reaction tubes during protein precipitation

Intra- and inter-daily variation posed a problem for determining relative concentration of the drug over three days. In order to increase the initial volume of extraction, high quality reaction tubes were first tested for resistance to ACN, in order to avoid damage to the LC column or PEG contamination due to plastic leaching. Although the manufacturer assures resistance to ACN for up to 24 hours incubation in polypropylene products,[198,201] the reaction tubes were tested for resistance before proceeding. No PEG was detected for up to 60 minutes of incubation (data not shown). Protein precipitation was not affected by incubation in plastic reaction tubes as opposed to glass vials, which indicated that further work could be performed without risk of contamination or decreased efficiency in the larger plastic reaction tubes.

3.4.3.2 Increasing the number of replicates and the starting volume of extraction

Increasing the starting volume for extraction to 1 ml and the number of processed replicates to four ensured that there was no significant difference between the intensity values between each day, and slightly improved CV values (Table 3.1). This may have been simply due to lower pipetting error at higher volumes. Alternatively, extracting 1 µg of EFV in 1 ml as opposed to 100 ng in 100 µl may have mitigated variation caused by MS accuracy at the lower end of the limit of detection. Increasing the number of experimental replicates to four allowed for the detection and potential removal of outliers while still maintaining three replicates for statistical validity. Outliers and variation between samples may be as a result of the manual extraction procedure. As the number of steps required during a procedure (operational complexity) increases, the possibility of variation due to error increases.[202] Automation of procedures often minimises operational complexity, as well as "hands-on time", resulting in lower %CV values between replicates.[202,203] Processing four replicates on sequential days did not significantly reduce the %CV values when compared to the samples processed after -20^{o}C. Due to processing the samples manually, the stored four experimental replicates per condition over three days would have had to be processed in daily batches to reduce the operational complexity. It was therefore decided to process the samples daily without freezing.

3.4.3.3 Extraction of EFV from the organic phase

ACN is miscible in water, but when a larger volume of 50% ACN was used to reconstitute the EFV pellet after extraction, a phase separation was visible. Phase separation of miscible organic solvents and water due to "salting-out" has been well documented.[204,205] The extraction of organic solutes can also be performed with ACN and water, with or without salt.[206] The phase separation observed was likely to be as a result of the phenol red, a polar organic molecule used in tissue culture.[206] EFV is relatively insoluble in water (0.093 mg/L) ,[194] and thus was expected to be present mostly in the organic ACN phase. Phenol red (354 g/mol) separated mostly in to the aqueous phase, but was still present in the organic phase as it is soluble in both water and ACN. The peak at 15.96 in the full scan in both the aqueous and organic fractions had an m/z of 353, identifying it as phenol red ionised in negative mode (Figure 3.4 and 3.5).

A full scan only detected EFV in the organic phase, indicating a higher concentration than the aqueous phase. The SRM assay confirmed this, as the EFV intensity was ~100 fold higher in the organic phase than in the aqueous phase. In addition, a large contaminant of 352 m/z was present in the blank sample (2% ACN) following the water fraction, identified as a phenolic acid.[207] Therefore only the organic

fraction was analysed in further experiments, as the blank samples following the organic phase samples did not contain the contaminant, indicating that the organic phase samples were also somewhat less complex (Figure 3.4 and 3.5).

3.4.4 Comparing gradient elution and isocratic elution for detection optimisation

An isocratic elution is preferable for analysis of simple samples, or samples that occupy 20 – 40% of the separation space in a scouting gradient run.[208] Other studies have found that a gradient elution is faster, more selective, and has a higher resolution even in samples that are specifically suited to an isocratic elution.[209]– Sensitivity and resolution were both increased when using the gradient elution, with an average intensity of $3.24x10^5$ compared to $1.36x10^4$ for the isocratic elution, resulting in a sharper peak with a higher intensity (Figure 3.6). A gradient elution separates molecules within a complex mixture, causing them to elute at different times based on their hydrophobicity. Control over the elution of an analyte in a complex mix allows for simplification and optimisation of the detection of the analyte of interest.

As fewer molecules elute at a time, ion suppression is less likely to occur. Ion suppression is most commonly caused by endogenous organic or inorganic molecules that are present in the samples to be analysed after extraction.[210] Highly polar molecules such as phenol red or organic molecules such as lipids and peptides are ion suppressor agents. Exogenous molecules such as PEG are also considered ion suppressor agents.[210,211] The presence of these non-volatile or less volatile molecules can cause a decrease the evaporation efficiency of the droplet, causing fewer analytes to reach the gas phase.[210,211]

Another cause of ion suppression is due to competition of compounds for the maximum ionisation efficiency.[210] Molecules of higher mass and more abundant molecules are more likely to supress lower mass and less abundant molecules.[211] As fewer analytes are ionised, the signal is decreased, which leads to a decreased detection ability or inability to detect the analyte. In order to minimise the unpredictable effects of ion suppression it is therefore preferable to use the gradient method over the isocratic elution for further experiments. Phenol red, lipids, and other molecules remain in the organic phase after extraction with ACN, as this protein precipitation method does not remove these molecules. The increased sensitivity and specificity of the gradient method was also advantageous for detection of EFV

in the lysate with low cell numbers, when the total volumetric space available and thus the total concentration of EFV would be lower.

Over several runs, the retention time of the EFV peak of the gradient method drifted from elution at 14.46 to 19.93 minutes (data not shown). This drift indicated that the equilibration of the column may not have been sufficient prior to sample introduction. Equilibration of the column ensures that the entire column is covered uniformly with 2% solvent B. Incomplete equilibration results in areas of the column containing a higher percentage of solvent B, which would change the binding of the analytes to the column, thus causing drifting retention times between samples. Subsequent to the increase of equilibration time, the retention time remained stable (data not shown). For adequate equilibration, it is recommended to be between two and ten column volumes.[209] At a flow rate of 300 µl/minute, the five minute equilibration time amounted to approximately two column volumes. The extended 15 minute equilibration amounted to six column volumes.

3.5 Conclusion

Optimisation of EFV extraction, sample processing, and the elution gradient was performed. ACN precipitation was selected over CM precipitation for EFV due to higher extraction efficiency. Inter- and intra- sample variation was deemed too high for semi-quantitative analysis when processing 100 µl from three replicates, necessitating a higher starting volume and more replicates. In order to prevent damage to the LC column and a decrease in analyte detection sensitivity, the extraction method in high quality reaction tubes was tested for PEG contaminants prior to increasing the starting volume for processing. PEG was not found as a contaminant for up to 60 minutes incubation and detection by SRM was not decreased by this method. The inter- and intra- daily variation between samples was decreased when 1 ml of four replicates was processed. EFV detection was further improved by extraction of the organic phase containing the majority of EFV, as well as the use of a gradient elution as opposed to an isocratic elution. The equilibration time at the end of the gradient was also increased to prevent retention time drift over an extended period of time. The optimised methods for EFV extraction were used for all further analysis.

Chapter 4: Relative EFV concentration in neuronal cell culture over three days

4.1 Introduction

EFV is a small lipophilic molecule that diffuses passively across most cell membranes, with a low solubility and a high permeability.[212] It is highly bound to plasma proteins (99.5%) and is only able to pass through the BBB in its unbound form. Entry into CNS is by passive diffusion with no active transport back into the systemic circulation.[65,213] Although only a small amount of EFV is able to pass through the BBB into the CNS, it is still estimated to be 26 times higher than the IC50 for wild type HIV-1.[65] CSF measurements are considered to be an acceptable estimate of the brain tissue drug concentration, and are more safely obtained from patients.[214,215]

During HIV treatment with ARV drugs, it is vital to ensure that the drug plasma concentration always remains above a certain level in order to achieve systemic viral suppression, and below a certain level in order to minimise toxicity.[216] Once the elimination of the drug is balanced by the administration of the drug - when the average concentration of the drug remains the same over time - it is said to have reached a steady state. EFV reaches its steady state within 6-10 days after initiation of dosing. The half-life is between 40-55 hours, although this varies greatly depending on the metabolism of the drug in individuals, which can be altered by genetic polymorphism.[217–219]

A challenging factor in modelling the effect of EFV on the development of proliferating NES cells is adequately imitating the *in vivo* pharmacokinetics of EFV *in vitro.* In order to gain deeper understanding of the chemical stability of the drug, as well as the mechanism of degradation, forced degradation studies have been previously performed using a range of pH values in various buffer formulations.[220–223]

EFV degradation follows first order kinetics in buffers ranging from pH 0.6 – 12.8 at 60°C, whereby the drug is eliminated at a rate proportional to the drug concentration.

The stability of EFV in solution was optimal at a neutral pH and did not degrade when exposed to temperatures up to 70°C, even after 30 days of exposure.[222] In a more acidic solution of pH4, EFV was stable in solution up to 60°C. In basic solutions, EFV tended to degrade more rapidly.[220–222]

NES cells are grown in serum free media supplemented with growth factors. The pH of the media ranges from pH 6-8 over three days when kept at 37°C and 5% CO_2. It is therefore important to understand the

degradation profile of EFV in these specific cell culture conditions to properly model the treatment-elimination profile.

In vivo, EFV is metabolised primarily by the cytochrome p450 CYP2B6, mostly in the liver. EFV regulates its own metabolism by activating the constitutive androstane receptor that induces CYP2B6 transcription.[48] Mutations of CYP2B6 have been linked to elevated EFV concentrations in plasma, as well as various CNS side effects associated with EFV treatment and early discontinuation of treatment.[117,224,225] CYP2B6 is found in the liver and in the CNS parenchyma, including neuronal, glial, and epithelial cells. CYP2A6 and CYP3A4, secondary metabolisers of EFV, are not found in any CNS tissue (Human Protein Atlas available from www.proteinatlas.org).[226] CYP2B6 follows atypical kinetics in the liver, and its activity in the CNS tissue differs from that in the liver.[227–229] Over an extended treatment period in mice, CYP2B6 expression increases dramatically after an initial delay with the onset of treatment. This may indicate that CYP2B6 induction only occurs once a steady-state is reached or higher levels of EFV begin to accumulate and that a higher rate of metabolism occurs with extended exposure.[229]

This chapter aims to establish a dosage regimen that mimics the *in vivo* EFV exposure in a developing neural system. First, the movement of EFV in cell culture was assessed in order to clarify whether EFV crosses the membrane of the NES cells. Next, the degradation of EFV in cell culture conditions was assessed in order to gain insight into whether the components of the media at 37°C and 5% CO_2 would affect the stability of the drug. Assessing the degradation of EFV through relative concentration studies would also indicate whether EFV is metabolised by the NES cells.

By analysing the movement and degradation patterns of EFV within these culture conditions, a treatment schedule can be designed in order to attempt to approximate the exposure of NES cells to EFV *in vivo.* EFV in the form of an FDC is administered once every 24 hours, reaching a steady state within approximately ten days.[39,218] This work aims to assess EFV in NES cell culture over three days, with dosing at estimated biologically relevant concentrations every 24 hours.[62,71,72,230]

4.2 Materials and methods

4.2.1 Cell culture preparation

This study used human-derived non-transformed NES cells which were kindly donated by the Austin-Smith group at the Cambridge Stem Cell Institute. The cell line was derived from 5-6 week old foetal hindbrains (Carnegie stage 15–17),[123] and were maintained in culture as follows: Adherent dishes were coated with proteins to provide an environment conducive to NES cell adherence and growth.[231] Plates were coated with Poly-L-Ornithine (100 µg/ml in phosphate buffered saline (PBS) (Invitrogen Gibco) and incubated for 30 minutes at 37˚C. The plates were then washed with PBS and coated with laminin (2 µg/ml in PBS) for 8-12 hours at 37˚C. The laminin was washed off with PBS and could either be stored at 4˚C for up to three weeks or used immediately.

4.2.2 Media and supplements used for tissue culture

The minimal amount (5 ml) of DMEM: Hams F12 medium (Invitrogen Gibco), supplemented with penicillin/streptomycin (1:100 v/v, Lonza), N2 supplement (1:100 v/v, Invitrogen Gibco), B27 supplement (1:1000 v/v, Invitrogen Gibco), epidermal growth factor (EGF, 0.01 ng/µl, Invitrogen Gibco) and fibroblast growth factor 2 (FGF2-b, 0.01 ng/µl, Invitrogen Gibco) was added to pre-coated plates. Cells were seeded onto adherent cell culture plates (TPP) by spotting onto plates containing pre-warmed media. The plates were rapidly slid back and forth to ensure even distribution of the cells and incubated at 37°C, 95% humidity and 5% carbon dioxide (CO_2). Once confluence was reached (roughly every three days), cells were lifted using Tryp-LE (Gibco), and transferred onto a larger plate, ensuring cell density remained at minimum between 3-4x10^4 cells/cm^2, as cell to cell contact is necessary for optimal maintenance of the culture.[123] Media was changed every 24 hours.

4.2.3 Standard curve

A standard curve was created to assess the relationship between signal intensity and EFV concentration in both the supernatant and lysate. Fresh media (1 ml) with and without cells was spiked with 1, 0.5, 0.25, 0.125, 0.0625, 0.03125 µg/ml of EFV; extracted as described in chapter 3, section 3.2.1.2; and analysed on the TSQ according to the method described in chapter 2 section 2.2.3. All data analysis was performed as described in chapter 3, section 3.2.5. The intensity and concentration values were $\log_2$ transformed for ease of interpretation.

4.2.4 DMSO viability assay

The vehicle for drug delivery used in this work was DMSO. Previous work in the Blackburn Laboratory has shown that up to 0.5% DMSO does not affect the viability of SHSY-5Y cells. To ensure that the same was true for NES cells, a DMSO dose response was performed with a doubling concentration from 0.125 to 2%. The proposed treatment vehicle concentration (0.05%) was also tested. Cell viability was assessed using 3-(4, 5-dimethylthiazolyl-2)-2, 5-diphenyltetrazolium bromide (MTT). At each time point the media was removed, cells were gently washed with warmed PBS to remove dead cells, and 0.5 mg/ml of MTT in base media was added to each well (1 ml). The cells were then incubated for 30 minutes. The media was then aspirated and 200 µl DMSO (100%) was added to solubilise the formazan crystals. This was followed by gentle agitation for 10 minutes at room temperature. The formation of purple formazan crystals is used as an indicator of cell viability. Absorbance values were recorded by the iMark microplate reader (Biorad) at 595 nm and analysed in the Microplate Manager software. Viability was measured as a percentage of the control (100% viability), and a t-test was performed to confirm significance.

4.2.5 Drug internalization by cells

Once EFV was successfully spiked into and extracted from media and cell lysate fractions, it was necessary to determine whether EFV was able to enter the NES cells as well as whether the ACN drug extraction followed by MS analysis was sufficient to detect the potentially low levels of EFV within the

cells. Based on a review of the literature, the estimated foetal plasma as - opposed to the foetal CNS concentration - of 1.05 μg/ml was used as the treatment concentration as there are currently mixed reviews estimating that the gestational age of BBB formation ranges from eight weeks to mid-gestation in non-human primates.[232–234] Cells were seeded, left to settle overnight, and then treated with 0.525 (half of the estimated concentration), 1.05, and 2.1 (double the estimated concentration) μg/ml of EFV. After 24 hours the supernatant was collected, and the cells harvested. Both fractions were subjected to ACN protein precipitation and analysed on the TSQ. Statistical analysis and visualization were performed with Skyline, Excel, and Prism (methods described in chapter 3, section 3.2.1.2 and 3.2.5).

4.2.6 Relative concentration of EFV over three days

EFV was administered to NES cells every 24 hours to approximate the current therapeutic dosing schedule of EFV.[218] The relative concentration was measured by MS every 24 hours to assess the accumulation or degradation of EFV.

Adherent six-well plates were seeded with NES cells and allowed to settle overnight (12 hours) after which fresh media containing 1.05 μg/ml EFV was added to each well (T0). From this point, the two conditions being tested were as follows:

Condition 1 – every 24 hours, media containing EFV was removed and the cells were washed with pre-warmed PBS. The old media was replaced with fresh media containing 1.05 μg/ml EFV (re-treatment).

Condition 2 – every 24 hours, media containing EFV was removed and cells were washed with pre-warmed PBS. Fresh media only was added (single treatment).

After treatment at 24 hours, 48 hours, and 72 hours, four replicates from each condition were harvested. The media (supernatant) was removed and retained. The cells were then washed with pre-warmed PBS to remove dead cells and any residual EFV, lifted, and pelleted in fresh tubes. The cell pellet was then resuspended in 1 ml fresh media. EFV was extracted with the ACN precipitation technique, which caused cell lysis and protein precipitation. The samples were analysed on the TSQ using the optimised SRM target list. Every 24 hours, four T0 replicates of fresh media spiked with 1.05 μg/ml EFV were processed concurrently. Treatment conditions 1 and 2 were repeated with cell free samples.

4.2.7 Normalizing with cell count and cell viability assays.

The mean cell count was normalised to the cell viability to take into account apoptotic cells with intact membranes but not metabolically active.[235] The EFV intensity signal of the lysate was then normalised to the viable cell count, assumed to be representative of the viable cell population. This would indicate the amount of EFV per viable cell. T-tests were performed to assess if there was a significant difference in the EFV signal every 24 hours.

4.2.7.1 Cell counting

Preliminary data showed that EFV was found inside the NES cells after treatment (Figure 4.3). NES cells have a doubling time of ~24 hours, making it necessary to normalize to the cell count over 72 hours.[123] A higher cell number could also impact the amount of drug detected in the lysate fraction, as more cells would result in higher total intracellular volume. Cells were seeded onto six-well plates and following overnight adherence, were treated with EFV, repeating conditions 1 and 2 (section 4.2.6). Cells were counted manually at 24 hours, 48 hours, and 72 hours in triplicate using the Trypan Blue cell viability assay (Sigma Aldrich). Each condition consisted of three biological replicates which were seeded from three separate plates in triplicate. This resulted in a total of nine replicates in each condition in order to control for variation due to seeding density.

A t-test was performed between the re-treat and single treatment condition to assess whether the treatment schedule had an effect on the cell count. The mean values of each technical replicate were used for normalisation to cell viability, resulting in three replicates at each time point in each condition.

4.2.7.2 Cell viability

Following seeding onto six-well plates and overnight adherence, cells were treated with the predicted foetal plasma concentration (1.05 µg/ml) of EFV.[62,71,72,230] A control and vehicle control (0.05% DMSO) were prepared. Viability was assessed using an MTT assay for the re-treat and single treatment conditions. T-tests were performed between the treatment conditions to assess whether the schedule has an effect on the cell viability. The cell viability was then reported as a percentage of the control condition absorbance value (100% viability).

4.3 Results

4.3.1 Standard curve

Standard curves were created to ascertain whether a linear relationship between the signal intensity and EFV concentration exists. Supernatant and lysate fractious were spiked with known EFV concentrations. The final estimated injection amount ranged from 9.7 pg – 40 ng. Intensity and concentration values were logged to more easily visualise the results. Both lysate and media extraction curves showed linearity over the range of EFV amount injected (Figure 4.1) with an average raw intensity of 1.14 $x10^3$ at the lower end. This indicated that intensities as low as 1.14 $x10^3$ could still be used to assess relative concentration when EFV was extracted in the presence of total cellular protein. The highest raw intensity detected that was still in the linear range was 2.3 $x10^7$.

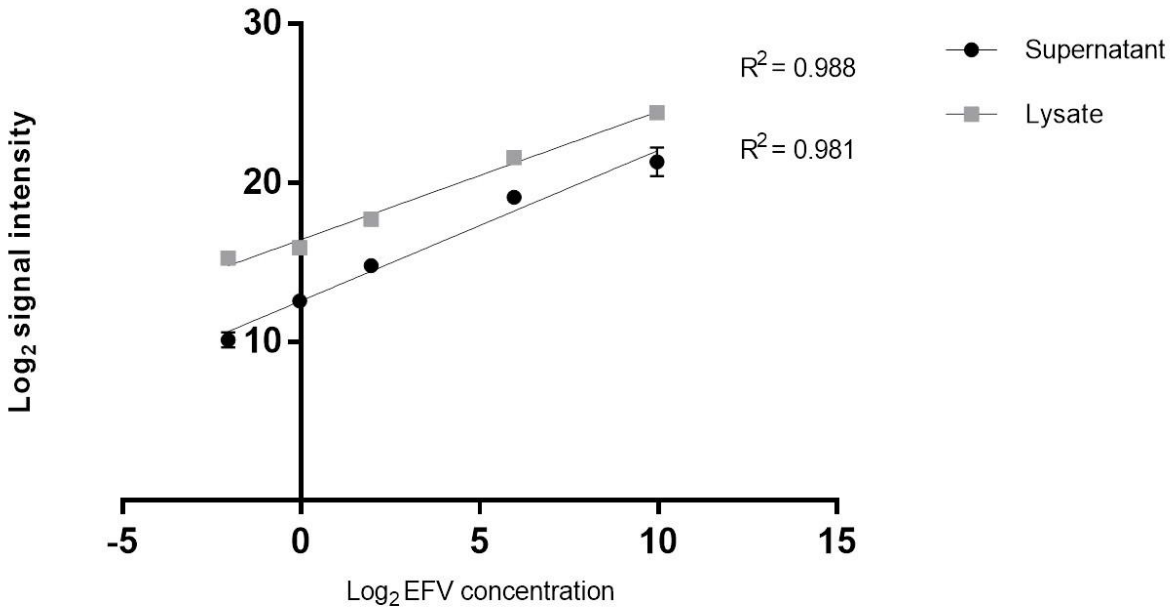

Figure 4.1: Standard curve of EFV extracted from spiked lysate and supernatant. EFV was spiked in a range of concentrations from 1 to 0.03125 µg/ml with a final injected amount estimated to be between 9.7 pg – 40 ng. Raw intensity values and concentration values were log_2 transformed for ease of visualisation. The EFV concentration range displayed a linear relationship with signal intensity.

4.3.2 DMSO viability assay

The control condition absorbance value was set as 100% cell viability. NES cells showed statistically significant sensitivity to DMSO from 0.25%. Cell viability was not affected at 0.05% (Figure 4.2).

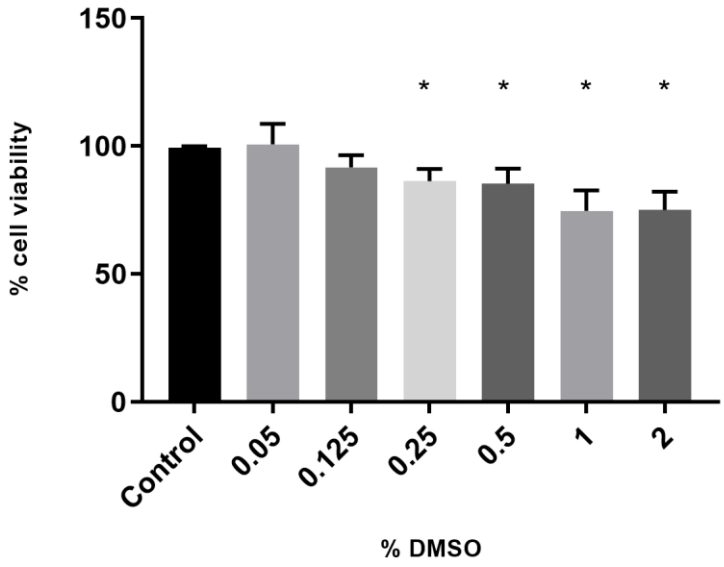

Figure 4.2: DMSO dose response in NES cells. NES cells were treated with DMSO at varying concentrations. Cell viability showed a slight but insignificant decrease at 0.125% DMSO. At 2% DMSO, there was 30% decrease in cell viability. The * indicates a significant ($p < 0.05$) decrease in the cell viability compared to the control after 24 hours. The final concentration of DMSO used during EFV treatment (0.05%) did not have a significant effect on cell viability.

4.3.3 Internalisation of EFV by NES cells over 24 hours

NES cells were treated with 0.525, 1.05, and 2.1 µg/ml of EFV to determine whether EFV was internalized by the NES cells after 24 hours. In all cases, EFV was detected in both the supernatant and cell lysate fractions. When treated with 0.525 µg/ml, the lysate to supernatant ratio was 0.18. The lysates to supernatant ratios of the higher treatment concentrations of 1.05 and 2.1 µg/ml were 0.12 and 0.11, respectively (Figure 4.3 and table 4.1).

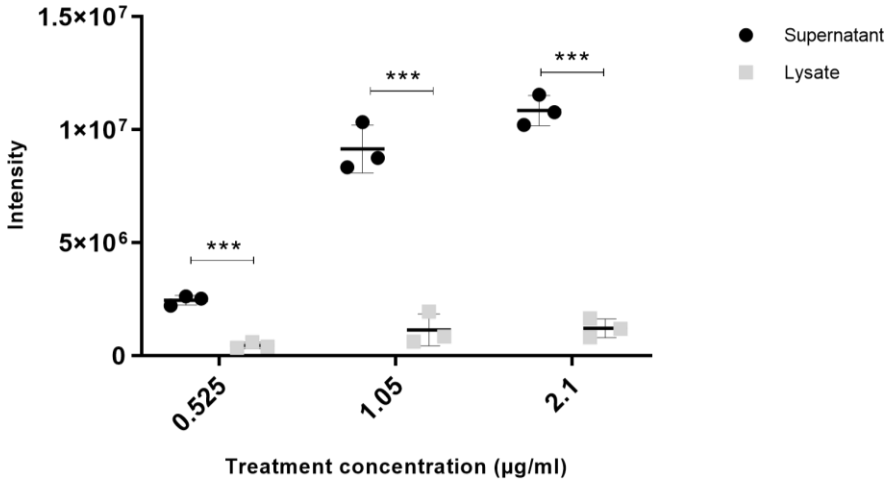

Figure 4.3: Assessment of internalisation of EFV by NES cells. NES cells were treated with increasing concentrations of EFV. Detection of EFV in the lysate indicated that EFV was potentially able to cross the cell membrane. *** indicate significant values of $p < 0.0001$.

Table 4.1 Lysate to supernatant ratio of EFV

EFV concentration (µg/ml)	Lysate to supernatant ratio
0.0525	0.18
1.05	0.12
2.1	0.11

4.3.4 Relative concentration of EFV over three days

EFV was extracted at 24, 48, and 72 hours from both the cell lysate and the media supernatant. EFV was also extracted from a cell free control. Each day, a T0 sample was created as a control for extraction and detection efficiency. All replicates had acceptable CV values (CV < 20%) as suggested by the FDA.[195]

4.3.4.1 Cell free control

Re-treatment: The signal intensity increased significantly with each subsequent treatment. From 24 to 48 hours there was a 1.8-fold change ($p = 0.005$) and from 48 to 72 hours there was a 2.7-fold change ($p = 0.001$).

Single treatment: There was a -0.19-fold change in signal intensity between 24 and 48 hours ($p = 0.0002$), and a -0.2-fold change between 48 and 72 hours ($p = 0.0006$).

T0: The T0 samples were not significantly different between 24 and 48 hours, and between 48 and 72 hours. Between the samples prepared at 24 and 72 hours, there was -0.5 fold change ($p = 0.023$).

The first set of samples processed at 24 hours contained two conditions that had been treated 24 hours before, and one condition that had been spiked with an equivalent amount immediately before processing (T0). The signal intensity between these three conditions was not found to be significantly different (Figure 4.4).

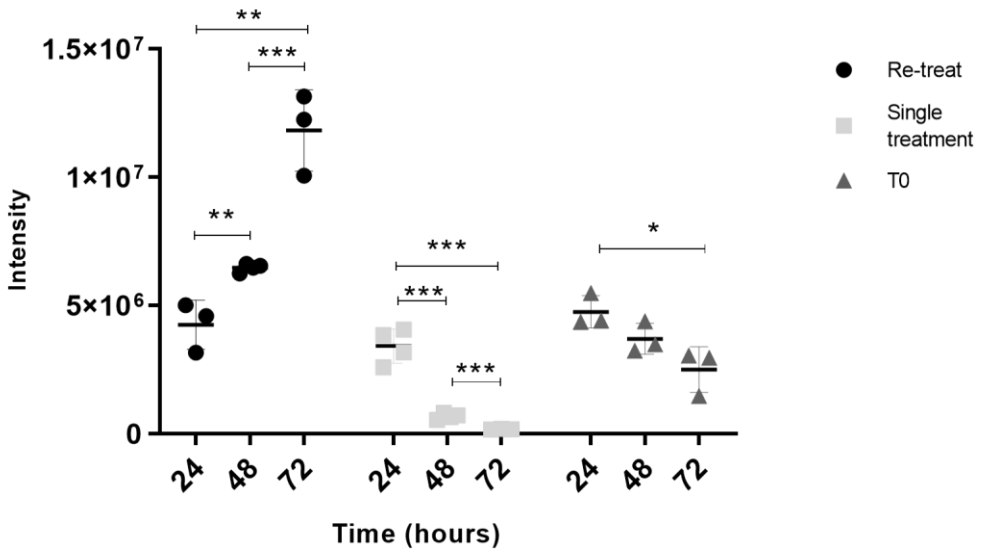

Figure 4.4: Relative intensity of EFV over 72 hours in cell free media. Cell free samples were treated according to the treatment schedules. In the re-treat condition, EFV concentration increased significantly with each successive treatment as EFV degradation was not caused by the media or cell culture conditions. In the single treatment condition EFV concentration decreased significantly with each successive media change. Each successive T0 was not significantly different from the previous T0 sample. * indicates $p < 0.01$, ** indicates $p < 0.001$, *** indicates $p < 0.0001$.

4.3.4.2 Supernatant:

After 24 hours the supernatant for the two conditions (re-treatment and single treatment) had EFV signal intensity values that were not significantly different from each other ($p > 0.05$), as expected. When compared to the T0 sample prepared at 24 hours, the signal intensity was not significantly different. In the re-treatment condition there was a 1.3-fold change in the relative intensity of EFV between 24 and 48 hours ($p = 0.01$), and a -0.6-fold change between 48 and 72 hours ($p = 0.0001$). After 72 hours, the signal intensity was 0.66-fold lower than the T0 samples ($p = 0.01$). The single treatment condition showed a -0.13-fold change in relative EFV intensity between 24 and 48 hours ($p=0.0007$), and a -0.22-fold change between 48 and 72 hours ($p = 0.0029$) (Figure 4.5).

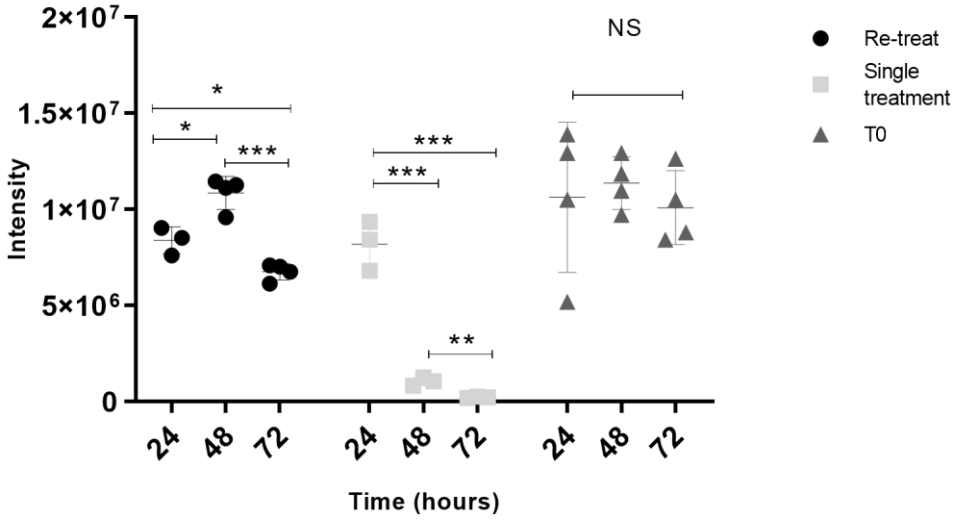

Figure 4.5: EFV relative intensity over 72 hours in the supernatant. Cells were plated and treated according to the treatment schedules. In the re-treat condition, EFV intensity significantly increased and subsequently decreased significantly by 72 hours. In the single treatment condition the EFV relative intensity decreased with each successive media change. T0 replicates were not found to be significantly different from each other. The signal intensity at T0 was not found to be significantly different to the signal intensity measured at 24 hours in both conditions. * indicates $p < 0.01$, ** indicates $p < 0.001$, *** indicates $p < 0.0001$.

4.3.5 Normalizing intensity data

4.3.5.1 Cell counting

As cell counting is variable by nature, a total of nine replicates were used to estimate an average cell count each day in both treatment conditions. There was no significant difference in the growth between the re-treatment and single treatment conditions (Supplementary Figure S1).

4.3.5.2 Viability assays

Treatment with the predicted foetal plasma concentration resulted in a slight decrease (9%) in cell viability although this was not statistically significant. In all four conditions, conversion of the MTT reagent into formazan crystals (indicating viability) increased after 48 hours, and then decreased after 72 hours (Figure 4.6). This trend was observed in repeat experiments (data not shown).

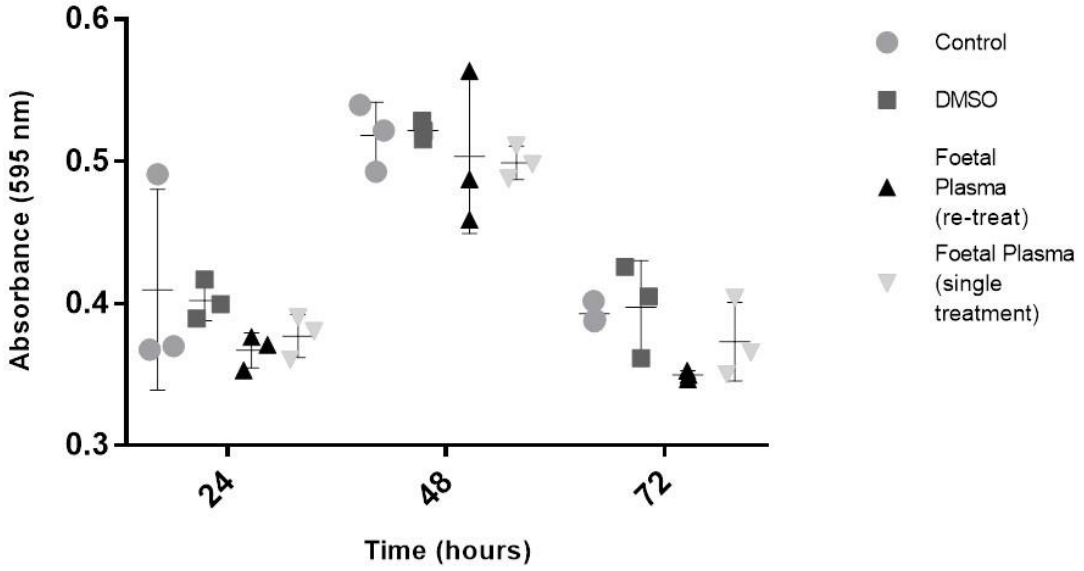

Figure 4.6: Cell viability assay. Viability of NES cells was assessed by an MTT assay when exposed to the estimated biologically relevant concentration of EFV (1.05 µg/m) over 72 hours. The DMSO condition contained 0.05% DMSO (vehicle control). There was no significant difference between the four conditions. In all conditions, there was a significant increase in cell viability (inferred by metabolism) at 48 hours, and a subsequent significant decrease at 72 hours.

4.5.5.3 Viable cell count

Once normalised, the viable cell count between the two treatment conditions were not significantly different (Figure 4.7).

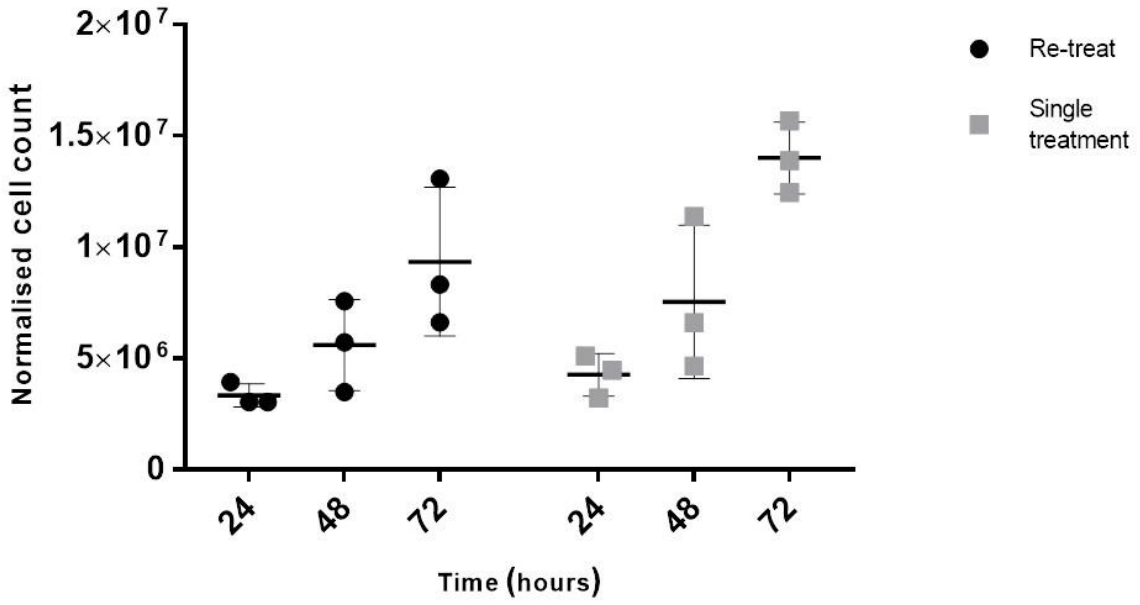

Figure 4.7: Cell count normalised to cell viability data. When the cell count was normalised to the cell viability data, there was no significant difference in the viable cell count between the two treatment schedules.

4.3.6 Normalised lysate intensity values

The cell lysate intensity values were normalised to the viable cell count. This value represents the relative concentration of EFV per cell (figure 4.8).

Re-treatment: When normalized to viable cell count, there was a 2-fold increase in the signal intensity of the cell lysate of re-treatment condition between 24 and 48 hours ($p = 0.014$), and then decreased -2- fold between 48 and 72 hours ($p = 0.0017$). The relative EFV concentrations at 24 and 72 hours were not significantly different from each other ($p = 0.504$).

Single treatment: After normalisation, intensity values decreased -0.3-fold between 24 and 48 hours (p = 0.0051), and then a further -0.5-fold decrease from 48 to 72 hours (p = 0.025). Lysate to supernatant ratios of EFV increased roughly 2-fold every 24 hours. An accumulation of EFV was detected *in vivo* over a period of eight days or five weeks (Table 4.2).

Table 4.2: Comparison of *in vitro* lysate to supernatant ratio to *in vivo* tissue to plasma ratio

Time	Lysate to supernatant ratio in NES cell culture	Tissue to plasma ratio *in vivo*	
24 hours	0.0064	**Macaque**	3.7 ([172])
48 hours	0.0116	**Rodent**	9.5 ([236])
72 hours	0.0204	**Macaque**	12.7 ([172])

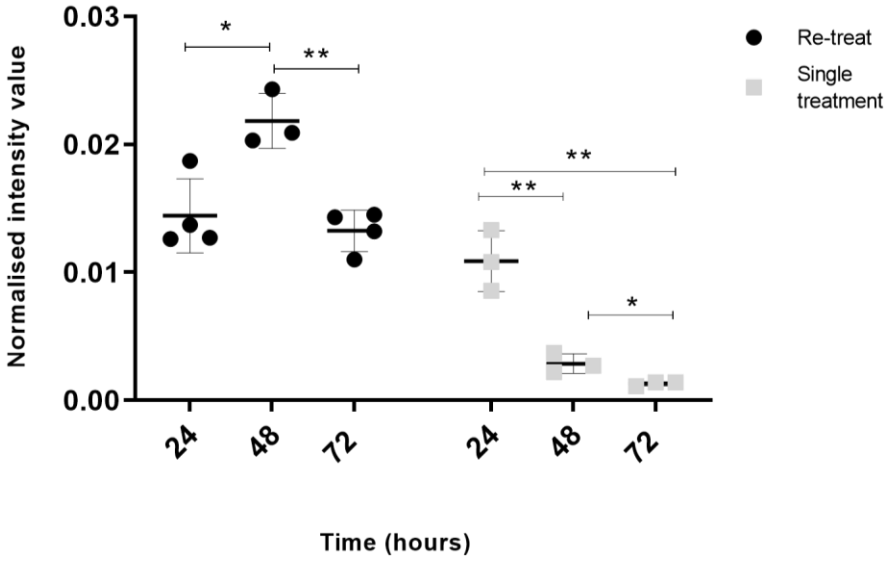

Figure 4.8: EFV relative intensity over 72 hours in the cell lysate. Signal intensity values were normalised to the viable cell count. The EFV signal intensity in the re-treatment condition increased significantly between 24 and 48 hours, and subsequently decreased significantly between 48 and 72 hours. The signal intensity decreased significantly with each subsequent media change in the single treatment condition. * indicates $p < 0.01$, ** indicates $p < 0.001$, *** indicates $p < 0.0001$.

4.4 Discussion

4.4.1 Standard curves

To create a treatment schedule of EFV in the *in vitro* NES cell culture model, an understanding of the movement and degradation of the drug both in media and when exposed to cells was required. In this work, it was adequate to measure the relative quantity of EFV between days. SRM assays are highly sensitive, and can quantify purified analytes at amounts as low as 0.2-2 fmol.[237] The TSQ Vantage has a linear dynamic range in excess of four orders of magnitude, making it a useful tool for drug detection assays in more complex mixtures.[238] The standard curves for both media and lysate spiked with EFV showed linearity when measuring intensity over spiked drug amount from 9.7 pg to 40 ng. Observing linearity at the lower end was important as is improved the chance of the measured values falling within the linear range. It was hypothesised the concentration of EFV within the cells would be on the lower end, as the cell density and small intracellular volume would not sequester a large fraction of the EFV (assuming passive diffusion into the cells). Linearity at the lower end would therefore allow the relative concentration to be inferred even in cell lysates with very low concentrations of EFV.

4.4.2 DMSO viability assay

Contrary to findings in SHSY-5Y cell lines, DMSO appeared to cause a decrease in NES cell viability in concentrations below 0.5%. SHSY-5Y is an immortalised cell line derived from a tumorigenic neuroblastoma, which may alter the response to various insults. The NES cells used in this work are non-immortalised human foetal derived cells. Their origin may make them more susceptible to DMSO compared to tumour derived cell lines.

4.4.3 Drug internalisation

Prior to treatment it was necessary to establish if EFV was able to enter the cells, as lack of detectable intracellular EFV would suggest active excretion, effective metabolism, or inability to enter this particular cell type. With increasing concentrations of EFV, the ratio of EFV found in the cell lysate when compared to the supernatant decreased (Figure 4.3, table 4.1). In a study modelling the movement and transportation of EFV in plasma using the "inverse" Michaelis-Menton equation, it was suggested that EFV transport diffusion movement was mostly passive.[239] The model also predicted that when the concentration increased in a volumetric space, the collective movement of the particles would initially increase and then decrease when approaching equilibrium, as passive transport is dependent on a concentration gradient.[212] According to these findings, EFV may move mostly via passive diffusion in the CNS, with higher concentrations moving into the CNS and neural tissue immediately after the initial treatments which may account for rapid CNS side effects.[240]

4.4.4 Relative concentrations of EFV over three days

The raw intensity values of both the lysate and supernatant were found to fall within the linear range of the standard curve. This indicated that an increase in the intensity value was proportional to an increase in the concentration, allowing for inferences about the concentration to be made from the signal intensity.

4.4.4.1 Supernatant

Re-treatment: The relative concentration in the re-treat and the single treatment conditions were equivalent 24 hours post treatment, which is expected as at this point the conditions were exactly the same. When compared to the T0 sample that was spiked with EFV immediately before processing, there was no significant difference in the intensity values. This also occurred in the cell free control. This indicates that after 24 hours in NES culture media EFV is not significantly degraded by the culture conditions (Figure 4.4). It also indicates that EFV is not significantly metabolised by the cells after 24

hours (Figure 4.5). The T0 sample prepared at 72 hours was significantly lower than the samples prepared at 24 hours. Over the 72 hours the signal intensity of T0 followed a downward trend. This was not seen in repeat experiments and in subsequent MS analysis indicating that it was not a MS technical variation. It was therefore attributed to experimenter error.

After 48 hours, the EFV relative concentration increased, and subsequently decreased significantly after 72 hours. The relative concentration at 72 hours was lower than the T0 sample, indicating that degradation of EFV had occurred. In order to determine whether this was due to degradation caused by culture conditions or degradation due to metabolism, the relative concentration trend of the supernatant was compared to that of the cell-free re-treatment condition. When there were no cells present, the relative EFV concentration increased every 24 hours with re-treatment. When cells were present, the relative intensity followed the same increasing trend for the first 48 hours, and then decreased significantly (Figure 4.4 and 4.5). EFV is known to activate the transcription of the cytochrome CYP2B6, thus inducing its own metabolism.[48] EFV is most likely being metabolised by CYPB26, as the secondary cytochromes that metabolise EFV have not been found in neuronal cells, whereas CYP2B6 has.[226] The significant decrease observed at 72 hours may be due to the accumulation of EFV and the subsequent up-regulation of its metabolism. In mice, CYP2B6 activation increased 4-fold during extended treatment compared to short term treatment indicating that as EFV levels increase, a concurrent increase of CYP2B6 occurs and the metabolism of EFV increases.[229]

Single treatment: EFV was detected in the supernatant up to 72 hours post treatment, subsequent to two drug free media changes. Passive diffusion of EFV from within the cells could not account for the relatively high concentration remaining in the supernatant. Rather, upon inspection of the cell free single treatment control, a similar trend is observed leading to the following hypothesis:

EFV is a highly lipophilic molecule, allowing it to diffuse easily into the brain tissue which is made up of roughly 60% fatty acids.[241] High CNS penetrance of ARVs is a desired characteristic as it is associated with improved viral suppression in the CSF.[242] In order to maintain cell adhesion in culture, the growth surface of disposable polystyrene plates are treated to become more hydrophilic.[243] The sides walls of the dish are not treated for cell growth, thus it is possible that the lipophilic EFV molecule would be strongly attracted to the hydrophobic areas of the plastic, creating a large reservoir of EFV which diffuses back into fresh drug free media even after two instances of complete media removal and PBS washes. A

reservoir of EFV as seen in the single treatment condition may also contribute to the accumulation of EFV in the cell free re-treat condition.

4.4.4.2 Normalisation of lysate signal intensity to viable cell count

Cell counting: In biological systems, contact inhibition is the means by which cells stop growing or proliferating when they come into contact with other cells. This process is important for organ development as well as general tissue and muscle health. Aberrations in this process lead to cancer or tumorigenesis.[244] In neuronal cell culture, contact inhibition regulates mitosis in non-transformed cell lines, inhibiting proliferation and initiating apoptosis. Dead cells were found to inhibit further proliferation, and removal of dead cells resulted in an increase in proliferation.[245] Pavel et al. (2018)[244] found that high density cell culture resulted in a decrease in autophagy and an increase in apoptosis, leading to a reduction in overall cell viability. During apoptosis, the cell membrane stays intact while the organelles begin to disintegrate.[235] The mitochondria become compromised through the intrinsic or mitochondrial pathway, which is a main process in apoptosis.[235] In cell culture macrophages or microglia are often not present, meaning that apoptotic cells are not engulfed and can remain within the population of live cells. In this work cell counting was performed by using a dye exclusion method, whereby the dye used is unable cross an intact cell membrane. Apoptotic cells maintain an intact membrane, which may have given false inflated readings for live cell count.[246]

Cell viability: An MTT assay assesses the viability of the cells based on mitochondrial function. As cell density increases, apoptosis increases, and mitochondria begin to disintegrate, leading to decreasing viability.[235,244] Due to the cell membrane staying intact, the cell count does not decrease proportionally to the viability reading of the culture. When testing multiple treatment concentrations as well as control and vehicle control conditions, the same trend was observed whereby the viability initially increased between 24 and 48 hours, and then decreased between 48 and 72 hours. This supports the idea that at high density, regardless of the treatment conditions, there was a decrease in viability which was likely caused by apoptosis.[244]

By normalising the cell count data to the cell viability, an estimate of the number of viable cells can be attained. This normalised count is referred to as the viable cell count. Supernatant values were not normalised to the viable cell count, as the intracellular volume was not considered likely to affect the supernatant volume. Although the volume of the NES cells has not been established, based on the

average volume of fibroblasts and osteoblasts (2-4 pL respectively), even after 72 hours, the cell count would not be high enough for the intracellular volume to significantly impact supernatant volume.

4.4.4.3 Lysate:

Re-treatment: When normalised to the viable cell count, the relative concentration of EFV followed the same trend as observed in the supernatant whereby there was an initial increase after 48 hours, followed by a significant decrease after 72 hours. The hypothesis that an accumulation of EFV resulted in an increased metabolism of the drug between 48 and 72 hours can also be applied based on the trend of cell lysate relative concentration.

When normalising to the viable cell count, the relative concentration of EFV decreases after 48 hours, indicating that there is less EFV present per cell after 72 hours (Figure 4.8). Based on diffusion and transport studies, EFV is transported passively across a concentration gradient.[212] If CYP2B6 activity is induced by EFV accumulation, then the rate of metabolism of EFV would increase, resulting in a lower intracellular concentration (Figure 4.5).

This work aims to model the exposure of NES cells to EFV. Although somewhat simplistic, one can compare the tissue to plasma ratio to the lysate to supernatant ratio of EFV. EFV is predicted to accumulate *in vivo* due to its high lipophilicity. This was confirmed in rat and macaque studies, whereby the tissue to plasma ratio ranged from 3.7 – 12.7.[172]

Similarly, when re-treated with EFV over 72 hours, the lysate to supernatant ratio essentially doubles with each re-treatment (Table 4.2). More data would be needed in order to determine whether EFV accumulates in the cells in a time dependent manner or simply a concentration dependent manner, but at first sight, the data presented here would support the hypothesis that passive transport across the cell membrane is rate limiting and that true equilibrium may not have been achieved in a 24 hour period.

Based on these findings, it appears that once EFV accumulates, it induces its own metabolism. It is important to note that this only occurs more than 48 hours post treatment. This indicates that in order to understand the more global cellular response to EFV, data needs to be collected prior to and subsequent to the initiation of the metabolism of the drug. Short term studies investigating the effects

of EFV over 24 hours or less may not determine a true biological response to EFV over time as metabolism has not been initiated at that point.[120,121]

Single treatment: Relative EFV concentration in the cell lysate followed the same trend before and after normalisation. In both cases, EFV concentration showed a significant decrease after the first media change and decreased again after the second media change. EFV was still detected in the lysate even after two washes, supporting the hypothesis of the culture vessel plastic acting as an EFV reservoir. The trend observed in the single-treatment lysate and supernatant followed the same trend as the cell free control. It is possible that at such low concentrations, the number of viable cells present did not affect the passive diffusion of EFV. Modelling of EFV transport found that at concentrations lower than 0.97 µg/ml, EFV passive movement is increased, and the drug can move in and out of the system with ease.[212] Based on this, it is possible that EFV is still detected even with extremely low supernatant concentrations due to increased passive diffusion into the cells.

4.5 Conclusion

The aim of this chapter was to assess the movement and degradation of EFV in NES cell culture conditions. Establishing whether EFV was being degraded by the conditions and/or metabolised by the cells was necessary to attempt to mimic the *in vivo* conditions of exposure in a developing neural system. The plastic cell culture dishes appeared to act as a reservoir of EFV which, although assumed to be fairly consistent across conditions, may have caused the model to be less biologically relevant. EFV was able to enter the NES cells, most probably by passive diffusion.[212,239] The stability of EFV was not significantly affected in cell-free cell culture conditions, indicating that the media did not cause degradation of the cells. A decrease in the relative EFV concentration in cell containing conditions was therefore most probably due to EFV inducing its own metabolism by CYP2B6 in the NES cells once reaching a threshold concentration.[224,226,228,247] Interestingly, the ratio of lysate to supernatant (as a rudimentary proxy for tissue to plasma ratio) was found to increase over time but not with an increasing concentration at a single time point. *In vivo,* EFV does indeed accumulate in the CNS tissue over time and is potentially underestimated when using CSF concentration as an approximation.[172,236]

This chapter indicated that a 24 hour re-treatment schedule was sufficient to use as an initial model for foetal neural exposure to EFV, as the drug was metabolised by the cells and not degraded by the cell culture conditions. Metabolism of EFV appeared to be initiated at least 48 hours post EFV treatment, indicating the necessity for longer term studies.

These data implied that there was a biologically relevant interaction between the cells and the drug, as opposed to the cells being exposed to an un-metabolised form of EFV, increasing every 24 hours.

4.6 Summary

The preceding three chapters aimed to develop a biologically relevant treatment schedule of EFV in NES cell culture in order to approximate the exposure of foetal neural progenitor cells to EFV *in utero.* Human derived NES cells were used in this work, which require specialised stem cell culture techniques. This cell type has also not been extensively researched. It was therefore important to assess the movement and degradation of EFV in these specific cell culture conditions. Prior to working with EFV in cell culture, a method of EFV detection using targeted MS was created. The optimal detection of neat EFV (99.4% purity) was in 50% ACN, in negative ionisation mode. A targeted SRM assay was developed, resulting in a target list containing five transitions, each optimised for collision energy. Once the assay was established, a standard curve was created for neat EFV in ACN in order to confirm that signal intensity and concentration showed a linear relationship over a concentration range.

Following detection optimisation, a method for EFV extraction from the cell culture was optimised. This was performed for both the lysate and the media fractions. ACN protein precipitation was selected as the extraction technique for subsequent experiments. The extraction method was further optimised in order to decrease variation between inter-sample and inter-day processing. Various other optimisation steps were performed to improve the detection of EFV, including gradient optimisation and sample concentration prior to MS analysis.

Once the detection and extraction of EFV was optimised, a standard curve was created using lysate and supernatant fractions spiked with EFV. This determined that the concentration and intensity has a linear relationship over a concentration range when EFV was extracted from a complex mixture. Further experiments were then performed to gain insight into the behaviour of EFV within the cell culture conditions. From this it was determined that EFV was able to enter NES cells, that it was metabolised by the cells, and that it was not degraded by the cell culture conditions. The estimated biologically relevant concentration of EFV and the concentration of the drug delivery vehicle did not cause a significant decrease in the cell count or the cell viability.

Based on the overall findings of these method development chapters, future experiments modelling the exposure of NES cells to EFV *in utero* were conducted as follows: After adhering to tissue culture plates overnight, NES cells were treated with 1.05 µg/ml of EFV in 0.05% DMSO. Every 24 hours, the media was removed and replaced with new media containing freshly spiked EFV (1.05 µg/ml).

4.5.1 Future work and limitations

The limitations acknowledged in this work indicate the necessary steps to further optimise the drug detection assay as well as to better model neural progenitor exposure to EFV *in utero*.

4.5.1.2 Decreasing variability between samples

Multiple attempts were made to decrease the inter-sample and inter-day variability. Although this was somewhat achieved, future work should include an internal standard that can be used to normalise intensity values. Larger sample starting volume and more replicates would serve to decrease variation.

4.5.1.3 Improvement of processing techniques

Variability between samples may have also been due to the manual processing of multiple samples per day, as well as the unavoidable multiple transfer steps during processing. An automated drug extraction technique or one that can be performed with fewer transfer steps would ensure more reliable and accurate results, mitigating human error and differential sample loss during processing.

4.5.1.4 Assessing the effect of the EFV reservoir

Based on this work it appears that EFV is absorbed into the untreated sides of the plastic cell culture dishes. With appropriate controls this may not have affected the comparative ability of the assay within these particular conditions, although it may cause the assay to be less biologically relevant. Future work could further elucidate whether the resultant reservoir of EFV diffusing into the media and cells affects the biological inference. This may necessitate optimisation of the cell culture conditions in order to mitigate the effect of the plastic absorption of EFV.

4.5.1.5 Detection of metabolites to validate assumptions

Based on the literature and the findings in this work, it is assumed that EFV activates its metabolism by the cytochrome CYP2B6. MS analysis can be used to detect various metabolites of EFV, which can clarify if EFV is indeed being metabolised by the cells. Metabolite analysis can also give insight into whether EFV is only metabolised by CYP2B6 in neural cells, or whether other secondary cytochromes also play a role in the CNS metabolism of EFV.

Chapter 5: Proteomic analysis of the effects of EFV in NES cells over 72 hours.

5.1 Introduction

The FDC consisting of EFV, FTC, and TFV is prescribed to pregnant, HIV-positive women in South Africa regardless of their CD4+ cell count and stage of pregnancy.[37,248] EFV is classified as a category D drug (positive evidence of foetal risk); case studies and animal studies suggest that EFV exposure may cause CNS malformations including incomplete neural tube closure (encephalocoele), myelomeningocele, craniofacial malformations such as cleft palate, and increased risk of spontaneous abortion.[76,78–81,249] Despite these findings, based on the small number of case studies and few small cohort studies, EFV exposure during pregnancy is not considered to be associated with an increased risk for CNS malformations or neurologic deficits, and is therefore used as a first line treatment for HIV-positive pregnant women.[91,250,251]

The protection that the ARV treatment affords a child born to an HIV-positive mother is invaluable, allowing the child to live a healthy, HIV-free life. Recently there have been reports of HEU children showing subtle neurological deficits, although not potentially fatal or as debilitating as the malformations such as encephalocoele or myelomeningocele, neurological deficits can affect HEU children throughout their lives, from school age to adulthood. Deficits in areas such as mental cognition, mathematic ability, verbal IQ, full scale IQ, memory, and language expression have been noted in cohort studies that follow HEU children longitudinally as opposed to a single assessment for malformations at birth.[99,106,116,252] Assessment of the effects of EFV during development is important as some skills only develop as the child ages. Some neurocognitive deficits, for example those due to early brain injury in pre-term births, can be diminished over time due to plasticity, or can only be detected at old age due to a vulnerability to neurodegeneration (the sleeper effect).[253] Exposure to toxic compounds such as EFV during early neurodevelopment may cause deficits that are not detectable upon birth, but rather emerge at a later stage affecting plasticity or causing a vulnerability to insult.[253] Thus, the potential effects of EFV on HEU children is an important public health issue that needs to be addressed. Currently, the neurocognitive deficits seen in HEU children are attributed to perinatal HIV exposure,[97] perinatal ARV exposure,[85,254] poor

maternal health,[113,114] or poor socioeconomic background.[113,114] In adults, the effects of EFV are well documented at a systemic level and in the CNS as a whole, but not on a molecular level. Characterization of the effects of EFV on foetal neural development is also lacking. The present study aims to elucidate the effect of EFV on developing neurons by treating human foetal- derived NES cells with estimated biologically relevant concentrations of EFV. Animal models are time consuming and expensive, making cell models appealing for initial discovery work. The human-derived NES cells used in this work offer a more biologically relevant model than cell lines with a tumorigenic background.[255]

Changes in the proteome caused by EFV treatment in NES cells can be characterised with MS. By using discovery proteomics, one can create a systematic snapshot in time of all the proteins within a biological network. Discovery proteomics aims to identify all the proteins within the system, post-translational modifications, protein localisation, protein interactions, and protein turnover.[127] The proteome is used to characterise the global molecular effects of EFV on NES cells when treated at an estimated biologically relevant concentration of 1.05 µg/mL. The treatment schedule for this experiment was determined by previous empirical evidence (Chapters 2-4). In an HIV-free experimental system, the potential effects of EFV on neurocognitive function during foetal neural development and in the postnatal CNS can be determined. This could lead to a broader understanding of HEU children and highlight the need for further studies and early intervention strategies. Characterising the molecular effects of EFV in neural cells may also be used to direct future research regarding adults suffering from persistent HAND or CNS side effects while on ARV treatment containing EFV. As a recommended first line constituent of combination treatment prescribed to HIV-positive patients in South Africa, gaining insights into the global cell-wide changes in the CNS may indicate a direction for future investigations into the safety profile of EFV.

5.2 Materials and methods

5.2.1 Sample preparation for MS

5.2.1.1 Cell culture and treatment of NES cells

NES cells were cultured according to the method described in chapter 4, section 4.2.1 and 4.2.2 in 6 cm dishes (TPP). Prior to plating, cells were counted using Trypan blue in order to ensure consistent seeding numbers across replicates. Cells were seeded with $4x10^4$ cells/cm^2 and allowed to adhere to the plates overnight (12 hours), followed by treatment with 0.05% DMSO (vehicle only control) or 1.05 µg/mL EFV in 0.05% DMSO (EFV treatment). Media was changed every 24 hours and replaced with fresh media either containing DMSO only (0.05%) for the control or EFV (1.05 µg/mL) for the treated condition, according to the treatment schedule determined in chapter 4.

5.2.1.2 Cell harvesting and lysis

After overnight adherence, five replicates were harvested (T0). Following the initiation of treatment, five replicates from the control and treated conditions were harvested every 24 hours, up to 72 hours. Cell pellets were snap-frozen in liquid nitrogen and stored at -80^{o}C. The sample lysis and digestion was performed following the method described in Jersie-Christensen, Abida, and Jesper (2016) with minor alterations.[256] Lysis buffer made up of 6 M guanidinium hydrochloride (GuHCl, Sigma Aldrich) in 100 mM Tris–HCl (pH 8.5, Sigma Aldrich) was heated to 90^{o}C before the addition of 200 µl to each replicate. Samples were heated to 90^{o}C for 20 minutes followed by sonication for 20 minutes. Heating and sonication was repeated for five rounds or until the lysate was clarified.

5.2.1.3 Protein quantitation

To ensure equivalent loading of peptide onto the column for MS analysis, the protein quantity was determined using the bicinchoninic acid assay (BCA) with the Pierce BCA Protein Assay Kit (Thermo Scientific). A standard curve using bovine serum albumin in lysis buffer was made in flat-bottomed 96 well plates (Greiner). The standard curve and the samples were prepared in triplicate. The absorbance values were read by the iMark microplate reader (Biorad) at 565 nm and analysed by the Microplate Manager software.

5.2.1.4 Digest and clean up

The remaining sample lysates (190 µl) were reduced and alkylated with 5 mM tris(2-carboxyethyl)phosphine (TCEP, Sigma Aldrich) and 10 mM iodoacetamide (IAA, Sigma Aldrich), followed by incubation at room temperature for one hour. Samples were then pre-digested with LysC at an enzyme to protein ratio of 1:100 for one hour at room temperature with gentle rotation, followed by dilution to a final volume of 1 M GuHCl with 25 mM Tris–HCl pH 8.5. Trypsin was added at an enzyme to protein ratio of 1:50 and incubated for 18 hours in a wet chamber at 37^{o}C. Samples were acidified post digestion with FA to a final concentration of 1% (pH 2-3) and then spun at 15 000 x *g* for five minutes to pellet insoluble material.

The peptide solutions were desalted following the stop and go extraction method.[257] Tips were packed in-house with c18 discs (Empore SPE Disks,C18, 47 mm) and equilibrated with 80% ACN, 0.1% FA (solvent B). The tips were loaded with 10 µg of peptide and washed with 2% ACN, 0.1% FA (solvent A). The peptide solution was eluted into clean tapered glass auto sampler inserts with 60% ACN, 0.1% FA (solvent C) and dried in the SpeedyVac vacuum concentrator (no heat). The dried peptides were resuspended in solvent A to a final concentration of 250 and 500 ng/µl for MS analysis.

5.2.2 Instrument parameters

Protein quantitation ideally ensures that the protein amount is constant in all the samples, although it is possible that protein loss occurs during subsequent preparation steps. A short gradient pilot sample was injected onto a Q-Exactive Orbitrap-quadrupole hybrid coupled to a Dionex UltiMate 3500 RSLC Nano-LC system (both Thermo Scientific) to determine the correct concentration and volume necessary to achieve a TIC intensity of 4 – 5 x10^{9}. The sample injection volume and sample concentration was adjusted equally across all samples as they were processed in parallel and assumed to have incurred similar loss due to processing. In order to achieve an optimal TIC, 5 µl of 500 ng/µl (a total of 2.5 µg peptide) was loaded onto a 2 cm trap column (5 µm Luna c18 beads, 100 µm ID, pore size 100 Å, Phenomenex, packed in-house) in 98% solvent A and 2% solvent B. Peptide was then eluted onto a 30 cm reverse phase analytical column (3.6 µm Aeris c18 beads, 75 µm ID, pore size 100 Å, Phenomenex, packed in-house). Peptides eluted over a 120 minute slope gradient, whereby solvent B increased from 6 – 40% between 10 – 80 minutes (curve of gradient = 3), and then from 40 – 80% between 80 - 85 minutes (curve of gradient = 7). This was followed by an 80% washout for 15 minutes before equilibration at 2% for 20 minutes. A 60-minute wash was performed after each analysis of three consecutive samples. Samples were analysed in

a randomized order to mitigate any technical bias introduced by instrument performance over time. The data acquisition was performed in positive mode. MS1 spectra collection settings were as follows: resolution: 70 000, range: 300-1750 m/z, automatic gain control (AGC): 3 x10^5, maximum injection time: 250 milliseconds (ms). Precursor ions were selected for fragmentation by a Top10 data dependent selection method. The MS2 spectra collection settings were as follows: resolution: 17 500, range: 200 – 2000 m/z, AGC: 1 x10^5, maximum injection time: 80 ms, isolation window: 2 m/z, dynamic exclusion: 30 seconds, and normalized collision energy: 28.

5.2.3 Data analysis

5.2.3.1 Statistical analysis

Raw MS data were imported into MaxQuant (v. 1.5.3.12) for peak identification and quantitation. The default settings were used with the following alterations. "Match between runs" was selected to identify unsequenced or unidentified peptides based on their mass and retention time;[150] LFQ was selected; the UniProt Human proteome protein sequence FASTA file was uploaded for the Andromeda database search (downloaded 2018/02/07); LysC and trypsin were selected as the digestion mode; and the FDR rate was set to 0.01. Summary statistics of the MS data were performed by an R script developed by Karsten Krug (Proteome Center Tuebingen, University of Tuebingen, Germany).

The protein groups text output from MaxQuant was imported into Perseus software[258] for visualisation of the data. The data was filtered by removal of contaminants, reverse hits, and protein groups with less than one unique peptide. LFQ intensity values were $\log_2$ transformed to aid visualisation, and protein groups with peptides detected in less than three replicates out of five per condition were removed. Perseus software was used to assess the protein expression profiles between conditions and visualized with heat maps.

LFQ values were normalised to T0 in both the control and treated conditions. A Student's t-test was performed to assess significant differences between control and treated groups at each time point. A one way ANOVA was used to assess a difference in expression over time, within either treatment condition.

5.2.3.2 Biological inference

Biological inference was performed in a series of steps to narrow the list of proteins of interest from broad interaction networks to specific pathways. Protein groups were converted to their gene identifiers using the UniProt database.[259] Through the CRUNCH environment (developed by Shaun Garnett, University of Cape Town), a STRING-db interaction network was generated for significantly differently regulated genes in each time point. STRING-db provides functional association networks and is a useful scaffold for the initial visualisation of the dataset.[260] The significantly deregulated genes were imported into Reactome to further interrogate the data. Reactome provides mechanistic detail of the protein interactions and uses over-representation analysis to rate the enrichment of super pathways and sub pathways in the dataset.[261] The list of user input proteins is assessed for over-representation by comparing whether there is more annotation matched to a pathway than would be expected by chance. The number of proteins in the set, the number of proteins annotated to the pathway, and the number of proteins annotated from the whole Reactome database are used to create the over-representation probability score.[261] Pathway navigation can be visualized through whole tissue diagrams as well as at a protein-to-protein level. The genes contained within the top five most significantly enriched pathways were identified in the STRING-db interaction pathway, and the interaction partners were investigated in order to obtain a broader view of the significantly differentially regulated genes at each time point.

5.3 Results

5.3.1 MS runs

A 2 µl injection of both low (250 ng/µl) and high (500 ng/µl) concentration samples was assessed. Based on the TIC, the high concentration samples were used for MS analysis. A total of 2.5 µg peptide (5 µl) was injected and eluted over 90 minutes on a 120-minute gradient (Figure 5.1). The steep drop towards the end of the gradient was found to be a common feature when using GuHCl lysis and protein precipitation (Blackburn Laboratory, unpublished). Of the 35 samples that were analysed, the chromatograms of two indicated low peptide levels (Figure 5.2, a). These samples were re-analysed with a higher injection volume, but the TIC was still sub-optimal (Figure 5.2, b) and were subsequently discarded. The TIC should be comparable between samples to decrease variation due to technical reasons (lack of detection due to low peptide levels as opposed to not being present in the sample).

During the sample analysis, the chromatography spray was disrupted. Before and after the analysis of the experimental samples, reference samples of SH-SY5Y were analysed for quality control purposes. Figure 5.3 shows that the chromatography spray had improved subsequent to the loss and repair of the spray. This can be seen by sharper less “fuzzy” lines. Unfortunately, due to time limitations, the samples analysed before the spray was repaired were not re-analysed.

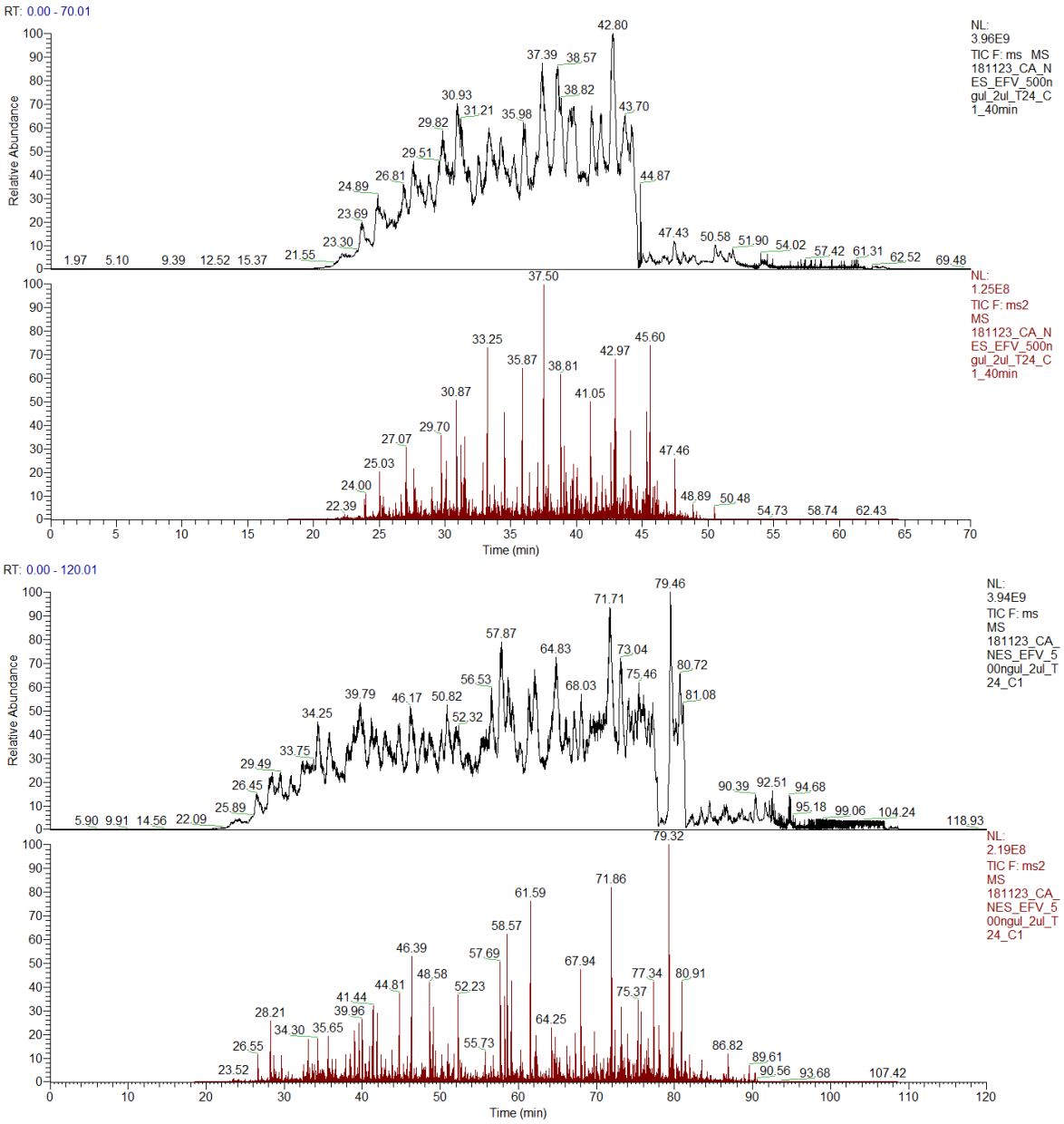

Figure 5.1: Optimisation of sample concentration and injection volume. **a)** The MS1 spectrum on a short, 70- minute gradient to determine the optimal injection volume. The TIC was 3.96 x10^9 with a 2 µl (1 µg) injection of the 500 ng/µl samples. **b)** The MS2 spectrum on the 70-minute gradient. **c)** The MS1 of an extended 120-minute gradient ensured optimal chromatography. The TIC was 4.74 x10^9 with a 5 µl (2.5 µg) injection of the 500 ng/µl samples. **d)** The MS2 spectrum on the 120-minute gradient

a)

b)

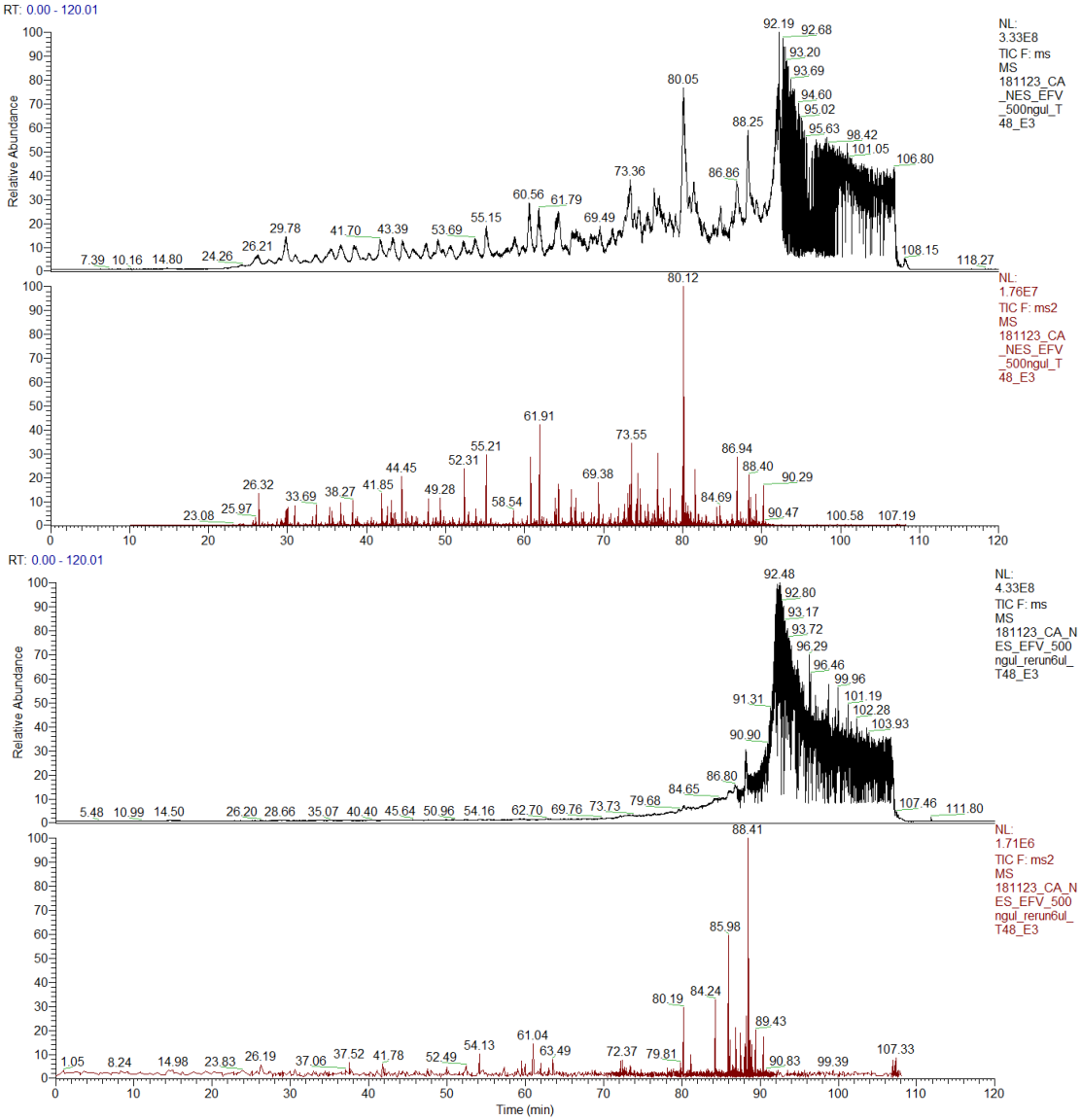

***Figure 5.2: Samples assessed for re-analysis*. a)** Low amount of peptide resulted in the chromatogram appearing low and flat, with limited MS2 detection compared to other samples. The TIC was 3.33 x10^8 due to the large peak at the end of the gradient. A similar peak was observed during wash samples and coincides with the high concentration of solvent B. Samples with low TIC were reanalysed. **b)** Samples were re-analysed with a 6 µl injection (3 µg). The flat TIC in MS1 (b) and in MS2 (c) indicates that there were very low levels of peptides left in the sample. These samples were subsequently discarded.

a)

b)

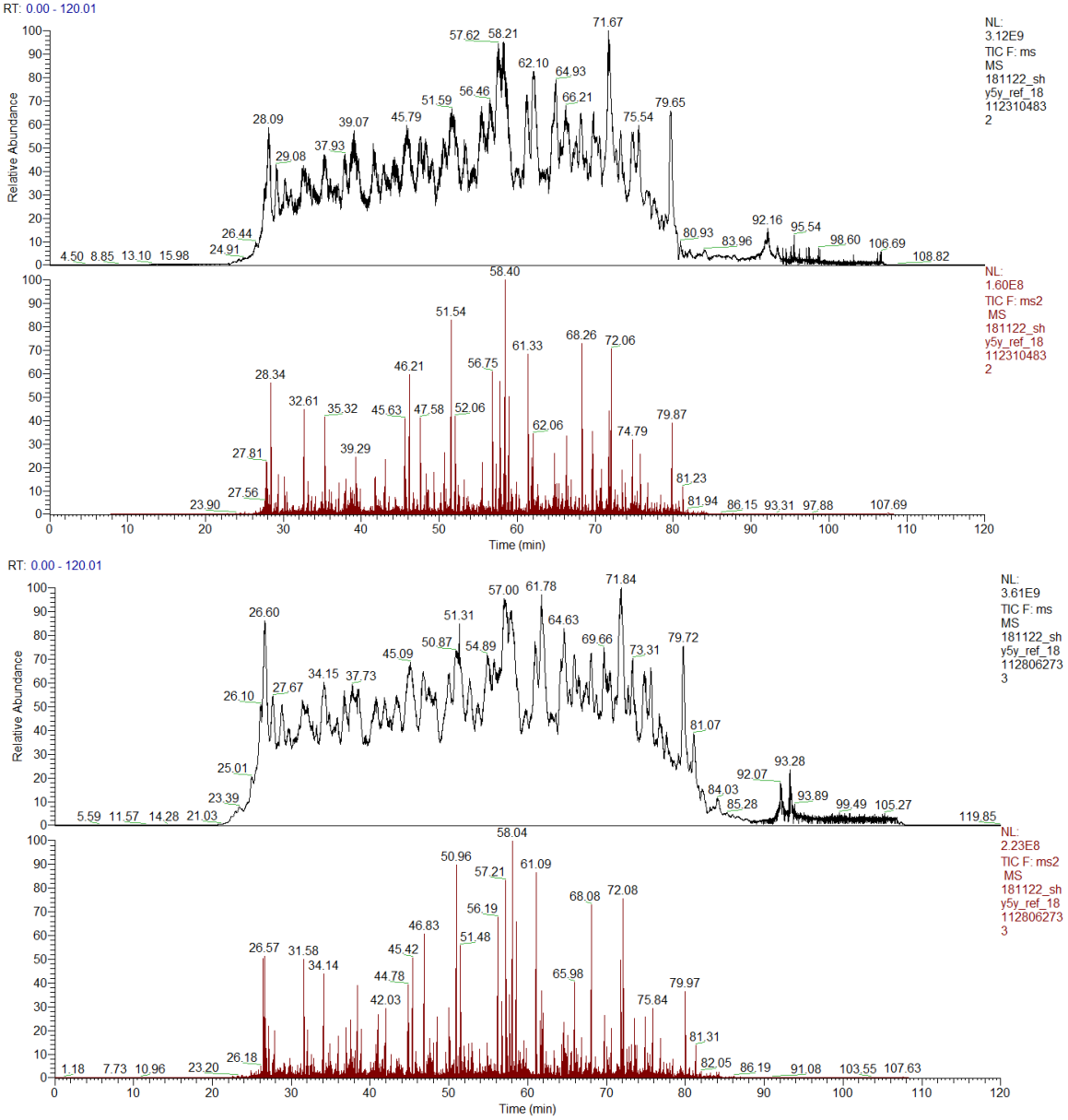

Figure 5.3: SH-SY5Y reference samples: a) Reference sample was analysed directly before the experimental samples. The spray at this point was considered acceptable. **b)** Reference sample analysed directly after the experimental samples (subsequent to repairing the spray). When comparing the two reference samples, the final reference sample had a sharper TIC than the initial reference, indicating an improved, stable spray. The TIC values of 3.12 x10^9 and 3.61 x10^9 respectively were similar between the two references

5.3.2 MaxQuant – data quality

A total of 286924 MS1 spectra and 1019253 MS2 spectra were detected across 35 samples. The Andromeda database search identified 1663 protein groups and 5844 peptides by MS2 spectrum to peptide matching. The digestion efficiency was indicated by the percentage of missed cleavages, 63.6% peptides with no missed cleavages, 29.7% with one, and 6.7% with two (Supplementary Figure S3). The MS2 identification for all samples was over 20%, which is considered acceptable (Supplementary Figure S4). The mass error was 0.8 +- 0.05 ppm in all samples analysed (Supplementary Figure S5).

5.3.3 Statistical analysis

5.3.3.1 Data visualisation

The protein groups text file was imported into Perseus for data visualisation. A total of 1663 protein groups were identified. After the data was filtered, 1332 protein groups remained. Scatter plots were used to assess the variation between samples, which was low (Pearson's correlation score > 0.95). The linearity indicates that proteomes were generally similar within treatment groups and between treatment groups (Supplementary Figure S6).

Hierarchical clustering showed very weak clustering between treatment groups. The clustering was not correlated to the order in which samples were run (data not shown). Hierarchical clustering performed with each treatment group separately tended to contain a mixture of T24 and T48 or T48 and T72. These results indicate that between control and treated groups the majority of the proteome remained unaltered at the time points analysed. Clustering of the replicates in the individual treatment groups indicated that the proteome changes were largely unaltered between 24 and 48 hours, and between 48 and 72 hours. However, the proteomes at 24 and 72 hours were distinct from each other (Figure 5.4). When comparing the variation between the replicates in each treatment condition, the standard deviation between the control samples increased at each time point and was more varied than the treated group. The variation between replicates of the treated samples decreased over time (Figure 5.5).

(a)

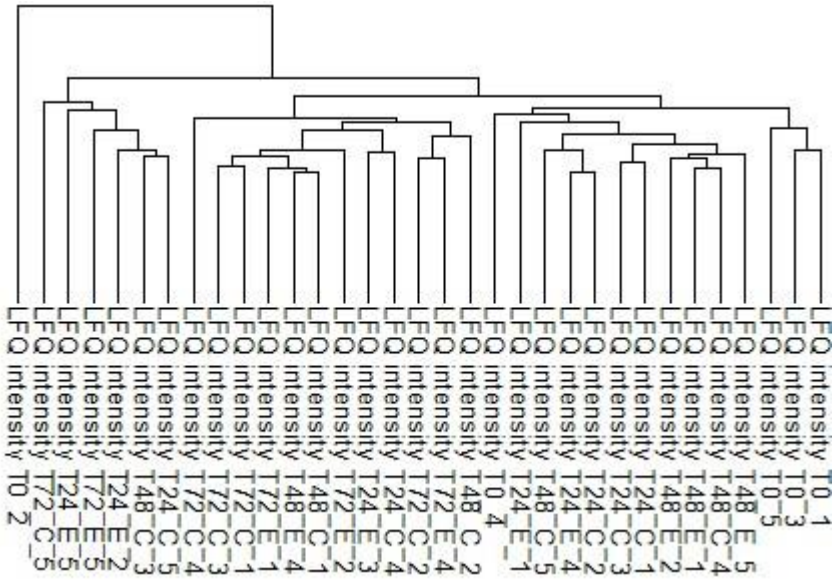

(b)

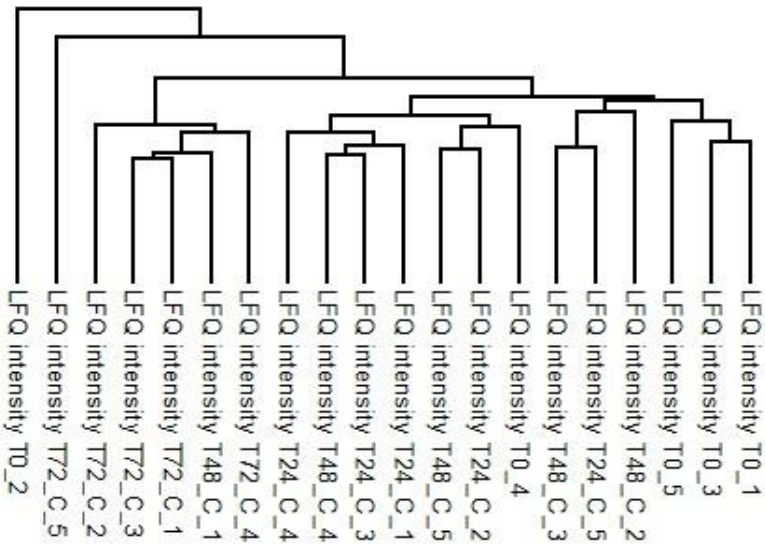

(c)

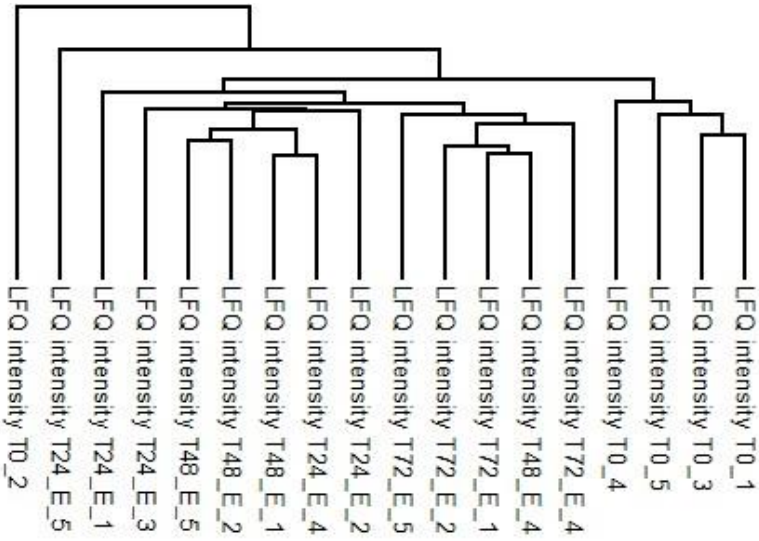

Figure 5.4: Hierarchical clustering of EFV treated NES samples over 72 hours. a) When analysed together, samples across both treatment conditions showed weak clustering. Treatment condition did not seem to have an appreciable effect on the proteome of the NES cells. The order of MS analysis was not correlated to the cluster groups, although there appeared to be weak clustering by time point and when hierarchical clustering was performed within the treatment group. In the control (b) and treated (c) conditions T24 and T48 clustered together and T48 and T72, but not T24 and T72.

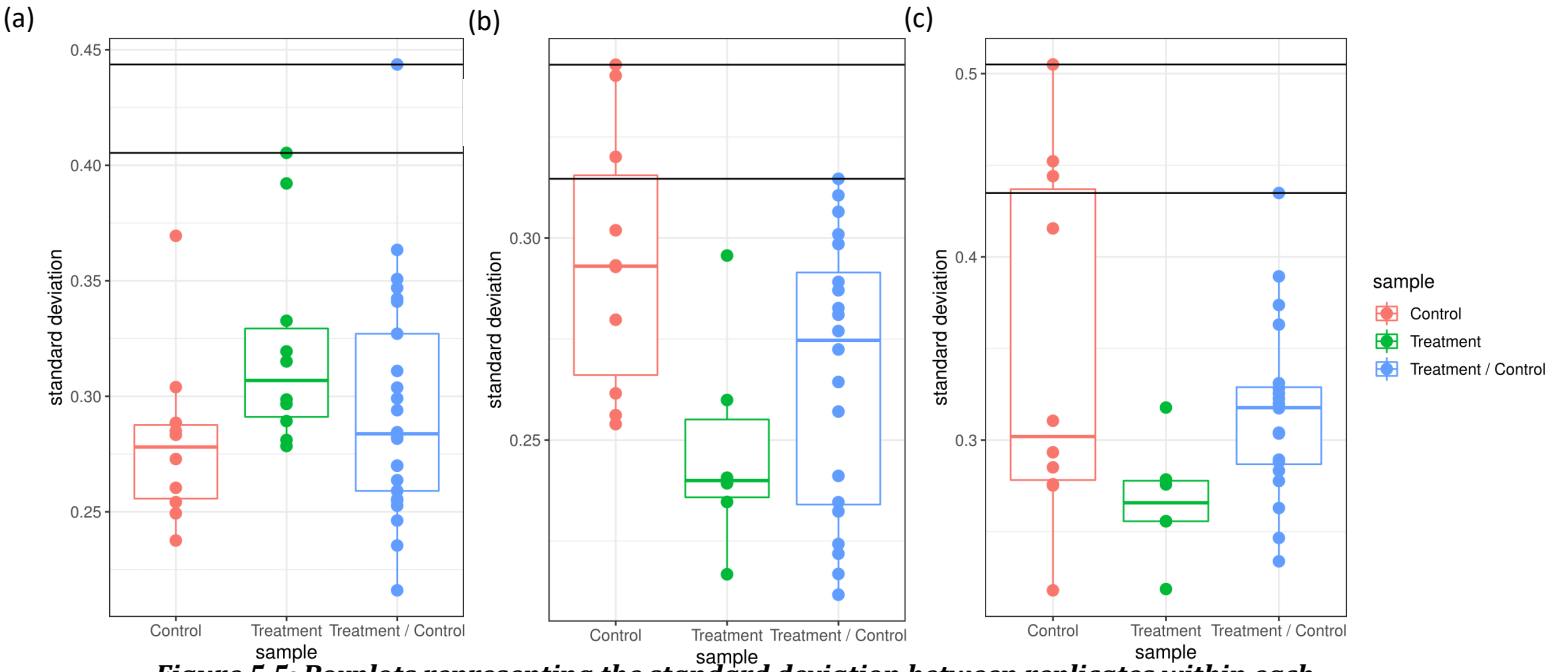

Figure 5.5: Boxplots representing the standard deviation between replicates within each condition group. a) At T24, control and treated samples had a similar spread of standard deviation within each group. The treatment group had a higher mean standard deviation. b) At T48, the standard deviation of the control group was higher and has more variation than the treated group. c) At T72, the mean standard deviation in the control group was higher than the treated group and the data points had a larger distribution. The variation of standard deviation increased in the control over time, with T72 having the most variation between replicates.

5.3.3.2 Differential statistics

Of the 1332 protein groups remaining after filtering, 131 were found to be significantly differentially regulated ($p < 0.05$) across all three time points following the Student's t-test. Protein group names were imported into Uniprot[259] and converted to their gene identifier, to which they will be referred to in the following sections. After 24, 48, and 72 hours of EFV treatment, 26, 39, and 80 protein groups were differentially regulated, respectively. The total protein groups identified and significant protein groups at each time point are listed in table 5.1. All significantly differentially regulated protein groups across all time points are listed by gene name in supplementary table S4.

Table 5.1: Protein groups identified and significantly differentially regulated by EFV treatment.

Hours post-treatment	**Total protein groups identified**	**Total significant protein groups**
24	1488	26
48	1442	39
72	1487	80

5.3.3.3 Time course analysis

The change in expression of genes that were significantly differentiated at each time point was also analysed over the entire time course. T-tests were used to determine differential regulation between conditions, and ANOVA was used to detect differential regulation within conditions between time points (significance indicated with green shading for down-regulation and red shading for up-regulation). Genes of interest were selected based on Reactome pathway enrichment as well as STRING-db network interactions. The time course data of the expression of genes of interest are represented and described here. Section 5.4.5 further discusses of the specific genes and the enriched pathways

The trend for squalene synthase (FDFT1) in the treatment condition was opposite to that of the control over 72 hours and was significantly different to the control across all time points. Hydroxymethylglutaryl-CoA synthase (HGMCS1) expression decreased continuously during the time course when treated with EFV while HMGCS1 expression in the control condition initially decreased but then appeared to recover. Fatty acid synthase (FASN) was significantly down-regulated at 24 and 72 hours post treatment and followed a similar trend to the control condition. At 48 hours, the variation of FASN detected in the control was high and thus not statistically significant although still appeared to follow the same trend with decreased levels compared to the control (Figure 5.6).

Acetyl-CoA acetyltransferase (ACAT) and ATP citrate lyase (ACLY) were both significantly down-regulated in the treatment condition at 48 and 72 hours. Both genes followed the same trend as the control condition throughout the time course. Squalene epoxidase (SQLE) was significantly up-regulated at 48 hours in the treatment condition and followed an upward trend throughout the time course. In the control condition, SQLE initially decreased and then appeared to recover by 72 hours (Figure 5.7). The variation in all time points was high, although the trend indicates that there was a higher expression of SQLE across all time points in the treated condition than in the control.

Splicing factor subunits A1 and B1 (SF3A1 and SF3B1), as well as the U6 small nuclear RNA (snRNA)-associated protein (LSM4) followed the same trend in the treatment and control conditions. At 72 hours post treatment, all three genes were significantly down regulated in the treated samples (Figure 5.8). UBX domain protein (UBXN7) followed the same trend as the control but was significantly down-regulated at 48 hours post treatment. The cleavage and polyadenylation specificity factor subunit 1 (CPSF1) increased significantly at each time point in the control samples, and was significantly higher than the treatment samples at T72 (Figure 5.9).

Annexin 2 (ANXA2) decreased significantly across the time points in both the control and treatment conditions, as indicated by the green shading. At 72 hours, ANXA2 expression was significantly higher in the treated condition. Signal transducer and activator of transcription 3 (STAT3) had a significantly higher expression in the treatment condition at 24 hours. STAT3 decreased in the treatment condition at 48 hours and then increased by 72 hours, remaining below the level of STAT3 in the control, although not significantly (Figure 5.10). P21 activated kinase 2 (PAK2) and Ras related GTPase binding protein (RAC1) followed the same trend in the control and treated conditions with lower expression levels at 24 and 48 hours. PAK2 and RAC1 both showed a significant decrease at 72 hours in the treated condition (Figure 5.11). Glycogen synthase kinase 3β (GSK3B) and ß-catenin (CTNNB1) followed similar trends to the control samples, and were both significantly decreased in the treatment condition compared to the control at 72 hours (Figure 5.12).

Peptidyl prolyl isomerase E (PPIE) and the cytoplasmic linker gene (CLIP2) were the two most respectively down or up-regulated genes in the dataset. PPIE expression in the treatment samples was opposite to that of the control, resulting in a significant down regulation at 72 hours. CLIP2 regulation followed the same trend in the treatment condition as the control, but was significantly up-regulated in the treatment samples after 72 hours (Figure 5.13).

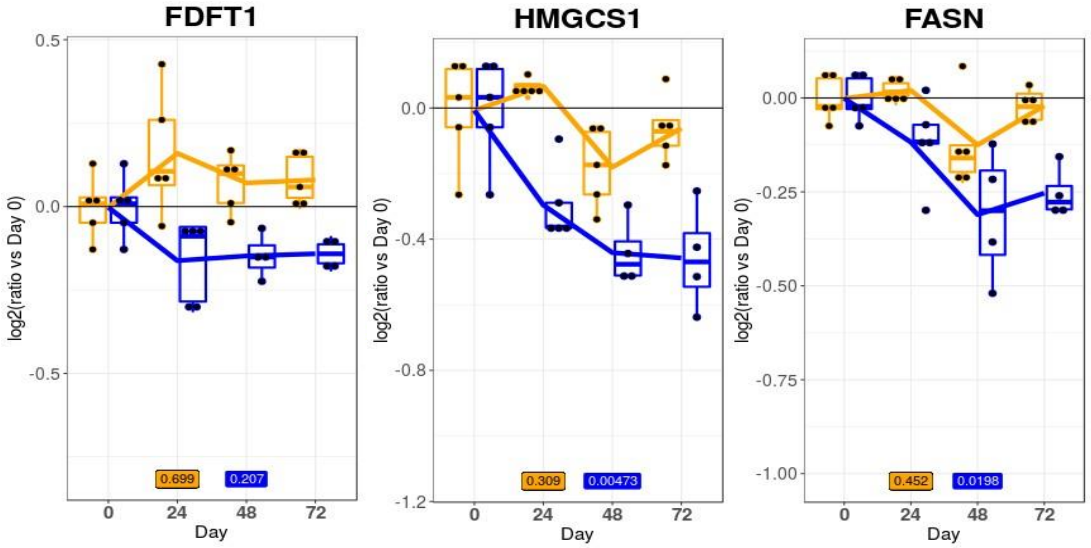

Figure 5.6: Time course graph of genes of interest significantly differentially regulated over 72 hours of EFV treatment enriching the cholesterol biosynthesis pathway. The yellow graph represents the control condition. The blue graph represents the EFV treatment condition. FDFT1, HMGCS1, and FASN enriched the cholesterol biosynthesis pathway. All three genes were down-regulated in the treatment condition. FDFT1 and HMGCS1 were down-regulated compared to the control across all three time points. FASN was significantly down-regulated at 24 and 72 hours.

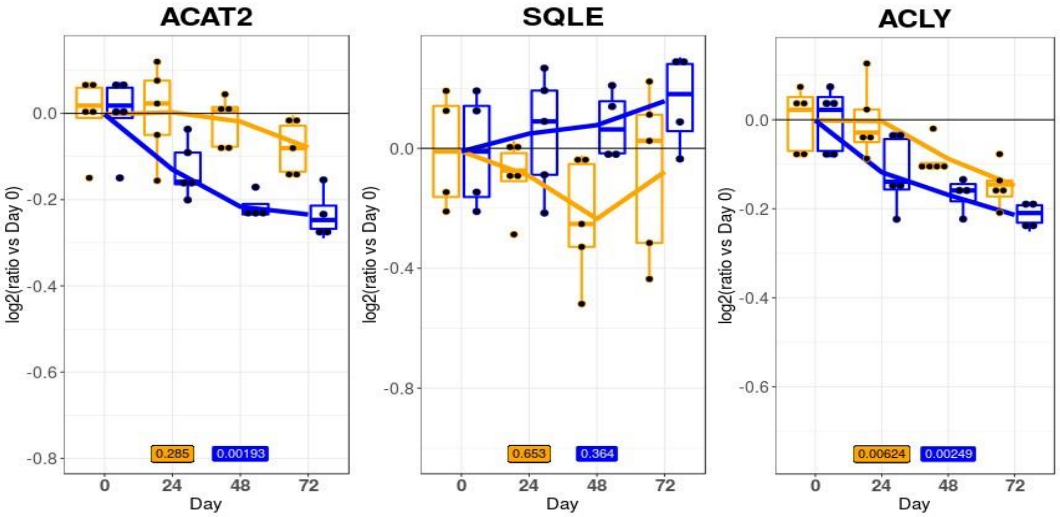

Figure 5.7: Time course graph of genes of interest significantly differentially regulated over 72 hours of EFV treatment enriching the cholesterol biosynthesis and fatty acid synthesis pathways. The yellow graph represents the control condition. The blue graph represents the EFV treatment condition. All three genes enriched the cholesterol biosynthesis pathways. ACAT2 and ACLY were down-regulated compared to the control across 72 hours. SQLE was up-regulated compared to the control across 72 hours, but only significantly different at 48 hours post-EFV treatment.

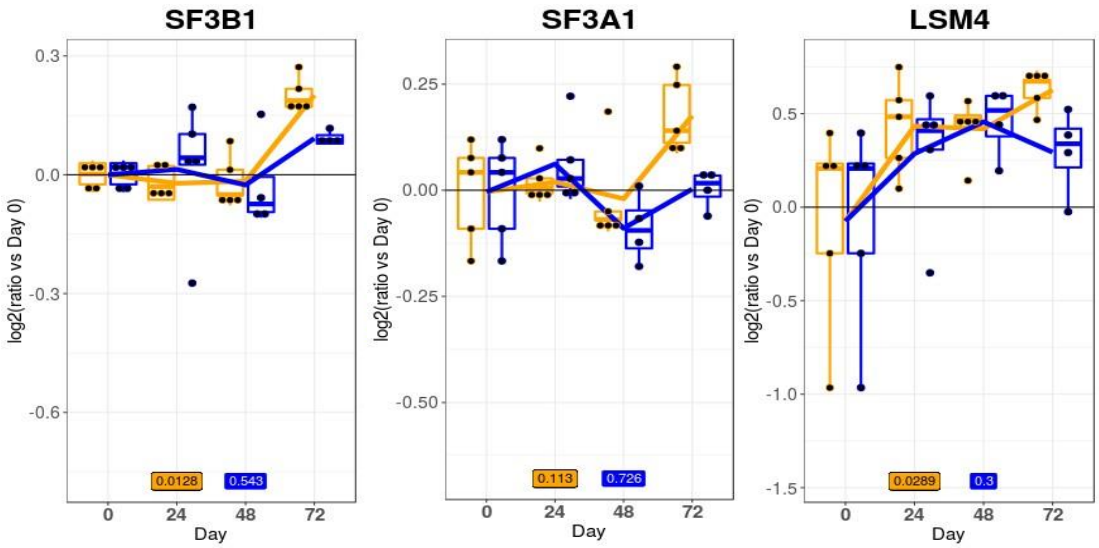

Figure 5.8: Time course graph of genes of interest significantly differentially regulated over 72 hours of EFV treatment enriching the mRNA splicing pathway. The yellow graph represents the control condition. The blue graph represents the EFV treatment condition. All three genes enriched mRNA processing pathways and followed similar trends in the control and treated conditions up to 48 hours post-treatment. At 72 hours, all three genes were down-regulated in the treated compared to the control condition.

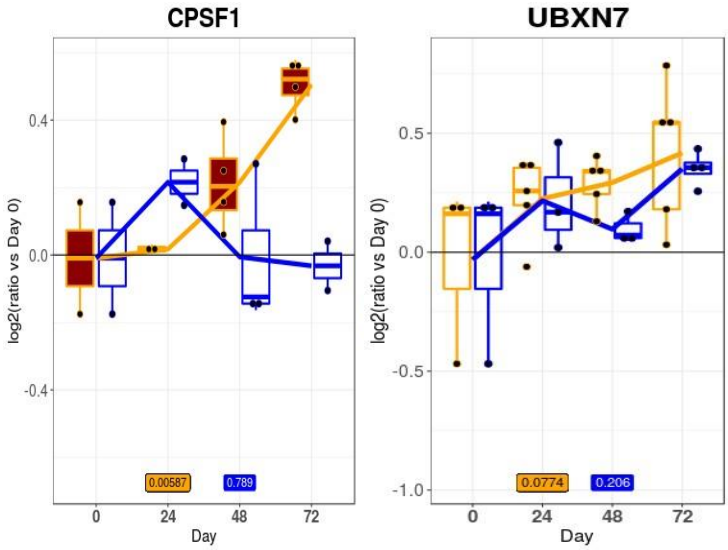

Figure 5.9: Time course graph of genes of interest significantly differentially regulated over 72 hours of EFV treatment related to immune response. The yellow graph represents the control condition. The blue graph represents the EFV treatment condition. CPSF1 enriched the mRNA splicing pathway and is known to interact with UBXN7, which was significantly down-regulated at T48 in the treatment samples. The red shading indicated a significant increase in the intensity of CPSF1 in the control condition across the time points.

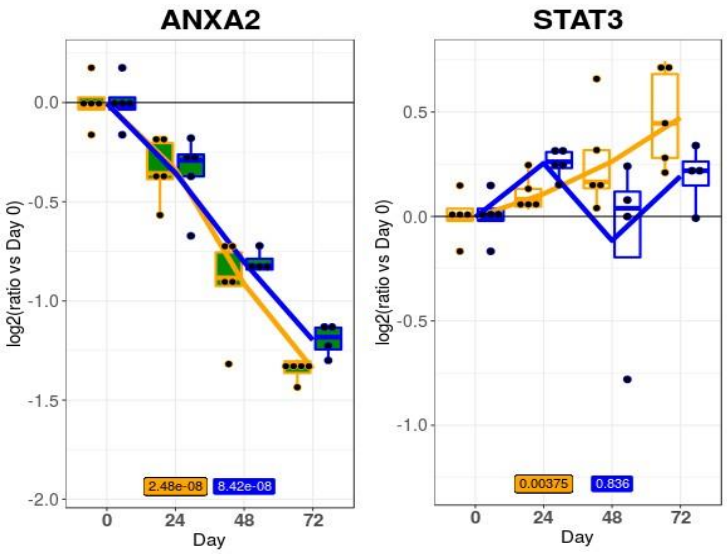

Figure 5.10: Time course graph of genes of interest significantly differentially regulated over 72 hours of EFV treatment enriching the JAK/STAT signaling pathway. The yellow graph represents the control condition. The blue graph represents the EFV treatment condition. ANXA2 enriched the JAK/STAT signalling pathway and was up- regulated at 72 hours post-treatment compared to the control. STAT3 was significantly up-regulated at 24 hours and subsequently decreased to levels below the control, although not significantly. The green shading indicates a significant decrease in intensity between each time point in both the control and treated samples.

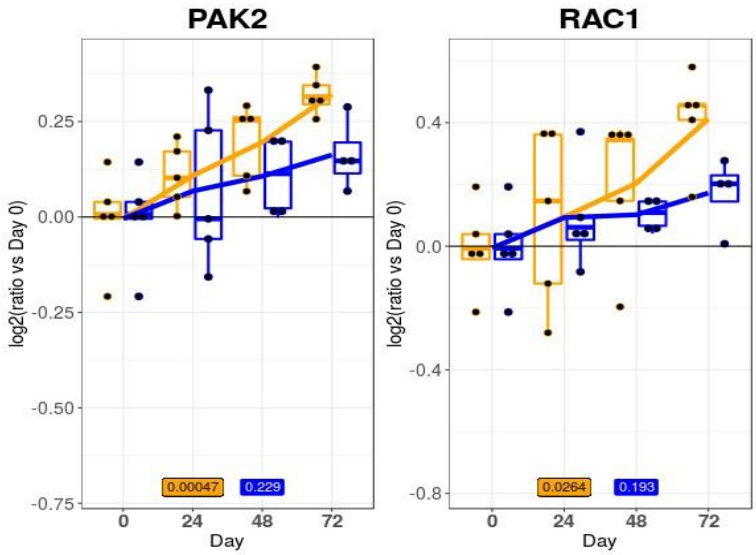

Figure 5.11: Time course graph of genes of interest significantly differentially regulated over 72 hours of EFV treatment enriching the JAK/STAT and Wnt signaling pathways. The yellow graph represents the control condition. The blue graph represents the EFV treatment condition. PAK2 and RAC1 enriched the JAK/STAT and Wnt signalling pathways respectively, and both were significantly down-regulated after 72 hours. The down-regulation of both genes appears to begin at 48 hours, although this is not significant.

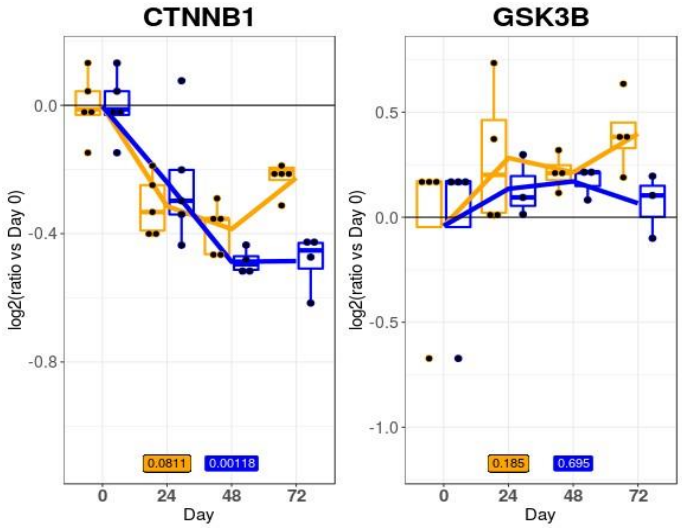

Figure 5.12: Time course graph of genes of interest significantly differentially regulated over 72 hours of EFV treatment enriching the Wnt signaling pathway. The yellow graph represents the control condition. The blue graph represents the EFV treatment condition. CTNNB1 and GSK3B both enriched the Wnt signalling pathway. In both cases, the gene regulation appeared to follow the same trend as the control until 72 hours, where both genes were significantly down regulated compared to the control.

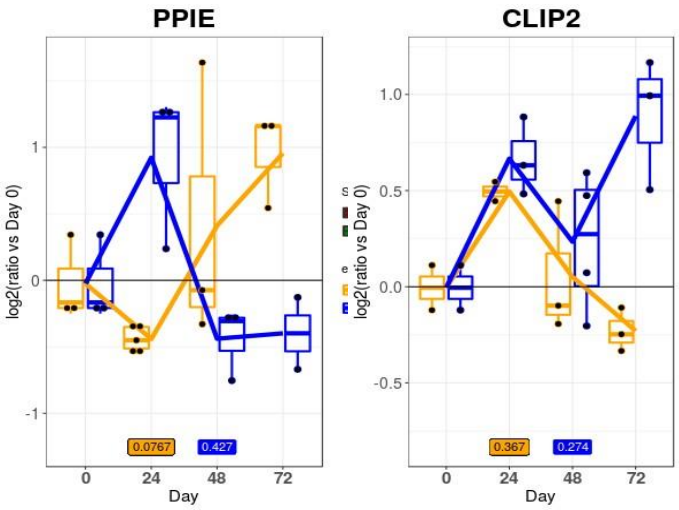

Figure 5.13: Time course graph of genes of interest that were the most highly differentially regulated over 72 hours of EFV treatment. The yellow graph represents the control condition. The blue graph represents the EFV treatment condition. PPIE was the most highly down-regulated gene in the data set and enriched the mRNA splicing pathways. PPIE was initially up-regulated with EFV treatment compared to the control at 24 hours, and was subsequently down-regulated at 72 hours. CLIP2 was not found in any of the enriched pathways, but was the most highly up-regulated gene in the data set. CLIP2 initially followed the same trend as in the control, and was highly up-regulated at 72 hours.

5.3.4 Biological inference

5.3.4.1 STRING-db and Reactome analysis

The top five most significantly enriched Reactome pathways in each time point were selected for further analysis. The genes contained within each pathway were extracted from the differentially regulated gene list in order to assess significance and fold change values (Supplementary tables S1-S3). All differentially regulated genes from each time point were imported into STRING-db for further investigation. Genes found within the enriched pathways and their interactions with various other genes not within the enriched pathways were investigated.

5.3.4.1.1 T24

The top three most significantly enriched pathways were linked to cholesterol biosynthesis and related functions and contained the genes FDFT1, HMGCS1, and FASN. All three genes were down regulated in response to treatment (Table 5.2 and 5.3). The fourth most significantly enriched pathway, carboxyterminal post-translational modifications of tubulin, contained TUBA1B gene, which was down regulated in the EFV treatment group (Table 5.3). The fifth most significant pathway, HSP90 chaperone cycle for steroid hormone receptors (SHR), contained genes TUBA1B, DYNC1LI1, and DNAJA1, which were down, up, and down regulated respectively in the treatment group (Table 5.3). TUBA1B was linked to DYNC1LI1 and CAP2 (an unknown protein that appears to be able to interact with actin, GeneCards) in the interaction network (Figure 5.15).

Table 5.2: Reactome top five most significantly enriched pathways at T24 post EFV treatment

Pathway	p-value	% entities found
Activation of gene expression by SREBF (SREBP)	2.18E-08	8.57
Regulation of cholesterol biosynthesis by SREBP (SREBF)	7.30E-08	6.98
Metabolism of steroids	1.30E-04	1.87
Carboxyterminal post-translational modifications of tubulin	3.03E-04	5.77
HSP90 chaperone cycle for steroid hormone receptors (SHR)	7.17E-04	4.29

Table 5.3: Genes enriching the top five most significantly enriched Reactome pathways at T24 post EFV treatment.

Gene ID	Fold Change (log2)	p-value	Pathway	
FASN	-0.138	0.048	Activation of gene expression by SREBF (SREBP)/Regulation of cholesterol biosynthesis by SREBP (SREBF)/Metabolism of steroids	
FDFT1	-0.322	0.023		
HMGCS1	-0.362	0.001		
TUBA1B	-0.064	0.038	Carboxyterminal post-translational modifications of tubulin	HSP90 chaperone cycle for steroid hormone receptors (SHR)
DNAJA1	0.14	0.041		
DYNC1LI1	-0.138	0.041		

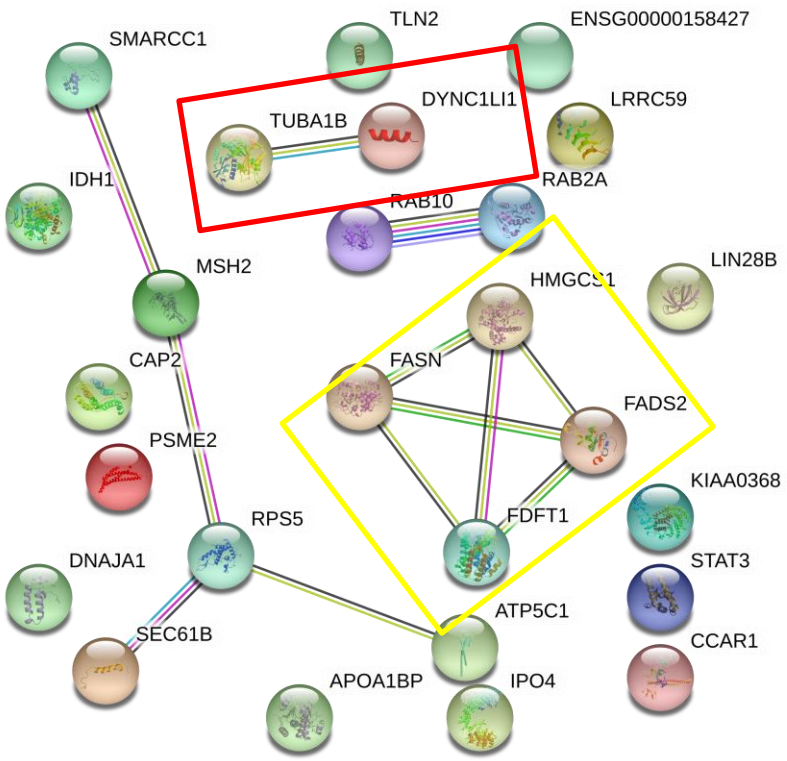

Figure 5.15: STRING-db interaction network of deregulated genes at T24 post EFV treatment. Genes contained in the cholesterol biosynthesis related pathways are indicated with a yellow box. FASN gene shows interactions with FADS2 and STAT3. Genes contained within the carboxyterminal post-translational modifications of tubulin and HSP90 chaperone cycle for SHR pathways are indicated with a red box. One of the genes in the SHR pathway (DNAJA1) is not found in the cluster. TUBA1B gene shows an interaction with CAP2 gene.

5.3.4.1.2 T48

The top four most significantly enriched pathways were linked to cholesterol biosynthesis and related functions and contained the genes FDFT1, HMGCS1, and SQLE. FDFT1 and HMGCS1 were down- regulated in response to treatment, and SQLE was up-regulated (Table 5.4 and 5.5). The genes clustered together in the STRING-db interaction network and showed interactions with genes involved in fatty acid biosynthesis (ACLY) and mitochondrial fatty acid beta-oxidation (ETFA) (Figure 5.16). The fifth most significantly enriched pathway was prefoldin mediated transfer of substrate to CCT/TriC (Table 5.4), enriched by CCT2 and TUBB4B, which were both down regulated in the EFV treatment group (Table 5.5). TUBB4B is a major constituent of microtubules, while CCT2 is involved in microtubule and actin protein folding (GeneCards).

Table 5.4: Reactome top five most significantly enriched pathways at T48 post EFV treatment

Pathway	p-value	% entities found
Activation of gene expression by SREBF (SREBP)	1.56E-07	8.57
Regulation of cholesterol biosynthesis by SREBP (SREBF)	5.16E-07	6.98
Metabolism of steroids	1.05E-04	2.18
Cholesterol biosynthesis	1.12E-04	5.56
Prefoldin mediated transfer of substrate to CCT/TriC	1.42E-04	10.35

Table 5.5: Genes enriching the top five most significantly enriched Reactome pathways at T48 post EFV treatment

Gene ID	Fold Change (log2)	p-value	Pathway
ACAT2	-0.197	0.001	Activation of gene expression by SREBF (SREBP)/Regulation of cholesterol biosynthesis by SREBP (SREBF)/Metabolism of steroids/Cholesterol biosynthesis
FDFT1	-0.219	0.004	
HMGCS1	-0.261	0.011	
SQLE	0.313	0.022	
CCT2	-0.082	0.021	Prefoldin mediated transfer of substrate to CCT/TriC
TUBB4B	-0.098	0.043	

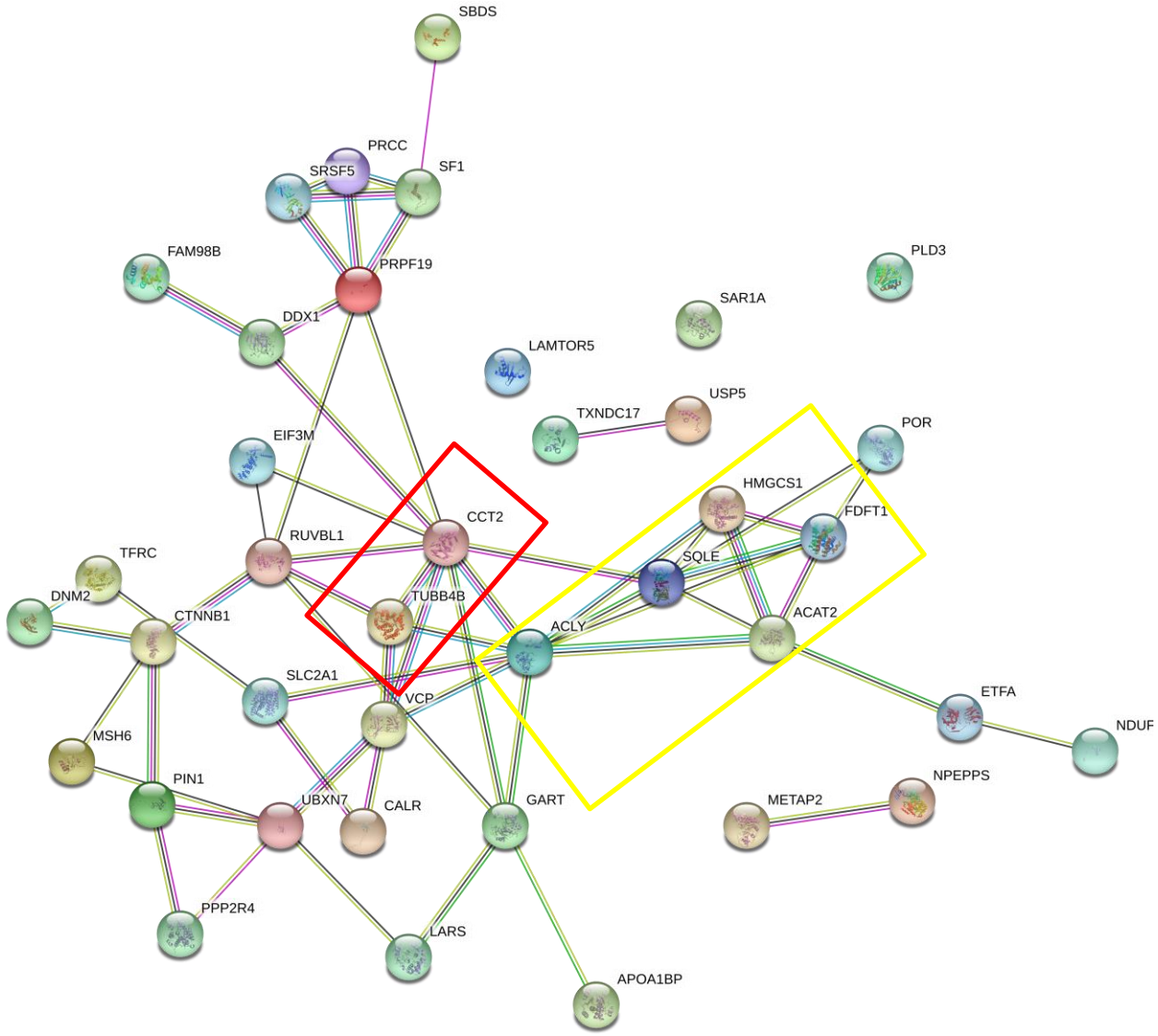

Figure 5.16: STRING-db interaction network of deregulated genes at T48 post EFV treatment.
Clusters of genes contained within the four most significantly enriched pathways, all of which relate to cholesterol biosynthesis, are indicated with a yellow box. Genes contained in the fifth most enriched pathway, prefoldin mediated transfer of substrate to CCT/TriC, are indicated with a red box. Interactions between multiple genes in the cholesterol biosynthesis related pathways and ACLY, involved in fatty acid biosynthesis, can be observed. ACLY and SQLE both link the cholesterol biosynthesis pathways to the prefoldin transfer pathway highlighted in red.

5.3.4.1.3 T72

The top two most significantly enriched Reactome pathways were related to mRNA splicing and contained nine genes (Table 5.6 and 5.7). Of the nine genes in the enriched pathway, seven are part of a spliceosome complex (Figure 5.17). The second most significantly enriched pathway was activation of gene expression by SREBF (SREBP), containing FDFT1, HMGCS1, and FASN. The next most significantly enriched pathway was gene and protein expression by the Janus kinase (JAK)-STAT signaling after Interleukin-12 stimulation, containing ANXA2, PAK2, and SOD2, which were up, down, and up-regulated respectively. The fifth most significantly enriched pathway was signaling by Wnt, containing 11 genes (Table 5.6 and 5.7). Genes from the cholesterol biosynthesis pathway show interactions with ACLY, which in turn shows interactions with genes from the JAK/STAT (ANXA2) and Wnt (GSK3B) signaling pathways. GSK3B and CTNNB1 interact with multiple genes contained in the enriched Reactome pathways such as PAK2, SMARCA4, and SF3B1 (Figure 5.17).

Table 5.6: Reactome top five most significantly enriched pathways at T72 post EFV treatment

Pathway	p-value	% entities found
mRNA Splicing - Major Pathway	7.05E-06	4.86
mRNA Splicing	1.11E-05	4.59
Activation of gene expression by SREBF (SREBP)	1.15E-05	8.57
Gene and protein expression by JAKSTAT signaling after Interleukin-12 stimulation	1.45E-05	8.22
Signaling by WNT	2.25E-05	3.33

Table 5.7: Genes enriching the top five most significantly enriched Reactome pathways at T48 post EFV treatment

Gene ID	Fold Change (log2)	p-value	Pathway
CPSF1	-0.538	0.014	mRNA Splicing - Major Pathway/mRNA splicing
LSM4	-0.333	0.038	
PPIE	-1.354	0.029	
PRPF19	-0.134	0.022	
PRPF38A	-0.258	0.035	
SF3A1	-0.173	0.011	
SF3B1	-0.109	0.004	
SNRPF	0.866	0.018	
SRRM1	-0.153	0.015	
FASN	-0.233	0.001	Activation of gene expression by SREBF (SREBP)
FDFT1	-0.222	0.002	
HMGCS1	-0.396	0.005	
ANXA2	0.145	0.032	Gene and protein expression by JAK/STAT signalling after Interleukin-12 stimulation
PAK2	-0.158	0.029	
SOD2	0.118	0.021	
AP2S1	0.323	0.004	Signaling by WNT
CALM2	-0.229	0.009	
CDC73	-0.319	0.049	
CTNNB1	-0.259	0.003	
GSK3B	-0.331	0.049	
PSMB1	-0.118	0.025	
PSMB3	-0.174	0.035	
RAC1	-0.24	0.03	
RPN1	0.166	0.043	
SMARCA4	-0.133	0.003	
YWHAZ	0.122	0.008	

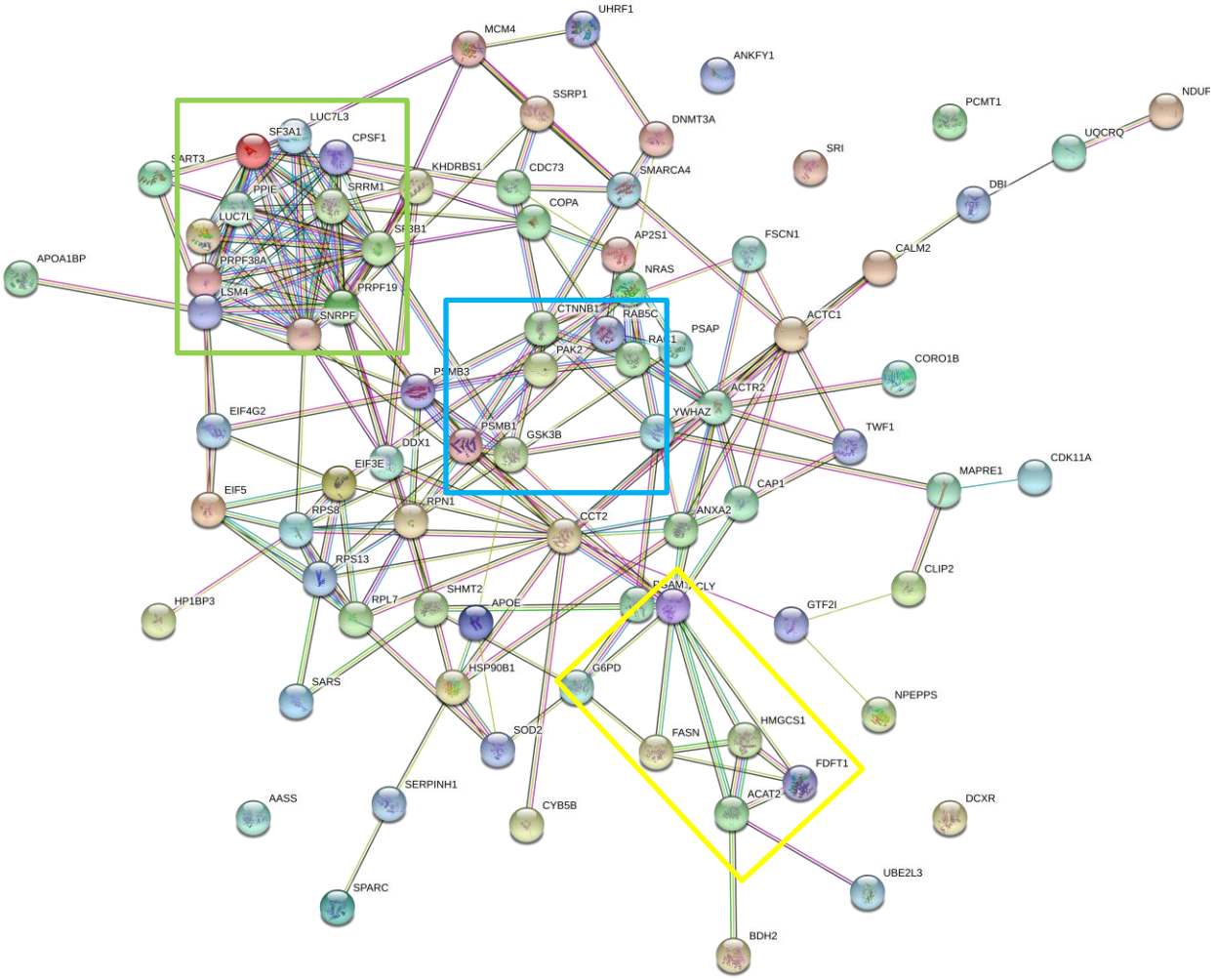

Figure 5.17: STRING-db interaction network of deregulated genes at T72 post EFV treatment. Clusters of genes found within the enriched pathway, mRNA splicing, is indicated by a green box. Genes found within the cholesterol biosynthesis pathway are indicated by a yellow box. A portion of the clusters of genes in the JAK/STAT and Wnt signalling pathways are indicated by a blue box.

5.4 Discussion

5.4.1 MS runs

Variations in TIC and LC should be minimised during MS analysis to allow for accurate comparison of samples. During sample analysis, the LC spray was disrupted, requiring repair and calibration prior to continuing sample analysis. The spray and the TIC intensity improved in subsequent runs, as seen in the reference sample after the experimental analysis when compared to the reference sample before experimental analysis (Figure 5.3). The improved TIC intensity may have been due to a more stable LC spray or the analysis continuing immediately after calibration. Due to limited instrument time, samples that had been analysed prior to LC failure but with poor spray were not re-analysed. Variations in data acquisition caused by unstable spray may have affected the detection of true differences between the treatment and control groups.

The two samples discarded due to low peptide level were not analysed sequentially and thus it is unlikely that the low TIC was due to a technical MS error. Peptide loss may have occurred during sample processing, most likely due to experimenter error.

5.4.2 MaxQuant

The total number of protein groups identified across 35 samples (1663) is low compared to similar previous work performed in the Blackburn Laboratory with human neural cell lines. In NES cells, over 3000 protein groups were identified and in SH-SY5Y and differentiated neural stem cells, between 3000 to 4000 protein groups were detected across samples.[262–264] The lower number of protein groups detected may have been due to using the GuHCl lysis method, as the previous work was prepared using filter aided sample preparation (FASP) methods. Upon inspection of reference samples of SH-SY5Y that was prepared with FASP methods and analysed after the experimental samples, 2028 total proteins groups were identified (data not shown). Identification of approximately 3000 protein groups in the reference sample is expected with optimal instrument function. This indicated that the low protein group identification in the experimental samples was not due to the sample preparation methods, but more likely due to a lower level of instrument performance. The

digestion efficiency in this work was low, as it is common for up to 90% of peptides to have no missed cleavages using FASP methods (Blackburn Laboratory, unpublished). Prior to trypsin digestion, pre-digestion with LysC was used to improve digestion efficiency. Therefore, the relatively low percentage of no missed cleavages may indicate that lysis with GuHCl causes disruption of effective digestion (Supplementary Figure S2). GuHCl was diluted to 1 M before trypsin digestion, which was below the recommended maximum of 2 M, but it is possible that the concentration of GuHCl was still too high for efficient trypsin activity.

Protein identification is also affected by the mass error, measured in parts per million (ppm), which can affect database searching. A lower ppm results in fewer candidate sequences, and thus results in a decreased risk of false positive matches. A ppm < 2 is considered a high mass accuracy. In this data set, the mass error remained close to 0.8 ppm across all samples (Supplementary Figure S4). This indicates that identification of the protein groups was accurate, even though the sensitivity was low.

5.4.3 Statistical analysis

5.4.3.1 Data visualisation

A core proteome is generally conserved between eukaryotes, and even more so within the same cell line.[265] A highly conserved proteome within a cell line would therefore not be expected to change dramatically with a low dosage treatment. Weak clustering of the treatment conditions indicate that changes in the proteome caused by EFV treatment are subtle, which would be expected (Figure 5.4). As the time course progressed, the control samples became more variable compared to the treatment samples (Figure 5.5). This may have been due to a common response caused by EFV treatment. It is unlikely that the variation in the control samples was caused by processing errors or a decrease in instrument performance over time with MS analysis, as subsequent to harvesting, all samples were processed and analysed in a randomised order.

5.4.3.2 Differential statistics

Protein groups identified by PSM were then subjected to statistical analysis. Of the 1663 identified protein groups, 131 were significantly different after filtering (described in section 5.2.3.1). In a similar experimental design in our laboratory assessing the effect of HIV-tat on differentiated neurons over three

time points, from 4104 identified protein groups, 280 were significantly differentially regulated after 48 hours. From this observation, it is not possible to conclude whether the low number of significant proteins was due to poor instrument performance and thus lower protein identifications, or due to EFV having a more subtle effect on the NES cells. The relatively low number of protein group identifications across all samples in this work may have restricted the sensitivity to detect changes in the proteome as well as the magnitude of those changes. This is an important factor to keep in mind during interpretation of the data, as well as for future work.

When analysed separately, the number of identified protein groups is higher in each time point than in the total number of protein groups remaining within the three time points. This was due to the criteria of filtering which required that at least three replicates in each group (in both treatment and control groups for all three time points) were required to contain valid values. This may therefore have excluded protein groups which reached the criteria within a single time point, but not in others.

5.4.3.2.1 Multiple testing corrections.

Multiple testing corrections (MTCs) are performed when many statistical tests are used to determine true significance. As the number of tests performed increases, so does the possibility of an apparently significant result being returned by chance. The level of significance is adjusted based on the number of tests performed, decreasing the chance of a false positive (type I error) occurring with an increasing number of tests. An adjusted level of significance will cause fewer results to pass the significance threshold, but those values that do pass are more likely to be truly significant than chance occurrences.

It has been suggested that in exploratory studies, which are designed to be followed by confirmatory studies, multiple testing corrections can be detrimental.[266–268] A false positive result can be easily removed once deemed insignificant after more rigorous testing, but a false negative (type II error) cannot be recovered. The nature of a shotgun proteomic experiment is hypothesis generating, with validation studies designed based on rational biological inference. The removal of significant values below the adjusted threshold, although statistically robust, does not consider the biology behind the results, and thus may limit the scope of confirmatory studies. In general, protein expression in an organism is tightly regulated, and this conservation is even observed across different eukaryotes.[265]

Small changes in the proteome may therefore not be directly proportional to the effect of the change; factors such as post-translational modifications also influence the function of proteins without affecting

protein expression. For this reason, many biologists are of the opinion that FDR and fold change cut off corrections, without taking the biology into account, are somewhat arbitrary and can lead to valuable data being lost.[269–271] When using the adjusted Benjamini-Hochberg[272] and Storey[273] FDR control, no significant values between the time points in either condition and between the two conditions were observed. It is possible that at the estimated biologically relevant concentration of 1.05 µg/mL, EFV did not have a significant effect on proliferating NES cells. Another possible explanation is that the low level of protein identification may have decreased the sensitivity of the experiment, resulting in fewer detected differences. Based on the literature, EFV has been found to cause extensive alterations to cellular mechanisms in cell culture, and thus no significant alterations in the proteome did not coincide with the ubiquitous empirical findings.[274]

Subsequently, the analysis was repeated without MTCs using the following rationale: Biological inference that focusses on protein interaction networks and pathway analysis applies additional stringency to proteins deemed significant ($p < 0.05$) as it ensures that proteins of interest are less likely to be significant by chance. A pathway enriched by multiple significantly different proteins is more likely to be a true result, as it contains evidence from multiple proteins.[275] Here, pathways containing a minimum of three genes were further discussed.

5.4.4 Biological inference

At all three time points, pathways related to cholesterol biosynthesis and metabolism were enriched by the same set of genes, which were differentially regulated throughout the time course. As cholesterol biosynthesis related pathways were in the top three and four pathways enriched in T24 and T48, respectively, it will be the only pathway discussed for these time points and will be discussed as an overview for across all three time points. The pathways that were enriched in T72, excluding cholesterol biosynthesis, will be discussed separately. Within each pathway, the functions of genes of interest are discussed based on existing literature. The functions of individual genes as well as the pathway as a whole are then discussed in the context of the response of NES cells to EFV treatment.

5.4.5 Enriched pathways:

5.4.5.1 Cholesterol Biosynthesis (activation of gene expression by SREBP)

The most significantly enriched pathways across the time points listed in tables 5.2, 5.4, and 5.6 contained FASN, HGMCS1, ACAT2, and FDFT1, which were all down-regulated throughout the 72 hours compared to the control, and followed a decreasing trend. SQLE was up-regulated significantly 48 hours post EFV treatment and increased throughout the time course (Figure 5.6 and 5.7). Cholesterol and fatty acid biosynthesis are interconnected pathways containing genes that were differentially regulated throughout the data set, including ACLY and FADS (Figure 5.18). All genes discussed in the following section were related to cholesterol or fatty acid biosynthesis and were found to be differentially regulated in EFV treatment, the majority of which were down-regulated.

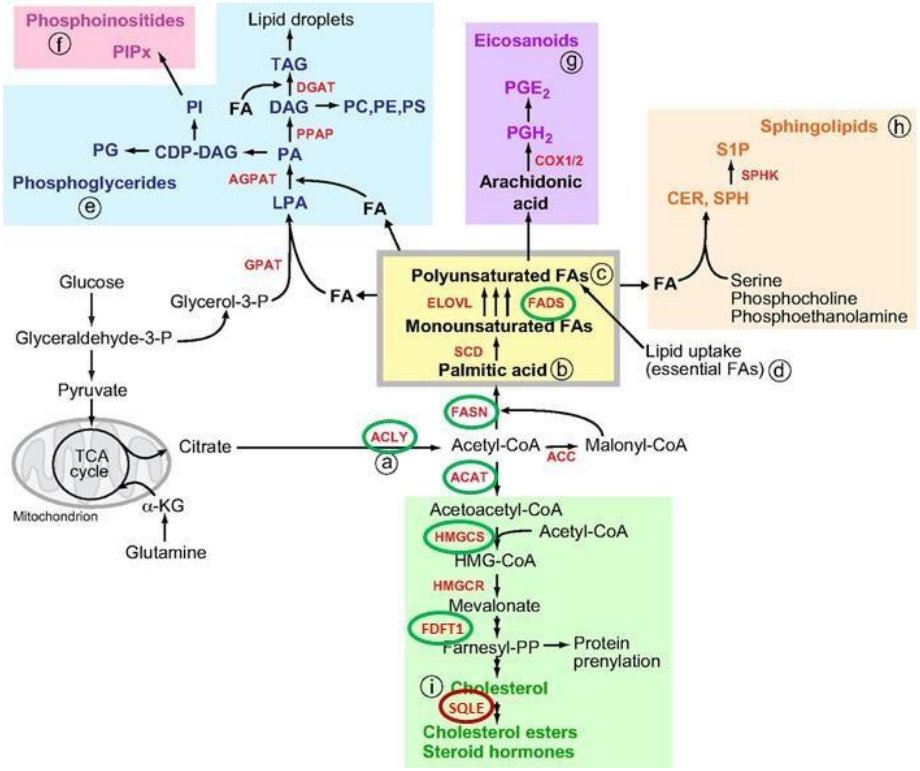

Figure 5.18: Schematic overview of cholesterol, fatty acid, phosphoglyceride, eicosanoid, and sphingolipid synthesis. Genes that were down-regulated following EFV treatment are circled in green. Genes that were up-regulated following treatment are circled in red. ACLY converts citrate to Acetyl-CoA, which is needed for both cholesterol and fatty acid biosynthesis. ACAT and FASN direct acetyl-CoA to the cholesterol and fatty acid synthesis pathways respectively. Adapted from Baenke et al., 2013.[276]

Cholesterol biosynthesis regulation is an essential component of healthy CNS function

Cholesterol is a lipid molecule that is essential for a large range of functions in animal cells including membrane structure and signal transduction.[277,278] Cholesterol also acts as a precursor for important molecules such as bile salts, vitamin D, and various steroid hormones. Acquisition of cholesterol is either through ingestion or can be synthesized *de novo* in the endoplasmic reticulum. Systemic cholesterol does not cross the BBB and therefore the cells in the CNS have to create cholesterol *de novo.*[278,279] Neurogenesis, and specifically synaptogenesis, is a cholesterol dependent process as neurite outgrowth requires plasma membrane growth.[280] Once synapses are formed, cholesterol synthesis plays an important role in vesicle formation and transmitter receptors for signalling.[281] Cholesterol is also an important component of myelin in the CNS that is required for efficient propagation of an action potential in axons and for general neuronal health.[282]

Aberrant regulation of cholesterol biosynthesis can lead to changes in proliferation and differentiation in stem cells.

Cholesterol biosynthesis is vital for embryonic development, and its aberrant synthesis can lead to serious malformation syndromes.[283] Cholesterol has a positive effect on self-renewal of stem cells, protects cells from apoptosis, and is vital in retaining the "stemness" of the cells.[284,285] Inhibition of cholesterol and fatty acid synthesis leads to spontaneous differentiation, and the level of synthesis continues to decline as differentiation progresses.[284–287] FASN, a key enzyme in *de novo* lipogenesis, is vital for neurogenesis and maintains the proliferation of neural stem cells.[288] Prolonged inhibition of FASN in murine neural stem cells resulted in a drastic reduction in cell proliferation, increased apoptosis within the cell population, and the altered expression of several stem cell markers, highlighting its importance in the maintenance and survival of proliferating cells.[288] ACLY links carbohydrate metabolism and fatty acid synthesis by converting citrate to acetyl CoA (Figure 5.18). ACLY has also been linked to the maintenance of pluripotency in stem cells, and was down- regulated significantly 48 hours post differentiation initiation following the removal of FGF in human embryonic stem cell culture.[289] The specific inhibition of ACLY in embryonic stem cells caused a subsequent decrease in the expression of several pluripotency markers.[289]

Stemness is a characteristic trait found in both stem cells and cancerous cells. The study of stemness in cancerous stem cells found in the CNS can give insight into non-cancerous neurogenesis. In glioma stem

cells, several components of the cholesterol and fatty acid synthesis pathways including ACLY, ACAT, HMGCS1, FDFT1, and SQLE are implicated in the maintenance of stemness. Upon differentiation of the glioma stem cells, the expression of the above mentioned genes decreased.[285,286] This further implicates cholesterol and fatty acid biosynthesis in the maintenance of a proliferating state in stem cells.

Components of the cholesterol biosynthesis pathway play a role in embryonic neural development as well as in the maintenance of a healthy adult neural system.

Cholesterol biosynthesis plays an important role in both the developing and adult CNS. FDFT1 is the first enzyme exclusively involved in the cholesterol biosynthesis pathway, and is therefore vital to many downstream processes. FDFT1 synthesizes lanosterol, from which steroids and cholesterol are derived, and has been implicated in multiple CNS defects.[280,290] The knockout of FDFT1 in mice resulted in reduction of the radial thickness of both the cortical wall and diencephalon, as well as increased apoptosis in new-born neurons.[280] Embryos also had smaller forebrains and an open neural plate, indicating incomplete neural tube closure.[290] Mutations in humans resulting in decreased FDFT1 production presented with structural brain malformations, global developmental delay, generalized seizures, and facial dysmorphisms.[291]

Lanosterol can be produced at low levels in adult neurons and has a neuroprotective effect by regulating mitochondrial uncoupling in response to reactive oxygen species (ROS) stress or neurotoxins.[292] The effect of MTPT, a neurotoxic compound that can induce a Parkinson's-like disease, was diminished when lanosterol was co-administered due to it mitochondrial uncoupling action.[293] Lowered levels of lanosterol have been implicated in both Parkinson's and Alzheimer's diseases, and increased levels has been identified to have a neuroprotective effect.[293,294]

Viral infection can regulate cholesterol biosynthesis to benefit its infection and replication.

As viruses display highly varied life cycles, the cellular response to viral infection is appropriately diverse. For example, Kaposi's sarcoma-associated herpesvirus (KSHV) produces micro RNAs (miRNA) that result in a down-regulation of HMGCS1 and FDFT1 transcripts, and subsequently protein levels, as a protective mechanism.[295] A final product of the cholesterol biosynthesis pathway, cholesterol 25-hydroxylase, converts cholesterol to 25-hydroxycholesterol and restricts replication of viruses such as

KSHV,[295] as well as blocking HIV and other enveloped viruses entry into cells.[296] Silencing cholesterol synthesis is therefore advantageous for the virus in order to establish latent infection,[295] although cholesterol is necessary for the lytic cycle of the virus.[295,297]

In contrast to this theory, upon infection with cytomegalovirus (CMV), primary bone marrow derived cells decreased cholesterol synthesis via a reduction in expression levels of HMGCS1 and SQLE (among others). The innate response to viral infection caused a reduction in sterol synthesis via the increased production of inteferons (IFN) IFN-γ or ß that act as transcriptional regulators to decrease sterol production, subsequently inhibiting viral infection.[298] In most cases of viral infection, including HIV, sterol biosynthesis down regulation via the inflammatory response acts an innate immune response to limit infectivity.[298,299]

The success of HIV can be partially attributed to its ability to hijack vital host processes, such as cholesterol and sterol synthesis. HIV up-regulates cholesterol biosynthesis, using lipid rafts to gain entry to cells and improve viral formation, budding, and infectivity.[279,300] Upon infection with HIV, proteins involved in cholesterol biosynthesis such as HMGCS1, SQLE, and FDFT1, among others, were up- regulated, improving viral infection in multiple different cell lines.[279,300] Decreasing cholesterol biosynthesis was therefore recommended as an adjuvant therapy to ARVs and was considered a desirable side effect of ARV treatment; however, hyperlipidaemia, lipodystrophy, insulin resistance, accelerated atherosclerosis, and coronary heart disease have been reported as side effects of certain protease inhibitor ARV drugs.[301,302] A reduction in cholesterol biosynthesis thus appears to be detrimental to both the host and the virus, indicating a need for more targeted treatment to mitigate these specific negative side effects in the host as a result of ARV treatment.[297]

EFV treatment causes a down-regulation in multiple components of cholesterol biosynthesis that is linked to deregulated proliferation, mitochondrial dysfunction, and CNS abnormalities. Treatment with EFV for 72 hours causes an overall down-regulation in genes relating to cholesterol biosynthesis in NES cells. Based on evidence from the literature, the down-regulation appears be a function of - or as a result of - a shift from proliferation towards differentiation, although this was not visibly apparent in the cells. Deregulated cholesterol biosynthesis may result in mitochondrial dysfunction via mitochondrial uncoupling. EFV has been well documented as a cause of disruption of mitochondrial function, causing mitochondrial depolarization, decreased membrane

potential, and increased ROS production in neuronal cells.[120,122] Mitochondrial damage from NRTI treatment is generally as a result of the inhibition of mitochondrial DNA (mtDNA) polymerase, or by inducing mtDNA mutations.[43,303] Although EFV does not inhibit mtDNA polymerase, mitochondrial toxicity is still common, indicating another mechanism of toxicity.[304] Deregulated fatty acid and cholesterol biosynthesis affect the mitochondria through uncoupling, which occurs when cells are exposed to toxic ROS. Uncoupling agents such as lanosterol decrease the mitochondrial inner membrane potential by causing protons to bypass ATP synthase, limiting mitochondrial ROS production.[305,306] The down-regulation of FDFT1 as a result of EFV treatment followed by a subsequent down-regulation of lanosterol synthesis would impact mitochondrial uncoupling, causing a subsequent increase in ROS production, which may indicate a mechanism by which EFV causes mitochondrial toxicity.[304] Mitochondrial toxicity in neuronal cells has been linked to various neurodegenerative diseases such as Alzheimer's, Parkinson's, amyotrophic lateral sclerosis (ALS), and Huntington's disease.[43,293,305,307,308]

Although the cells used for this work were proliferating neural stem cells, the mode of mitochondrial dysfunction may give insights into the mechanism of persistent HAND in the ARV era, which mimic various neurodegenerative diseases. The similarities seen in HAND and non-HIV related neurodegenerative diseases may be due to mitochondrial dysfunction, albeit with different aetiology.

Lowered cholesterol biosynthesis during embryonic development results in CNS malformations that are echoed in case studies implicating EFV as the cause of CNS abnormalities.

FDFT1, a major component of cholesterol biosynthesis, was down-regulated across all time points in NES cells when treated with EFV (Figure 5.6). The malformations caused by depletion of FDFT1, and deregulated cholesterol synthesis in general, echo some of the concerns surrounding EFV treatment during pregnancy. Case studies report defects neural tube closure, cleft palate, myelomeningocele, encephalocoele, and seizures where EFV treatment was the only known risk factor, although this has not been recognised as an increased risk from EFV.[78–81,117,119] FDFT1 depletion in mice models has similarly been linked to incomplete neural tube closure, cleft palate, craniofacial malformations, seizures and developmental delay.[280,283,290,291,309] Reduced cholesterol synthesis as observed with EFV treatment may contribute to developmental CNS abnormalities and explain the seemingly low risk of EFV exposure *in utero*, as reduced cholesterol biosynthesis causes early embryonic lethality. [280,290,309]

The embryonic and adult CNS requires cholesterol and fatty acid biosynthesis for optimal functioning. Although desirable for its adjuvant antiviral protection, the down-regulation of cholesterol biosynthesis with EFV treatment may offer a mechanistic explanation for some of the CNS side effects observed in adults with EFV treatment. Cholesterol deficiency in adults has been linked to Alzheimer's, Huntington's, Niemann Pick C disease, reduced synaptic activity, and neuronal loss.[308,310] These neurodegenerative diseases have a host of symptoms which can present as psychiatric problems, loss of cognitive function, cerebellar ataxia, and progressive dementia, among others.[308,310–312] Similarly, CNS side effects of EFV include confusion, lethargy, impaired concentration, amnesia, and depression.[49,50] Many cases reporting neuropsychiatric events resolve within two months, but in up to 50% of cases symptoms can persist for years, including a marked neuropsychological decline observed after three years of treatment that improved with treatment discontinuation.[50,219,313] These findings, along with the significant prevalence of HAND when otherwise under virologic control, indicates that ARVs, and specifically EFV, may contribute to the milder forms of HAND.[219] Based on the present work, one can speculate that the neurocognitive impairments associated with mild forms of HAND in the ARV era, specifically those associated with EFV treatment, may be caused by de-regulated cholesterol biosynthesis, which is linked to mitochondrial dysfunction and many neurocognitive disorders.[89,307]

5.4.5.2 mRNA Splicing – Major Pathway

mRNA splicing regulates and modulates gene expression.

One of the fundamental processes in the of regulation and modulation of gene expression is that of messenger RNA (mRNA) splicing and degradation, which influences gene regulation through transcription elongation, mRNA splicing, degradation, and mRNA export.[314,315] The spliceosome is made up of six small nuclear ribonucleoproteins (snRNPs) and polypeptides and is responsible for gene expression modulation through alternative splicing, which has been linked to specifying cell identity during neurogenesis,[316,317] as well as implicated in diseases such as various cancers[318,319] and ALS.[320]

mRNA splicing controls proliferation, differentiation, and survival in neuronal stem cells.

Splicing factors play an important role in proliferation or stemness maintenance.[316] Aberrant regulation of mRNA splicing factor SF3B1 from the U2 snRNP is often associated with cancer formation, and its

inhibition results in a reduction of proliferation.[318,321] SF3B1 and LSM4, a decapping protein from the U6 snRNP, are expressed at high levels in proliferating stem cells in the sub-ventricular zone (SVZ) in adult mice brains. Another mRNA processing gene, CPSF1, has also been specifically linked to stem cell growth, proliferation, and survival.[319]

Transcriptional profiling of adult brain stem cells revealed that RNA splicing and chromatin remodelling were prominent processes involved in adult neurogenesis and is vital for generating the complexity seen in the nervous system.[316] Alternative splicing in embryonic and adult neural stem cells regulates processes such as transcription factor activity, cell fate, axon guidance, the development of neurotransmitter receptors, and the switch between proliferation and differentiation.[316]

Deregulation of components of the spliceosome has been associated with weakened immune response.

The SF3 complex is essential for splicing in human cells, and its complete inhibition results in mRNA build up, depleted protein expression, and eventual cell death.[322] Protein depletion of the SF3A1 or SF3B1 subunits did not cause cell death, but resulted in a decreased immune response in mouse and human cells.[323] When challenged with gram negative bacterial lipopolysaccharide, inhibition of SF3A1 and SF3B1 resulted in a decreased expression of inflammatory cytokines tumour necrosis factor α (TNF-α) and interleukin 6 (IL-6), indicating that the two subunits are specifically required for a robust innate immune response.[323]

The SF3A and SF3B complexes also interact with PPIE, which was the most down-regulated gene expressed in response to EFV treatment (Supplementary table S1, Figure 5.13). PPIE is a nuclear localized cyclophillin, also termed spliceophillin or immunophillin,[324] that is important for the regulation of pre-mRNA splicing, chromatin remodelling, transcription coupled DNA repair, and degradation of single stranded or super coiled DNA.[324,325] Multiple genes in the deregulated mRNA pathway, including PPIE, CPSF1, and UBNX7, play a role in mRNA stability and degradation and have all been implicated in directly inhibiting transcription and replication of viruses such as influenza and HIV.[319,326] Interestingly, previous work in our laboratory found UBXN7 and CPSF subunits to be down-regulated in SH-SY5Y and differentiated neurons, respectively, in response to HIV-tat treatment.[262,263]

EFV treatment causes a down-regulation in components of spliceosomes, possibly affecting proliferation, differentiation, and immune response.

The down-regulation of multiple components of the mRNA splicing pathway is directly linked to immune response and anti-viral activity.[319,323,326] Following EFV treatment for 72 hours, multiple components of the mRNA splicing pathway were down-regulated. Splicing factors SF3A1 and SF3B1, implicated in a decreased inflammatory response, were both down regulated at 72 hours post treatment (Figure 5.8).[323] When exposed to a pathogen, the innate immune response initiates an increase in the production of inflammatory cytokines, which can be detrimental if not tightly controlled. HIV infection causes chronic inflammation, even in patients with virologic control, and has been suggested to contribute to the development of HAND.[327] Previous work in our laboratory found that upon treatment with viral tat protein, SF3A1 and SF3B1 were both up-regulated in neural cell lines.[328] Another study found that inflammatory cytokine IL-6 was significantly increased subsequent to cessation of ARV treatment in infected individuals.[329] This indicates that one of the mechanisms by which HIV causes inflammation may be via an up-regulation of SF3A1 and SF3B1, which in turn aids in the production of IL-6,[323] contributing to the inflammatory response caused upon HIV infection.

In this work, treatment with EFV in the absence of HIV or HIV proteins resulted in a down regulation of SF3A1 and SF3B1 after 72 hours. It has been suggested that HIV infection and the subsequent inflammation associated with it during pregnancy may be a risk factor for neurodevelopmental disorders seen in HEU children, and that the ARV drugs have a protective effect by reducing inflammation via the reduction of viral load.[97] The response to EFV seen in this work may support this whereby, aside from reducing the viral load, EFV also reduces an inflammatory response via signalling modulation and causes the subsequent reduction of expression of SF3A and SF3B subunits that are vital for an inflammatory immune response. On the other hand, if this response is maintained throughout foetal development, it may cause HEU children to be more susceptible to infections, as depletion of SF3A1 and SF3B1 have

been linked to a lowered immune response.[323] Perinatal exposure to ARVs has been linked to an increased susceptibility to infections such as rubella, herpes simplex virus, CMV, toxoplasmosis, and influenza, which have been linked to neurodevelopmental problems when exposed during infancy.[97,103,330] Neurodevelopmental delays suspected to be caused by *in utero* ARV exposure may therefore not be caused directly by the ARVs, but rather due to increased vulnerability to illness during early childhood.

CPSF1 and UBXN7, two components of the mRNA splicing pathway, were down-regulated in undifferentiated NES cells (Figure 5.9). Interestingly, previous work in the Blackburn Laboratory found the same trend, although to a higher degree, of down-regulation of both UBXN7 and CPSF1 in neural cells when exposed to HIV-tat.[328,331] Investigating the effects of EFV and HIV-tat treatment concurrently would indicate whether the regulation of mRNA genes related to immune response and viral inhibition would result in a synergistic or antagonistic interaction between the innate immune response and the ARV drug action.

5.4.5.3 Gene and protein expression by JAK-STAT signalling after Interleukin-12 stimulation

JAK/STAT pathway regulates the expression of inflammatory responses

The JAK/STAT pathway is activated via interferons and cytokines binding to cell surface receptors and phosphorylating the JAK proteins, which in turn phosphorylate the STAT proteins. Phosphorylated STAT translocates into the nucleus and activates transcription of various target genes. The JAK/STAT pathway can also be activated by ROS to increase transcription of protective proteins.[332] In response to viral infection, interferons activate the JAK/STAT pathway, and the production of cytokines such as IL-6 and TNF-α is subsequently increased.[333] Increased IL-6 and TNF-α levels in turn activate JAK, leading to chronic inflammation, which if not regulated can cause disruption of CNS function, including that of the BBB.[333–336] ANXA2 interacts with STAT3 as a receptor that modulates cytokine production via the JAK/STAT pathway. The silencing of ANXA2 in human-derived macrophages resulted in a down regulation of TNF-α and IL-6 production when stimulated with a pro-inflammatory molecule that activates JAK/STAT.[337]

The cell fate and proliferation of stem cells is modulated by components of the JAK/STAT pathway

The JAK/STAT pathway is considered to be an essential attribute to the stemness of cells, promoting self-renewal.[338,339] Transforming growth factor ß (TGF-ß), responsible for the epithelial to mesenchymal transition (EMT) switch, regulates the expression of STAT3 and ANXA2 and induces EMT, which is vital during neural tube formation and BBB development.[340,341] In breast cancer cells, inhibition of STAT3 resulted in lower levels of ANXA2 expression and decreased EMT, causing in a more epithelial

phenotype.[342] Together this indicates that the JAK/STAT pathway via ANXA2 and STAT3 regulates the maintenance of stemness.

Pathogenic viruses hijack the JAK/STAT machinery to gain entry into host cells.

In murine brain endothelial cells, ANXA2 was up-regulated in response to fungal infection, which resulted in an increase in fugal invasion of the BBB. The subsequent knockdown of ANXA2 resulted in a weakened immune response when challenged and inhibited the transmigration of the fungus across the BBB.[343] Both HIV and pathogenic *Cryptococcus neoformans* hijack ANXA2, the former using ANXA2 to improve viral entry and infectivity, [344,345] and the latter using ANXA2 to traverse the BBB.[343] HIV increases the production of IL-6 and TNF-α, and subsequently up-regulates expression of STAT proteins.[346,347] The JAK/STAT response to HIV and EFV both result in the increase of STAT3 (although transient with EFV treatment) and ANXA2 protein levels (Figure 5.10). It appears that EFV may lower cytokine production while HIV increases it, based on the observed down-regulated genes involved in cytokine regulation (SF3A1 and SF3B1) in response to EFV treatment (section 5.4.5.2). Common genes deregulated in EFV and HIV treatment require further investigation in order to determine whether the response is synergistic or antagonistic, and how it affects the efficacy of EFV.

Considering that HIV uses ANXA2 to gain entry into the host cell, it would be pertinent to investigate whether HIV uses ANXA2 to traverse the BBB, as *C.neoformans* does, to elucidate the mechanism by which HIV enters the CNS. HIV and IL-6 synergistically increase infected monocyte migration across *in vitro* models of the BBB, and STAT1 plays a role in HIV-induced BBB damage.[346] It is possible that HIV uses the up-regulation of IL-6 and subsequent up-regulation of ANXA2 as a means to enter the CNS. If HIV uses the JAK/STAT pathway for BBB traversal, then the increase in expression in response to EFV treatment may implicate a weakened BBB, due to EFV and HIV, as a cause of the CNS side effects seen with EFV treatment.

The down-regulation of JAK/STAT pathway genes may cause alterations to proliferation of NES cells.

Based on the link between cytokine production, JAK/STAT signalling, and the response to EFV, it appears that EFV may be able to alter the innate inflammatory immune response *in vitro* as a signalling molecule. If EFV does indeed affect IL and cytokine signalling, then it may contribute to the

mechanistic causes of HEU children being more susceptible to childhood illnesses.[97,103] Further investigation of the long-term effects of the deregulation of this pathway caused by EFV is also important, especially in the context of neurodevelopment. For example, a haploinsufficiency in mice of PAK2 resulted in abnormal synapse morphology and decreased synapse density. The mice also displayed characteristics of impaired social interactions.[348] Synapse formation is critical for memory and learning, and aberrant formation during neurogenesis may cause long term effects into adulthood, as seen in mice models.[348,349] Although behavioural deficits in humans are more complex, it is interesting to note that subtle behavioural differences have been detected in HEU children, including verbal IQ and language expression, which can have a major impact on social interactions.[99,116] It is possible that deregulated JAK/STAT signalling may affect normal neurogenesis and CNS development. PAK2 has been implicated in the control of proliferation in stem cells, possibly resulting in the decreased synapse density observed in the haploinsufficiency mouse model.[348] PAK2 expression is strongly associated downstream of phosphorylated STAT3 and its activation is further increased by RAC1.[350,351] In this work, the overall lower levels STAT3, RAC1, and PAK2 compared to the control indicates that the EFV treatment may affect the efficiency or rate of proliferation, possibly acting as a signalling molecule and altering the signal transduction of the JAK/STAT pathway (Figure 5.10 and 5.11).[350]

Phosphoproteomic analysis would give insight into the effects of EFV as a potential signal transducer and elucidate how the JAK/STAT pathway and its target genes are affected by EFV, and how this in turn may affect CNS development.

5.4.5.4 Wnt signalling

Wnt signalling transcriptional regulation modulates embryogenesis and neurogenesis

The Wnt signalling cascade is involved in many stages of embryonic development and plays an important role in both embryonic and adult neurogenesis.[352,353] Wnt signalling via the canonical pathway generally results in transcriptional regulation of various genes by CTNNB1. Briefly, Wnt ligands bind to the frizzled receptor and low-density lipoprotein cell surface receptors on target cells and initiate the transduction of signals to inhibit the cytoplasmic destruction complex. This complex consists of axin, adenomatous polyposis coli tumour suppressor protein, GSK3B, casein kinase 1, and protein

phosphatase 2A. Cytoplasmic CTNNB1 levels are normally low due to phosphorylation by the destruction complex, marking it for proteosomal degradation. In the presence of Wnt signalling, the destruction complex is destabilized and is thus unable to phosphorylate CTNNB1, which subsequently accumulates in the cytoplasm, translocates into the nucleus, and induces the expression of various Wnt target genes.[354]

The proliferative state of neural stem cells is maintained by the Wnt signalling pathway

Wnt signalling via CTNNB1, the transcriptional activator of the Wnt pathway, is required for the maintenance of neural stem cells; a loss of signalling induces neural, glial, and oligodendral differentiation. [355–357] GSK3B constitutes part of the destruction complex that phosphorylates CTNNB1 in the absence of Wnt signalling, and its inhibition results in the stabilization of cytoplasmic CTNNB1, which promotes self-renewal in stem cells and protection from premature differentiation.[353,358,359] By knocking out CTNNB1, the differentiation blockade caused by GSK3B inhibition is alleviated and cells begin to differentiate.[358,359] Ablation of CTNNB1 also decreased the rate of proliferation and increases the number of cells exiting the proliferation cycle and differentiating, controlling the size of the precursor pool and, by extension, the size of the nervous system is thus partially controlled by CTNNB1.[357]

Mutations affecting Wnt signalling result in aberrant craniofacial patterning and neurogenesis

During embryogenesis, GSK3B and CTNNB1 have multiple functions, including participating in skeletal patterning. In mouse knockout models, all homozygous null GSK3B mice had a cleft palate, as well as other skeletal dysmorphism. The cleft palate phenotype could only be rescued early in foetal development, indicating the importance of GSK3B for craniofacial patterning during early embryonic development.[360] CTNNB1 null mice die in early embryonic development with brain and craniofacial malformations, and conditional knockout of CTNNB1 results in severe dendrite malformation followed by neuronal death.[361,362] In humans, mutations of CTNNB1 present with “dose sensitive” developmental delay, postnatal microcephaly, progressive ataxia, and spasticity.[363,364]

Viral replication can be modulated by Wnt signalling

The activated Wnt pathway and its constituents have been implicated in HIV positive long-term non-progressors (LTNP), whereby viral control is achieved without the help of ARVs.[303] The activated Wnt pathway is suggested to improve cell survival in LTNPs and contribute to a stronger antiviral response by regulation of cytokine activity.[303] Inhibition of GSK3B, mimicking Wnt signalling, causes an increase in CTNNB1 and a decrease in viral replication.[365–367] When treated with HIV, an up-regulation of GSK3B was detected in neuronal cells leading to a decrease in CTNNB1 and an increase in viral replication.[365–367] This occurs due to the HIV gp120 envelope protein blocking Wnt signalling and preventing CTNNB1 from entering the nucleus, where it is able to repress HIV replication by binding to the HIV promoter region.[367,368]

EFV treatment in proliferating NES cells may cause a shift towards differentiation and points to a possible mechanism of CNS side effects with EFV treatment.

Of the 11 genes enriching the Wnt signalling pathway in response to EFV treatment, eight were down-regulated, including the transcriptional regulator CTNNB1, which would likely cause a decrease in the transcription of Wnt target genes of the canonical pathway.[353,354] In both the control and treated conditions, GSK3B expression initially increased, which correlates to a decrease in CTNNB1 (Figure 5.12), as increased GSK3B expression would result in more CTNNB1 being phosphorylated and marked for degradation.[353,354] After 72 hours of exposure, both GSK3B and CTNNB1 expression increased in the control, which was unexpected as GSK3B expression results in CTNNB1 degradation. This may be explained by phosphoproteomic analysis, as more CTNNB1 may be phosphorylated and marked for degradation at this particular point in time, as opposed to lowered expression levels due to degradation.[353,354]

Both GSK3B and CTNNB1 were down regulated in the treatment group compared to the control group (Figure 5.12). The inhibition or knockdown of both of these genes results in differentiation of embryonic or neural stem cells, [356–359] indicating that the EFV treated NES cells may be progressing towards differentiation or are proliferating less efficiently. EFV has been implicated as potentially causing risk to foetal neural development as seen in animal studies and case studies where neural tube defect is reported with EFV as the only known risk factor.[78–81] Interestingly, a cleft palate has been observed in monkeys and humans after exposure to EFV during foetal development,[82,249,254,369] as seen with GSK3B knockout mice.[360] EFV toxicity in children has also resulted in progressive ataxia,[118]

as seen with mutated CTNNB1 genes.[363,364] The down-regulation of expression of GSK3B and CTNNB1, both of which are involved in early brain and craniofacial development, may indicate the mechanism by which EFV can cause the above-mentioned malformations.

CTNNB1 also plays a role in BBB maintenance, as well as inhibits viral replication as part of an innate antiviral response. If EFV causes a down-regulation of CTNNB1 in CNS tissue, the BBB may be weakened and the viral replication inhibition by CTNNB1 would be decreased in the CNS. This would be a concerning outcome, as that would imply that EFV treatment makes the CNS more vulnerable to HIV infection via a damaged BBB, reduced innate replication inhibition, and increased vulnerability to a peripheral inflammatory response. If this were the case, persistent HAND with undetectable plasma viral load or EFV-related CNS side effects may be due to a continuous neuroinflammatory response or a temporarily higher CNS viral load, caused by a weakened BBB.[370]

5.4.5.5 Themes in enriched pathways briefly summarised and discussed.

Multiple deregulated pathways point to a shift towards differentiation of proliferating NES cells.

Each enriched pathway contained multiple genes that participate in the maintenance of stem cells. Down-regulation of the various genes discussed was consistently linked to a shift from proliferation to differentiation. The NES cells used in this work were treated with EGF and FGF in order to maintain a proliferating state and no morphological changes that indicated differentiation were visually observed during the treatment period.[123]

One of the most highly up-regulated genes in the data set was CLIP2. Although not present in any of the enriched pathways, CLIP2 is associated with microtubules and cytoskeleton formation, and is an important regulator of neurite, axon, and dendrite formation during differentiation.[317] Initially, CLIP2 expression in the control and treated conditions was equivalent, but 72 hours post-treatment, CLIP2 expression increased compared to the control. The up-regulation of CLIP2 in the treated condition further supports the hypothesis that NES cells shift towards differentiation with increased length of exposure to EFV (Figure 5.13).

In the treatment condition, many of the down-regulated proteins follow similar trends to the control condition with slightly lowered expression (Figure 5.7, 5.8, and 5.11). Multiple genes involved in

cholesterol biosynthesis decreased in expression over time in both conditions, which may possibly indicate that the shift towards differentiation was caused in part by the drug-delivery vehicle, DMSO. A depletion of ANXA2 was observed in both the treated and control samples and has been linked to causing the inhibition of STAT3 activation by EGF, [342] one of the factors used to maintain proliferation in NES cells. Based on this evidence, it is possible that the vehicle, DMSO, acts as a signalling molecule, which ultimately causes EGF signal to be weakened and ineffective at maintaining proliferation.

DMSO is widely used as a vehicle for drug delivery as it is considered to be genetically inactive. Recently, subtle gene expression modulation was observed with concentrations as low as 0.05% DMSO.[371] High concentrations of DMSO administered at 0.5% has also been shown to decrease pluripotency markers and cause stem cells to be more susceptible to differentiation signals.[372–374] In this work, DMSO was administered at a final concentration of 0.05% and was not found to impact cell viability significantly at

0.125%. DMSO above 1% resulted in 80% survival compared to the control, although this trend was not statistically significant (Chapter 4, section 4.3.2). No visual morphological changes were observed in cells treated with 0.01 and 0.1% of DMSO[373] or in the current work with 0.05%. The down-regulation of various genes related to differentiation in both conditions indicates that an assessment of the proteome of DMSO treated NES cells is necessary in order to determine whether DMSO is an appropriate vehicle when working with this cell line. The effects of EFV treatment may also need to be re-evaluated using a different drug-delivery vehicle, but it is still possible to interpret the effects of EFV on the NES cells due

to differential regulation. A significant difference between the conditions, even if following the same trend, indicates that EFV caused a response in the cells. Even so, conclusions must be drawn with caution, as effects of the EFV treatment may be inflated due to DMSO increasing membrane permeability.[373]

EFV treatment may cause a disruption in normal inflammatory response in NES cells

One of the outcomes of down-regulation of cholesterol biosynthesis in the context of HIV infection is the subsequent decrease in viral replication, due to viral dependence on cholesterol for replication and infectivity. A decrease in cholesterol biosynthesis is therefore a desired side effect of ARV treatment.

The inflammatory response system and regulation of cholesterol synthesis are tightly linked functions, both of which were down-regulated in response to EFV treatment. A decreased inflammatory response is another desired side effect of ARV treatment, and possibly occurs with EFV treatment caused by a down regulation of SF3A1 and SF3B1. In the context of foetal development, this would contribute to protection from the increased inflammation caused by maternal HIV infection.[327] On the other hand, a decreased immune response during foetal development may cause increased susceptibility to infection at during early childhood development.[97]

Based on the findings in this work, it appears that EFV reduces an innate immune response through the reduction of cytokine production. EFV caused a reduction in SF3A1 and SF3B1 protein levels after 72 hours, which is known to cause a reduction in IL-6 and TNF-α cytokines.[323] Inhibition or down-regulation of components of the cholesterol biosynthesis pathway, as seen during the 72 hour time-course, further decrease IL-6 and TNF-α expression,[336] which results in limited activation of the JAK/STAT pathway and subsequently limits the JAK/STAT inflammatory immune response. A reduced immune response caused by EFV may offer an important avenue for future research, as HEU children are more susceptible to various infections which can affect neurodevelopment when contracted during childhood.[97,103,330] Negative neurodevelopmental outcomes in HEU children due to childhood infections can be easily minimised by early intervention strategies to boost immune function in HEU children immediately postnatally.

Malformations caused by deregulated genes mirror malformations suspected to be caused by EFV exposure in utero

Various differentially regulated genes in the enriched pathways were associated with CNS malformations or disorders. A reduction in cholesterol biosynthesis and depletion of certain genes such as PAK2 are both linked to synapse malformation which is a vital component in memory and learning.[349] When depleted in mouse models, multiple deregulated genes in this work such as FDFT1, GSK3B, and CTNNB1 cause embryonic lethality or malformations that echo those seen in cases where EFV is the sole risk factor. For example, the cleft palate phenotype, which has been implicated in exposure to EFV and the depletion of GSK3B during embryo development, is also a phenotype of cholesterol deficiencies.[283,309,360,375] Given that cholesterol depletion is commonly seen during ARV treatment, the link between EFV, cholesterol deficiency, and birth defects is one that requires further investigation. These observations indicate a possible molecular mechanism for the potential

dangerous effects of *in utero* exposure to EFV that have yet to be confirmed or denied. In order to detect even a small increase in the incidence of rare disorders, such as incomplete neural tube formation, a very large sample size is required. There is a paucity of data regarding the effects of EFV when used during pregnancy, with most studies consisting of few participants and poorly matched control groups. Although EFV is generally considered safe for use during pregnancy, it is still classed as a category D drug and thus needs further investigation.

Based on the observation that EFV treatment may cause cells to cease proliferation prematurely, and that the expression of essential proteins for craniofacial and brain development were decreased, it would be pertinent to assess whether the altered protein levels persist over a longer period of time, as well as during differentiation and maturation. Diffusion tensor imaging (DTI) neuroimaging studies in HEU children found abnormalities in the CNS which may represent microscopic deficits in axonal structure, which are suggested to be as a result of abnormal cell proliferation or aberrant pruning.[252] This supports the hypothesis that EFV treatment may cause a premature exit from proliferation and promote differentiation in NES cells. The abnormal axonal structure observed in HEU children DTI results correlated to subtle neurological defects in the HEU children,[252] which further indicates the need for a deeper understanding of the safety profile of EFV for HEU children, and how exposure may affect them throughout development.

A comparison of the response to EFV and HIV-tat treatment shows similarities and differences that necessitate further investigation.

This work and previous work in our laboratory highlight differences and similarities in the response of neural cells to HIV and EFV. In some cases, down-regulation occurred in response to EFV treatment, and up-regulation in response to HIV-tat treatment as seen with SF3A1, SF3B1, and GSK3B. In other cases, the regulation of the gene was in the same direction but of a different magnitude, as seen with a small decrease in UBXN7 in response to EFV, and a large decrease in response to HIV-tat. Further research to elucidate the potentially synergistic effects of EFV and the innate immune response when challenged with HIV may improve our understanding of the aetiology of persistent HAND and CNS side effects in the ARV treatment era.

Proteome changes observed subsequent to predicted initiation of EFV metabolism may be caused by EFV metabolites

The majority of differentially regulated genes occurred between 48 and 72 hours post EFV treatment. Based on the findings from previous chapters that indicate that NES cells begin to metabolise EFV more rapidly between 48 and 72 hours, the changes seen in the proteome may be caused as a result of the up-regulation of EFV metabolism. The major metabolite of EFV, 8-hydroxy-EFV, is metabolised by the CYP2B6 cytochrome and has been implicated in causing various CNS side effects seen with EFV treatment.[274,376] It is thus plausible that the alterations in the proteome seen after 72 hours, which correlates to the hypothesised initiation of EFV metabolism (Chapter 4, section 4.4.4), may be due to a response to the increase in the 8-hydroxy-EFV metabolite as opposed to un-metabolised EFV.

5.5 Conclusion

The benefits of ARV usage are undeniable and have changed HIV from a death sentence to a chronic, manageable illness. HIV-infected patients on ARV treatment live longer, relatively healthy lives. ARV treatment has also resulted in a substantial decrease the in incidence of HIV transmission *in utero,* allowing HIV-positive mothers to give birth to HIV-negative children. Thus, ARV treatment for HIV- positive pregnant women is a top priority in order to protect both the mother and the child. As the population of children born with HIV infection decreases, the population of those exposed to ARVs *in utero* increases, highlighting the need to address the potential long-term effects of exposure to often toxic drugs during a critical developmental period.

EFV is a first line treatment in South Africa that is administered as part of an FDC, with pregnant women being priority patients regardless of the stage of pregnancy. Although the overarching opinion is that EFV is safe for use in pregnancy, the fact that EFV causes CNS toxicity in adults makes its safety profile in vulnerable foetuses questionable. This study, among others, has shown that EFV can cause global cellular changes with negative side effects that may persist throughout the life on an HEU child if not sufficiently recognized and mitigated as early as possible.

EFV appears to cause proliferating NES cells either to become less efficient at proliferating, or to begin to prepare for differentiation. The potential differentiation initiation was found to be a function of all four enriched pathways, indicating that it is highly probable that this was a true effect. EFV treatment caused deregulation in multiple signalling pathways, possibly disrupting Wnt and JAK/STAT signalling, both of which are vital for embryonic development. Treatment with EFV caused a major overall down-regulation of the cholesterol biosynthesis pathway, which is important for not only embryonic development but also general CNS health. EFV was also implicated in affecting the activation of the inflammatory response through multiple pathways, which could have both positive and negative effects in terms of foetal development.

Although this study was performed in proliferating NES cells, thus making it a model specifically for early neural development, many of the effects caused by aberrant expression of the genes in the deregulated pathways echo the effects of EFV not only in foetal neurogenesis and development, but also in the CNS of adult HIV positive people suffering from HAND. This work can therefore be extrapolated to some degree to explain the effect of EFV on the adult CNS, which also contains a population of neuronal stem cells. By analysing EFV in isolation, it may be possible to tease apart the

effects of HIV and EFV, as well as to elucidate potential synergistic effects that may occur due to the ability of HIV to hijack many vital cellular processes. This work has elucidated multiple pathways of interest for further analysis involving not only neurogenesis but also mature neurons in the presence of EFV, which may lead to vital pre-clinical data to improve the protection of both the foetal and adult CNS in the ARV era.

5.6 Limitations

5.6.1 Electing to not use MTC subsequent to initial statistical analysis

There are many opinions that posit that discovery work followed by pathway analysis and validation mitigates the need for MTC, which can result in the loss of valuable information. Not using MTC in this work is considered a limitation as the decision was made subsequent to observing that MTCs recommended for proteomic data were too stringent for this work. Low protein identification, possibly due to poor instrument performance or poor protein extraction and digestion by GuHCl lysis protocol, limits the present work, since significantly dysregulated but lower abundant proteins may have been missed. This study would need to be repeated in order to determine the cause of low numbers of statistically significant results.

5.6.2 The EFV vehicle, DMSO, may have caused a proteomic response

Based on observations in both the treatment and control conditions, it is suspected that DMSO might have an effect on NES cell proliferation and signalling. This may have caused the effect of DMSO and EFV on the cells to be conflated. At higher concentrations, DMSO is also known to increase membrane permeability, and thus may have exaggerated the effects of EFV *in vitro.*

5.6.3 Inaccurate modelling of *in vivo* EFV concentration *in vitro.*

Prior to performing a proteomic analysis of NES cells exposed to EFV, the concentration of EFV in cell culture conditions over time was analysed. Although it was attempted to make the dosage and the treatment schedule as biologically relevant as possible, the conditions used for NES cell culture effectively resulted in the highly lipophilic EFV molecule being absorbed into the plastic tissue culture plates, creating a reservoir. EFV accumulates in the CNS but it is not known to what extent, and therefore the final concentration of EFV that the cells were exposed to may not be as biologically relevant as intended.

5.6.4 Poor MS quality and protein extraction

Based on previous reports from the Blackburn Laboratory, the Q-Exactive instrument was not operating optimally, resulting in relatively low peptide and protein group identification. During sample analysis, the LC spray was inconsistent, but due to time limitations on the instrument, it was not possible to re-analyse samples analysed during a period of poor chromatographic spray. Together, these factors may have caused the sensitivity of the experiment decrease.

5.7 Future Research

5.7.1 Investigating the effects of EFV during neuronal differentiation and in mature neurons.

This work focused on investigating the effects of EFV on NES cells during proliferation. In order to create a broader overview of the effects of EFV on neural development, it would be pertinent to assess the effects of EFV on the NES cells during differentiation as well as once matured in the presence of EFV. Work assessing the effects of EFV on mature neurons not exposed during maturation would offer insights into the potential effects of EFV in the adult CNS, as suggested in this work. Based on findings in chapter 4 (section 4.4.4), EFV may only initiate its own metabolism after reaching a threshold concentration. This indicates that studies of EFV should extend for more than 72 hours, as this would allow for insight into the effect of EFV and its metabolites on the neural system. Further investigation of the metabolites and the upstream processes involved in EFV metabolism in the neural system would further improve our understanding of how EFV affects the CNS.

5.7.2 Phosphoproteomic analysis to assess signalling pathways

Based on the findings elucidated by pathway analysis, EFV can affect transcriptional regulation of genes within immune response and signalling pathways, as well as potentially acting as a signalling molecule that modulates signal transduction. Phosphoproteomic analysis would offer insight into the signal transduction networks that are affected by EFV in NES cells and mature neurons.

5.7.3 Assessing synergy or antagonistic effects caused by co-treatment with HIV-tat and EFV.

EFV treatment resulted in the deregulated expression of several genes that were also deregulated with HIV-tat treatment. The next investigation would thus be to establish how these responses change when exposed to both EFV and HIV or HIV-tat. This work would be vital in gaining a deeper understanding of the persistent presence of HAND, even in patients with undetectable viral loads, as well as the synergistic and/or antagonistic effects of HIV and EFV in the CNS.

5.7.4 Comparing the effects of metabolised and unmetabolised EFV

Polymorphisms of the primary metaboliser of EFV, CYP2B6, cause slow drug metabolism, resulting in higher EFV plasma levels. Slow metabolisers have an increased risk of experiencing CNS side effects and are more likely to discontinue EFV treatment.[377] An assessment of the molecular effects of EFV in slow metabolisers, as well as the molecular effects of pure 8-hydroxy-EFV would help to improve the current knowledge of the safety profile of EFV and its metabolites in order to optimise the efficacy and toxicity profile of EFV.

References

1. Statistics South Africa. *Mid-Year Population Estimates 2018*.; 2018.

2. Haase AT. Pathogenesis of lentivirus infections. *Nature*. 1986;322:130-136. doi:10.1038/322130a0.

3. Doitsh G, Galloway NLK, Geng X, et al. Pyroptosis drives CD4 T-cell depletion in HIV-1 infection. *Nature*. 2014;505(7484):509-514. doi:10.1038/nature12940.Pyroptosis.

4. Biancotto A, Iglehart SJ, Vanpouille C, et al. HIV-1–induced activation of CD4(+) T cells creates new targets for HIV-1 infection in human lymphoid tissue ex vivo. *Blood*. 2008;111(2):699-704. doi:10.1182/blood-2007-05-088435.

5. Ho DD, Neumann AU, Perelson AS, Chen W, Leonard JM, Markowitz M. Rapid turnover of plasma virions and CD4 lymphocytes in HIV-1 infection. *Nature*. 1995;373(6510):123-126. doi:10.1038/373123a0.

6. Statistics South Africa. *Mid-Year Population Estimates*.; 2016. doi:Statistical release P0302.

7. WHO (World Health Organisation). HIV/AIDS fact sheet. 2016.

8. Iwelunmor J, Blackstone S, Veira D, et al. Toward the sustainability of health interventions implemented in sub-Saharan Africa: a systematic review and conceptual framework. *Implement Sci*. 2015;11(1):43. doi:10.1186/s13012-016-0392-8.

9. Sharp PM, Hahn BH. Origins of HIV and the AIDS pandemic. *Cold Spring Harb Perspect Med*. 2011;1(1):1-22. doi:10.1101/cshperspect.a006841.

10. Esté JA, Telenti A. HIV entry inhibitors. *Lancet*. 2007;370(9581):81-88. doi:10.1016/S0140-6736(07)61052-6.

11. Chan DC, Kim PS. HIV entry and its inhibition. *Cell*. 1998;93(5):681-684. doi:10.1016/S0092-8674(00)81430-0.

12. Zheng YH, Lovsin N, Peterlin BM. Newly identified host factors modulate HIV replication. *Immunol Lett*. 2005;97(2 SPEC. ISS.):225-234. doi:10.1016/j.imlet.2004.11.026.

13. Das K, Arnold E. HIV-1 reverse transcriptase and antiviral drug resistance. Part 1. *Curr Opin Virol*. 2013;3(2):111-118. doi:10.1016/j.coviro.2013.03.012.

14. Goldgur Y, Craigie R, Cohen GH, et al. Structure of the HIV-1 integrase catalytic domain complexed with an inhibitor: a platform for antiviral drug design. *Proc Natl Acad Sci U S A*. 1999;96(23):13040-13043. doi:10.1073/pnas.96.23.13040.

15. Burke TR, Fesen MR, Mazumder a, et al. Hydroxylated aromatic inhibitors of HIV-1 integrase. *J Med Chem*. 1995;38(21):4171-4178. doi:10.1021/jm00021a006.

16. Wensing AMJ, van Maarseveen NM, Nijhuis M. Fifteen years of HIV Protease Inhibitors: raising the barrier to resistance. *Antiviral Res*. 2010;85(1):59-74. doi:10.1016/j.antiviral.2009.10.003.

17. Kohl NE, Emini EA, Schleif WA, et al. Active human immunodeficiency virus protease is required for viral infectivity. *Proc Natl Acad Sci*. 1988;85(13):4686-4690. doi:10.1073/pnas.85.13.4686.

18. Brik A, Wong C-H. HIV-1 protease: mechanism and drug discovery. *Org Biomol Chem*. 2003;1(1):5-14. doi:10.1039/b208248a.

19. Lange JMA, Ananworanich J. The discovery and development of antiretroviral agents. *Antivir Ther*. 2014;19:5-14. doi:10.3851/IMP2896.

20. Zapor MJ, Cozza KL, Wynn GH, Wortmann GW, Armstrong SC. Antiretrovirals, Part II: focus on non-protease inhibitor antiretrovirals (NRTIs, NNRTIs, and fusion inhibitors). *Psychosomatics*.

2004;45(6):524-535. doi:10.1176/appi.psy.45.6.524.

21. De Clercq E. The role of non-nucleoside reverse transcriptase inhibitors (NNRTI) in the therapy of HIV-1 infection. *Antiviral Res*. 1998;38(3):153-179.

22. Encyclopaedia Britannica. Retrovirus infection and reverse transcription. Encyclopaedia Britannica, Inc.

23. Larder B, Darby G, Richman D. HIV with reduced sensitivity to zidovudine (AZT) isolated during prolonged therapy. *Science (80-)*. 1989;243:1731-1734.

24. Montaner JSG, Reiss P, Cooper D, et al. A Randomized, Double-blind Trial Comparing Combinations of Nevirapine, Didanosine, and Zidovudine for HIV-Infected Patients. *Jama*. 1998;279(12):930. doi:10.1001/jama.279.12.930.

25. Scott H, Squires K, Hughes MD, et al. A controlled trial of two nucleoside analogues plus indinavir in persons with human immunodeficiency virus infection and CD4 cell counts of 200 per cubic millimeter or less. *N Engl J Med*. 1997;337:785-791. doi:10.1056/NEJMoa012295.

26. CASCADE Collaberation. Survival after introduction of HAART in people with known duration of HIV-1 infection. *Lancet*. 2000;355:1158-1159.

27. Crum NF, Riffenburgh RH, Wegner S, et al. Comparisons of Causes of Death and Mortality Rates Among HIV-Infected Persons. *JAIDS J Acquir Immune Defic Syndr*. 2006;41(2):194-200. doi:10.1097/01.qai.0000179459.31562.16.

28. Bangsberg DR, Kroetz DL, Deeks SG. Adherence-resistance relationships to combination HIV antiretroviral therapy. *Curr HIV/AIDS Rep*. 2007;4(2):65-72. doi:10.1007/s11904-007-0010-0.

29. Chesney MA, Ickovics JR, Chambers DB, et al. Self-reported adherence to antiretroviral medications among participants in HIV clinical trials: the AACTG adherence instruments. Patient Care Committee & Adherence Working Group of the Outcomes Committee of the Adult AIDS Clinical Trials Group (AACTG). *AIDS Care*. 2000;12(3):255-266. doi:10.1080/09540120050042891.

30. Chesney M. Factors affecting adherence to antiretroviral therapy. *Clin Infect Dis*. 2000;30:S171-S176. doi:10.1086/313849.

31. Bhatt NB, Baudin E, Meggi B, et al. Nevirapine or efavirenz for tuberculosis and HIV coinfected patients: Exposure and virological failure relationship. *J Antimicrob Chemother*. 2015;70(1):225-232. doi:10.1093/jac/dku348.

32. Lalloo UG. Efavirenz and Nevirapine Interactions with Rifampicin: Resolving the Dilemmas? *Clin Infect Dis*. 2009;48:1760-1762. doi:10.1086/599115.

33. South African National AIDS Council. *South Africa Global AIDS Response Progress Report*.; 2016.

34. Best BM, Letendre SL, Koopmans P, et al. Low CSF Concentrations of the Nucleotide HIV Reverse Transcriptase Inhibitor, Tenofovir. *J Acquir Immune Defic Syndr*. 2013;59(4):376-381. doi:10.1097/QAI.0b013e318247ec54.LOW.

35. Nirogia R, Bhyrapunenia G, Kandikerea V, et al. Pharmacokinetic profiling of efavirenz–emtricitabine–tenofovir fixed dose combination in pregnant and non-pregnant rats. *Biopharm Drug Dispos*. 2012;28(33):265-277. doi:10.1002/bdd.

36. Moodley T, Moodley D, Sebitloane M, Maharaj N, Sartorius B. Improved pregnancy outcomes with increasing antiretroviral coverage in South Africa. *BMC Pregnancy Childbirth*. 2016:1-10. doi:10.1186/s12884-016-0821-3.

37. Republic of South Africa Department of Health. *FDC Circular*.; 2016.

38. De Clercq E. Antiviral drugs in current clinical use. *J Clin Virol*. 2004;30(2):115-133. doi:10.1016/j.jcv.2004.02.009.

39. Rakhmanina NY, van den Anker JN. Efavirenz in the Therapy of HIV Infection. *Natl Institutes Heal*. 2011;6(1):95-103. doi:10.1517/17425250903483207.Efavirenz.

40. Raines C, Radcliffe O, Treisman GJ. Neurologic and psychiatric complications of antiretroviral agents. *J Assoc Nurses AIDS Care*. 2005;16(5):35-48. doi:10.1016/j.jana.2005.07.004.

41. Vivithanaporn P, Gill MJ, Power C. Impact of current antiretroviral therapies on neuroAIDS. *Expert Rev Anti Infect Ther*. 2011;9(4):371-374. doi:10.1586/eri.10.179.

42. Margolis AM, Heverling H, Pham P a., Stolbach A. A Review of the Toxicity of HIV Medications. *J Med Toxicol*. 2014;10(1):26-39. doi:10.1007/s13181-013-0325-8.

43. Zhang Y, Song F, Gao Z, et al. Long-term exposure of mice to nucleoside analogues disrupts mitochondrial DNA maintenance in cortical neurons. *PLoS One*. 2014;9(1):1-7. doi:10.1371/journal.pone.0085637.

44. Mayer KH, Ramjee G. The current status of the use of oral medication to prevent HIV transmission. *Curr Opin HIV AIDS*. 2015;10(4):226-232. doi:10.1097/COH.0000000000000170.

45. Roell KR, Reif DM, Motsinger-Reif A a. An introduction to terminology and methodology of chemical synergy-perspectives from across disciplines. *Front Pharmacol*. 2017;8(APR):1-11. doi:10.3389/fphar.2017.00158.

46. Basavapathruni A, Bailey CM, Anderson KS. Defining a Molecular Mechanism of Synergy between Nucleoside and Nonnucleoside AIDS Drugs. *J Biol Chem*. 2004;279(8):6221-6224. doi:10.1074/jbc.C300523200.

47. Bousquet L, Pruvost A, Guyot AC, Farinotti R, Mabondzo A. Combination of tenofovir and emtricitabine plus efavirenz: In vitro modulation of ABC transporter and intracellular drue accumulation. *Antimicrob Agents Chemother*. 2009;53(3):896-902. doi:10.1128/AAC.00733-08.

48. Faucette SR, Zhang T, Moore R, et al. Relative Activation of Human Pregnane X Receptor versus Constitutive Androstane Receptor Defines Distinct Classes of CYP2B6 and CYP3A4 Inducers. *J Pharmacol Exp Ther*. 2014;320(1):72-80. doi:10.1124/jpet.106.112136.Relative.

49. Cavalcante GIT, Capistrano VLM, Cavalcante FSD, et al. Implications of efavirenz for neuropsychiatry: a review. *Int J Neurosci*. 2010;120(12):739-745. doi:10.3109/00207454.2010.520541.

50. Dalwadi D a., Ozuna L, Harvey BH, Viljoen M, Schetz J a. Adverse Neuropsychiatric Events and Recreational Use of Efavirenz and Other HIV-1 Antiretroviral Drugs. *Pharmacol Rev*. 2018;70(3):684-711. doi:10.1134/S2070048211050036.

51. Kenedi CA, Goforth HW. A Systematic Review of the Psychiatric Side-Effects of Efavirenz. *AIDS Behav*. 2011;15:1803-1818. doi:10.1007/s10461-011-9939-5.

52. Masliah E, DeTeresa RM, Mallory ME, Hansen L a. Changes in pathological findings at autopsy in AIDS cases for the last 15 years. *AIDS*. 2000;14(1):69-74. doi:10.1097/00002030-200001070-00008.

53. de Almeida SM, Letendre S, Ellis R. Human immunodeficiency virus and the central nervous system. *Braz J Infect Dis*. 2006;10(1):41-50. doi:/S1413-86702006000100009.

54. Sagar V, Pilakka-Kanthikeel S, Pottathil R, Saxena SK, Nair M. Towards nanomedicines for neuroAIDS. *Rev Med Virol*. 2014;24(2):103-124. doi:10.1002/rmv.1778.

55. Hauser KF, Knapp PE. *Interactions of HIV and Drugs of Abuse. The Importance of Glia, Neural Progenitors, and Host Genetic Factors*. Vol 118.; 2014. doi:10.1016/B978-0-12-801284-0.00009-9.

56. van Arnhem L a., Bunders MJ, Scherpbier HJ, et al. Neurologic Abnormalities in HIV-1 Infected Children in the Era of Combination Antiretroviral Therapy. *PLoS One*. 2013;8(5):1-6. doi:10.1371/journal.pone.0064398.

57. Maschke M, Kastrup O, Esser S, Ross B, Hengge U, Hufnagel a. Incidence and prevalence of neurological disorders associated with HIV since the introduction of highly active antiretroviral therapy (HAART). *J Neurol Neurosurg Psychiatry*. 2000;69:376-380. doi:10.1136/jnnp.69.3.376.

58. Hogan C, Wilkins E. Neurological complications in HIV. *Clin Med J R Coll Physicians London*. 2011;11(6):571-575. doi:10.7861/clinmedicine.11-6-571.

59. Woods SP, Moore DJ, Weber E, Grant I. Cognitive neuropsychology of HIV-associated neurocognitive disorders. *Neuropsychol Rev*. 2009;19(2):152-168. doi:10.1007/s11065-009-9102-5.

60. Saylor D, Dickens AM, Sacktor N, et al. HIV-associated neurocognitive disorder — pathogenesis and prospects for treatment. *nat rev neurol*. 2016;12(4):234-248. doi:10.1038/nrneurol.2016.27.HIV-associated.

61. Heaton RK, Franklin DR, Ellis RJ, et al. HIV-associated neurocognitive disorders before and during the era of combination antiretroviral therapy: Differences in rates, nature, and predictors. *J Neurovirol*. 2011;17(1):3-16. doi:10.1007/s13365-010-0006-1.

62. Ene L, Duiculescu D, Sm R, Victor. How much do antiretroviral drugs penetrate into the central nervous system? *J Med Life*. 2011;4(4):432-439.

63. Calcagno A, Di Perri G, Bonora S. Pharmacokinetics and Pharmacodynamics of Antiretrovirals in the Central Nervous System. *Clin Pharmacokinet*. 2014;53(10):891-906. doi:10.1007/s40262-014-0171-0.

64. WHO (World Health Organisation). *NEW WHO Recommendations Formulated for the 2013 Guidelines on HIV Testing and Counselling, Antiretroviral Therapy (ART) and HIV Service Delivery*.; 2013.

65. Best BM, Koopmans PP, Letendre SL, et al. Efavirenz concentrations in CSF exceed IC50 for wild-type HIV. *J Antimicrob Chemother*. 2011;66(2):354-357. doi:10.1093/jac/dkq434.

66. World Health Organization. Antiretroviral drugs for treating pregnant women and preventing HIV infection in infants. *Geneva WHO*. 2010;(April):1-117. doi:WHO/HIV/2012.6.

67. South African National Department of Health. *National Consolidated Guidelines for the Prevention of Mother-To-Child Transmission of HIV (PMTCT) and the Managment of HIV in Children, Adolescents and Adults*.; 2015. www.doh.gov.za.

68. Goga AE, Dinh T, Jackson DJ, et al. Population–level effectiveness of PMTCT Option A on early mother–to–child (MTCT) transmission of HIV in South Africa: implications for eliminating MTCT. *J Glob Health*. 2016;6(2):1-10. doi:10.7189/jogh.06.020405.

69. (Unaids) JUNP on H. *Progress Report*.; 2017. doi:UNAIDS/JC2923E.

70. Brent RL. Utilization of Animal Studies to Determine the Effects and Human Risks of Environmental Toxicants (Drugs, Chemicals, and Physical Agents) Robert. *Pediatrics*. 2004;113(4).

71. Colbers A, Greupink R, Burger D. Pharmacological considerations on the use of antiretrovirals in pregnancy. *Curr Opin Infect Dis*. 2013;26:575-588. doi:10.1097/QCO.0000000000000017.

72. Else LJ, Taylor S, Back DJ, Khoo SH. Pharmacokinetics of antiretroviral drugs in anatomical sanctuary sites: The fetal compartment (placenta and amniotic fluid). *Antivir Ther*. 2011;16(8):1139-1147. doi:10.3851/IMP1918.

73. Stek a. M, Best BM, Luo W, et al. Effect of pregnancy on emtricitabine pharmacokinetics. *HIV Med*. 2012;13(4):226-235. doi:10.1111/j.1468-1293.2011.00965.x.

74. Flynn PM, Mirochnick M, Shapiro DE, et al. Pharmacokinetics and Safety of Single-Dose Tenofovir Disoproxil Fumarate and Emtricitabine in HIV-1-Infected Pregnant Women and Their Infants. *Antimicrob Agents Chemother*. 2011;55(12):5914-5922. doi:10.1128/AAC.00544-11.

75. Zash R, Jacobson DL, Diseko M, et al. Comparative safety of antiretroviral treatment regimens in pregnancy. *JAMA Pediatr*. 2017;171(10). doi:10.1001/jamapediatrics.2017.2222.

76. Malaba TR, Phillips T, Le Roux S, et al. Antiretroviral therapy use during pregnancy and adverse birth outcomes in South African women. *Int J Epidemiol*. 2017;46(5):1678-1689. doi:10.1093/ije/dyx136.

77. Food and Drug Administration (FDA). *SUSTIVA (Efavirenz) Prescribing Information*.; 2011.

78. Fundarò C, Genovese O, Rendeli C, Tamburrini E, Salvaggio E. Myelomeningocele in a child with intrauterine exposure to efavirenz. *AIDS*. 2002;16(299-300).

79. Saitoh A, Hull AD, Franklin P, Spector S a. Myelomeningocele in an infant with intrauterine exposure to efavirenz. *J Perinatol*. 2005;25:555-556. doi:10.1038/sj.jp.7211343.

80. Santis M De, Carducci B, Santis L De, Cavaliere AF, Straface G. Periconceptional Exposure to Efavirenz and Neural Tube Defects. *Arch Intern Med*. 2001;161(reaction 3):1455-1457.

81. Gudu W, Bekele D. Encephalocele following a periconceptional exposure to efavirenz: A case report. *J Perinatol*. 2013;33(12):987-988. doi:10.1038/jp.2013.121.

82. Bera E, McCausland K, Nonkwelo R, Mgudlwa B, Chacko S, Majeke B. Birth defects following exposure to efavirenz-based antiretroviral therapy during pregnancy: a study at a regional South African hospital. *AIDS*. 2010;24(2):283-289. doi:10.1097/QAD.0b013e328333af32.

83. Bisio F, Nicco E, Calzi A, et al. Pregnancy outcomes following exposure to efavirenz-based antiretroviral therapy in the Republic of Congo. *New Microbiol*. 2015;38(2):185-192.

84. Knapp KM, Brogly SB, Muenz DG, et al. Prevalence of congenital anomalies in infants with in utero exposure to antiretrovirals. *Pediatr Infect Dis J*. 2012;31(2):164-170. doi:10.1097/INF.0b013e318235c7aa.

85. Sibiude J, Mandelbrot L, Blanche S, et al. Association between Prenatal Exposure to Antiretroviral Therapy and Birth Defects: An Analysis of the French Perinatal Cohort Study (ANRS CO1/CO11). *PLoS Med*. 2014;11(4). doi:10.1371/journal.pmed.1001635.

86. Van Dyke RB, Chadwick EG, Hazra R, Williams PL, Seage GR. The PHACS SMARTT study: Assessment of the safety of in utero exposure to antiretroviral drugs. *Front Immunol*. 2016;7(MAY). doi:10.3389/fimmu.2016.00199.

87. Kranick SM, Nath A. Neurologic complications of HIV-1 infection and its treatment in the era of antiretroviral therapy. *Continuum (Minneap Minn)*. 2012;18(6 Infectious Disease):1319-1337. doi:10.1212/01.CON.0000423849.24900.ec.

88. Giunta B, Ehrhart J, Obregon DF, et al. Antiretroviral medications disrupt microglial phagocytosis of β-amyloid and increase its production by neurons: implications for HIV-associated neurocognitive disorders. *Mol Brain*. 2011;4(1):23. doi:10.1186/1756-6606-4-23.

89. Shao L, Martin M V, Watson SJ, et al. Mitochondrial involvement in psychiatric disorders. *Ann Med*. 2008;40(4):281-295. doi:10.1080/07853890801923753.

90. Ford N, Mofenson L, Shubber Z, et al. Safety of efavirenz in the first trimester of pregnancy : an updated systematic review and meta-analysis. *AIDS*. 2014;28:123-131. doi:10.1097/QAD.0000000000000231.

91. Ford N, Calmy A. Efavirenz is not a known teratogen. *Pediatr Infect Dis J*. 2012;31(9):999. doi:10.1097/INF.0b013e31825c36fc.

92. Gatzeva-topalova PZ, Warner LR, Pardi A, Carlos M. Congenital Anomalies and in utero Antiretroviral Exposure in HIV-exposed Uninfected Infants. *JAMA Pediatr*. 2015;1169(11):48-55. doi:10.1001/jamapediatrics.2014.1889.

93. Evans C, Jones CE, Prendergast AJ. HIV-exposed, uninfected infants: new global challenges in the era of paediatric HIV elimination. *Lancet Infect Dis*. 2016;16(6). doi:10.1016/S1473-3099(16)00055-4.

94. Cusick SE, Georgieff MK. The Role of Nutrition in Brain Development: The Golden Opportunity of the "First 1000 Days." *J Pediatr*. 2016;175:16-21. doi:10.1016/j.jpeds.2016.05.013.The.

95. Le Doare K, Bland R, Newell M-L. Neurodevelopment in Children Born to HIV-Infected Mothers by Infection and Treatment Status. *Pediatrics*. 2012;130(5):e1326-e1344. doi:10.1542/peds.2012-0405.

96. Brackis-Cott E, Kang E, Dolezal C, Abrams EJ, Mellins CA. The impact of perinatal HIV infection on older school-aged children's and adolescents' receptive language and word recognition skills. *AIDS Patient Care STDS*. 2009;23(6):415-421. doi:10.1089/apc.2008.0197.

97. Spaulding AB, Yu Q, Civitello L, et al. Neurologic outcomes in HIV-exposed/uninfected infants exposed to antiretroviral drugs during pregnancy in Latin America and the Caribbean. *AIDS Res Hum Retroviruses*. 2016;32(4):AID.2015.0254. doi:10.1089/AID.2015.0254.

98. Nozyce ML, Huo Y, Williams PL, et al. Safety of in utero and neonatal antiretroviral exposure: cognitive and academic outcomes in HIV-exposed, uninfected children 5-13 years of age. *Pediatr Infect Dis J*. 2014;33(11):1128-1133. doi:10.1097/INF.0000000000000410.

99. Kerr SJ, Puthanakit T, Vibol U, et al. Neurodevelopmental outcomes in HIV-exposed-uninfected children versus those not exposed to HIV. *AIDS Care*. 2014;26(11):1327-1335. doi:10.1080/09540121.2014.920949.

100. Rice ML, Zeldow B, Siberry GK, et al. Evaluation of risk for late language emergence after in utero antiretroviral drug exposure in HIV-exposed uninfected infants. *Pediatr Infect Dis J*. 2013;32(10):e406-13. doi:10.1097/INF.0b013e31829b80ee.

101. Rice ML, Buchanan AL, Siberry GK, et al. Language Impairment in Children Perinatally Infected with HIV Compared With Children Exposed and Without Infection. *J Dev Behav Pediatr*. 2011;(October 2015):1. doi:10.1097/DBP.0b013e318241ed23.

102. Sirois PA, Huo Y, Williams PL, et al. Safety of perinatal exposure to antiretroviral medications: developmental outcomes in infants. *Pediatr Infect Dis J*. 2013;32(6):648-655. doi:10.1097/INF.0b013e318284129a.

103. Filteau S. The HIV-exposed, uninfected African child. *Trop Med Int Heal*. 2009;14(3):276-287. doi:10.1111/j.1365-3156.2009.02220.x.

104. Smith R, Chernoff M, Williams PL, et al. Impact of Human Immunodeficiency Virus Severity on Cognitive and Adaptive Functioning during Childhood and Adolescence. *Pediatr Infect Dis*. 2012;31(6):1-11. doi:10.1097/INF.0b013e318253844b.Impact.

105. Abubakar A, Holding P, Van Baar A, Newton CRJC, Van de Vijver FJR, Espy KA. The performance of children prenatally exposed to HIV on the A-not-B task in Kilifi, Kenya: A preliminary study. *Int J Environ Res Public Health*. 2013;10(9):4132-4142. doi:10.3390/ijerph10094132.

106. Nicholson L, Chisenga M, Siame J, Kasonka L, Filteau S. Growth and health outcomes at school age in HIV-exposed, uninfected Zambian children: Follow-up of two cohorts studied in infancy. *BMC Pediatr*. 2015;15(1):1-10. doi:10.1186/s12887-015-0386-8.

107. Barret B, Tardieu M, Rustin P, et al. Persistent mitochondrial dysfunction in HIV-1-exposed but uninfected infants: clinical screening in a large prospective cohort. *AIDS*. 2003;17(12):1769-1785. doi:10.1097/00002030-200308150-00006.

108. Divi RL, Einem TL, Fletcher SLL, et al. Progressive mitochondrial compromise in brains and livers of primates exposed in utero to nucleoside reverse transcriptase inhibitors (NRTIs). *Toxicol Sci*. 2010;118(1):191-201. doi:10.1093/toxsci/kfq235.

109. Holmes MJ, Robertson FC, Little F, et al. Longitudinal increases of brain metabolite levels in 5-10 year old children. *PLoS One*. 2017;12(7):1-14. doi:10.1371/journal.pone.0180973.

110. Williams PL, Marino M, Malee K, Brogly S, Hughes MD, Mofenson LM. Neurodevelopment and in utero antiretroviral exposure of HIV-exposed uninfected infants. *Pediatrics*. 2010;125(2):e250-60. doi:10.1542/peds.2009-1112.

111. Malee KM, Tassiopoulos K, Siberry G, et al. Mental health functioning among children and adolescents with perinatal HIV infection and perinatal HIV exposure. *AIDS Care*.

2011;23(12):1533-1544. doi:10.1080/09540121.2011.575120.

112. Sugandhi N, Rodrigues J, Kim M, et al. HIV-exposed infants: Rethinking care for a lifelong condition. *Aids*. 2013;27(0 2):S187-S195. doi:10.1097/QAD.0000000000000090.

113. Ngoma MS, Hunter JA, Harper JA, et al. Cognitive and language outcomes in HIV-uninfected infants exposed to combined antiretroviral therapy in utero and through extended breast-feeding. *Aids*. 2014;28 Suppl 3(416):S323-30. doi:10.1097/QAD.0000000000000357.

114. Springer P, Laughton B, Tomlinson M, Harvey J, Esser M. Neurodevelopmental status of HIV-exposed but uninfected children: A pilot study. *South African J Child Heal*. 2012;6:51-55. doi:10.7196/SAJCH.409.

115. Walker SP, Wachs TD, Gardner JM, et al. Child development: risk factors for adverse outcomes in developing countries. *Lancet*. 2007;369:145-157. doi:10.3945/ajcn.114.101071.

116. Van Rie A, Mupuala A, Dow A. Impact of the HIV/AIDS Epidemic on the Neurodevelopment of

Preschool-Aged Children in Kinshasa, Democratic Republic of the Congo. *Pediatrics*.

2008;72(2):181-204. doi:10.1038/nature13314.A.

117. Pinillos F, Dandara C, Swart M, et al. Case report: Severe central nervous system manifestations associated with aberrant efavirenz metabolism in children: the role of CYP2B6 genetic variation. *BMC Infect Dis*. 2015;16(1):56. doi:10.1186/s12879-016-1381-x.

118. Hauptfleisch MP, Moore DP, Rodda JL. Efavirenz as a cause of ataxia in children. *South African*

Med J. 2015;105(11):897-898. doi:10.7196/SAMJ.2015.v105i11.9451.

119. Chersich MF, Urban MF, Venter FWD, et al. Efavirenz use during pregnancy and for women of child-bearing potential. *AIDS Res Ther*. 2006;3:1-6. doi:10.1186/1742-6405-3-11.

120. Purnell PR, Fox HS. Efavirenz Induces Neuronal Autophagy and Mitochondrial Alterations. *J Pharmacol Exp Ther*. 2014;351(2):250-258. doi:10.1124/jpet.114.217869.

121. Funes HA, Blas-garcia A, Esplugues J V., Apostolova N. Efavirenz alters mitochondrial respiratory function in cultured neuron and glial cell lines. *J Antimicrob Chemother*. 2015;70(8):2249-2254. doi:10.1093/jac/dkv098.

122. Funes HA, Apostolova N, Alegre F, et al. Neuronal bioenergetics and acute mitochondrial dysfunction: A clue to understanding the central nervous system side effects of efavirenz. *J Infect Dis*. 2014;210(9):1385-1395. doi:10.1093/infdis/jiu273.

123. Tailor J, Kittappa R, Leto K, et al. Stem cells expanded from the human embryonic hindbrain stably retain regional specification and high neurogenic potency. *J Neurosci*. 2013;33(30):12407-12422. doi:10.1523/JNEUROSCI.0130-13.2013.

124. Elkabetz Y, Panagiotakos G, Al Shamy G, Socci ND, Tabar V, Studer L. Human ES cell-derived neural rosettes reveal a functionally distinct early neural stem cell stage. *Genes Dev*. 2008;22(2):152-165. doi:10.1101/gad.1616208.

125. Garnett S. Generating a Proteomic Profile of Neurogenesis. 2019;24.

126. Ishihama Y. Proteomic LC – MS systems using nanoscale liquid chromatography with tandem mass spectrometry. *J Chromatogr A*. 2005;1067:73-83. doi:10.1016/j.chroma.2004.10.107.

127. Zhang Y, Fonslow BR, Shan B, Baek M-C, Yates III JR. Protein Analysis by Shotgun/Bottom-up Proteomics. *Chem Rev*. 2013;113(4):2343-2394. doi:10.1021/cr3003533.Protein.

128. Aguilar M-I. Reversed-phase high-performance liquid chromatography. In: *Methods in Molecular Biology*. Vol 251. ; 2004:9-23. doi:10.1016/S0378-4347(00)81282-7.

129. Henzel WJ, Watanabe C, Stults JT. Protein identification: The origins of peptide mass fingerprinting. *J Am Soc Mass Spectrom*. 2003;14(9):931-942. doi:10.1016/S1044-0305(03)00214-9.

130. Walch A, Rauser S, Deininger SO, Höfler H. MALDI imaging mass spectrometry for direct tissue analysis: A new frontier for molecular histology. *Histochem Cell Biol*. 2008;130(3):421-434. doi:10.1007/s00418-008-0469-9.

131. Kebarle P. A brief overview of the present status of the mechanisms involved in electrospray mass spectrometry. *J Mass Spectrom*. 2000;35:804-817. doi:10.1007/s12517-014-1353-7.

132. Fenn JB, Mann M, Meng CK, Wong SF, Whitehouse CM. Electrospray ionization for mass spectrometry of large biomolecules. *Science (80-)*. 1989;246(4926):64-71.

133. Konermann L, Ahadi E, Rodriguez AD, Vahidi S. Unraveling the mechanism of electrospray ionization. *Anal Chem*. 2013;85(1):2-9. doi:10.1021/ac302789c.

134. Wilm M. Principles of Electrospray Ionization. *Mol Cell Proteomics*. 2011;10(7):M111.009407. doi:10.1074/mcp.M111.009407.

135. Wysocki VH, Resing KA, Zhang Q, Cheng G. Mass spectrometry of peptides and proteins. *Methods*. 2005;35:211-222. doi:10.1016/j.ymeth.2004.08.013.

136. Aebersold R, Mann M. Mass spectrometry-based proteomics. *Nature*. 2003;422(6928):198-207. doi:10.1038/nature01511.

137. Lange V, Picotti P, Domon B, Aebersold R. Selected reaction monitoring for quantitative proteomics: A tutorial. *Mol Syst Biol*. 2008;4(222). doi:10.1038/msb.2008.61.

138. Scigelova M, Makarov A. Orbitrap Mass Analyzer – Overview and Applications in Proteomics. *Proteomics*. 2006;6(S2):16-21. doi:10.1002/pmic.200600528.

139. Hu Q, Noll RJ, Li H, Makarov A, Hardman M, Cooks RG. The Orbitrap: A new mass spectrometer. *J Mass Spectrom*. 2005;40(4):430-443. doi:10.1002/jms.856.

140. Michalski A, Damoc E, Hauschild J, et al. Mass Spectrometry-based Proteomics Using Q Exactive, a High-performance Benchtop Quadrupole Orbitrap Mass Spectrometer. *Am Soc Biochem Mol Biol*. 2011;10(9):1-11. doi:10.1074/mcp.M111.011015.

141. Gallien S, Duriez E, Crone C, Kellmann M, Moehring T, Domon B. Targeted Proteomic Quantification on Quadrupole-Orbitrap Mass Spectrometer. *Am Soc Biochem Mol Biol*. 2012;11(12):1709-1723. doi:10.1074/mcp.O112.019802.

142. Jedrychowski MP, Huttlin EL, Haas W, Sowa ME, Rad R, Gygi SP. Evaluation of HCD- and CID-type Fragmentation Within Their Respective Detection Platforms For Murine Phosphoproteomics. *Mol Cell Proteomics*. 2011;10(12):M111.009910. doi:10.1074/mcp.M111.009910.

143. Graves PR, Haystead TA. Molecular biologists guide to proteomics. *Microbiol Mol Biol Rev*. 2002;66(1):39-63. doi:10.1128/MMBR.66.1.39.

144. Tao WA, Aebersold R. Advances in quantitative proteomics via stable isotope tagging and mass spectrometry. *Curr Opin Biotechnol*. 2003;14(1):110-118. doi:10.1109/ICAIS.2002.1048050.

145. Chahrour O, Cobice D, Malone J. Stable isotope labelling methods in mass spectrometry-based quantitative proteomics. *J Pharm Biomed Anal*. 2015;113:2-20. doi:10.1016/j.jpba.2015.04.013.

146. Mann M. Functional and quantitative proteomics using SILAC. *Mol Cell Biol*. 2006;7(December):952-959.

147. Ross PL, Huang YN, Marchese JN, et al. Multiplexed Protein Quantitation in Saccharomyces cerevisiae Using Amine-reactive Isobaric Tagging Reagents. *Mol Cell Proteomics*. 2004;3:1154-1169. doi:10.1074/mcp.M400129-MCP200.

148. Wilm M, Mann M. Analytical properties of the nanoelectrospray ion source. *Anal Chem*.

1996;68(1):1-8. doi:10.1021/ac9509519.

149. Wilm MS, Mann M. Electrospray and Taylor-Cone theory, Dole's beam of macromolecules at last? *Int J Mass Spectrom Ion Process*. 1994;136(2-3):167-180. doi:10.1016/0168-1176(94)04024-9.

150. Cox J, Hein MY, Luber CA, Paron I, Nagaraj N, Mann M. Accurate Proteome-wide Label-free Quantification by Delayed Normalization and Maximal Peptide Ratio Extraction, Termed MaxLFQ. *Mol Cell Proteomics*. 2014;13(9):2513-2526. doi:10.1074/mcp.M113.031591.

151. Wang M, You J, Bemis KG, Tegeler TJ, Brown DPG. Label-free mass spectrometry-based protein quantification technologies in proteomic analysis. *Briefings Funct Genomics Proteomics*. 2008;7(5):329-339. doi:10.1093/bfgp/eln031.

152. Bondarenko P V., Chelius D, Shaler TA. Identification and relative quantitation of protein mixtures by enzymatic digestion followed by capillary reversed-phase liquid chromatography - Tandem mass spectrometry. *Anal Chem*. 2002;74(18):4741-4749. doi:10.1021/ac0256991.

153. Cox J, Mann M. MaxQuant enables high peptide identification rates, individualized p.p.b.-range mass accuracies and proteome-wide protein quantification. *Nat Biotechnol*. 2014;26(12):1367-1372. doi:10.1038/nbt.1511.

154. Weisser H, Nahnsen S, Grossmann J, et al. An Automated Pipeline for High-Throughput Label-Free Quantitative Proteomics. *J Proteome Res*. 2013;12:1628-1644. doi:10.1021/pr300992u.

155. Cox J, Neuhauser N, Michalski A, Scheltema R a, Olsen J V, Mann M. Andromeda: a peptide search engine integrated into the MaxQuant environment. *J Proteome Res*. 2011;10(4):1794-1805. doi:10.1021/pr101065j.

156. Käll L, Storey JD, Maccoss MJ, Noble WS. Posterior Error Probabilities and False Discovery Rates : Two Sides of the Same Coin. *J Proteome Res*. 2008;7:40-44.

157. Al Shweiki MHDR, Mönchgesang S, Majovsky P, Thieme D, Trutschel D, Hoehenwarter W.

Assessment of Label-Free Quantification in Discovery Proteomics and Impact of Technological Factors and Natural Variability of Protein Abundance. *J Proteome Res*. 2017;16(4):1410-1424. doi:10.1021/acs.jproteome.6b00645.

158. Pino LK, Searle BC, Bollinger JG, Nunn B, Maclean B, Maccoss MJ. The Skyline ecosystem : Informatics for quantitative mass spectrometry proteomics. *Mass Spectrom Rev*. 2017:1-16. doi:10.1002/mas.21540.

159. MacLean B, Tomazela DM, Shulman N, et al. Skyline: An open source document editor for creating and analyzing targeted proteomics experiments. *Bioinformatics*. 2010;26(7):966-968. doi:10.1093/bioinformatics/btq054.

160. Bereman M, Maclean B, Tomazela DM, Liebler DC, MacCoss MJ. The Development of Selected Reaction Monitoring Methods for Targeted Proteomics via Empirical Refinement. *Proteomics*. 2012;12(8):1134-1141. doi:10.1002/pmic.201200042.The.

161. Zhang B, Verberkmoes NC, Langston MA, Uberbacher E, Hettich RL, Samatova NF. Detecting Differential and Correlated Protein Expression in Label-Free Shotgun Proteomics. *J Proteome Res*. 2006;5:2909-2918. doi:10.1021/pr0600273.

162. Food and Drug Administration (FDA), Center for Drug Evaluation and Research (CDER), Center for Biologics Evaluation and Research (CBER). *Guidance for Industry Expedited Programs for Serious Conditions – Drugs and Biologics*.; 2014.

163. Food and Drug Administration (FDA). *Human Immunodeficiency Virus-1 Infection : Developing Antiretroviral Drugs for Treatment Guidance for Industry Human Immunodeficiency Virus-1 Infection : Developing Antiretroviral Drugs for Treatment Guidance for Industry*.; 2015.

164. Luan Q, Xi Y, Gan N, Cao Y, Li T, Chen Y. A facile colorimetric aptamer assay for small molecule detection in food based on a magnetic single-stranded DNA binding protein-linked composite probe. *Sensors Actuators B Chem*. 2017;239:979-987. doi:https://doi.org/10.1016/j.snb.2016.08.123.

165. Soh JH, Lin Y, Rana S, Ying JY, Stevens MM. Colorimetric Detection of Small Molecules in Complex Matrixes via Target-Mediated Growth of Aptamer-Functionalized Gold Nanoparticles. *Anal Chem*. 2015;87(15):7644-7652. doi:10.1021/acs.analchem.5b00875.

166. Cheng S, Shi F, Jiang X, Wang L, Chen W, Zhu C. Sensitive Detection of Small Molecules by Competitive Immunomagnetic-Proximity Ligation Assay. *Anal Chem*. 2012;84(5):2129-2132. doi:10.1021/ac3001463.

167. Taylor AE, Keevil B, Huhtaniemi IT. Mass spectrometry and immunoassay: How to measure steroid hormones today and tomorrow. *Eur J Endocrinol*. 2015;173(2):D1-D12. doi:10.1530/EJE-15-0338.

168. Mullins GR, Bazydlo LAL. Technical Comparison of Immunoassay and Mass Spectrometry. *Med lab Manag*. 2016:2.

169. Hopfgartner G, Bourgogne E. Quantitative high-throughput analysis of drugs in biological matrices by mass spectrometry. *Mass Spectrom Rev*. 2003;22(3):195-214. doi:10.1002/mas.10050.

170. Szabó PT, Kele Z. Electrospray mass spectrometry of hydrophobic compounds using dimethyl sulfoxide and dimethylformamide as solvents. *Rapid Commun Mass Spectrom*. 2001;15(24):2415-2419. doi:10.1016/S1570-7946(09)70603-0.

171. Strzelecka D, Holman SW, Eyers CE. Evaluation of dimethyl sulfoxide (DMSO) as a mobile phase additive during top 3 label-free quantitative proteomics. *Int J Mass Spectrom*. 2015;391:157-160. doi:10.1016/j.ijms.2015.07.004.

172. Curley P, Rajoli RKR, Moss DM, et al. Efavirenz Is Predicted To Accumulate in Brain Tissue: an In Silico, In Vitro, and In Vivo Investigation. *Antimicrob Agents Chemother*. 2017;61(1):e01841-16. doi:10.1128/AAC.01841-16.

173. Thermo Scientific. HESI-II Probe User Guide. 2009;(April):1-26.

174. Nirogi R, Bhyrapuneni G, Kandikere V, et al. Simultaneous quantification of a non-nucleoside reverse transcriptase inhibitor efavirenz, a nucleoside reverse transcriptase inhibitor emtricitabine and a nucleotide reverse transcriptase inhibitor tenofovir in plasma by liquid chromatography positive io. *Biomed Chromatogr*. 2009;23(4):371-381. doi:10.1002/bmc.1125.

175. Avery LB, Parsons TL, Meyers DJ, Hubbard WC. A highly sensitive ultra performance liquid chromatography-tandem mass spectrometric (UPLC-MS/MS) technique for quantitation of protein free and bound efavirenz (EFV) in human seminal and blood plasma. *October*.

2010;878(31):3217-3224. doi:10.1097/OPX.0b013e3182540562.The.

176. Applied Biosystems. A simple and rapid LC-MS / MS method for the simultaneous determination of nine antiretroviral drugs commonly used in Europe (protease Inhibitors and non-nucleoside reverse transcriptase inhibitors). *Appl Biosyst*.

177. Pruvost A, Theodoro F, Agrofoglio L, Negredo E, Henri Benech. Specificity enhancement with LC-

positive ESI-MS/MS for the measurement of nucleotides: application to the quantitative determination of carbovir triphosphate, lamivudine triphosphate and tenofovir diphosphate in human peripheral blood mononuclear cells. *J Mass Spectrom*. 2008;43:224-233. doi:10.1002/jms.

178. Wishart DS, Feunang YD, Marcu A, et al. HMDB 4.0: The human metabolome database for 2018.

Nucleic Acids Res. 2018;46(D1):D608-D617. doi:10.1093/nar/gkx1089.

179. Kind T, Tsugawa H, Cajka T, et al. Identification of small molecules using accurate mass MS/MS

search. *Mass Spectrom Rev*. 2018;37(4):513-532. doi:10.1002/mas.21535.

180. MacLean B, Tomazela DM, Abbatiello SE, et al. Effect of Collision Energy Optimisation on the Measurement of Peptides by Selected Reaction Monitoring (SRM) Mass Spectrometry. *Anal Chem*. 2010;0(0). http://dx.doi.org.ezproxy2.library.usyd.edu.au/10.1021/ac102179j.

181. Mcdonald GR, Hudson AL, Dunn SMJ, et al. Bioactive Contaminants Leach from Disposable Laboratory Plasticware Bioactive Contaminants Leach from Disposable Laboratory Plasticware G. *Science (80-)*. 2008;322(November):917. doi:10.1126/science.1162395.

182. Lewis LK, Robson MH, Vecherkina Y, Ji C, Beall GW. Interference with spectrophotometric analysis of nucleic acids and proteins by leaching of chemicals from plastic tubes Interference with spectrophotometric analysis of nucleic acids and proteins by leaching of chemicals from plastic tubes. *Biotechniques*. 2010;48:297-302. doi:10.2144/000113387.

183. D'Avolio A, Sciandra M, Siccardi M, et al. A new assay based on solid-phase extraction procedure with LC-MS to measure plasmatic concentrations of tenofovir and emtricitabine in HIV infected patients. *J Chromatogr Sci*. 2008;46(6):524-528. doi:10.1093/chromsci/46.6.524.

184. Roškar R, Lušin TT. *Analytical Methods for Quantification of Drug Metabolites in Biological Samples*.; 2012. doi:10.5772/51676.

185. Alshammari TM, Al-Hassan AA, Hadda TB, Aljofan M. Comparison of different serum sample extraction methods and their suitability for mass spectrometry analysis. *Saudi Pharm J*. 2015;23(6):689-697. doi:10.1016/j.jsps.2015.01.023.

186. Bonfiglio R, Bonfiglio R, King R, et al. The effects of sample preparation methods on the variability of the electrospray ionization response for model drug compounds. *Rapid Commun Mass Spectrom*. 1999;13(12):1175-1185. doi:10.1002/(SICI)1097-0231(19990630)13:12<1175::AID-RCM639>3.0.CO;2-0.

187. Govender K, Gibhard L, Du Plessis L, Wiesner L. Development and validation of a LC-MS/MS method for the quantitation of lumefantrine in mouse whole blood and plasma. *J Chromatogr B Anal Technol Biomed Life Sci*. 2015;985:6-13. doi:10.1016/j.jchromb.2015.01.015.

188. Huang Y, Gandhi M, Greenblatt RM, Gee W, Lin ET, Messenkoff N. Sensitive analysis of anti-HIV drugs, efavirenz, lopinavir and ritonavir, in human hair by liquid chromatography coupled with tandem mass spectrometry. *Rapid Commun Mass Spectrom*. 2008;22(21):3401-3409. doi:10.1002/rcm.3750.Sensitive.

189. Xu X, Lan J, Korfmacher WA. Rapid LC / MS / MS Method Development for Drug Discovery A three-checkpoint paradigm. *Anal Chem*. 2005;77:389-394. doi:10.1021/ac053476f.

190. Polson C, Sarkar P, Incledon B, Raguvaran V, Grant R. Optimization of protein precipitation based upon effectiveness of protein removal and ionization effect in liquid chromatography-tandem mass spectrometry. *J Chromatogr B Anal Technol Biomed Life Sci*. 2003;785(2):263-275. doi:10.1016/S1570-0232(02)00914-5.

191. Jung BH, Rezk NL, Bridges AS, Corbett AH, Kashuba ADM. Simultaneous determination of 17 antiretroviral drugs in human plasma for quantitative analysis with liquid chromatography–tandem mass spectrometry. *Biomed Chromatogr*. 2007;21:1095-1104. doi:10.1002/bmc.

192. Veldkamp A, Harris M, Montaner JS, et al. The steady-state pharmacokinetics of efavirenz and nevirapine when used in combination in human immunodeficiency virus type 1-infected persons. *J Infect Dis*. 2001;184(1):37-42. doi:10.1086/320998.

193. Srivastava P, Moorthy GS, Gross R, Barrett JS. A Sensitive and Selective Liquid Chromatography/Tandem Mass Spectrometry Method for Quantitative Analysis of Efavirenz in Human Plasma. *PLoS One*. 2013;8(6):1-9. doi:10.1371/journal.pone.0063305.

194. National Center for Biotechnology Information. CID=64139 (efavirenz). PubChem Compound Database. https://pubchem.ncbi.nlm.nih.gov/compound/64139. Accessed July 12, 2018.

195. Food and Drug Administration (FDA). *Methods, Method Verification and Validation*. Vol 1.7.; 2014.

196. Trufelli H, Palma P, Giorgio Famiglini and AC. An overview of matrix effects in liquid chromatography-mass spectrometry. *Mass Spectrom Rev*. 2011;30:491-509. doi:10.1002/mas.

197. Kingshott P, Mcarthur S, Thissen H, Castner DG, Griesser HJ. Ultrasensitive probing of the protein resistance of PEG surfaces by secondary ion mass spectrometry. 2002;23:4775-4785.

198. Eppendorf Research ® plus. *Chemical Resistance*.; 2015.

199. Jordaan MA, Shapi M. Investigation of the solvent-dependent photolysis of a nonnucleoside reverse-transcriptase inhibitor, antiviral agent efavirenz. *Antivir Chem chemotheray*. 2017;25:94-104.

200. Fic E, Kedracka-Krok S, Jankowska U, Pirog A, Dziedzicka-Wasylewska M. Comparison of protein precipitation methods for various rat brain structures prior to proteomic analysis. *Electrophoresis*. 2010;31(21):3573-3579. doi:10.1002/elps.201000197.

201. Ewald K. *Chemical Stability of Consumables*.; 2012.

202. Dundas N, Leos NK, Mitui M, Revell P, Rogers BB. Comparison of Automated Nucleic Acid Extraction Methods with Manual Extraction. *J Mol Diagnostics*. 2008;10(4):311-316. doi:10.2353/jmoldx.2008.070149.

203. Guryca V, Roeder D, Piraino P, et al. Automated Sample Preparation Platform for Mass Spectrometry-Based Plasma Proteomics and Biomarker Discovery. *Biology (Basel)*. 2014;3:205-219. doi:10.3390/biology3010205.

204. Frankforter G, Cohen L. Equilibria in the systems, water, acetone, and inorganic salts. *J Am Chem Soc*. 1914;36:1103–1134. doi:10.1021/ja02183a005.

205. Tabata M, Kumamoto M, Nishimoto J. Chemical Properties of Water-Miscible Solvents Separated and Their Application to Solvent Extraction. *Anal Sci*. 1994;10(383-388).

206. Leggett DC, Jenkins TF, Miyares PH. Salting-Out Solvent Extraction for Preconcentration of Neutral Polar Organic Solutes from Water Differential Densometrlc Analysis of Equilibria in Highly Concentrated Media : Determination of the Aqueous Second Acid Dissociation Constant of H2S. *Anal Chem*. 1990;62:1355-1356. doi:10.1021/ac00212a029.

207. Simirgiotis MJ, Benites J, Areche C, Sepúlveda B. Antioxidant Capacities and Analysis of Phenolic Compounds in Three Endemic Nolana Species by HPLC-PDA-ESI-MS. *Molecules*. 2015;20:11490-11507. doi:10.3390/molecules200611490.

208. Dolan JW. Making the Most of a Gradient Scouting Run. *LCGC North Am*. 31:30-35.

209. Schellinger AP, Carr PW. Isocratic and gradient elution chromatography: A comparison in terms of speed, retention reproducibility and quantitation. *J Chromatogr A*. 2006;1109(2):253-266. doi:10.1016/j.chroma.2006.01.047.

210. Antignac J, Wasch K De, Monteau F, Brabander H De, Le B. The ion suppression phenomenon in liquid chromatography – mass spectrometry and its consequences in the field of residue analysis. *Anal Chim Acta*. 2005;529:129-136. doi:10.1016/j.aca.2004.08.055.

211. Annesley TM. Ion suppression in mass spectrometry. *Clin Chem*. 2003;49(7):1041-1044. doi:10.1002/ar.1090380206.

212. Nemaura T. Modelling Transportation of Efavirenz: Inference on possibility of mixed modes of transportation and kinetic solubility. *Front Pharmacol*. 2015;6:1-7. doi:10.3389/fphar.2015.00121.

213. Yilmaz A, Watson V, Dickinson L, Back D. Twenty-four hour efavirenz pharmacokinetics in cerebrospinal fluid and plasma. *Antimicrob Agents Chemother*. 2012;(June). doi:10.1128/AAC.06311-11.

214. Liu X, Smith BJ, Chen C, et al. Evaluation of Cerebrospinal Fluid Concentration and Plasma Free Concentration As a Surrogate Measurement for Brain Free Concentration. *Drug Metab Dispos*. 2006;34(9):1443-1447. doi:10.1124/dmd.105.008201.

215. Nagaya Y, Nozaki Y, Takenaka O, et al. Investigation of utility of cerebrospinal fluid drug concentration as a surrogate for interstitial fluid concentration using microdialysis coupled with cisternal cerebrospinal fluid sampling in wild-type and Mdr1a (-/-) rats. *Drug Metab Pharmacokinet*. 2016;31:57-66. doi:10.1016/j.dmpk.2015.10.003.

216. Csajka C, Marzolini C, Fattinger K, et al. Population pharmacokinetics and effects of efavirenz in patients with human immunodeficiency virus infection. *Clin Pharmacol Ther*. 2003;73(1):20-30. doi:10.1067/mcp.2003.22.

217. Ribaudo HJ, Haas DW, Tierney C, et al. Pharmacogenetics of plasma efavirenz exposure after treatment discontinuation: an Adult AIDS Clinical Trials Group Study. *Clin Infect Dis*. 2006;42(December 2005):401-407. doi:10.1086/499364.

218. Food and Drug Administration (FDA). *Highlights of Prescribing Information: Efavirenz Tablets*.; 2014. https://www.accessdata.fda.gov/drugsatfda_docs/label/2016/091471orig1s000lbl.pdf.

219. Apostolova N, Funes HA, Blas-Garcia A, Galindo MJ, Alvarez A, Esplugues J V. Efavirenz and the CNS: What we already know and questions that need to be answered. *J Antimicrob Chemother*. 2015;70(10):2693-2708. doi:10.1093/jac/dkv183.

220. Maurin M, Rowe S, Blom K, Pierce M. Kinetics and mechanism of hydrolysis of efavirenz. *Pharm Res*. 2002;19(4):517-521. doi:10.3184/146867809X471117.

221. Hamrapurkar PD, Patil PS, Phale MD, Shah N, Pawar SB. Optimization and Validation of Rp-Hplc Stability-Indicating Method for Determination of Efavirenz and its Degradation Products. *Int J Appl Sci*. 2010;8(2):155-165.

222. Kakde RB, Kale DL. Stability Study and Densitometric Determination of Efavirenz in Tablet by Normal Phase Thin Layer Chromatography. *Int J Pharmtech Res*. 2011;3(3):1889-1896.

223. Nikalje AP, Rao BU. Stability-indicating HPLC method for the determination of efavirenz in bulk drug and in pharmaceutical dosage form. *African J Pharm Pharmacol*. 2009;3(12):634-650. http://www.academicjournals.org/journal/AJPP/article-abstract/4D6CDE427788.

224. Wyen C, Hendra H, Siccardi M, et al. Cytochrome P450 2B6 (CYP2B6) and constitutive androstane receptor (CAR) polymorphisms are associated with early discontinuation of efavirenz-containing regimens. *J Antimicrob Chemother*. 2011;66(9):2092-2098. doi:10.1093/jac/dkr272.

225. Cross HM, Chetty S, Asukile MT, Hussey HS, Lee Pan EB, Tucker LM. A proposed management algorithm for late-onset efavirenz neurotoxicity. *South African Med J*. 2018;108(4):271. doi:10.7196/SAMJ.2018.v108i4.12914.

226. Uhlén M, Fagerberg L, Hallström BM, et al. Tissue-based map of the human proteome. *Science (80-)*. 2015;347(6220):1260419. doi:10.1126/science.1260419.

227. Miksys S, Tyndale RF. Brain Drug-Metabolizing Cytochrome P450 Enzymes are Active In Vivo , Demonstrated by Mechanism-Based Enzyme Inhibition. *Neuropsychopharmacology*. 2009;34(3):634-640. doi:10.1038/npp.2008.110.Brain.

228. Ward BA, Gorski JC, Jones DR, Hall SD, Flockhart DA, Desta Z. The Cytochrome P450 2B6 (CYP2B6) Is the Main Catalyst of Efavirenz Primary and Secondary Metabolism : Implication for HIV/AIDS Therapy and Utility of Efavirenz as a Substrate Marker of CYP2B6 Catalytic Activity. *J Pharmacol Exp Ther*. 2003;306(1):287-300. doi:10.1124/jpet.103.049601.

229. Grilo NM, João Correia M, Miranda JP, et al. Unmasking efavirenz neurotoxicity: Time matters to the underlying mechanisms. *Eur J Pharm Sci*. 2017;105(April):47-54. doi:10.1016/j.ejps.2017.05.010.

230. Cressey TR, Stek A, Capparelli E, et al. Efavirenz Pharmacokinetics During the Third Trimester of Pregnancy and Postpartum. *J Acquir Immune Defic Syndr*. 2012;59(3):245-252.

231. Walicke P, Cowan WM, Ueno N, Baird a, Guillemin R. Fibroblast growth factor promotes survival of dissociated hippocampal neurons and enhances neurite extension. *Proc Natl Acad Sci U S A*. 1986;83(9):3012-3016. doi:10.1073/pnas.83.9.3012.

232. Ek CJ, Angelo BD, Lehner C, Nathanielsz P, Li C, Mallard C. Expression of tight junction proteins and transporters for xenobiotic metabolism at the blood – CSF barrier during development in the nonhuman primate (P.hamadryas). *Reprod Toxicol*. 2015;56:32-44. doi:10.1016/j.reprotox.2015.06.047.

233. Ek CJ, Dziegielewska KM, Habgood MD, Saunders NR. Barriers in the developing brain and Neurotoxicology. *Neurotoxicology*. 2012;33(3):586-604. doi:10.1016/j.neuro.2011.12.009.

234. Saunders NR, Liddelow S a., Dziegielewska KM. Barrier mechanisms in the developing brain. *Front Pharmacol*. 2012;3 MAR(March):1-18. doi:10.3389/fphar.2012.00046.

235. Elmore S. Apoptosis: A review of programmed cell death. *Toxicol Pathol*. 2007;35(4):495-516. doi:10.1016/j.biotechadv.2011.08.021.Secreted.

236. Thompson CG, Bokhart MT, Sykes C, et al. Mass spectrometry imaging reveals heterogeneous efavirenz distribution within putative HIV reservoirs. *Antimicrob Agents Chemother*. 2015;59(5):2944-2948. doi:10.1128/AAC.04952-14.

237. Zhi W, Wang M, She JX. Selected reaction monitoring (SRM) mass spectrometry without isotope labeling can be used for rapid protein quantification. *Rapid Commun Mass Spectrom*. 2011;25(11):1583-1588. doi:10.1002/rcm.5023.

238. Thakur RA, Kiyonami R, Mcnally J, Cook K, Zabrouskov V. *The Importance of Linear Dynamic Range for Small Molecule and Targeted Peptide LC-MS / MS Quantitation*.; 2008.

239. Nemaura T. Stochastic Modelling of Solution Particle Movement: An Individual Case of Coupled Concentration Gradient Dependent and Independent Movements of Efavirenz. *J Appl Math Phys*. 2017;5(January):1027-1034. doi:10.4236/jamp.2017.55090.

240. Nemaura T. Derived wave of gradient driven diffusion' s convective flux of efavirenz. *J Phys*

Commun. 2018;2:055008. doi:https//doi.org/10.1088/2399-6528/aac0f0.

241. Change C-Y, Ke D-S, Chen J-Y. Essential fatty acids and human brain. *Acta Neurol Taiwan*. 2009;18(4):231-241. http://ovidsp.ovid.com/ovidweb.cgi?T=JS&PAGE=reference&D=emed9&NEWS=N&AN=2009642885.

242. Cusini A, Vernazza PL, Yerly S, et al. Higher CNS Penetration-Effectiveness of Long-Term Combination Antiretroviral Therapy is Associated With Better HIV-1 Viral Suppression in Cerebrospinal Fluid". *J Acquir Immune Defic Syndr*. 2013;62(1):e118-e119. doi:10.1097/QAI.0b013e3182809d9f.

243. Ryan JA. Evolution of Cell Culture Surfaces. *BioFiles*. 2008;21:8-11. http://www.sigmaaldrich.com/technical-documents/articles/biofiles/evolution-of-cell.html.

244. Pavel M, Renna M, Park SJ, et al. Contact inhibition controls cell survival and proliferation via YAP/TAZ-autophagy axis. *Nat Commun*. 2018;9(1). doi:10.1038/s41467-018-05388-x.

245. Sipahi R, Zupanc GKH. Stochastic cellular automata model of neurosphere growth: Roles of proliferative potential, contact inhibition, cell death, and phagocytosis. *J Theor Biol*. 2018;445:151-165. doi:10.1016/j.jtbi.2018.02.025.

246. Cummings BS, Wills LP, Schneellmann RG. Measurement of Cell Death in Mammalian Cells. *Curr Protoc Pharmacol*. 2004;(Lemasters 1999):1-30. doi:10.1002/0471141755.ph1208s25.Measurement.

247. Nightingale S, Chau TTH, Fisher M, et al. Efavirenz and metabolites in CSF; relationship with *CYP2B6* c.516G>T genotype and perturbed blood-brain barrier due to tuberculous meningitis. *Antimicrob Agents Chemother*. 2016;60(May):AAC.00280-16. doi:10.1128/AAC.00280-16.

248. Western Cape Government. *The Western Cape Consolidated Guidelines for HIV Treatment: Prevention of Mother- to- Child Transmission of HIV (PMTCT), Children, Adolescents and Adults. 2018 (Amended Version)*. Vol 2018.; 2018.

249. Shanske AL. Bilateral oblique facial clefts and extremity anomalyin an infant after intrauterine efavirenz exposureand review of its teratogenic risk. *AIDS*. 2012;26:1775–1779.

250. Ford N, Mofenson L, Shubber Z, et al. Safety of efavirenz in the first trimester of pregnancy: an updated systematic review and meta-analysis. *AIDS*. 2014;28 Suppl 2:S123-31. doi:10.1097/QAD.0000000000000231.

251. Chaudhury S, Williams PL, Mayondi GK, et al. Neurodevelopment of HIV-Exposed and HIV-Unexposed Uninfected Children at 24 Months. *Pediatrics*. 2017;140(4):e20170988.

252. Tran LT, Roos A, Fouche J-P, et al. White Matter Microstructural Integrity and Neurobehavioral Outcome of HIV-Exposed Uninfected Neonates. *Medicine (Baltimore)*. 2016;95(4):e2577. doi:10.1097/MD.0000000000002577.

253. Luciana M. Cognitive development in children born preterm : Implications for theories of brain plasticity following early injury. *Dev Psychopathol*. 2003;15:1017-1047.

254. Brogly SB, Abzug MJ, Watts DH, et al. Birth defects among children born to HIV-infected women: Pediatric AIDS Clinical Trials Protocols 219 and 219C. *Pediatr Infect Dis J*. 2010;29(8):721-727. doi:10.1097/INF.0b013e3181e74a2f.Birth.

255. Popova D, Karlsson J, Jacobsson SOP. Comparison of neurons derived from mouse P19 , rat PC12 and human SH-SY5Y cells in the assessment of chemical- and toxin-induced neurotoxicity. *BMC Pharmacol Toxicol*. 2017;18:1-11. doi:10.1186/s40360-017-0151-8.

256. Jersie-Christensen RR, Sultan A, Olsen J V. Simple and Reproducible Sample Preparation for Single- Shot Phosphoproteomics with High Sensitivity. *Phospho-Proteomics Methods Protoc Methods Mol Biol*. 2016;1355:251-260. doi:10.1007/978-1-4939-3049-4.

257. Rappsilber J, Ishihama Y, Mann M. Stop and Go Extraction Tips for Matrix-Assisted Laser Desorption/Ionization, Nanoelectrospray, and LC/MS Sample Pretreatment in Proteomics. *Anal Chem*. 2003;75:663–670. doi:10.1021/ac026117i.

258. Tyanova S, Temu T, Sinitcyn P, et al. The Perseus computational platform for comprehensive analysis of (prote)omics data. *Nat Meth*. 2016;13(9):731-740. http://dx.doi.org/10.1038/nmeth.3901.

259. The Uniprot Consortium. UniProt: a worldwide hub of protein knowledge. *Nucleic Acids Res*. 2019;47(November 2018):506-515. doi:10.1093/nar/gky1049.

260. Szklarczyk D, Morris JH, Cook H, et al. The STRING database in 2017: quality-controlled protein – protein association networks, made broadly accessible. *Nucleic Acids Res*. 2017;45(Database issue):362-368. doi:10.1093/nar/gkw937.

261. Fabregat A, Jupe S, Matthews L, et al. The Reactome Pathway Knowledgebase. *Nucleic Acids Res*. 2018;46(Database Issue):649-655. doi:10.1093/nar/gkx1132.

262. Gurwitz KT, Burman RJ, Murugan BD, et al. Time-Dependent, HIV-Tat-Induced Perturbation of Human Neurons In Vitro: Towards a Model for the Molecular Pathology of HIV-Associated Neurocognitive Disorders. 2017;10(May):1-16. doi:10.3389/fnmol.2017.00163.

263. Ganief T, Gqamana P, Garnett S, et al. Quantitative proteomic analysis of HIV-1 Tat-induced dysregulation in SH-SY5Y neuroblastoma cells. *Proteomics*. 2017;17(6):1-12. doi:10.1002/pmic.201600236.

264. Garnett S. Generating a Proteomic Profile of Neurogenesis. 2009;24.

265. Weiss M, Schrimpf S, Hengartner MO, Lercher MJ, Von Mering C. Shotgun proteomics data from multiple organisms reveals remarkable quantitative conservation of the eukaryotic core proteome. *Proteomics*. 2010;10:1297-1306. doi:10.1002/pmic.200900414.

266. Diz AP, Carvajal-rodríguez A, Skibinski DOF. Multiple Hypothesis Testing in Proteomics: A Strategy for Experimental Work. *Mol Cell Proteomics*. 2011;10:1-10. doi:10.1074/mcp.M110.004374.

267. Althouse AD. Adjust for Multiple Comparisons? It's Not That Simple. *Ann Thorac Surg*.

2016;101(5):1644-1645. doi:10.1016/j.athoracsur.2015.11.024.

268. Ranstam J. Multiple P-values and Bonferroni correction. *Osteoarthr Cartil*. 2016;24(5):763-764. doi:10.1016/j.joca.2016.01.008.

269. Draghici S. Statistical intelligence: effective analysis of high-density microarray data. *Drug Discov Today*. 2002;7(11):55-63.

270. Karp NA, Lilley KS. Design and Analysis Issues in Quantitative Proteomics Studies. *Proteomics*. 2007;7(S1):42-50. doi:10.1002/pmic.200700683.

271. Carvalho PC, Yates III JR, Barbosa VC. Improving the TFold test for differential shotgun proteomics. *Bioinformatics*. 2012;28(12):1652-1654. doi:10.1093/bioinformatics/bts247.

272. Benjamini Y, Hochberg Y. Controlling the False Discovery Rate : A Practical and Powerful Approach to Multiple Testing. *R Stat Soc*. 1995;57(1):289-300.

273. Storey JD. The false positive discovery rate: A Bayesian interpretation and the q-value. *Ann Stat*. 2003;31(6):2013-2035.

274. Apostolova N, Blas-garcia A, Galindo MJ, Esplugues J V. Efavirenz: What is known about the cellular mechanisms responsible for its adverse effects. *Eur J Pharmacol*. 2017;812:163-173. doi:10.1016/j.ejphar.2017.07.016.

275. Pascovici D, Handler DCL, Wu JX, Haynes PA. Multiple testing corrections in quantitative proteomics : A useful but blunt tool. *Proteomics*. 2016;16:2448-2453. doi:10.1002/pmic.201600044.

276. Baenke F, Peck B, Miess H, Schulze A. Hooked on fat : the role of lipid synthesis in cancer metabolism and tumour development. *Dis Model Mech*. 2013;6:1353-1363. doi:10.1242/dmm.011338.

277. Incardona JP, Eaton S. Cholesterol in signal transduction. *Curr Opin Cell Biol*. 2000;12:193-203.

278. Cerqueira NMFSA, Oliveira EF, Gesto DS, et al. Cholesterol Biosynthesis: A Mechanistic Overview. *Biochemistry*. 2016;55:5483-5506. doi:10.1021/acs.biochem.6b00342.

279. Zheng Y, Plemenitas A, Fielding CJ, Peterlin BM. Nef increases the synthesis of and transports cholesterol to lipid rafts and HIV-1 progeny virions. *PNAS*. 2003;100(14):1-6.

280. Saito K, Dubreuil V, Arai Y, et al. Ablation of cholesterol biosynthesis in neural stem cells increases their VEGF expression and angiogenesis but causes neuron apoptosis. *PNAS*. 2009;106(20):8350-8355.

281. Pfrieger FW. Cholesterol homeostasis and function in neurons of the central nervous system. *Cell Mol Life Sci*. 2003;60:1158-1171. doi:10.1007/s00018-003-3018-7.

282. Niebroj-dobosz I, Rafaowska J, Fidziañska A, Gadamski R, Grieb P. Myelin composition of spinal cord in a model of amyotrophic lateral sclerosis (ALS) in SOD1 G93A transgenic rats. *Folia Neuropthologica*. 2007;45(4):236-241.

283. Porter FD, Herman GE. Malformation syndromes caused by disorders of cholesterol synthesis. *J Lipid Res*. 2011;52(July 2010):6-34. doi:10.1194/jlr.R009548.

284. Mejia-Pous C, Damiola F, Gandrillon O. Cholesterol synthesis-related enzyme oxidosqualene cyclase is required to maintain self-renewal in primary erythroid progenitors. *Cell Prolif*. 2011;44(6):441-452. doi:10.1111/j.1365-2184.2011.00771.x.

285. Kim HY, Kim DK, Bae S, et al. Farnesyl diphosphate synthase is important for the maintenance of glioblastoma stemness. *Exp Mol Med*. 2018;50(137). doi:10.1038/s12276-018-0166-2.

286. Yasumoto Y, Miyazaki H, Vaidyan LK, et al. Inhibition of Fatty Acid Synthase Decreases Expression of Stemness Markers in Glioma Stem Cells. *PLoS One*. 2016;11(1):1-14. doi:10.1371/journal.pone.0147717.

287. Wang L, Zhang T, Wang L, et al. Fatty acid synthesis is critical for stem cell pluripotency via promoting mitochondrial fission. *EMBO J*. 2017;36(10):1330-1347. doi:10.15252/embj.201695417.

288. Knobloch M, Braun SMG, Zurkirchen L, et al. Metabolic control of adult neural stem cell activity by Fasn-dependent lipogenesis. *Nature*. 2013;493(7431):226-230. doi:10.1038/nature11689.Metabolic.

289. Moussaieff A, Rouleau M, Kitsberg D, et al. Glycolysis-Mediated Changes in Acetyl-CoA and Histone Acetylation Control the Early Differentiation of Embryonic Stem Cells Article Glycolysis-Mediated Changes in Acetyl-CoA and Histone Acetylation Control the Early Differentiation of Embryonic Stem Cells. *Cell Metab*. 2015;21:392-402. doi:10.1016/j.cmet.2015.02.002.

290. Tozawa R, Ishibashi S, Osuga J, et al. Embryonic Lethality and Defective Neural Tube Closure in Mice Lacking Squalene Synthase. *J Biol Chem*. 1999;274(43):30843-30848.

291. Coman D, Vissers LELM, Riley LG, et al. Squalene Synthase Deficiency: Clinical, Biochemical, and Molecular Characterization of a Defect in Cholesterol Biosynthesis. *Am J Hum Genet*. 2018;103(1):125-130. doi:10.1016/j.ajhg.2018.05.004.

292. Nieweg K, Schaller H, Pfrieger FW. Marked differences in cholesterol synthesis between neurons and glial cells from postnatal rats. *J Neurochem*. 2009;109:125-134. doi:10.1111/j.1471-4159.2009.05917.x.

293. Lim L, Wong LC, Shui GH, et al. Lanosterol induces mitochondrial uncoupling and protects dopaminergic neurons from cell death in a model for Parkinson's disease. *Cell Death Differ*. 2012;19:416-427. doi:10.1038/cdd.2011.105.

294. Kölsch H, Heun R, Jessen F, et al. Alterations of cholesterol precursor levels in Alzheimer' s disease. *BBA - Mol Cell Biol Lipids*. 2010;1801(8):945-950. doi:10.1016/j.bbalip.2010.03.001.

295. Serquina AKP, Kambach DM, Sarker O, Ziegelbauer JM. Viral MicroRNAs Repress the Cholesterol Pathway, and 25-hydroxycholesterol Inhibits Infection. *Am Soc Microbiol*. 2017;8(4).

296. Liu S, Aliyari R, Chikere K, et al. Interferon-Inducible Cholesterol-25-Hydroxylase Broadly Inhibits Viral Entry by Production of 25-Hydroxycholesterol. *Immunity*. 2013;38(1):92-105. doi:10.1016/j.immuni.2012.11.005.Interferon-Inducible.

297. Balakrishnan S, Tastan O, Carbonell J, Klein-seetharaman J. Alternative paths in HIV-1 targeted human signal transduction pathways. *BMC Genomics*. 2009;10:1-13. doi:10.1186/1471-2164-10-S3-S30.

298. Blanc M, Hsieh WY, Robertson KA, et al. Host Defense against Viral Infection Involves Interferon Mediated Down-Regulation of Sterol Biosynthesis. *PLoS Biol*. 2011;9(3). doi:10.1371/journal.pbio.1000598.

299. del Real G, Jiménez-baranda S, Mira E, et al. Statins Inhibit HIV-1 Infection by Down-regulating Rho Activity. *J Exp Med*. 2004;200(4):541-547. doi:10.1084/jem.20040061.

300. Wout BVJ, Swain JV, Schindler M, et al. Nef Induces Multiple Genes Involved in Cholesterol Synthesis and Uptake in Human Immunodeficiency Virus Type 1-Infected T Cells. *J Virol*. 2005;79(15):10053-10058. doi:10.1128/JVI.79.15.10053.

301. Liang J-S, Distler O, Cooper DA, et al. HIV protease inhibitors protect apolipoprotein B from degradation by the proteasome : A potential mechanism for protease inhibitor-induced hyperlipidemia. *Nat Med*. 2001;7(12):1327-1331.

302. Pramfalk C, Angelin B, Eriksson M, Parini P. Cholesterol regulates ACAT2 gene expression and enzyme activity in human hepatoma cells. *Biochem Biophys Res Commun*. 2007;364:402-409. doi:10.1016/j.bbrc.2007.10.028.

303. Wu JQ, Dwyer DE, Dyer WB, Yang YH, Wang B, Saksena NK. Genome-wide analysis of primary CD4+ and CD8+ T cell transcriptomes shows evidence for a network of enriched pathways associated with HIV disease. *Retrovirology*. 2011;8(18):1-21. doi:10.1186/1742-4690-8-18.

304. Li M, Sopeyin A, Paintsil E. Combination of Tenofovir and Emtricitabine with Efavirenz Does Not Moderate Inhibitory Effect of Efavirenz on Mitochondrial Function and Cholesterol Biosynthesis in Human T Lymphoblastoid Cell Line. *Antimicrob Agents Chemother*. 2018;62(9):e00691-18.

305. Andrews ZB, Diano S, Horvath TL. Mitochondrial uncoupling proteins in the CNS: In support of function and survival. *Nat Rev Neurosci*. 2005;6(November 2015):829-840. doi:10.1038/nrn1767.

306. Mailloux RJ, Harper M. Uncoupling proteins and the control of mitochondrial reactive oxygen species production. *Free Radic Biol Med*. 2011;51(6):1106-1115. doi:10.1016/j.freeradbiomed.2011.06.022.

307. Petrozzi L, Ricci G, Giglioli NJ, Siciliano G, Mancuso M. Mitochondria and Neurodegeneration. *Biosci Rep*. 2007;27:87-104. doi:10.1002/9780470725207.ch13.

308. Crews L, Masliah E. Molecular mechanisms of neurodegeneration in Alzheimer's disease. *Hum Mol Genet*. 2010;19(1):12-20. doi:10.1093/hmg/ddq160.

309. Keber R, Motaln H, Wagner KD, et al. Mouse Knockout of the Cholesterogenic Cytochrome P450 Lanosterol 14α -Demethylase (Cyp51) Resembles Antley-Bixler Syndrome. *J Biol Chem*. 2011;286(33):29086-29097. doi:10.1074/jbc.M111.253245.

310. Martín MG, Pfrieger F, Dotti CG. Cholesterol in brain disease: sometimes determinant and frequently implicated. *EMBO Rep*. 2014;15(10):1036-1052.

311. Roos RAC. Huntington's disease: a clinical review. *Orphanet J Rare Dis*. 2010;5(40):2-9.

312. Dubois B, Feldman HH, Jacova C, et al. Revising the definition of Alzheimer's disease: a new

lexicon. *Lancet*. 2010;9(November). doi:10.1016/S1474-4422(10)70223-4.

313. Clifford DB, Evans S, Yang Y, et al. Long Term Impact of Efavirenz on Neuropsychological Performance and Symptoms in HIV Infected Individual (ACTG 5097s). *HIV Clin Trials*. 2009;10(6):343-355. doi:10.1310/hct1006-343.Long-Term.

314. Huch S, Muller M, Muppavarapu M, Gommlich J, Balagopal V, Nissan T. The decapping activator Edc3 and the Q/N-rich domain of Lsm4 function together to enhance mRNA stability and alter mRNA decay pathway dependence in Saccharomyces cerevisiae. *Biol Open*. 2016;5:1388-1399. doi:10.1242/bio.020487.

315. Carey KT, Wickramasinghe VO. Regulatory Potential of the RNA Processing Machinery: Implications for Human Disease. *Trends Genet*. 2018;34(4):279-290. doi:10.1016/j.tig.2017.12.012.

316. Lim DA, Suarez-Farinas M, Naef F, et al. In vivo transcriptional profile analysis reveals RNA splicing and chromatin remodeling as prominent processes for adult neurogenesis. *Mol Cell Neurosci*. 2006;31:131-148. doi:10.1016/j.mcn.2005.10.005.

317. Madgwick A, Fort P, Hanson PS, et al. Neural Differentiation Modulates the Vertebrate Brain Specific Splicing Program. *PLoS One*. 2015;10(5):e0125998. doi:10.1371/journal.pone.0125998.

318. Biamonti G, Catillo M, Pignataro D, Montecucco A, Ghigna C. The alternative splicing side of cancer. *Semin Cell Dev Biol*. 2014;32:30-36. doi:10.1016/j.semcdb.2014.03.016.

319. Zhang B, Lui Y, Liu D, Yang L. Targeting cleavage and polyadenylation specific factor 1 via shRNA inhibits cell proliferation in human ovarian cancer. *J Biosci*. 2017;42(3):417-425. doi:10.1007/s12038-017-9701-x.

320. Saris CGJ, Groen EJN, Van Vught PWJ, et al. Gene expression profile of SOD1-G93A mouse spinal cord, blood and muscle. *Amyotrohpic Lateral Scler Front Degener*. 2013;14:190-198. doi:10.3109/21678421.2012.749914.

321. G S, R R, I P, et al. The GeneCards Suite: From Gene Data Mining to Disease Genome Sequence Analysis. *Curr Protoc Bioinforma*. 2016;54(1).

322. Tanackovic G, Kramer A. Human Splicing Factor SF3a , but Not SF1 , Is Essential for Pre-mRNA Splicing In Vivo. *Mol Biol Cell*. 2005;16(March):1366-1377. doi:10.1091/mbc.E04.

323. Arras L De, Alper S. Limiting of the Innate Immune Response by SF3A-Dependent Control of MyD88 Alternative mRNA Splicing. *PLoS Genet*. 2013;9(10):e1003855. doi:10.1371/journal.pgen.1003855.

324. Yao Q, Li M, Yang H, Chai H, Fisher W, Chen C. Roles of Cyclophilins in Cancers and Other Organ Systems. *World J Surg*. 2005;29:276-280. doi:10.1007/s00268-004-7812-7.

325. Rajiv C, Davis TL. Structural and Functional Insights into Human Nuclear Cyclophilins. *Biomolecules*. 2018;8(161). doi:10.3390/biom8040161.

326. Wang Z, Liu X, Zhao Z, et al. Cyclophilin E Functions as a Negative Regulator to Influenza Virus Replication by Impairing the Formation of the Viral Ribonucleoprotein Complex. *PLoS One*. 2011;6(8):e22625. doi:10.1371/journal.pone.0022625.

327. Deeks SG. Immune Dysfunction, Inflammation, and Accelerated Aging in Patients on Antiretroviral Therapy. *Top HIV Med*. 2009;17(4).

328. Gurwitz K. Unravelling molecular mechanisms of HIV associated neurocognitive disorders through proteomics. 2015;(October).

329. Neuhaus J, Jr DRJ, Baker J V, et al. Markers of Inflammation, Coagulation and Renal Function Are Elevated in Adults with HIV Infection. *J Infect Dis*. 2010;201(12):1788-1795. doi:10.1086/652749.Markers.

330. Adler C, Haelterman E, Barlow P, Marchant A, Levy J. Severe Infections in HIV-Exposed Uninfected Infants Born in a European Country. *PLoS One*. 2015;10(8):1-14. doi:10.1371/journal.pone.0135375.

331. Ganief TA. A network analysis based proteomic and transcriptomic investigation into HIV-Tat induced neuronal dysfunction and the neuroprotective effect of lithium By. 2015;(September).

332. Martindale JL, Holbrook NJ. Cellular Response to Oxidative Stress: Signaling for Suicide and Survival. *J Cell Physiol*. 2002;192:1-15. doi:10.1002/jcp.10119.

333. Taylor JM, Minter MR, Newman AG, Zhang M, Adlard PA, Crack PJ. Type-1 interferon signaling mediates neuro-inflammatory events in models of Alzheimer's disease. *Neurobiol Aging*. 2014;35:1012-1023. doi:10.1016/j.neurobiolaging.2013.10.089.

334. Plata-Salaman CR, Turrin NP. Cytokine interactions and cytokine balance in the brain: relevance to neurology and psychiatry. *Mol Psychiatry*. 1999;4:303-306.

335. Maes OC, Chertkow HM, Wang E, Schipper HM. Stress Gene Deregulation in Alzheimer Peripheral Blood Mononuclear Cells. 2011;(March). doi:10.1007/978-1-60761-956-7.

336. Jougasaki M, Ichiki T, Takenoshita Y, Setoguchi M. Statins suppress interleukin-6-induced monocyte chemo-attractant protein-1 by inhibiting Janus kinase/signal transducers and activators of transcription pathways in human vascular endothelial cells. *Br J Pharmacol*. 2010;159:1294-1303. doi:10.1111/j.1476-5381.2009.00612.x.

337. Li Q, Laumonnier Y, Syrovets T, Simmet T. Plasmin Triggers Cytokine Induction in Human Monocyte-Derived Macrophages. *Arterioscler Thromb Vasc Biol*. 2007;27:1383-1389. doi:10.1161/ATVBAHA.107.142901.

338. Ramalho-santos M, Yoon S, Matsuzaki Y, Mulligan RC, Melton DA. "Stemness": Transcriptional Profiling of Embryonic and Adult Stem Cells. *Science (80-)*. 2002;298:597-601.

339. Kiger AA, Jones DL, Schulz C, Rogers MB, Fuller MT. Stem Cell Self-Renewal Specified by JAK-STAT Activation in Response to a Support Cell Cue. *Science (80-)*. 2001;294:2542-2546.

340. Hay ED. The Mesenchymal Cell , Its Role in the Embryo , and the Remarkable Signaling Mechanisms That Create It. *Dev Dyn*. 2005;233:706-720. doi:10.1002/dvdy.20345.

341. Rocha MR, Barcellos-de-Souza P, Sousa-Squiavinato ACM, et al. Annexin A2 overexpression associates with colorectal cancer invasiveness and TGF-ß induced epithelial mesenchymal transition via Src/ANXA2/STAT3. *Sci Rep*. 2018;8(11285):1-11. doi:10.1038/s41598-018-29703-0.

342. Wang T, Yuan J, Zhang J, et al. Anxa2 binds to STAT3 and promotes epithelial to mesenchymal transition in breast cancer cells. *Oncotarget*. 2015;6(31):30975-30992.

343. Fang W, Fa Z, Xie Q, et al. Complex Roles of Annexin A2 in Host Blood – Brain Barrier Invasion by Cryptococcus neoformans. *CNS Neurosci Ther*. 2017;23:291-300. doi:10.1111/cns.12673.

344. Mei M, Ye J, Qin A, et al. Identification of novel viral receptors with cell line expressing viral receptor-binding protein. *Sci Rep*. 2015;5(7935):1-6. doi:10.1038/srep07935.

345. Rai T, Mosoian A, Resh MD. Annexin 2 Is Not Required for Human Immunodeficiency Virus Type 1 Particle Production but Plays a Cell Type-Dependent Role in Regulating Infectivity . *J Virol*. 2010;84(19):9783-9792. doi:10.1128/JVI.01584-09.

346. Chaudhuri A, Yang B, Gendelman HE, Persidsky Y, Kanmogne GD. STAT1 signaling modulates HIV-1 – induced inflammatory responses and leukocyte transmigration across the blood-brain barrier. *Blood*. 2008;111(4):2062-2072. doi:10.1182/blood-2007-05-091207.The.

347. Peng H, Sun L, Jia B, et al. HIV-1-infected and immune-activated macrophages induce astrocytic differentiation of human cortical neural progenitor cells via the STAT3 pathway. *PLoS One*. 2011;6(5). doi:10.1371/journal.pone.0019439.

348. Wang Y, Zeng C, Li J, et al. PAK2 Haploinsufficiency Results in Synaptic Cytoskeleton Impairment and Autism-Related Behavior. *Cell Rep*. 2018;24(8):2029-2041. doi:10.1016/j.celrep.2018.07.061.

349. Mayford M, Siegelbaum SA, Kandel ER. Synapses and Memory Storage. *Cold Spring Harb Perspect Biol*. 2012;4:a005751.

350. Deng W, Wu L, Bu L, et al. PAK2 promotes migration and proliferation of salivary gland adenoid cystic carcinoma. *Am J Transl Res*. 2016;8(8):3387-3397.

351. Renkema GH, Pulkkinen K, Saksela K. Cdc42/Rac1-Mediated Activation Primes PAK2 for Superactivation by Tyrosine Phosphorylation. *Mol Cell Biol*. 2002;22(19):6719-6725. doi:10.1128/MCB.22.19.6719.

352. Ille F, Sommer L. Wnt signaling: multiple functions in neural development. *Cell Mol Life Sci*. 2005;62:1100-1108. doi:10.1007/s00018-00.

353. Nusse R, Fuerer C, Ching W, et al. Wnt Signaling and Stem Cell Control. *Cold Spring Harb Symp Quant Biol*. 2008;73:59-66.

354. Logan CY, Nusse R. The Wnt signaling pathway in development and disease. *Annu Rev Cell Dev Biol*. 2004;20:781-810. doi:10.1146/annurev.cellbio.20.010403.113126.

355. Wrobel CN, Mutch CA, Swaminathan S, Taketo MM, Chenn A. Persistent expression of stabilized β-catenin delays maturation of radial glial cells into intermediate progenitors. *Dev Biol*. 2007;309(2):285-297.

356. Wexler EM, Paucer A, Kornblum HI, Palmer TD, Geschwind DH. Endogenous Wnt Signaling Maintains Neural Progenitor Cell Potency. *Stem Cells*. 2009;27(5):1130-1141. doi:10.1002/stem.36.Endogenous.

357. Zechner D, Fujita Y, Hulsken J, et al. ß-Catenin signals regulate cell growth and the balance between progenitor cell expansion and differentiation in the nervous system. *Dev Biol*.

2003;258:406-418. doi:10.1016/S0012-1606(03)00123-4.

358. Ye S, Tan L, Yang R, et al. Pleiotropy of Glycogen Synthase Kinase-3 Inhibition by CHIR99021 Promotes Self-Renewal of Embryonic Stem Cells from Refractory Mouse Strains. *PLoS One*. 2012;7(4):e35892. doi:10.1371/journal.pone.0035892.

359. Wray J, Kalkan T, Gomez-lopez S, et al. Inhibition of glycogen synthase kinase-3 alleviates Tcf3 repression of the pluripotency network and increases embryonic stem cell resistance to differentiation. *Nat Cell Biol*. 2012;13(7):838-845. doi:10.1038/ncb2267.Inhibition.

360. Liu KJ, Arron JR, Stankunas K, Crabtree GR, Longaker MT. Chemical rescue of cleft palate and midline defects in conditional GSK-3 b mice. *Nature*. 2007;446(March):79-82. doi:10.1038/nature05557.

361. Gao X, Arlotta P, Macklis JD, Chen J. Conditional Knock-Out of ß-Catenin in Postnatal-Born Dentate Gyrus Granule Neurons Results in Dendritic Malformation. *J Neurosci*. 2007;27(52):14317-14325. doi:10.1523/JNEUROSCI.3206-07.2007.

362. Brault V, Moore R, Kutsch S, et al. Inactivation of the β-catenin gene by Wnt1-Cre-mediated deletion results in dramatic brain malformation and failure of craniofacial development. *Development*. 2001;128:1253-1264.

363. de Ligt J, Willemsen MH, van Bon BWM, et al. Diagnostic Exome Sequencing in Persons with Severe Intellectual Disability. *N Engl J Med*. 2012;367(20):1921-1929. doi:10.1056/NEJMoa1206524.

364. Dubruc E, Putoux A, Labalme A, Rougeot C, Sanlaville D, Edery P. A New Intellectual Disability Syndrome Caused by CTNNB1 Haploinsufficiency. *Am J Med Genet Part A*. 2014;164A:1571-1575. doi:10.1002/ajmg.a.36484.

365. Maggirwar SB, Tong N, Ramirez S, Gelbard HA, Dewhurst S. HIV-1 Tat-Mediated Activation of Glycogen Synthase Kinase-3ß Contributes to Tat-Mediated Neurotoxicity. *J Neur*. 1999;73:578-586.

366. Kumar A, Zloza A, Moon RT, Watts J, Tenorio AR, Al-harthi L. Active ß-Catenin Signaling Is an Inhibitory Pathway for Human Immunodeficiency Virus Replication in Peripheral Blood Mononuclear Cells. *J Virol*. 2008;82(6):2813-2820. doi:10.1128/JVI.02498-07.

367. Narasipura SD, Henderson LJ, Fu SW, Chen L, Kashanchi F, Al-harthi L. Role of ß-Catenin and TCF/LEF Family Members in Transcriptional Activity of HIV in Astrocytes. *J Virol*. 2012;86(4):1911-1921. doi:10.1128/JVI.06266-11.

368. Butler JS, Dunning EC, Murray DW, Doran PP, Byrne JMO. HIV-1 Protein Induced Modulation of Primary Human Osteoblast Differentiation and Function Via a Wnt/ß-Catenin-Dependent Mechanism. *J Orthop Res*. 2013;31(2):218-226. doi:10.1002/jor.22196.

369. Antiretroviral Pregnancy Registry Steering Committee. *The Antiretroviral Pregnancy Registry Interim Report*. Vol 2018.; 2018.

370. Lengfeld JE, Lutz SE, Smith JR, et al. Endothelial Wnt/β-catenin signaling reduces immune cell infiltration in multiple sclerosis. *PNAS*. 2017;114(7):E1168–E1177. doi:10.1073/pnas.1609905114.

371. Moskot M, Jak J, Kloska A, Piotrowska E. The Role of Dimethyl Sulfoxide (DMSO) in Gene Expression Modulation and Glycosaminoglycan Metabolism in Lysosomal Storage Disorders on an Example of Mucopolysaccharidosis. *Int J Mol Sci*. 2019;20(304):1-18. doi:10.3390/ijms20020304.

372. Jasmin, Spray DC, Carlos A, Carvalho C De, Mendez-otero R. Chemical Induction of Cardiac Differentiation in P19 Embryonal Carcinoma Stem Cells. *Stem Cells Dev*. 2010;19(3). doi:10.1089/scd.2009.0234.

373. Pal R, Krishna M. Diverse effects of dimethyl sulfoxide (DMSO) on the differentiation potential of human embryonic stem cells. *Arch Toxicol*. 2012;86:651-661. doi:10.1007/s00204-011-0782-2.

374. Czysz K, Minger S, Thomas N. DMSO Efficiently Down Regulates Pluripotency Genes in Human Embryonic Stem Cells during Definitive Endoderm Derivation and Increases the Proficiency of Hepatic Differentiation. *PLoS One*. 2015;10(2):e0117689. doi:10.1371/journal.pone.0117689.

375. Jira P. *Cholesterol Metabolism Deficiency*. Vol 113. 1st ed. Elsevier B.V.; 2013. doi:10.1016/B978- 0-444-59565-2.00054-X.

376. Brandmann M, Nehls U, Dringen R. 8-Hydroxy-Efavirenz, the Primary Metabolite of the Antiretroviral Drug Efavirenz, Stimulates the Glycolytic Flux in Cultured Rat Astrocytes. *Neurochem Res*. 2013;38(12):2524-2534. doi:10.1007/s11064-013-1165-2.

377. Nolan D, Phillips E, Mallal S. Efavirenz and CYP2B6 polymorphism: implications for drug toxicity and resistance. *Clin Infect Dis*. 2006;42(December):408-410. doi:10.1086/499369.

Supplementary Data

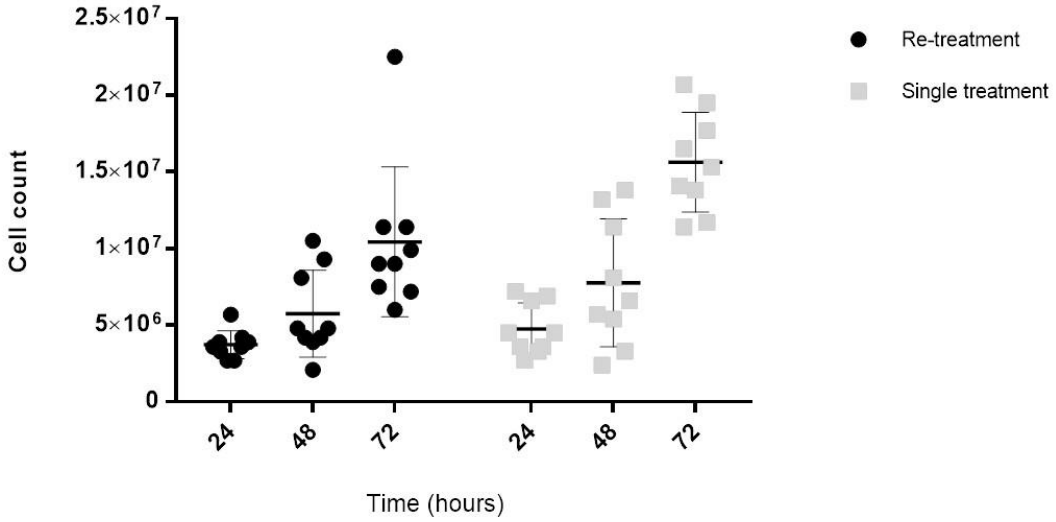

Figure S1: Cell count over 72 hours when treated with EFV. Cells were treated according to the two treatment schedules. Each condition had a total of nine replicates that were harvested every 24 hours and manually counted with the Trypan Blue cell counting assay. The differences in cell counts between the two conditions were not significantly different, although there appeared to be a slight but insignificantly lower count after 72 hours in the re-treatment condition.

Table S1: Significantly differentially regulated genes in T24 with EFV treatment

Gene ID	Fold change (Log_2)	p-value
ATP5C1	0.157	0.011
CAP2	-0.174	0.016
CCAR1	-0.154	0.016
DNAJA1	0.140	0.041
DYNC1LI1	-0.138	0.041
FADS2	-0.265	0.006
FASN	-0.138	0.048
FDFT1	-0.322	0.023
HMGCS1	-0.362	0.001
IDH1	-0.151	0.039
IPO4	0.444	0.021
KIAA0368	0.256	0.007
LIN28B	0.160	0.023
LRRC59	-0.324	0.024
MSH2	0.119	0.042
PSME2	0.128	0.031
RAB10	-0.270	0.010
RAB2A	0.128	0.047
RPS5	-0.198	0.020
SEC61B	0.611	0.040
SMARCC1	0.212	0.033
STAT3	0.147	0.018
TLN2	0.344	0.016
TMSB15B	-0.857	0.027
TUBA1B	-0.064	0.038
APOA1BP	-0.292	0.050

Table S2: Significantly differentially regulated genes in T48 with EFV treatment		
Gene ID	**Fold change (Log_2)**	**p-value**
ACAT2	-0.197	0.001
ACLY	-0.081	0.018
APOA1BP	-0.398	0.026
CALR	0.168	0.003
CCT2	-0.082	0.021
CTNNB1	-0.102	0.044
DDX1	-0.107	0.046
DNM2	-0.093	0.016
EIF3M	0.139	0.006
ETFA	-0.197	0.043
FAM98B	-0.278	0.023
FDFT1	-0.219	0.004
GART	-0.163	0.034
HMGCS1	-0.261	0.011
LAMTOR5	-0.288	0.020
LARS	-0.147	0.038
METAP2	-0.322	0.017
MSH6	-0.251	0.046
NDUFS1	-0.259	0.008
NPEPPS	-0.129	0.021
PIN1	-0.249	0.005
PLD3	-0.178	0.014
POR	-0.156	0.003
PPP2R4	0.347	0.018
PRCC	0.178	0.004
PRPF19	-0.119	0.019
RUVBL1	-0.064	0.029
SAR1A	0.147	0.042
SBDS	-0.208	0.049
SF1	0.080	0.033
SLC2A1	-0.573	0.030
SQLE	0.313	0.022
SRSF5	-0.349	0.039
TFRC	0.472	0.026
TUBB4B	-0.098	0.043
TXNDC17	-0.172	0.001
UBXN7	-0.196	0.018
USP5	0.056	0.031
VCP	-0.073	0.049

Table S3: Significantly differentially regulated genes in T72 with EFV treatment		
Gene ID	Fold change (Log_2)	p-value
AASS	0.226	0.007
ACAT2	-0.155	0.007
ACLY	-0.066	0.045
ACTC1	0.319	0.040
ACTR2	0.179	0.038
ANKFY1	0.376	0.007
ANXA2	0.145	0.032
AP2S1	0.323	0.004
APOA1BP	-0.349	0.036
APOE	0.168	0.040
BDH2	-0.455	0.020
CALM2	-0.229	0.009
CAP1	-0.188	0.004
CCT2	-0.056	0.031
CDC73	-0.319	0.049
CDK11A	0.152	0.026
CLIP2	1.117	0.049
COPA	0.102	0.030
CORO1B	-0.445	0.032
CPSF1	-0.538	0.014
CTNNB1	-0.259	0.003
CYB5B	-0.265	0.028
DBI	-0.156	0.050
DCXR	-0.264	0.012
DDX1	-0.180	0.015
DNMT3A	0.136	0.024
EIF3E	-0.193	0.016
EIF4G2	-0.084	0.049
EIF5	-0.367	0.040
FASN	-0.233	0.001
FDFT1	-0.222	0.002
FSCN1	0.242	0.019
G6PD	0.250	0.036
GSK3B	-0.331	0.049
GTF2I	-0.098	0.049
HMGCS1	-0.396	0.005
HP1BP3	-0.134	0.016
HSP90B1	0.065	0.043
KHDRBS1	-0.230	0.042
LSM4	-0.333	0.038
LUC7L	-0.437	0.046

LUC7L3	-0.383	0.019
MAPRE1	-0.225	0.042
MCM4	-0.072	0.029
NDUFB11	-0.307	0.009
NPEPPS	-0.111	0.009
NRAS	0.123	0.002
PAK2	-0.158	0.029
PCMT1	0.240	0.037
PGAM1	0.135	0.011
PPIE	-1.354	0.029
PRPF19	-0.134	0.022
PRPF38A	-0.258	0.035
PSAP	-0.270	0.049
PSMB1	-0.118	0.025
PSMB3	-0.174	0.035
RAB5C	-0.105	0.031
RAC1	-0.240	0.030
RPL7	-0.185	0.047
RPN1	0.166	0.043
RPS13	-0.128	0.016
RPS8	0.141	0.016
SARS	-0.227	0.048
SART3	-0.225	0.037
SERPINH1	0.130	0.033
SF3A1	-0.173	0.011
SF3B1	-0.109	0.004
SHMT2	0.160	0.018
SMARCA4	-0.133	0.003
SNRPF	0.866	0.018
SOD2	0.118	0.021
SPARC	0.158	0.035
SRI	-0.122	0.019
SRRM1	-0.153	0.015
SSRP1	-0.096	0.047
TWF1	-0.199	0.037
UBE2L3	-0.390	0.050
UHRF1	-0.271	0.039
UQCRQ	0.585	0.025
YWHAZ	0.122	0.008

Table S4: The log_2 fold change of significantly differentially regulated ($p < 0.05$) genes in the EFV treatment condition compared to the control over 72 hours.

Gene ID	EFV_24	EFV_48	EFV_72
AASS			0.226051985
ACAT2		-0.197335632	-0.155244843
ACLY		-0.081066736	-0.065701131
ACTC1			0.319075036
ACTR2			0.179065109
ANKFY1			0.376258304
ANXA2			0.145280186
AP2S1			0.323101758
APOA1BP	-0.292019861	-0.398311366	-0.349498123
APOE			0.1683741
ATP5C1	0.156601932		
BDH2			-0.454698704
CALM2			-0.229432766
CALR		0.168240919	
CAP1			-0.187581016
CAP2	-0.174103534		
CCAR1	-0.154105444		
CCT2		-0.082012302	-0.056048559
CDC73			-0.318998605
CDK11A			0.151562687
CLIP2			1.117413907
COPA			0.102147937
CORO1B			-0.444615409
CPSF1			-0.537768338
CTNNB1		-0.10180373	-0.259199393
CYB5B			-0.265496434
DBI			-0.155945485
DCXR			-0.26435659
DDX1		-0.107166206	-0.180080323

DNAJA1	0.13993827		
DNM2		-0.092746525	
DNMT3A			0.135759725
DYNC1LI1	-0.138355186		
EIF3E			-0.19299421
EIF3M		0.139349909	
EIF4G2			-0.083618832
EIF5			-0.366597851
ETFA		-0.196723636	
FADS2	-0.265345043		
FAM98B		-0.278464695	
FASN	-0.137777574		-0.232712644
FDFT1	-0.321702705	-0.218780143	-0.221640884
FSCN1			0.241824984
G6PD			0.250131711
GART		-0.16348609	
GSK3B			-0.330965738
GTF2I			-0.097651269
HMGCS1	-0.362220449	-0.260686886	-0.395591236
HP1BP3			-0.133686846
HSP90B1			0.06494082
IDH1	-0.150721799		
IPO4	0.444272561		
KHDRBS1			-0.230279521
KIAA0368	0.255843629		
LAMTOR5		-0.288057976	
LARS		-0.146560599	
LIN28B	0.160403616		
LRRC59	-0.324030828		
LSM4			-0.333162882
LUC7L			-0.437158687

MAPRE1			-0.225374795
MCM4			-0.071720181
METAP2		-0.321904969	
MSH2	0.119388084		
MSH6		-0.251419032	
NDUFB11			-0.306676274
NDUFS1		-0.259212128	
NPEPPS		-0.129434585	-0.110551767
NRAS			0.122985745
PAK2			-0.158471253
PCMT1			0.239640951
PGAM1			0.135335936
PIN1		-0.248838539	
PLD3		-0.178277578	
POR		-0.155635268	
PPIE			-1.354399645
PPP2R4		0.346841337	
PRCC		0.178044921	
PRPF19		-0.119265927	-0.133575327
PRPF38A			-0.258222858
PSAP			-0.269540545
PSMB1			-0.117819553
PSMB3			-0.174354001
PSME2	0.127549351		
RAB10	-0.269609422		
RAB2A	0.127834658		
RAB5C			-0.105111257
RAC1			-0.240205549
RPL7			-0.185108562
RPN1			0.166123957
RPS13			-0.128457268
RPS8			0.141379339

RUVBL1		-0.064492353	
SAR1A		0.147260183	
SARS			-0.227025669
SART3			-0.225111154
SBDS		-0.207532417	
SEC61B	0.610764539		
SERPINH1			0.129712985
SF1		0.079859447	
SF3A1			-0.172811858
SF3B1			-0.109148744
SHMT2			0.160241531
SLC2A1		-0.573487884	
SMARCA4			-0.133435068
SMARCC1	0.212019598		
SNRPF			0.866089834
SOD2			0.118300502
SPARC			0.158418024
SQLE		0.312757545	
SRI			-0.122350996
SRRM1			-0.15306555
SRSF5		-0.349192207	
SSRP1			-0.095695216
STAT3	0.146624578		
TFRC		0.471813357	
TLN2	0.344359789		
TMSB15B	-0.857042084		
TUBA1B	-0.064395233		
TUBB4B		-0.098069445	
TWF1			-0.199145087
TXNDC17		-0.172060836	
UBE2L3			-0.389743257
UBXN7		-0.196118545	

UHRF1		-0.270599342
UQCRQ		0.585083921
USP5	0.055862943	
VCP	-0.073076308	
YWHAZ		0.122406091

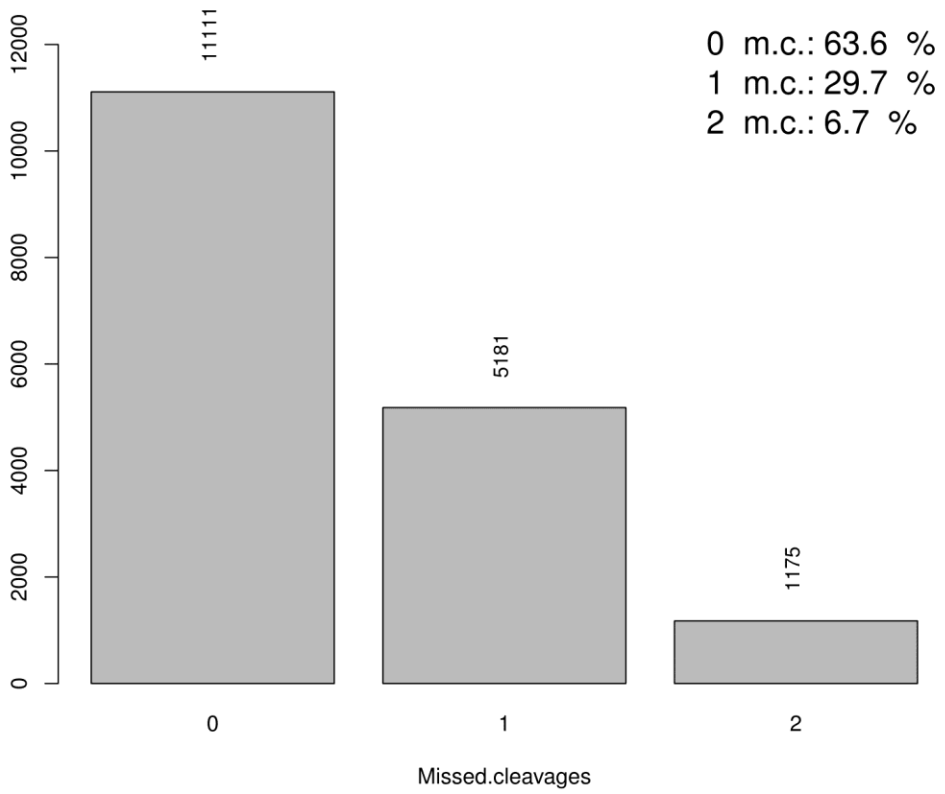

Figure S2: Assessment of digestion efficiency based on missed cleavages.

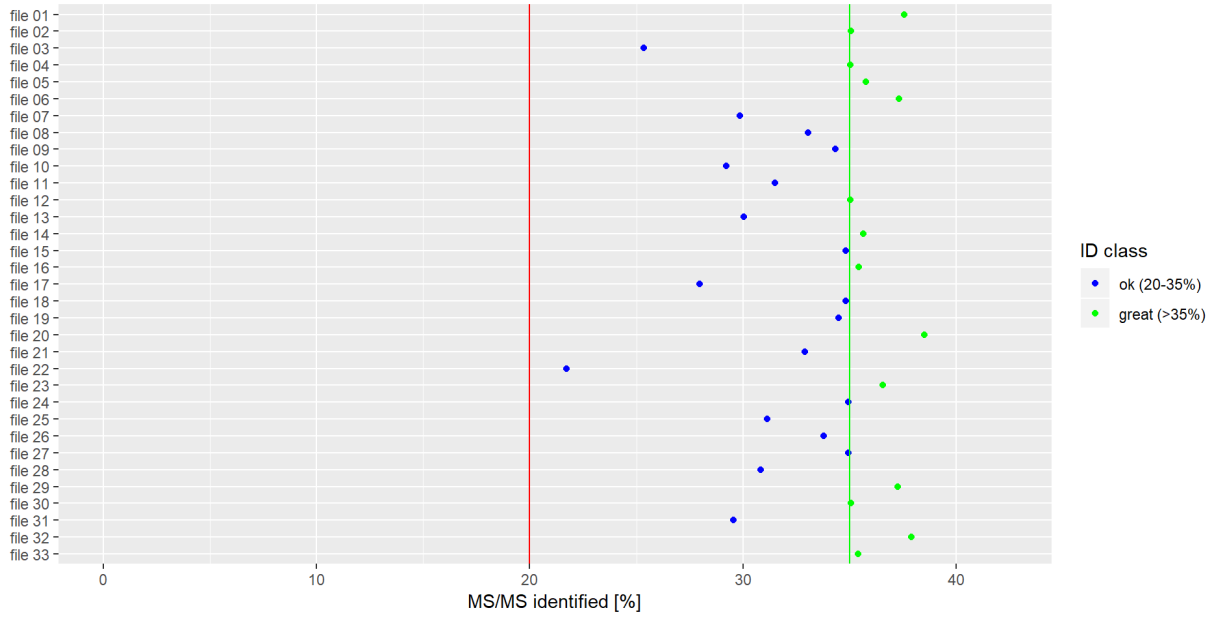

Figure S3: MS/MS identification rate per raw file. A 20% or higher identification rate was achieved in all raw files.

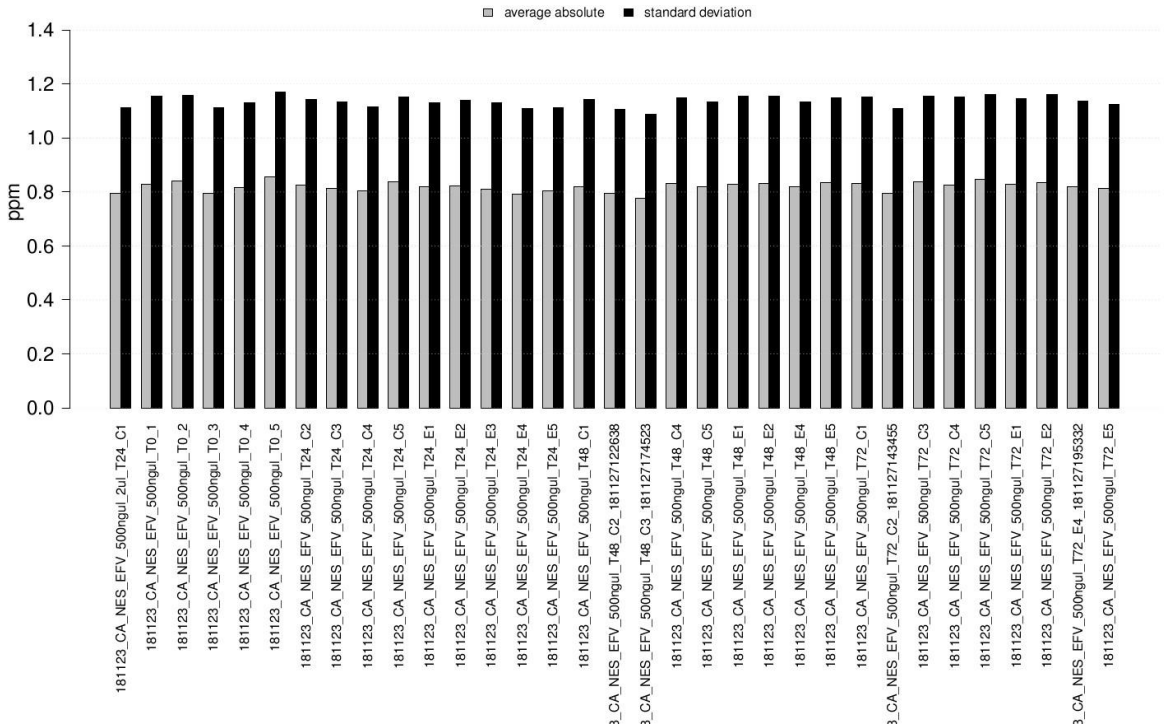

Figure S4: The average mass error of the MS instrument in each sample, measured in parts per million.The mass error across all samples was 0.8 +-0.5 ppm

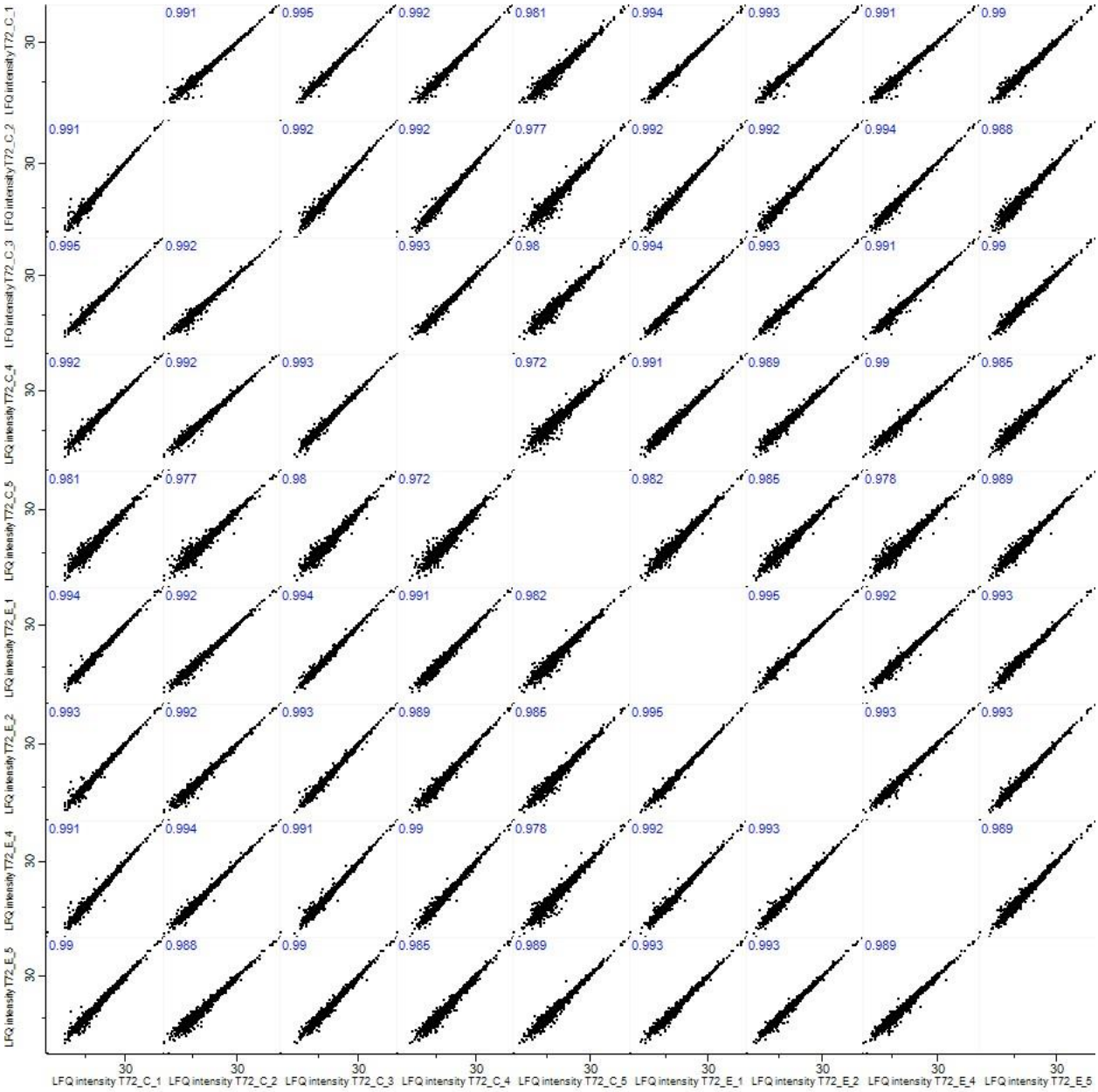

Figure S5: A multi-scatter plot containing replicates from control and treated samples in T72. LQF intensity values from each replicate are plotted against each other replicate in order to assess variation. Pearson's correlation scores indicate the amount of variation between two samples. Scores > 0.95 indicate low variation between samples.